Designing the Stem Cell Microenvironment for Guided Connective Tissue Regeneration

Danielle R. Bogdanowicz

Submitted in partial fulfillment of the requirements for the degree of Doctor of Philosophy

in the Graduate School of Arts and Science

Columbia University

2017

ABSTRACT

Designing the Stem Cell Microenvironment for Guided Connective Tissue Regeneration

Danielle R. Bogdanowicz

Injuries to connective tissues such as ligaments and tendons are common, and rather than healing, repair typically results in fibrosis, or the formation of mechanically inferior and disorganized scar tissue. This fibrotic repair response is due in part to inflammation, during which the injury site is invaded by a number of cell types, including macrophages, neighboring fibroblasts, and homed stem cells or progenitor cells. Activation of macrophages is believed to be modulated by communications with fibroblasts and stem cells, prompting either a pro-fibrotic or a pro-regenerative response. Beyond changes to the cellular microenvironment, fibrosis also results in changes to the organization and mechanical properties of the matrix microenvironment. For healthy fibrous connective tissues, the matrix is comprised of aligned collagen fibers, while scar tissue is disorganized and exhibits weaker mechanical properties than healthy tissue. To date, the nature of the cell-cell and cell-matrix interactions and their relevance in tissue healing or repair remain understudied.

To better understand the cellular and matrix-based cues that direct scar formation versus tissue regeneration, and using anterior cruciate ligament (ACL) injuries as a model, Aim 1 of this thesis tests the hypothesis that *in vitro* models of cellular communications between fibroblasts, macrophages, and mesenchymal stem cells (MSC) can be used to determine the effects of cellular interactions on macrophage activation and fibrosis. In Aim 2, the contribution of matrix-based cues (alignment and mechanical properties) to the inflammatory and fibrotic response, as well as their modulation of cellular interactions, were examined. Findings from these two aims reveal that 1) communications between native tissue fibroblasts and macrophages drive inflammation and fibrosis, while stem cells modulate the repair process through a combination of trophic signaling and immunomodulatory roles, and 2) matrix alignment and mechanical properties exert combined regulation on cell response during inflammation. From a clinical application perspective, stem cells delivered in conjunction with an engineered matrix that provides the critical cues for driving stem cell immunomodulation and trophic signaling will be essential for promoting

tissue regeneration and minimizing fibrosis. In particular, an aligned matrix with an elastic modulus similar to that of developing connective tissue may serve to further minimize inflammation and scar formation, and activate stem cell-guided regeneration of mechanically functional connective tissue.

TABLE OF CONTENTS

LIST OF FIGURES AND TABLES

LIST OF ABBREVIATIONS

ACL: Anterior Cruciate Ligament
AD: Angular Deviation
ADSC: Adipose-Derived Stem Cell
AFM: Atomic Force Microscopy
ALP: Alkaline Phosphatase
APC: Allophycocyanin
ASTM: American Society for Testing and Materials
ATR: Attenuated Total Reflectance
AuPd: Gold-Palladium
bFGF: Basic Fibroblast Growth Factor
BMP: Bone Morphogenetic Protein
BSA: Bovine Serum Albumin
cDNA: Complementary Deoxyribose Nucleic Acid
COX: Cyclooxygenase
CPC: Cetylpyridinium Chloride
CSD: Circular Standard Deviation
DAPI: 4',6-Diamidino-2-Phenylindole, Dihydrochloride
DCM: Dichloromethane
DI: Deionized
DMEM: Dulbecco's Modified Eagle's Medium
DMF: Dimethylformamide
DNA: Deoxyribose Nucleic Acid
DT: Doubling Time
E_{mod}: Elastic Modulus
E_{bulk}: Bulk Elastic Modulus
E_{local}: Local Elastic Modulus
ECM: Extracellular Matrix
EDTA: Ethylenediaminetetraacetic Acid
EGF: Epidermal Growth Factor
EGTA: N,N,N',N'-tetraacetic Acid
ELISA: Enzyme-Linked Immunosorbent Assay
FABP4: Fatty Acid Binding Protein 4
FACS: Fluorescence Activated Cell Sorting
FAK: Focal Adhesion Kinase
Fb: Fibroblast
FC: Fold Change
Fn: Fibronectin
FBS: Fetal Bovine Serum
FITC: Fluorescein Isothiocyanate
F/S: Fully Supplemented
FTIR: Fourier Transform Infrared
GAPDH: Glyceraldehyde-3-Phosphate Dehydrogenase

GDF: Growth Differentiation Factor
G-CSF: Granulocyte Colony-Stimulating Factor
HCl: Hydrochloric Acid
HGF: Hepatocyte Growth Factor
HLA: Human Leukocyte Antigen
HSC: Hematopoietic Stem Cell
IDO: Indoleamine 2,3-Dioxygenase
IFN: Interferon
IGF: Insulin-Like Growth Factor
IL: Interleukin
iPSC: Induced Pluripotent Stem Cell
LPS: Lipopolysaccharide
MΦ: Macrophage
MIP-1α: Macrophage Inflammatory Protein-1α (alpha)
MA: Mean Vector Angle
MAP: Mitogen-Activated Kinase
MHC: Major Histocompatibility Complex
MMP: Matrix Metalloproteinase
Mo: Monocyte
mRNA: Messenger RNA
MSC: Mesenchymal Stem Cell
MVL: Mean Vector Length
NaAc: Sodium Acetate
NaCl: Sodium Chloride
NaOH: Sodium Hydroxide
NBF: Neutral-Buffered Formalin
NEAA: Non-Essential Amino Acids
NO: Nitric Oxide
OC: Osteocalcin
OHP: Hydroxyproline
OP: Osteopontin
P/S: Penicillin-Streptomycin
PBC: Peripheral Blood Cell
PBMC: Peripheral Blood Mononuclear Cell
PBS: Phosphate Buffered Saline
PCL: Poly-ε-caprolactone
PD: Population Doublings
PDGF: Plated-Derived Growth Factor
PDL: Periodontal Ligament
PDO: Polydioxanone
PEG: Poly(ethylene glycol)
PEG-DA: Poly(ethylene glycol) Diacrylate
PEUUR: Poly(ester urethane)Urea

PGE2: Prostaglandin E2
PLGA: Poly(lactic-*co*-glycolic) Acid
PLLA: Poly-L-lactic Acid
PDMS: Polydimethylsiloxane
PMA: Phorbol 12-myristate 13-acetate
PMMA: Poly(methyl methacrylate)
pNP: p-Nitrophenol
PPAR-γ: Peroxisome Proliferator-Activated Receptor-γ (Gamma)
PVA: Poly(vinyl alcohol)
qRT-PCR: Quantitative Reverse Transcription Polymerase Chain Reaction
RF: Radiofrequency
RGD: Arginylglycylaspartic acid
RPMI: Roswell Park Memorial Institute
RNA: Ribonucleic Acid
SEM: Scanning Electron Microscopy
SMA: Smooth Muscle Actin
TDSC: Tendon-Derived Stem Cell
TGF-β1: Transforming Growth Factor-β1 (beta 1)
TGF-β3: Transforming Growth Factor-β3
THF: Tetrahydrofuran
TNF: Tumor Necrosis Factor
TSG: Tumor Suppressor Gene
UTS: Ultimate Tensile Strength
UV: Ultraviolet
VEGF: Vascular Endothelial Growth Factor
Y: Yield Strength
2-ME: 2-Mercaptoethanol

ACKNOWLEDGEMENTS

During my time at Columbia University, I have had the opportunity and privelege to work with an incredible group of faculty, students, and staff. I would like to thank my thesis advisor, Professor Helen H. Lu, for her mentorship and guidance throughout my graduate career. I would also like to thank and acknowledge my thesis committee – Professor Samuel K. Sia, Professor Lance C. Kam, Dr. William N. Levine, and Professor Nikolaj Gadegaard – who have offered invaluable feedback, insight, and direction throughout my thesis project development, execution, and completion.

I am also tremendously appreciative of my colleagues in the Biomaterials and Interface Tissue Engineering Laboratory, who have shared knowledge, advice, and thoughtful discussion with me throughout my tenure at Columbia. I would like to thank the past and present graduate students and post-doctoral scholars in my lab, including Dr. Siddarth Subramony, Dr. Philip Chuang, Dr. Sagaw Prateepchinda, Dr. Margaret Boushell, Dr. Xinzhi Zhang, Dr. Nancy Lee, Dovina Qu, Christopher Mosher, Philip Brudnicki, Dr. Cevat Erisken, and Dr. Jennifer Robinson, as well as the undergraduate and high school students who have worked directly with me, including Larisa Bowen-Dodoo, Taylor Wright, Stephanie Wells, Alexa Mazur, Christopher Eom, Victoria Xu, Busra Ozlu, and Temitope Akinade.

I am also incredibly thankful to the many collaborators who have been generous in sharing their time, expertise, and equipment over the years. Thank you to Professor Ozgur Sahin and Dr. Nicola Mandriota for help with atomic force microscopy studies. Thanks to Dr. Brian Jones for sharing his custom-built uniaxial tensile testing equipment, as well as Professor Michael Sheetz and Dr. Thomas Iskratsch for immunohistochemistry protocols. I would also like to thank Professor Edward Botchwey and Claire Segar at Georgia Institute of Technology for THP-1 culture protocols and for their guidance in the design and execution of THP-1 studies.

In addition to those who directly supported my research at Columbia, I would like to thank the outstanding mentors I have had during my undergraduate and graduate careers. Thank you to my professors at Rensselaer Polytechnic Institute, especially Dr. Deanna Thompson and Dr. James Cooper, as well as Dr. Holger Babbe at Janssen Research & Development, for supporting and encouraging my pursuit of a graduate degree, and for serving as fantastic role models and teachers.

Finally, I would like to thank my family and friends for their unending support, encouragement, and love throughout this process. To my parents – thank you for believing in me, for celebrating every milestone throughout this process, big or small, and for keeping me motivated. Thank you also to my brother for your encouragement and support during this journey. Finally, I would like to thank the rest of my family and my friends for being my cheerleaders and for serving as an incredible support system. Without the support of you all, I never could have made it to this point, and for that I am eternally grateful.

Research funding for the studies in this thesis has been provided by the National Science Foundation Graduate Research Fellowship Program (NSF GRFP), the Columbia Fu Foundation School of Engineering and Applied Sciences Presidential Fellowship, and the National Institutes of Health (R01-AR055280).

DEDICATION

This thesis is dedicated to my Popi - because of you, I will always work hard to do and be my best, while also remembering to stop and smell the roses.

CHAPTER 1: INTRODUCTION

1.1. Specific Aims

Mesenchymal stem cells (MSC) play an important role in tissue homeostasis and regeneration through their capacity for multipotent differentiation, immunomodulation, and promotion of healing through trophic signaling. It is thus not surprising that MSC are of increasing interest as a treatment modality for injury and disease in a number of tissue types. In fibrous connective tissues, MSC have been shown to mitigate the inflammatory response following acute injury, and promote proliferation and matrix synthesis by native tissue fibroblasts. Still, therapies that utilize MSC delivery as an adjuvant for tissue engineering approaches to connective tissue repair have yielded mixed results *in vivo*. This is likely due to inadequate synergistic signaling to delivered MSC by the surrounding microenvironment, resulting in an unpredictable cell response following delivery.

To this end, there is significant interest in investigating the impact of each of the various components of the connective tissue microenvironment on MSC response *in vitro* in order to develop an optimal stem cell microenvironment to promote stem cell-guided connective tissue regeneration. The native microenvironment is comprised of a combination of stimuli which serve as cues for stem cell activation and healing response. These cues include cellular communications with other cell types, interactions with the underlying matrix, soluble signaling cues, and physical/mechanical cues. Current attempts to engineer an artificial microenvironment capable of modulating stem cell response aim to mimic one or more of the signals provided by the native connective tissue microenvironment to coax stem cells to participate in tissue regeneration. Still, an optimal artificial matrix for promoting stem cell-guided regeneration of connective tissues has yet to be developed.

This thesis focuses on gaining a better understanding of the roles that MSC play in connective tissue injury and repair, as well as determining the critical matrix-based cues that are capable of promoting stem cells' regenerative capabilities. This will be achieved through the study of cell-cell and cell-matrix interactions using a series of *in vitro* culture models which mimic the cellular and structural microenvironment within fibrous connective tissue under healthy and injured conditions. This thesis is guided by the **hypotheses** that 1) mimicking the cell-cell communications between native tissue fibroblasts, macrophages, and stem cells following connective tissue injury will elucidate the effects of macrophage accumulation on scar tissue formation, as well as uncover the regenerative roles of stem cells during repair,

and 2) matrix-based cues contribute to the inflammatory and fibrotic response following connective tissue injury, and can therefore be tuned in order to modulate the fibrotic response and promote stem cell-guided connective tissue regeneration.

The specific aims of this thesis are outlined below:

Aim 1: **Evaluate the role of cellular interactions between fibroblasts, macrophages, and mesenchymal stem cells during connective tissue injury and repair.**

Hypotheses:

1. Interactions between fibroblasts and macrophages will mimic the early inflammatory response following connective tissue injury, resulting in pro-inflammatory activation of macrophages and a pro-fibrotic response by fibroblasts.
2. Interactions between MSC and both fibroblasts and macrophages will mitigate the inflammatory response and contribute to healing through:
    a. Enhanced fibroblast healing response, as observed through increased fibroblast proliferation and matrix synthesis.
    b. Decreased macrophage pro-inflammatory activation.

Aim 2: **Investigate the contribution of matrix-based cues (alignment and mechanical properties) to the inflammatory and fibrotic response, as well as their modulation of cellular interactions during connective tissue healing.**

Hypotheses:

1. Differences in matrix alignment and mechanical properties will impact:
    a. Initial MSC attachment, spreading, and alignment, resulting in differences in cell proliferation, and differentiation.
    b. Fibroblast alignment, proliferation, matrix synthesis, and phenotypic response.
    c. Macrophage inflammatory activation, in terms of attachment and cytokine release.
2. Matrix alignment and mechanical properties can be tuned to modulate the inflammatory response during connective tissue healing.

This thesis aims to model the changes that occur within the connective tissue microenvironment following injury, in order to assess the impact that these changes have on stem cell behavior, as well as uncover the role of MSC in connective tissue injury and healing. Specifically, heterotypic interactions between MSC, native ligament fibroblasts, and infiltrating macrophages during injury, inflammation, repair, and remodeling will be modeled using a series of co-culture and tri-culture models (**Aim 1**). These interactions will be further evaluated in 3D using a series of electrospun nanofiber-based matrices to assess the contributions of matrix alignment and mechanical properties (**Aim 2**) on the healing response.

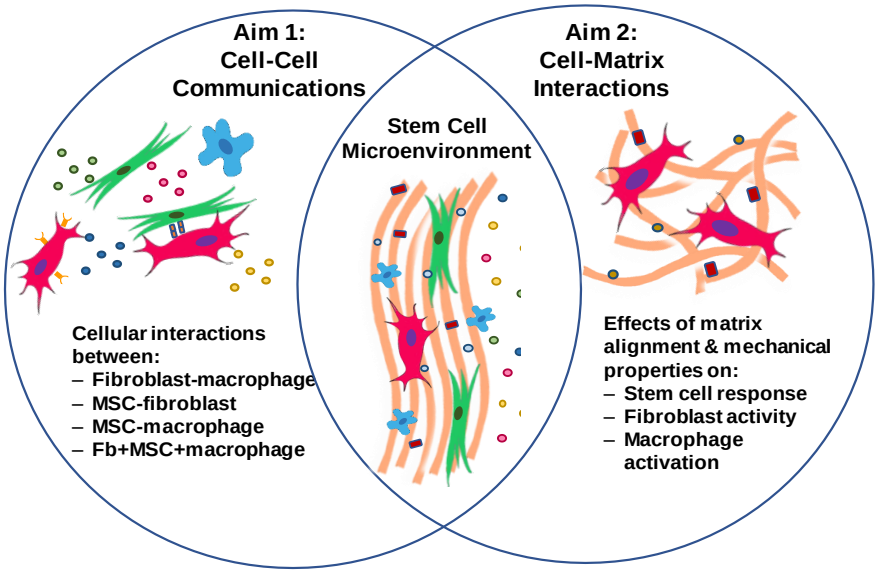

Figure 1.1: Engineering the Connective Tissue Microenvironment for Stem Cell-Guided Tissue Regeneration.

Identification of the environmental cues that are crucial to modulation of stem cell response to promote stem cell-guided tissue repair requires a better understanding of the environmental cues that are present following connective tissue injury, as well as elucidation of the factors which may be critical in promoting stem cell-guided tissue regeneration. This thesis aims to uncover the cell-cell communications and cell-matrix interactions that serve to promote stem cell trophic signaling, immunomodulation, and activation in terms of proliferation, matrix synthesis, and differentiation, in order to design an implantable matrix to promote stem cell-guided tissue repair following connective tissue injury. This matrix should serve to 1) modulate the inflammatory response following injury, as well as 2) promote stem cell-guided regeneration of tissue in exchange for scar tissue formation. To this end, the interactions between native

ligament fibroblasts and infiltrating macrophages will first be assessed (*Aim 1, Chapter 2*) to gain a better understanding of the inflammatory microenvironment following injury. Next, the roles that MSC play in controlling the inflammatory response and promoting healing (*Aim 1, Chapter 3*) will be investigated. Once the effects of MSC on tissue healing have been uncovered, a series of electrospun nanofiber-based matrices will be designed and optimized (*Aim 2, Chapter 4*) in order to assess the effects of matrix alignment and mechanical properties on stem cells (*Aim 2, Chapter 5*), as well as native ligament fibroblasts (*Aim 2, Chapter 6*) and infiltrating macrophages (*Aim 2, Chapter 7*). Finally, the interactions between all three cell types will be assessed on these nanofiber matrices, in order to determine the impact of matrix-based cues on the healing response following connective tissue injury (*Aim 2, Chapter 8*). Results from these studies will yield the optimal matrix properties for design of an artificial stem cell microenvironment for the delivery and activation of stem cells to promote stem cell-guided tissue regeneration following connective tissue injury.

Aim 1 will focus on the design and optimization of 2D co-culture and tri-culture systems in order to model the heterotypic cellular interactions observed within the ligament during injury, inflammation, repair, and remodeling. Following connective tissue injury, multiple cell types accumulate at the injury site, including resident and recruited inflammatory cells, homed stem/progenitor cells, as well as native ligament fibroblasts from the surrounding tissue(1;2). However, the cellular interactions between these various cell types at the wound site following injury, and during inflammation and healing, remain elusive(3). Therefore, the communications between native ligament fibroblasts, macrophages which arrive early in the inflammatory response and are present throughout the healing process, and migratory MSC, which home to the injury site throughout healing, will be assessed both individually and in tandem. Following injury, emigration of inflammatory cells from the circulatory system to the site of injury occurs, dumping mass numbers of leukocytes to initiate an inflammatory response. Critical among these cells is a population of macrophages, which are recruited to the wound site and begin to accumulate within 24 hours of injury, and continue to migrate to the injury throughout early- and late-stage healing(4). Using anterior cruciate ligament (ACL) injuries as a model, initial studies will focus on modeling the interactions between native ligament fibroblasts and macrophages during inflammation and early wound healing (*Chapter 2*). Beginning within 24-48 hours following injury, monocytes in the blood undergo extravasation and migrate to the injury site,

where they become activated and can differentiate into macrophages. These cells continue to infiltrate the wound site throughout the inflammatory process, and are found to be present for the duration of the healing process. It has been previously observed that macrophages are essential in tissue repair, as they are responsible not only for the clearance of debris, but also the release of signaling molecules that promote fibroblast proliferation, as well as extracellular matrix synthesis and degradation(1). Still, the mechanisms behind these interactions are not well-understood. Toward this objective, a co-culture model will be used to assess the nature of these communications.

After gaining a better understanding of the cellular microenvironment during inflammation, this thesis will focus on developing a series of co- and tri-culture models which mimic the heterotypic interactions between stem cells and both native ligament fibroblasts and macrophages in order to identify the role of stem cells in fibrous connective tissue healing (*Chapter 3*). As inflammation subsides and early wound healing begins, MSC and other progenitors are homed to the injury site, and continue to infiltrate this location throughout wound healing and late-stage remodeling. While the role of MSC following their arrival is not completely understood, it is believed that the release of trophic signaling factors plays a role in promoting the healing capacity of resident fibroblasts, as well as attenuating the inflammatory response, to allow for functional healing. The first study in *Chapter 3* will serve to model the interactions between MSC and native ligament fibroblasts within the connective tissue microenvironment during wound healing. It is believed that MSC are capable of encouraging proliferation, matrix synthesis, and remodeling by native cells. In addition to their ability to promote tissue regeneration, MSC have also been shown to modulate inflammatory response and attenuate inflammation(5). Both *in vitro* and *in vivo* studies suggest that MSC have the ability to suppress the immune response to inflammatory cells, including T cells, B cells, and natural killer cells. In the second study in *Chapter 3*, the heterotypic interactions between MSC and macrophages during connective tissue healing will be modeled. This model will be utilized to assess the immunomodulatory effects of MSC on macrophage activation. According to others, contact with MSC results in increased expression of CD206, an anti-inflammatory marker, by human peripheral blood monocytes, indicating that MSC are capable of encouraging alternative activation of macrophages toward an anti-inflammatory phenotype(6). Still, the impact of macrophages on MSC response remains largely unstudied. Finally, in the third study of *Chapter 3*, a tri-culture model incorporating ligament fibroblasts,

MSC, and macrophages will be used in order to recapitulate the cellular environment within connective tissue during healing. With this model, the role of heterotypic cellular interactions between all three cell types on cell behavior during early and late-stage wound healing response can be assessed. Each of the models designed in *Chapters 2* and *3* will be utilized in **Aim 2** to study the effects of matrix-based cues (fiber alignment and mechanical properties) on the heterotypic cellular interactions between these three cell types during connective tissue injury and healing.

The objective of **Aim 2** is to determine the effects of changes in matrix alignment and mechanical properties on the connective tissue healing response. Therefore, this aim will focus on elucidating the impact of matrix alignment and mechanical properties on the cell-matrix interactions of each of the cell types assessed in **Aim 1** using electrospun nanofiber-based matrices. Healthy connective tissues, including the ligament, are comprised of fibrous, mostly collagenous connective tissue(7), aligned parallel to the direction of loading. However, following injury, fibroblasts and other cells are activated to quickly fill the tissue void, resulting in the formation of scar tissue, which is often disorganized when compared to healthy connective tissue, with and increased incidence of defects and observed collagen fiber misalignment(8). This disorganization has been shown to affect cellular alignment on scar tissue(9) and results in differences in mechanical properties as compared to healthy connective tissue(10).

Electrospun nanofibers have been used previously to recapitulate the fibrillar structure of connective tissues such as the ligament(11), skeletal muscle(12), and skin(13). To study the effects of changes in matrix alignment and stiffness on cell response, electrospun nanofiber-based matrices will be designed, characterized, and optimized to exhibit 1) unaligned vs. aligned fiber morphologies and 2) soft vs. stiff mechanical properties (*Chapter 4*). In order to accomplish this, polydimethylsiloxane (PDMS), an inert, nontoxic polymer with outstanding flexibility, will be added to poly-ε-caprolactone (PCL) fibers, to create nanofibers comprised of a PDMS-PCL polymer blend. PDMS is fabricated by mixing dimethylsiloxane monomer with its corresponding cross-linking agent and altering the ratio of base polymer to crosslinking agent has been shown to change the elasticity of the resultant elastomer(14). PDMS with varying ratios of base to crosslinker has previously been used as a 2D substrate for studying the effects of matrix stiffness on cell behavior(15-19). PDMS-PCL nanofiber meshes will be electrospun in aligned and unaligned fiber orientations and characterized in terms of fiber diameter, pore size, alignment, surface

chemistry and surface energy, in order to confirm that PDMS was successfully incorporated into fibers, while maintaining the same topography and structure as PCL-only fibers. The mechanical properties of the optimized PDMS-PCL fibers and PCL-only fibers will also be assessed at both the bulk and local levels, to confirm that the addition of PDMS to PCL fibers results in lower mechanical properties.

Chapter 5 will focus on studying the effects of fiber alignment and mechanical properties on the behavior of MSC. Previous work studying human MSC on unaligned vs. aligned poly-lactic-*co*-glycolic acid (PLGA) nanofibers has shown that MSC alignment can be modulated by the alignment of underlying fibers, as MSC were observed to orient themselves along the direction of fibers by day 1. MSC on aligned fibers proliferated more extensively and synthesized more matrix than cells on unaligned substrates(20). Additionally, studies have shown that cellular mechanotransduction systems are capable of sensing the surrounding microenvironment and transducing these stimuli into biochemical signals, which in turn translate into controlled functional responses(21-23). Specific to MSC, the mechanical properties of the microenvironment appear to be important to lineage specification and ultimately, differentiation(21). Still, the mechanisms behind these interactions remain elusive.

Next, in *Chapter 6*, the effects of matrix alignment and mechanical properties on the response of native ligament fibroblasts will be assessed, in terms of cell adhesion and alignment, proliferation, and matrix synthesis. Study of human rotator cuff fibroblasts on aligned and unaligned PLGA nanofibers suggests that fiber alignment plays a role in fibroblast attachment and spreading, as well as integrin expression, resulting in differences in matrix synthesis and organization(24). In *Chapter 7*, the effects of fiber alignment and mechanical properties on macrophage activation toward a pro-inflammatory or anti-inflammatory pathway will be determined. Previous work using the murine macrophage-like RAW 264.7 cell line has shown that macrophage activation toward a pro-inflammatory phenotype can be modulated by the alignment of electrospun poly (L-lactic) acid (PLLA) fibers, as observed through an upregulation in the secretion of pro-inflammatory cytokines(25).

Finally, this thesis will culminate with assessment of the cellular interactions between all three cell types on each of the matrices designed in *Chapter 4*, in order to uncover the effects of matrix-based cues on the heterotypic interactions between MSC, fibroblasts, and macrophages during and following connective tissue injury, using a 3D tri-culture model (*Chapter 8*). After assessing the impacts of matrix

cues on the response of each cell type individually, as well as in tri-culture, it will be possible to identify the optimal matrix cues for mitigating the inflammatory response and promoting stem cell-guided tissue regeneration. These findings will be used toward determining the required design parameters for an engineered matrix for implantation following connective tissue injury, which can serve as 1) a vehicle for the delivery and subsequent activation of autologous mesenchymal stem cells, or 2) an acellular implant to modulate the inflammatory response and promote stem cell-mediated tissue regeneration by homed stem cells or progenitor cells.

In combination, these two aims will allow for a better understanding of the changes that occur immediately following ligament injury, as well as throughout the healing process, and the impacts that these changes have on prompting a pro-fibrotic versus pro-regenerative healing response. These strategies can be translated to serve as a physiologically-relevant 3D model for studying both cell-matrix and cell-cell interactions in connective tissue under healthy and injured conditions. Additionally, by gaining a better understanding of the cellular and matrix-based cues responsible for MSC behavior in healthy and injured connective tissue, these cues could be utilized to develop an artificial matrix, which could then be seeded with exogenous MSC and delivered to the injury site to promote stem cell-guided connective tissue regeneration following injury. This would aid in generation of a mechanically functional tissue replacement, which is critical for connective tissue engineering. And while in this study, the anterior cruciate ligament (ACL) is utilized as a model for connective tissue repair, this artificial microenvironment could be designed for application in the regeneration of other fibrous connective tissues, such as other ligaments, tendons, muscle, and skin, to promote scarless healing and regeneration of a mechanically functional replacement tissue following injury.

1.2. Background and Significance

1.2.1 Mesenchymal Stem Cells & The Stem Cell Niche

1.2.1.1 Mesenchymal Stem Cells

Mesenchymal stem cells (MSC) are a heterogeneous population of non-hematopoietic, multipotent cells first discovered in the adult bone marrow(26-28), which were observed to form bone following heterotopic bone transplantation(26). They exhibit a fibroblast-like morphology and are able to self-renew, or replicate as undifferentiated cells, and can also differentiate toward mesenchymal lineages(29), including

bone, cartilage, and fat, as well as skin(30), tendon/ligament(31-33), muscle(34), and bone marrow stroma(35;36). In addition to cells derived from the bone marrow, stem cells have been found to reside in other mesenchymal tissues, including fat(37), skin(38), tendon(39), periodontal ligament(40), and dental pulp(41), to name a few. These cells are believed to contribute to the ability of adult tissues to regenerate and repair following injury and aging(42).

While there is currently no known gene expression profile for the definitive identification of MSC, the Mesenchymal and Tissue Stem Cell Committee at the International Society of Cellular Therapy (ISCT) has devised a set of minimal criteria for defining these cells(43). Specifically, cells must be substrate-adherent, differentiate into osteocytes, adipocytes, and chondrocytes, and exhibit a specific expression profile of a subset of surface markers. Specifically, MSC must express CD90/Thy1, CD73, and CD105(43). In addition to these, Stro-1 is the most widely accepted and well-known MSC marker, as this marker is correlated with cells' ability to form colonies, a hallmark characteristic of MSC *in vitro*(44). However, the exact function of Stro-1 expression is not known, and its expression is not unique to MSC and can be found in other cell types including nucleated erythroid cells, limiting the use of Stro-1 as a standalone marker for MSC identification(45). Further, MSC are observed to gradually lose their expression of this marker during *in vitro* expansion, limiting its use beyond MSC isolation and early culture. Additionally, the markers which are absent from the surface of MSC include CD34 (hematopoietic and endothelial cell marker), CD45 (leukocyte marker), CD11b (monocytes and macrophages), CD79-α or CD19 (B cell markers), and human leukocyte antigen (HLA) class II surface molecules (antigen-presenting cells and lymphocytes)(43). Other markers such as CD117 and CD31 are commonly referred to as negative MSC markers(43).

There is great interest in utilizing MSC for clinical applications because of their trophic capacity to promote tissue repair and remodeling, and their ability to modulate the immune response following injury(46). Mesenchymal stem cells actively respond to stress or injury similarly to cells in the adaptive and innate immune systems following pathogen exposure or apoptosis(47). While undifferentiated MSC do not express major histocompatibility complex (MHC) class II antigens, these molecules are observed to be upregulated on the cell surface following exposure to the inflammatory microenvironment(48). Mesenchymal stem cells have been shown to influence the immune system through the secretion of a variety of soluble factors including indoleamine 2,3-dioxygenase (IDO)(49), nitric oxide(50), transforming

growth factor (TGF)-β(51), prostaglandin E2 (PGE2)(51;52), and tumor necrosis factor stimulated gene-6 protein (TSG-6)(53). Early studies on the immunosuppressive potential of MSC found that cells derived from humans(54-57), baboons(58), and mice(59;60) are all capable of suppressing T cell proliferation and inflammatory cytokine secretion. Since then, it has been reported that MSC are also able to suppress the proliferation and cytokine release of other inflammatory cell types, including B cells, antigen-presenting cells, and natural killer cells. Specific to connective tissues, MSC have been shown to reduce the infiltration of inflammatory cells within the tendon and tendon-to-bone interface in animal models, promoting repair(61).

In addition to their role in immunomodulation, MSC have been reported to enhance fibroblast proliferation and collagen matrix synthesis via paracrine signaling(62). These cells serve as a source of cytokines and proteinases essential to angiogenesis and tissue regeneration, including vascular endothelial growth factor (VEGF), matrix metalloproteinases (MMPs), insulin-like growth factor-1 (IGF-1), hepatocyte growth factor (HGF), TGF-β, and basic fibroblast growth factor (bFGF)(63). Specific to connective tissues, MSC promote scarless healing within the tendon and tendon-to-bone interface through secretion of factors that stimulate fibroblast proliferation, promote angiogenesis, inhibit apoptosis, and minimize fibrosis(61;64;65).

1.2.1.2 The Mesenchymal Stem Cell Niche in Connective Tissue

In order to better understand stem cell behavior and tissue-specific response, it is important to account for the cells' tissue of origin. As MSC have been shown to reside in a number of different tissues, both mesenchymal and non-mesenchymal in origin, it is likely that common features among the MSC microenvironment must exist in order to modulate cell function. Toward this point, in 1978, Schofield proposed the existence of distinct, finite microenvironments within tissue, known as "stem cell niches," that serve to house and support stem cells(66). While the niche was first described within the hematopoietic system, stem cell niches have since been identified in a number of tissues.

The term "niche" has historically been used to describe the anatomic location of stem cells within adult tissues. More recently, it is believed that the niche is comprised of the collective cellular, structural, and signaling cues that modulate stem cell participation in tissue maintenance and generation and repair(67;68). The exact components that make up the stem cell niche remain controversial and differ

between tissues and niche locations. It is postulated that the niche is comprised of an extracellular matrix (ECM), other non-cellular constituents, and heterologous cell populations that can communicate with stem cells. These elements, along with homologous stem cell communication, are largely responsible for the maintenance of stem cell self-renewal.

Stem cells and other progenitor cells have been found in tendon and ligaments throughout the body(31;39;69). However, the anatomic location of the niche in these tissues is largely unknown. It has been proposed that stem and progenitor cells within these tissues reside in a perivascular niche, located close to blood vessels which can replenish depleted MSC populations by recruiting cells from the bone marrow, as shown in *Figure 1.2*. The perivascular niche has been implicated in the maintenance of stem cell populations in other tissues, such as neural tissue(70-72), dental pulp(73), and the bone marrow stroma(35;36). This suggests that signaling, as well as cellular interactions from the blood, have an important effect on stem cell maintenance and function.

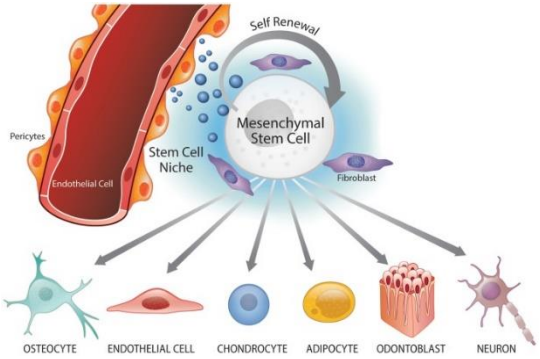

Figure 1.2: Schematic of the perivascular niche and regulation of mesenchymal stem cell lineage specification; from Oh *et al.*(277)

On the other hand, more recent studies suggest that populations of MSC reside within the tissue proper, and cells rely more heavily on direct contact with the surrounding ECM and inhabitant cell types for maintenance and regulation of function. In tendons, a stem cell niche was identified through tracking the location of tendon stem cells within mouse patellar tendons. It was observed that these cells reside between parallel collagen fibril chains, suggesting the potential importance of the ECM in maintaining the tendon stem cell niche(39). In recent years, populations of adult stem cells capable of multilineage differentiation have been identified in tendons(39) and ligaments(40). Still, the various cues responsible for the maintenance of a population of multipotent stem cells within tendons and ligaments have yet to be uncovered. To better understand these cues, there is growing interest in developing an *in vitro* environment mimetic of the connective tissue milieu.

1.2.2 Engineering the Stem Cell Microenvironment In Vitro

The local delivery of MSC to sites of injury is an attractive option to facilitate tissue healing. Early MSC delivery methods have utilized bolus injection of cells either systemically via intravenous or intra-arterial delivery, or locally via direct injection to the injury site(74;75). Systemic delivery is the easiest of the two options and relies on MSC homing or migration to the site of injury and inflammation(74). While MSC migration to the injury location is possible, the number of MSC that reach the injured tendon/ligament tissue is limited(76). Additionally, intravenous injection typically results in a buildup of MSC in the lungs, limiting the number of stem cells available for homing(77). Additional complications such as arterial thrombosis have been reported in limbs where MSC were delivered via the circulatory system(77). Alternatively, a local intralesional injection offers direct delivery of MSC to the injury site; however, stem cell survival at the injury site can be compromised due to lack of oxygen and nutrients to support viability. It has been observed that, while equine embryonic stem cells persisted at the injury site for as long as three months following injection into an equine flexor tendon lesion, MSC showed less than 5% survival within the first 10 days following injection(78). Further, in both instances, the inflammatory microenvironment has been shown to have a negative effect on MSC survival, as pro-inflammatory cytokines have been shown to diminish MSC proliferation and self-renewal, and promote cell death. Despite promising effects of MSC delivery on tendon healing, transplantation of MSC alone has resulted in ectopic bone formation within the tendon following delivery(79;80).

These findings suggest that, while MSC may be a valuable cell source for promoting tissue regeneration following injury, without proper stimuli from the surrounding microenvironment, the ability of MSC to home to the injury site and participate in tissue regeneration is compromised. Therefore, engineering of an artificial microenvironment capable of directing MSC response following delivery to an injury is an appealing strategy for addressing these limitations. To this end, investigating the impact of each of the various components of the connective tissue microenvironment on MSC activity and tendon/ligament lineage commitment *in vitro* is vital. It has been shown that through optimization of a number of these components, as shown in *Figure 1.3*, it may be possible to mimic the signals provided by the connective tissue microenvironment to control MSC response and promote stem cell-guided tissue regeneration. The current progress in engineering each of these individual aspects of the connective tissue microenvironment

in vitro are described in more detail in the following sections, with the goal of determining which environmental cues are vital for controlling stem cell response to promote stem cell-guided connective tissue regeneration.

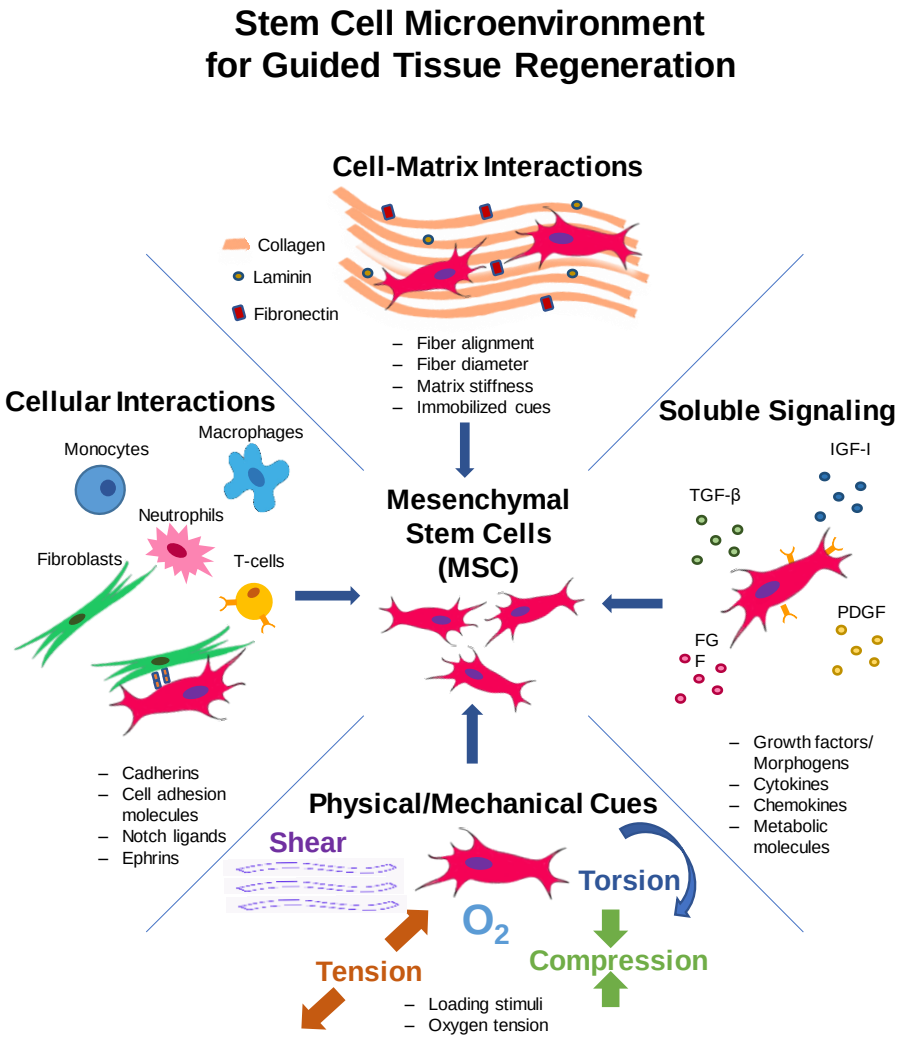

Figure 1.3: Schematic of the various cues present within the connective tissue cell microenvironment. These stimuli, ranging from cellular cues to matrix-based cues to exogenous mechanical stimulation, have been observed to modulate stem cell response.

1.2.2.1 Cellular Interactions

The healthy vs. injured cellular microenvironment in connective tissue is shown in *Figure 1.4.* The cellular microenvironment within healthy ligaments and tendons largely consists of elongated fibroblasts, which lie parallel to the tissues' collagen fibrils, with multiple cell processes extended to aid in the synthesis of organized matrix, and allow for paracrine interactions and cell-cell communications via gap junctions

between cells(81;82). Following injury, the cellular microenvironment changes abruptly, as the tissue is invaded by neighboring fibroblasts, as well as inflammatory cells, recruited to the injury site via chemotactic signaling agents(83). Specifically, neutrophils, pro-inflammatory and anti-inflammatory macrophages, as well as other immune cells including T cells and mast cells, are found at the wound site(1).

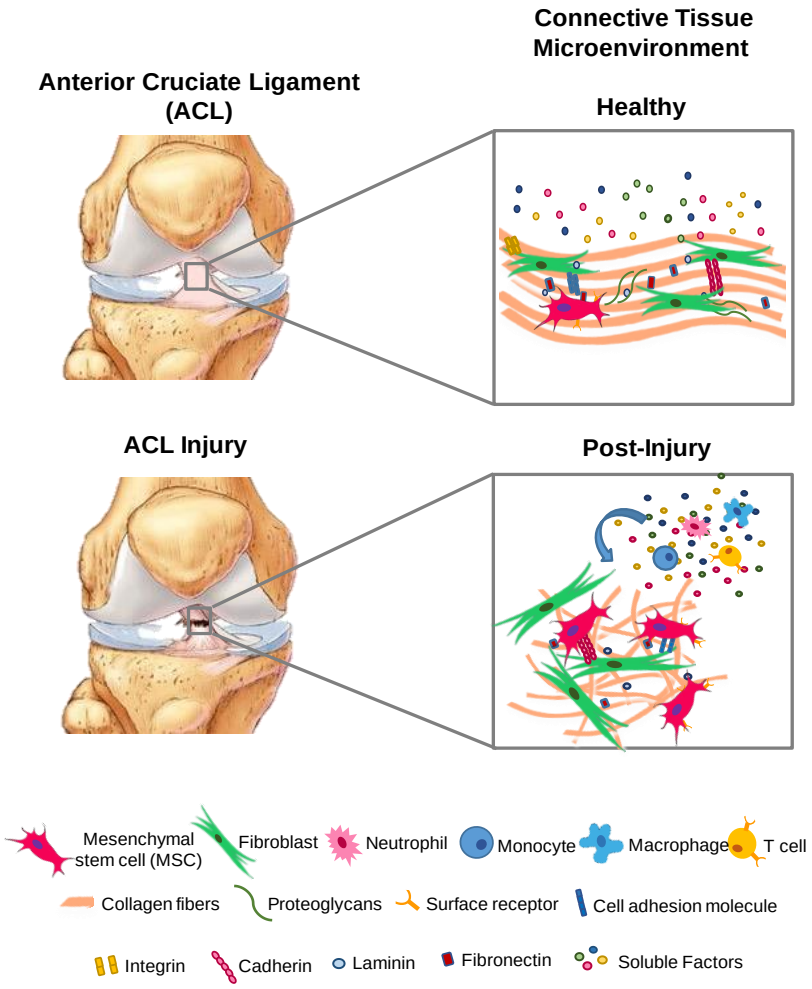

Figure 1.4: Schematic of the connective tissue cell microenvironment before and after injury.

In vitro co- and tri-culture models with MSC have been developed in order to 1) promote lineage-specific differentiation of MSC and 2) elucidate the trophic signaling and immunomodulatory effects of MSC on other cell types. As healthy fibrous connective tissues are largely comprised of tissue-specific fibroblasts, the majority of co- and tri-culture models for ligament and tendon tissue engineering involve fibroblasts (*Table 1.1*). Segregated co-culture models provide a means for isolating the response of individual cell types, to assess the impact of ligament/tendon cell paracrine signaling on MSC differentiation(84-88). Lee *et al*. assessed the response of MSC to co-culture with ACL fibroblasts using a transwell co-culture model, and found that expression of ligament-related markers, including types I and III collagen and tenascin-C, was upregulated by co-cultured MSC by day 7(84). Similarly, Luo *et al*. found that both proliferation and expression of tenogenic markers were enhanced for MSC in transwell co-culture with Achilles tendon cells after 14 and 21 days(87). In work by Lovati *et al*.,

equine MSC were co-cultured with fragments of digital flexor tendons using a segregated transwell model. Results show that MSC in co-culture expressed greater levels of decorin, tenomodulin, and tenascin-C, and aggregated to form 3D tissue-like structures, which stained positively for type I collagen by day 15(88). These results suggest that paracrine signaling between MSC and cells within tendon tissue may be capable of inducing tenogenic differentiation of MSC.

To assess the effects of direct contact between MSC and ligament fibroblasts, mixed co-culture models have also been utilized. Canseco *et al*. developed a mixed co-culture model, in which autologous porcine ACL cells and MSC were cultured in varying co-culture ratios (3:1, 1:1, 1:3 MSC:ACL fibroblasts). A co-culture ratio of 1:1 resulted in increased expression of type I collagen and tenascin-C at day 28, as well as increased tenascin-C staining compared to MSC controls, though histological staining was not different from fibroblast single-culture controls(89). To assess the effects of co-culture on each cell type individually, Kramer *et al*. performed mixed co-culture of male human MSC and female periodontal ligament cells at varying ratios (1:1, 2:1, 10:1 MSC:PDL cells), and were able to isolate individual cell types using Y chromosome labeling. Results show that co-culture increased MSC expression of periodontal ligament-related markers at day 7(90).

Co- and tri-culture models can also be used to analyze the effects of MSC on tendon/ligament cell response. To better understand the trophic effects of MSC on fibroblasts, Proffen *et al*. used a mixed co-culture model of porcine ACL fibroblasts with either adipose-derived stem cells (ADSC) or MSC isolated from peripheral blood (PBMC)(62). Co-culture of ADSC with fibroblasts results in increased expression of both types I and III collagen by day 14, while no such effect of co-culture was found with PBMC co-culture. Additionally, proliferation and procollagen synthesis were increased for fibroblasts in co-culture with ADSC at days 7 and 14(62). Work by Manning *et al*. examined the combined trophic and immunomodulatory roles of MSC using a tri-culture model with mixed and segregated culture of mouse MSC, macrophages, and tendon fibroblasts(91). Results from this study show that, contact between fibroblasts and MSC during transwell culture with macrophages suppressed fibroblast expression of pro-inflammatory and matrix degradation markers, suggesting an immunomodulatory role of MSC during inflammation and wound healing.

While the above studies are important for understanding cellular communications between MSC and native connective tissue cell types, other researchers have also studied these interactions on physiologically relevant matrices to understand the role that cell-matrix interactions play in modulating communications between cell types. Wang *et al*. assessed the effects of a 3D microenvironment on MSC fibrochondrogenic differentiation through the use of a tri-culture model in which bovine MSC were seeded in a 3D agarose hydrogel and cultured with osteoblasts and fibroblasts to promote ligament-to-bone interface regeneration(92). It was noted that MSC in hydrogels in both single-culture and tri-culture exhibited greater expression of types I and II collagen compared to monolayer controls, suggesting that 3D culture facilitates MSC differentiation *in vitro*(92). In work by Fan *et al*., human MSC were seeded on fibrous hybrid gelatin/silk fibroin scaffolds and cultured in segregated co-culture with ACL fibroblasts(3). In this study, MSC proliferation and collagen production were increased at both 7 and 14 days compared to single-culture of MSC on gelatin/silk fibroin scaffolds. In addition, expression of types I and III collagen were increased at days 7 and 14, with increased expression of tenascin-C at day 14 in co-culture(3). He *et al*. similarly used knitted silk scaffolds for tri-culture of MSC with fibroblasts and osteoblasts for ligament-to-bone regenerative applications(93). In this study, rabbit MSC, osteoblasts, and fibroblasts were seeded on individual scaffolds and cultured separately for 7 days, at which point the three scaffolds were sutured together to achieve a scaffold comprised of an osteoblast-only region, overlapping osteoblast-MSC region, MSC-only region, overlapping MSC-fibroblast region, and fibroblast-only region. Results from this study show that MSC in direct contact with fibroblasts while also exposed to paracrine signaling from osteoblasts undergo differentiation toward a fibrocartilage lineage, based on increased expression of Sox9 and aggrecan after 21 days in tri-culture(93).

Collectively, these studies highlight the importance of studying cellular interactions on a physiologically relevant 3D matrix *in vitro*, and show that the underlying matrix plays an important role in modulating MSC response for connective tissue regeneration.

Table 1.1: Summary of Studies Assessing the Role of Cell-Cell Interactions on Stem Cell-Guided Tissue Regeneration

MSC co-culture models

Study	Cell Types	Co-culture Model	Findings
Kramer *et al.*(90)	Human BMSC and periodontal ligament (PDL) cells	Mixed – 1:1, 2:1, 10:1 MSC:PDL cells	Increased expression of periodontal ligament-related markers by MSC at day 7
Lee *et al*.(94)	Human BMSC + murine skeletal myocytes	Mixed – 1:5 myocyte:BMSC	MSC incorporate into myotubes and express myogenic markers in co-culture; Increased nestin expression in myotubes following MSC incorporation
Lee & Kemp(95)	Human ADSC + murine skeletal myocytes	Mixed – 1:5 myocyte:ADSC	ADSC incorporate into myotubes and express myogenic markers in co-culture
Lee *et al.*(84)	Human BMSC and ACL fibroblasts	Segregated – transwell	Increased expression of ligament-related markers by MSC by day 7
Mizuno *et al.*(85)	Human BMSC and PDL cells	Segregated – transwell, conditioned medium	Increased proliferation and decreased mineralization potential by MSC in conditioned medium, upregulation in expression of 35 genes
Zhang *et al.*(86)	Rat BMSC and ligament fibroblasts	Segregated – permeable membrane	Increased expression of collagen I, collagen III and tenascin-C by BMSC in co-culture
Luo *et al.*(87)	Rat BMSC and tenocytes	Segregated – transwell	Increased proliferation and expression of tenogenic markers for MSC in co-culture compared to single-culture controls after 14 and 21 days
Beier *et al.*(96)	Rat BMSC and myoblasts	Mixed	Upregulation in myogenic markers MEF2 (myogenic enhancer factor 2) and α-sarcomeric actin by MSC
Canseco *et al.*(89)	Porcine BMSC and ACL fibroblasts	Mixed – 3:1, 1:1, 1:3	Increased expression of collagen I and tenascin-C and enhanced tenascin-C staining at day 28
Lovati *et al.*(88)	Equine BMSC and tendon fragments	Segregated – transwell	Positive collagen I staining, increased expression of decorin, tenomodulin, and tenascin-C after 15 days in co-culture
Proffen *et al.*(62)	Porcine ADSC/peripheral blood-derived MSC and ACL fibroblasts	Mixed	Increased expression of collagen I and collagen III by day 14 by ADSC in co-culture; proliferation and procollagen synthesis were increased for fibroblasts in co-culture with ADSC at days 7 and 14

MSC tri-culture models

Study	Cell Types	Tri-culture Model	Findings
Manning *et al.*(91)	Mouse BMSC, macrophages, and tendon fibroblasts	Mixed vs. transwell	Macrophages switch from M1 to M2 phenotype in tri-culture, resulting in release of less pro-inflammatory factors
Wang *et al.*(92)	Bovine BMSC, fibroblasts, and osteoblasts	Segregated on coverslips	BMSC exhibited greater fibrochondrogenic potential than ligament fibroblasts in tri-culture; growth of BMSC decreased while proteoglycan production and TGF-β3 expression increased by day 14

3D co-culture and tri-culture models

Study	Cell Types	3D Matrix Model	Findings
Fan *et al.*(3)	Human BMSC and ACL fibroblasts	Segregated with MSC on gelatin/silk hybrid scaffolds	Increased expression of ligament-related markers by MSC in co-culture
Schneider *et al.*(97)	Canine ADSC and tenocytes	Mixed in high density pellet culture; conditioned media	Active exchange of vesicles between cell types in monolayer; upregulation of collagen I/III, decorin, tenomodulin, MAP kinase pathway (Shc, Erk1/2), and scleraxis
He *et al.*(93)	Rabbit BMSC, ligament fibroblasts, osteoblasts	Mixed + segregated on hybrid fibrous silk scaffolds	Increased expression of fibrocartilage markers Sox9 and aggrecan after 21 days by MSC in direct contact with fibroblasts while exposed to paracrine signaling from osteoblasts
Wang *et al.*(92)	Bovine BMSC, ligament fibroblasts, and osteoblasts	Segregated with MSC in agarose hydrogel	Greater collagen I and collagen II expression, increased collagen synthesis by MSC in tri-culture

1.2.2.2 Cell-Matrix Interactions

The matrix microenvironment within fibrous connective tissues is comprised of mostly aligned type I collagen, as well as elastin, in a proteoglycan-rich matrix that functions to lubricate the tissue, as well as organize collagen fibril assembly(8;98). Type I collagen fibrils are crosslinked to one another in a staggered fashion to form fibers, the primary unit of tendons and ligaments. These fibers are aligned along the direction of load bearing, separated by type III collagen-positive fibrils(98).

Following injury, cells within the tissue are induced to synthesize a dense mat of largely collagenous fibrotic scar tissue(83). During scar formation, fibroblasts are triggered to form not only type I collagen, but also an increased amount of type III collagen(83;99-102). These collagen fibers are initially disorganized and randomly oriented, as opposed to the aligned fibrillar bundles observed in healthy tissue, with an increased presence of defects(8;103). Furthermore, due to its disorganized structure, this newly formed tissue is classically weaker than healthy connective tissues, unable to withstand physiological levels of loading(99;104).

Extensive research through the years has focused on designing biomaterials and forming 3-D extracellular matrix analogues which serve to mimic the collagenous fibers within connective tissues in order to direct MSC toward tendon/ligament lineages. To this end, matrices derived from either natural materials, such as silk and collagen, or synthetic materials, including the poly-α-hydroxyester family, have been developed and studied extensively for their effects on native tissue fibroblasts and MSC(105-107). Since fibrous connective tissues are largely made up of type I collagen, collagen-based gels have been used extensively as an engineered tendon/ligament matrix(105). However, due to the low mechanical properties of type I collagen hydrogels, fibrous matrices which can be woven to produce scaffolds with enhanced material properties have since been developed. Naturally-derived silk fibers have been explored for tendon/ligament tissue engineering, as the fibers can be woven into braids or ropes with mechanical properties similar to native tissue(108). Stem cells seeded on these substrates have been shown to proliferate and secrete collagen matrix(109). Similarly, synthetic materials such as PLLA, PLGA, PCL, and others have been used to produce fibrous meshes. These matrices are ideal for mimicking the structure of connective tissues, as they can be tuned in terms of fiber alignment(110) and diameter(111), as well as matrix mechanical properties(112). Current strategies to evaluate these matrices for promotion of tenogenic differentiation of MSC include optimization of matrix topography, matrix mechanical properties, and ECM components.

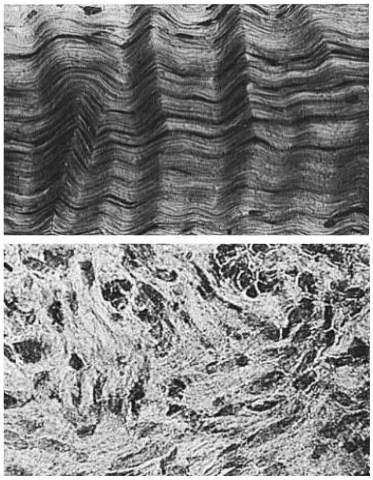

Figure 1.5: Scanning electron micrographs of healthy ligament tissue (top) and scar tissue (bottom); from Frank *et al.*(99)

A number of studies have evaluated the effects of matrix topography on tenogenic differentiation of MSC through fabrication of unaligned and aligned fibrous matrices which mimic the architecture of the native tissue (*Table 1.2*). Yin *et al*. reported that tendon-derived mesenchymal stem cells upregulated their expression of tendon-related markers, with decreased expression of osteogenic markers, on aligned PLLA fibers compared to unaligned fibers(113). These results suggest that aligned fibers are best suited for mimicking the structure of healthy connective tissues such as tendons and ligaments.

The mechanical properties of the underlying substrate can also be optimized to modulate MSC response (*Table 1.2*). It is well-established that tissue-adherent cells are capable of sensing and responding

to the stiffness of the tissue microenvironment(21). Foundational work by Engler *et al*. has shown that the stiffness of the underlying matrix can control MSC lineage commitment without the addition of chemical factors(22). Specific to fibrous connective tissues, MSC on polyacrylamide gels with mechanical properties similar to those of muscle are shown to undergo differentiation toward a muscle lineage, while cells on softer substrates differentiate toward nerve cells, and stiffer substrates result in osteogenic lineage commitment(114). Alternatively, it has also been shown that human MSC can be kept quiescent by growing them on polyacrylamide substrates that mimic the properties of marrow(115). Similarly, work by Sharma and Snedeker shows that for human MSC on acrylamide-bisacrylamide electrophoresis gels of varying stiffnesses, tenogenic marker expression is upregulated on matrices with mechanical properties similar to the native tendon, but not on stiffer substrates(116). Rehmann *et al*., however, observed a combination of tenogenic and osteogenic marker upregulation for MSC on polyethylene glycol (PEG)-tetranorbornene with higher stiffnesses(117). It has been speculated that intracellular changes resulting from alterations in matrix stiffness are a result of changes in integrin expression. Activation of these integrins results in activation of mitogen-activated protein (MAP) kinases, which have a downstream effect on the activation of Rho GTPases such as RhoA and ROCK, a key pathway in MSC differentiation(118).

In addition to the structure of the underlying ECM, ECM-bound factors and cell-ECM interactions in response to surface molecules are critical drivers of stem cell activity and homeostasis(119;120). Interactions between stem cells and the surrounding ECM are mediated through a number of cell receptors, including integrins. The extent of interaction between MSC and the matrix has an effect on MSC spreading and shape, which have been shown to be important for MSC response and lineage commitment. Surface functionalization with matrix ligands such as type I collagen and fibronectin have been used to modulate cell spreading and integrin expression, both of which have been shown to impact MSC response and lineage commitment (*Table 1.2*). Sharma and Snedeker assessed the effects of surface functionalization on MSC response by coating the surface of acrylamide-bisacrylamide gels with varying densities of collagen and fibronectin(116). Results show that MSC attachment is greater on collagen-coated surfaces than on fibronectin within 1 hour, with increased cell spreading on collagen at 24 hours. Additionally, tenogenic differentiation was achieved on collagen substrates but not fibronectin, as MSC on collagen coatings also exhibited an increase in the expression of scleraxis, tenomodulin, tenascin-C and type III collagen, while

fibronectin coatings resulted in enhanced Runx2 and ALP expression, suggesting differentiation toward an osteogenic lineage(116). This work suggests the importance on integrin-driven cell signaling in modulating cell response.

Table 1.2: Summary of Studies Assessing the Effects of Changes in Matrix Properties on Stem Cell-Guided Tissue Regeneration

Fiber Alignment

Study	Cell type	Scaffold	Results
Yin *et al.*(113)	Human TSPC	PLLA nanofibers – aligned and unaligned	Increased expression of tendon markers on aligned fibers, increased expression of osteogenic markers on unaligned fibers
Tang *et al.*(121)	Human GFP-expressing BMSC	Achilles tendon blocks of different angles (0°, 12°, 20°, 30°, 45°, 75° and 90°), collagen I gel	0° and 12° sections result in increased tenomodulin expression at day 3
Zhang *et al.*(122)	Human iPSC-derived MSC	Aligned and unaligned chitosan-based ultrafine fibers	Increased ALP expression and collagen staining on random fibers; increased tendon marker expression on aligned fibers
Popielarczyk *et al.*(123)	Equine BMSC	Polystyrene fibers – parallel vs. perpendicular	No major differences in gene expression or matrix synthesis between groups

Fiber Diameter

Study	Cell type	Scaffold	Results
Cardwell *et al.*(124)	Murine BMSC	Aligned and unaligned PEUUR mats with small (<1 μm), medium (1-2 μm) and large (>2 μm) diameters	Increased scleraxis expression on large fibers compared to medium fibers; increased collagen I expression on large fibers compared to small and medium fibers at day 14

Matrix Mechanical Properties

Study	Cell type	Scaffold	Results
Engler *et al.*(22)	Human BMSC	Polyacrylamide gels	Muscle cells can be generated using medium stiffness (20kPa) gels

1.2.2.3 Soluble Signaling

In addition to matrix-driven cell signaling, soluble signaling cues are also involved in driving cell response following connective tissue injury. Specific to tendons and ligaments, research has shown that, following injury, there is an increase in local concentrations of a number of growth factors, including bFGF, TGF-β, IGF-1, and platelet-derived growth factor (PDGF), all of which are active at multiple stages of the injury and healing process(125). To this end, there is interest in utilizing growth factor supplementation *in vitro* as a means of controlling MSC function and promoting differentiation (*Table 1.3*).

Both *in vitro* and *in vivo* studies have shown the potential of bFGF to act as a mitogen, as well as an angiogenic stimulator, and it has been proven to maintain MSC differentiation potential, stimulate proliferation, and induce fibroblastic differentiation. Specifically, at low doses, Hankemeier *et al*. showed that bFGF is capable of increasing MSC proliferation as observed at day 7, as well as promote a tenogenic phenotype through increased expression of types I and III collagen, as well as fibronectin and smooth muscle actin (SMA) at days 14 and 21(126). Sahoo *et al*. later incorporated bFGF into hybrid silk/PLGA fiber meshes and observed increased proliferation and matrix synthesis by MSC cultured on these substrates, resulting in enhanced scaffold mechanical properties within 3 weeks(127).

Another mitogenic factor, TGF-β, is produced by tendon and ligament fibroblasts, and has been shown to be active in all stages of fibrous connective tissue healing(128). In work by Holladay *et al*., stimulation with TGF-β1 results in synthesis of fibrocartilaginous matrix by equine tendon-derived stem cells, which is undesirable for fibrous connective tissue repair and regeneration(129). Jenner *et al*. also assessed the effects of TGF-β1 on human MSC on PLGA fibers and saw enhanced proliferation in all TGF-β1-containing groups at day 12, as well as increased collagen synthesis and synthesis per cell of both types I and III collagen(130).

Bone morphogenetic proteins (BMPs) have also been used to induce tenogenic differentiation. BMP-7, -12, -13 and -14 have been implicated in the neoformation and repair of tendons, and BMP-12 specifically has been shown to promote tendon differentiation and formation *in vitro* and *in vivo*(131-133). Multiple studies have shown that BMP-12 alone is enough to promote tenogenic differentiation of MSC culture *in vitro*, as observed through increased expression of tendon markers including tenomodulin, decorin, and scleraxis(133;134). Interestingly, for rat MSC on collagen sponges, increases in the expression of scleraxis and tenomodulin were observed over 14 days, after only 12 hours' exposure to BMP-12 on day 1. This 12-hour stimulation resulted in increased cell number, matrix synthesis, and expression of tendon markers after 21 days *in vivo*(135). Alternatively, Bottagisio *et al*. reported that BMP-12 or BMP-14 alone were insufficient for inducing tendon lineage commitment, and required the addition of TGF-β1 and VEGF to the culture medium to achieve tenogenesis(136). Clearly additional studies are needed to elucidate the effect of BMPs on MSC-mediated connective tissue response.

Growth differentiation factors (GDFs) are also members of the TGF-β superfamily and are closely related to BMPs. Factors such as GDF-5, -6, and -7 are believed to act as signaling molecules during tendon, ligament, and muscle development, and have been shown to induce neotendon/ligament formation *in vivo*(137). Adipose-derived MSC exposed to GDF-5 *in vitro* have been shown to undergo enhanced proliferation, with a dose-dependent increase in scleraxis and tenomodulin expression. High doses of GDF-5 also result in increased tenascin-C expression, suggesting tenogenic lineage commitment in these groups(138). Similar effects were observed for equine tendon-derived stem cells, in which there was an upregulation in the expression of tendon-related markers by day 28 in culture, and a concomitant downregulation in adipogenic and chondrogenic markers(129). However, when MSC were cultured on PLGA fibers, GDF-5 did not have any observable effects on MSC response compared to untreated controls(130).

IGF-1 has also been shown to be highly expressed during early inflammation(139), as it plays a significant role in the inflammatory and proliferative phases of wound healing(125;140). Additionally, IGF-1 has been applied to damaged tendons and was observed to mitigate inflammation and accelerate the functional recovery of the tissue(141). Used to stimulate MSC response, IGF-1 was observed to preserve the multipotency of equine tendon-derived stem cells over 28 days *in vitro*(129).

PDGF is a chemotactic agent, as well as a mitogen, and has been shown to promote protein synthesis by mesenchymal stem cells(142). PDGF has been observed to be elevated in the healing canine digital flexor tendon(143), and is thought to play a role in connective tissue healing by inducing the synthesis of other growth factors including IGF-1(142). In work which assesses the response of adipose-derived MSC on aligned collagen fibers doped with PDGF-containing nanoparticles, PDGF stimulation resulted in enhanced cell proliferation up to 7 days, and increased expression of tendon lineage markers, including tenomodulin and scleraxis at days 3, 7, and 14(144). These observations suggest that not only can PDGF be used to promote tendon lineage commitment by MSC, it can also be incorporated directly into scaffold materials to provide multiple cues to cells simultaneously.

Table 1.3: Summary of Studies Assessing the Effects of Soluble Cues on Stem Cell-Guided Connective Tissue Regeneration

2D Culture

Study	Cell type	Growth factor	Results
Hankemeier *et al.*(126)	Human BMSC	bFGF	Low doses of bFGF stimulate MSC proliferation and upregulate expression of collagen I, collagen III, fibronectin, α-SMA
Violini *et al.*(133)	Equine BMSC	BMP-12 (50 ng/ml)	Increased tenomodulin and decorin expression by MSC in BMP-12 on day 20
Park *et al.*(138)	Rat ADSC	GDF-5	Increased cell number at 100 ng/mL at days 3-12; increased expression of scleraxis and tenomodulin in 100 ng/ml, increased tenascin-C expression in 1000 ng/mL
Zhang *et al.*(145)	TDSC	Dexamethasone	All concentrations of dexamethasone result in suppressed collagen I expression and increased PPARγ and Sox9 expression at day 7
Mohanty *et al.*(134)	Equine UCB-MSC	BMP-12	Increased expression of scleraxis, tenomodulin, decorin, Mohawk, collagen-1α1
Reed & Johnson(146)	Equine UCB-MSC vs ADSC	FGF-2	FGF-2 results in increased proliferation by ADSC only
Holladay *et al.*(129)	Equine TDSC	IGF-1, GDF-5, TGF-β1	IGF-1 preserves multipotency; GDF-5 supplementation results in increased tenogenic gene expression and decreased adipogenic and chondrogenic expression by day 28; TGF- β1 results in fibrocartilage/scar matrix formation

3D Culture

Study	Cell type	Growth Factor	Scaffold	Results
Moreau *et al.*(147)	Human BMSC	FGF vs. EGF + TGF-β1	RGD-modified silk fibers	Increased matrix synthesis for bFGF+TGF-β1 compared to EGF
Jenner *et al.*(130)	Human BMSC	GDF-5	Braided PLGA fibers (Panacryl 2.0 suture material)	Increased collagen production and collagen synthesis per cell by day 12. No effect due to GDF5
Sahoo *et al.*(127)	Rabbit BMSC	bFGF	bFGF-releasing silk/PLGA fibers	Increased proliferation, total collagen production, and enhanced mechanical properties after 3 weeks
Lee *et al.*(135)	Rat BMSC	BMP-12	Collagen sponges	12 hr treatment w/ BMP results in increased scleraxis and tenomodulin expression at day 14 *in vitro*; increased cell number, matrix synthesis, and expression of tendon markers at day 21 *in vivo*
James *et al.*(148)	Rat ADSC	GDF-5	poly(DL-lactide-co-glycolide) (PLAGA) fiber scaffolds and films	Dose-dependent increase in cell proliferation, expression of tenogenic markers, and extracellular matrix markers beginning at day 7 on fibers
Bottagisio *et al.*(136)	Rabbit BMSC	BMP-12, BMP-14, TGF-β, VEGF	Fibrin-based constructs	Combination of factors results in tenogenic differentiation in monolayer and in 3D

1.2.2.4 Physical/Mechanical Stimuli

In addition to matrix-guided cues, mechanical stimulation is an important factor in modulating stem cell behavior within the tissue environment, especially in orthopaedic tissues. The primary modes of stimulation experienced by fibrous connective tissues such as tendons, ligaments, and muscles are tensile and torsional loading(105;149;150), the magnitudes of which are shown to vary among tissue types and anatomic locations(151). Specifically, tendons typically undergo greater levels of loading compared to ligaments, likely due to the forces generated by contracting muscles, and consequently tendons have been shown to have greater mechanical strength(151). A number of models have been developed to elucidate the effects of both tensile and torsional loading on the response of MSC in terms of cell proliferation, alignment, matrix synthesis and organization, as well as expression of tendon- and ligament-related genes, and optimized loading regimens have shown promise for modulating stem cell metabolic activity and promoting MSC differentiation toward tendon and ligament fibroblasts (*Table 1.4*).

The simplest approach to mechanical stimulation of cells is the application of static loads. While these methods have proven effective for guiding cell orientation and organized matrix synthesis, little effect on MSC differentiation or proliferation has been observed. Awad *et al*. seeded MSC in collagen gels at varying densities, and observed that contraction occurs to a greater extent in collagen gels with high cell densities compared to lower density gels(152). Additionally, for gels with higher cell densities, and consequently greater contraction, cells appeared more aligned with elongated nuclei compared to cells in less contracted gels(152). In another instance, van Eijk *et al*. tested the effect of varying the timing of static load application, and found that by loading MSC during seeding onto PLGA fibers, cell number was increased by day 5 compared to unloaded groups(153). Still, there were no observable differences in cell proliferation or differentiation after 23 days in culture for any loading regimen(153).

Due to the limited effects of static loading on MSC response, more physiologically relevant dynamic tensile stimulation regimens have been developed to guide cell response. In 2D, cyclic strain has been shown to not only encourage MSC alignment, but can also increase the expression of tendon- and ligament-related markers(84;154;155). In work by Xu *et al*., MSC grown on silicone substrates coated in fibronectin were exposed to 10% strain at a frequency of 1 Hz for 48 hours(118). Following mechanical stimulation, cells showed increased expression of tendon-related markers including collagen type I and III, tenascin-C,

and scleraxis. To better understand the mechanism behind these changes, the phosphorylation of focal adhesion kinase (FAK) was assessed, and was shown to increase about two-fold following within 30 minutes of the application of tensile loading. To determine whether this pathway was responsible for the observed changes in MSC differentiation, the FAK pathway was blocked using Y-27632 (a RhoA/ROCK inhibitor), cytochalasin-D (an inhibitor of actin polymerization), and PF 228 (a p21-activated kinase inhibitor). Results show that in all three groups, FAK activation was significantly decreased compared to loaded control, with attenuated expression of all four tenogenic markers, suggesting this pathway plays a role in MSC mechanotransduction and differentiation(118).

Still, overstimulation of MSC with mechanical stimuli can result in undesired cell response. By loading human MSC with varying degrees of strain, Morita *et al*. showed that MSC stimulated with 10% strain at a frequency of 1 Hz for 24 hours upregulated their expression of tendon-related markers compared to MSC that underwent 5% or 15% strain(155). Zhang and Wang similarly showed that for rabbit tendon-derived MSC, cyclic stretching at 4% strain at a frequency of 0.5 Hz for 12 hours resulted in increased type I collagen expression, while increasing the strain to 8% resulted in upregulation of type I collagen, as well as cartilage, bone, and fat-related markers such as type II collagen, Sox9, Runx2, and peroxisome proliferator-activated receptor (PPAR)-γ(156).

Extensive work by Butler *et al*. shows that mechanical stimulation of MSC can be used for both tendon and ligament tissue engineering applications. Initial work evaluated the effects of mechanical stimulation on MSC on type I collagen sponges. Scaffolds were loaded under cyclic tension to a maximum strain of 4% once every 5 minutes for 8 hours per day for 2 weeks(157;158). Results show that stimulated scaffolds exhibited increased mechanical properties compared to unstimulated scaffolds. Additionally, mechanically loaded sponges which were implanted into rabbit patellar tendon defects showed enhanced mechanical properties after harvest(157), as well as increased expression of types I and III collagen by MSC on loaded scaffolds, compared to unstimulated controls(158).

Increasing the complexity of applied loading regimens, Altman *et al*. seeded collagen gels with bovine MSC and subjected scaffolds to 10% tensile strain and 25% torsional strain at a rate of 1 cycle per minute. By day 14, cells showed increased expression of types I and III collagen and fibronectin, with no observable increases in bone or cartilage markers. Following these initial studies, human MSC were seeded

on silk fiber matrices and exposed to 45º rotation at a rate of $1.39x10^4$ Hz, which was applied 1, 3, 6, or 9 days after cell seeding, to assess the impact of temporal application of torsional strain on stem cell response. Results show that MSC metabolic activity was greatest on samples loaded 9 days after seeding(159).

Table 1.4: Summary of Studies Assessing the Effects of Physical/Mechanical Cues on Stem Cell-Guided Connective Tissue Regeneration

Static Loading

Study	Cells	Scaffold	Regimen	Findings
Awad *et al.*(152)	Rabbit BMSC	Collagen gels	Static stretch (contraction of collagen gels)	Greater contractions result in more aligned cells and elongated cell nuclei
Van Eijk *et al.*(153)	Goat BMSC	Braided PLGA	Static tension by spring wire	Greatest number of cells after 5 days on loaded scaffolds, no effect by 23 days
Kawasaki *et al.*(160)	Human PDL cells	Tissue culture plastic	Oxygen tension – hypoxia vs. anoxia	Upregulation of stem cell markers at hypoxic and anoxic conditions after 6 hr; anoxic: increased scleraxis expression

Dynamic Tensile Loading

Study	Cells	Scaffold	Regimen	Findings
Noth *et al.*(161)	Human BMSC	Collagen I gel	Cyclic stretch: stretching frequency of 1 Hz and amplitude of 3 mm was performed for 14 days (continuously for 8 h/day)	Increased collagen I, collagen III, elastin, and fibronectin expression and enhanced matrix production by loaded MSC by day 14
Juncosa-Melvin *et al.*(157)	Rabbit BMSC	Collagen sponge	Dynamic stretch	Improved biomechanics following tendon repair in a rabbit model
Juncosa-Melvin *et al.*(158)	Rabbit BMSC	Collagen sponge	Dynamic stretch	Increased collagen I and collagen III expression
Butler *et al.*(162)	Rabbit BMSC	Collagen gel/collagen gel-sponge composite	Tensile strain – bioreactor prior to implantation	Improved mech properties after 12 weeks *in vivo*
Shearn *et al.*(163)	Rabbit BMSC	Collagen sponges	1 Hz to produce a 2.4% post-to-post strain once every 5 min for 8 h/ day for 12 d	No difference in mechanical properties following *in vitro* culture, but improved mechanical properties for loaded scaffolds after implantation
Lee *et al.*(84)	Human BMSC	Flexcell®	1 Hz with 10% elongation for 2 days	Cells align perpendicular to strain; increased expression of collagen I, collagen III, and tenascin-C
Chen *et al.*(164)	Human BMSC	collagen I-coated Flexcell®	stretching of 3% or 10% surface elongation at 1 Hz for 8 or 48 hr	Increased MMP3 expression at 48 hr for 3% strain. Increased MMP3 expression for 10% stain group, but to a lesser extent. Downregulation of MSCP (stem cell differentiation marker) in both stretch groups

Kuo *et al.*(165)	Human BMSC	3D collagen I gels atop Flexcell®	Static tension: MSC contracting collagen gel OR dynamic tension: 7 days cyclic uniaxial strain at 1Hz for 30 min/day at 1% elongation	Collagen fiber alignment observed in stretched groups, increased collagen content following loading
Zhang *et al.*(166)	Rat BMSC	Silicon membrane	cyclic strain (10% at 1 Hz) for 3 h, 6 h, 12 h, 24 h, and 36 h	Increased collagen I and collagen III synthesis in loaded groups
Zhang *et al.*(86)	Rat BMSC	Silicon membrane	cyclic strain (10%, 1 Hz) was applied for different durations: 3, 6, 12, 24, and 36 h	Increased collagen III, collagen I, and tenascin-C expression
Nirmalanandhan *et al.*(167)	Rabbit BMSC	Collagen sponge	Varied peak strain, cycle number, and cycle repetition at 1 Hz for 8 h/day for 12 days	Ideal loading regimen consists of 2.4% strain, 3000 cycles/day, one cycle repetition
Nirmalanandhan *et al.*(168)	Rabbit BMSC	Collagen sponge	2.4% strain, 3000 cycles/day, one cycle repetition	Increased stiffness of scaffolds via crosslinking results in decreased mechanical properties after implantation *in vivo*
Abousleiman *et al.*(169)	Rat BMSC	Human umbilical veins	2% strain for 1 h=day at a frequency of 0.0167 Hz	Increased proliferation and collagen I/collagen III expression in loaded groups
Chokalingam *et al.*(170)	Mouse BMSC	Collagen sponge	Tensile - 2.4% peak strain for 20 s at 1 Hz followed by a rest period at 0% strain for 100 s (5 hr/day)	Increased collagen I expression and increased linear stiffness for loaded groups
Song *et al.*(154)	Rat BMSC	Silicon membrane	Dynamic stretch – cyclic uniaxial	Detectable tenascin-C and scleraxis, with increased collagen I and III expression in stretched samples
Zhang & Wang(156)	Rabbit TDSC	Silicon dish with microgrooves (3μm depth, 10 μm width)	Cyclic stretching of 4% or 8% at 0.5 Hz was applied to silicone dishes for 12 h.	Loading results in enhanced proliferation; increased collagen I expression for loaded samples, with no change in expression of fat or cartilage-related markers at 4% strain; increased expression of fat, cartilage, bone, and ligament markers with 8%
Doroski *et al.*(171)	Human BMSC	PEG hydrogel	10% strain, 1 Hz, 2 h strain/3 hr rest	Upregulation in tendon/ligament marker gene expression for loaded samples
Thomopoulos *et al.*(172)	Rat BMSC	Collagen matrix	Dynamic cyclic loading 1.5mm amplitude and 1Hz for 7 days	Increased scleraxis, collagen I, and aggrecan expression under compressive and tensile loading
Issa *et al.*(173)	Rat BMSC	Human umbilical vein	2% strain, 0.0167 Hz, 1 hr/day	Lowest seeding density results in greatest tensile strength after 7 days
Kreja *et al.*(174)	Human BMSC	Fibrous PLA scaffolds	Cyclic tensile - 1Hz 2% or 5%	No effect on gene expression, decreased MMP1, TIMP-2 expression with stretch

			strain, 1 hr/day, 15 days	
Xu *et al.*(118;175)	Human BMSC	Silicon chamber	stretch treatment at an amplitude of 10% and a frequency of 1 Hz for 48 h	Cells align perpendicular to strain, RhoA/ROCK, cytoskeletal organization, and FAK compose a “signaling network” that drives mechanical stretch-induced tenogenic differentiation of hMSCs
Morita *et al.*(155)	Human BMSC	Silicon rubber chamber	1-Hz uniaxial cyclic stretching of 5%, 10%, or 15% elongation over 24 h or 48 h	Expression of collagen I, collagen III, tenomodulin, and scleraxis are greatest for 10% strain group
Zhang & Wang(176)	Mouse TDSC	Patellar + Achilles tendons	*In vivo* – treadmill running; *in vitro* – 4% or 8% strain	Increased expression of both tenocyte (Coll I, tenomodulin) and non-tenocyte (LPL, Sox9, Runx2) markers in the high stimulation group (at day 5?)
Xu *et al.*(177)	Rabbit TDSC	P(LLA-CL)/collagen scaffolds	4% elongation in length and 0.5 Hz, 2 h per day for a total of 14 days	Increased proliferation w/ loading; increased expression of tendon markers and decreased chondrogenic marker expression with stretch; loading promotes healing in rabbit patellar tendon injury model

Dynamic Torsional Loading

Study	**Cells**	**Scaffold**	**Regimen**	**Findings**
Altman *et al.*(159)	Bovine BMSC	Collagen gel	Dynamic tensile (10%) and torsional (25%) strains applied at 1 cycle/minute	Observable collagen I, collagen III, and fibronectin synthesis by day 14, no detection of bone or cartilage markers
Chen *et al.*(178)	Human BMSC	Silk fiber matrix	45º rotation at $1.39x10^4$ Hz	Cell response is dependent on temporal application of mechanical stimulation

1.2.3 Combined Effects: Combining Cues to Engineer the Stem Cell Microenvironment

While *in vitro* results suggest that MSC metabolic activity and differentiation can be controlled through optimization of individual microenvironment components, *in vivo* studies using these models have yielded mixed results. Therefore, several groups have begun testing the effects of combining multiple environmental cues on the ability to control stem cell behavior (*Table 1.5*). In works by Nirmalanandhan *et al*., rabbit MSC were seeded on both type I collagen sponges and gels, and exposed to uniaxial tension. Results show that mechanical stimulation of MSC on sponges resulted in enhanced mechanical properties, while loading MSC on gels did not improve the elastic modulus of gels, suggesting that the combination of mechanical and matrix-based cues affects MSC response(179). Subramony *et al*. also assessed the combined effects of matrix and mechanical cues on MSC through application of uniaxial tension to MSC on unaligned and aligned PLGA nanofibers. It was determined that, while mechanical stimulation resulted in

increased cell proliferation and collagen synthesis on both aligned and unaligned fibers, the expression of ligament-related markers including scleraxis and tenascin-C were increased on aligned fibers only(32). Czaplewski *et al*. studied the impact of matrix composition and mechanical properties on the response of MSC to mechanical loading by seeding cells on braided fibers comprised of PLLA, PCL, or blends of the two polymers, braided using a range or braid angles. While matrix composition was observed to affect MSC attachment and spreading, braiding angle was shown to impact tendon- and ligament-lineage commitment, as fiber with large braid angles resulted in increased expression of tendon and ligament markers and downregulation of bone markers by day 10 compared to day 3(112). These studies show that, while mechanical stimulation is known to impact MSC commitment toward tendon and ligament lineages, matrix-based cues such as matrix organization or mechanical properties can be used as a means of further enhancing these observed effects.

In addition to synergistic matrix and mechanical cues, other studies have combined either matrix microenvironment or mechanical stimulation with chemical stimuli to promote MSC differentiation. Petrigliano *et al*. incorporated bFGF into PCL nanofibers and exposed human MSC seeded on fibers to uniaxial tensile loading(180). These combined stimuli led to an upregulation in the expression of tendon-specific markers including types I and III collagen and tenascin-C by day 21. Similarly, in work by the Altman group, MSC seeded on fibrous silk scaffolds were exposed to either FGF or EGF, followed by cyclic torsional loading. Sequential exposure to chemical and mechanical stimulation while in contact with a physiologically relevant matrix resulted in increased matrix production and cellular ingrowth into scaffolds, as well as enhanced differentiation toward ligament fibroblasts(181). In work by Subramony *et al*., human MSC on unaligned and aligned PLGA fibers were exposed to uniaxial tensile loading in the presence of bFGF. This combinatorial approach showed that exposure to bFGF resulted in enhanced MSC proliferation, while mechanical stimulation resulted in increased collagen synthesis and the upregulation of ligament-specific genes including types I and III collagen, tenascin-C, and tenomodulin, suggesting a synergistic effect due to MSC exposure to a combination of these cues on a physiologically relevant aligned fibrous substrate(33). Raabe *et al*. also developed an *in vitro* model which combines mechanical and chemical stimulation to promote differentiation of equine ADSC in type I collagen gel scaffolds(182). It was observed that high oxygen tension combined with exposure to GDF-5 or -7, as well as cyclic tensile strain, could

promote tenogenic differentiation, as observed through increased expression of types I and III collagen, cartilage oligomeric protein, and scleraxis by day 21 *in vitro*.

Each of these studies highlights the potential synergistic effects of exposing MSC to a combination of cues mimetic of the surrounding connective tissue microenvironment, either sequentially or simultaneously. While these studies have been successful for promoting MSC differentiation toward connective tissue lineages *in vitro*, future work will need to focus on determining whether these cues will be sufficient to promote MSC's regenerative capabilities *in vivo*. To this end, development of an implantable artificial microenvironment to control stem cell response and promote stem cell-guided tissue regeneration is an attractive option to augment stem cell-based treatments for connective tissue repair.

Table 1.5: Summary of Studies Assessing the Effects of Combined Microenvironmental Cues on Stem Cell-Guided Connective Tissue Regeneration

Study	Cells	Scaffold	Combined Cues	Findings
Nirmalanandhan *et al.*(179)	Rabbit BMSC	Collagen I sponge and gel	Matrix properties + mechanical stimulation	Loading results in increased mechanical properties for collagen sponges, but not collagen gels
Nirmalanandhan *et al.*(183)	Rabbit BMSC	Collagen I sponge and gel	Matrix properties + mechanical stimulation	Longer sponge constructs result in highest *in vitro* linear stiffness
Petrigliano *et al.*(180)	Rat BMSC	bFGF-coated PCL	Growth factors (bFGF) + mechanical stimulation	Upregulation of collagen I, collagen III, and tenascin-C expression over 21 days
Moreau *et al.*(181)	Human BMSC	Silk fiber matrix	Growth factors (bFGF, EGF) + mechanical stimulation	Rotation at 0.5 cycles/hr is optimal when combined with bFGF
Rowlands *et al.*(184)	Human BMSC	Collagen I, collagen IV, laminin, fibronectin-coated gels	Matrix components + matrix mechanical properties	Myogenic differentiation is achieved on all gel-protein combinations with stiffnesses >9 kPa
Farng *et al.*(185)	Mouse BMSC	Porous PCL scaffolds	Growth factors (GDF-5) + mechanical stimulation	Combined mechanical and chemical stimulation enhanced messenger RNA (mRNA) production of collagen I, collagen II, and scleraxis
Sharma & Snedeker(116)	Human BMSC	4-12% acrylamide-bis-acrylamide gels (10-110 kPa)	Matrix components (varying concentration of collagen, fibronectin) + matrix mechanical properties	Increased osteogenic differentiation on fibronectin-coated substrates, with decreased osteogenic marker expression with decreasing stiffness. Tenogenic marker expression enhanced on softer and collagen coated substrates.
Beier *et al.*(96)	Rat BMSC	Tissue culture plastic	Myoblast co-culture + growth factors (bFGF+dex)	Upregulation of myogenic markers (MEF2, α-sarcomeric actin) in co-culture with medium supplementation

Kishore *et al.*(186)	Human BMSC	Collagen fibers	Fiber alignment + BMP-12	Increased cell adhesion, decreased proliferation, increased expression of tendon-related markers and decreased expression of bone-related markers on aligned fibers. No effect of BMP-12.
Subramony *et al.*(20)	Human BMSC	Unaligned and aligned PLGA nanofibers	Matrix alignment + mechanical stimulation	Loaded MSC on aligned fibers produce both collagen I and collagen III, while predominantly collagen I is synthesized by loaded MSC on unaligned fibers. Upregulation of fibroblast marker expression on loaded aligned fibers only
Subramony *et al.*(33)	Human BMSC	Unaligned and aligned PLGA	Matrix alignment + mechanical stimulation + bFGF supplementation	bFGF results in increased proliferation while mechanical stimulation leads to increased matrix synthesis and upregulation in ligament-related gene expression
Cheng *et al.*(144)	Rat ADSC	Aligned and unaligned collagen fibers	Matrix alignment + PDGF release	Increased proliferation up to day 7 and increased expression of tendon markers on aligned PDGF-eluting fibers
Czaplewski *et al.*(112)	Human iPSC-derived MSC	Braided submicron fibrous scaffolds – PLLA vs. PCL	Matrix composition/ mechanical properties + mechanical stimulation	Increased expression of both ligament and bone-related markers on PLLA compared to PCL at day 3
Banks *et al.*(187)	Human ADSC	Collagen gel – crosslinked membranes (2.5 – 5 MPa)	Matrix mechanical properties + growth factors (PDGF-BB) (BMP-2, PDGF-BB)	Increased osteogenic differentiation and decreased adipogenic differentiation with increasing stiffness; PDGF-BB decreased ALP expression by ADSC on stiff substrates while BMP-2 increased ALP expression on soft substrates
Raabe *et al.*(182)	Horse ADSC	Collagen I gels	Growth factors (GDF-5, -6, -7) + oxygen tension + mechanical stimulation	GDF-5/GDF-7 supplementation results in enhanced expression of collagen I, collagen III, and scleraxis
Durant *et al.*(188)	Human BMSC	Fibrin gels	Growth factors (TGF-β) + oxygen tension	TGF-β supplementation and low oxygen tension results in increased cell number; increased collagen I & III expression with addition of TGF-β regardless of oxygen tension
Rehmann *et al.*(117)	Human BMSC	PEG-tetranorbornene (10-90 kPa)	Matrix components (collagen, fibronectin) + matrix mechanical properties + BMP-13, ascorbic acid	Increasing modulus and collagen content results in increased ligamentogenic/tenogenic gene expression and protein production in the presence of BMP-13 and ascorbic acid

1.3 Summary

Adult MSC represent a powerful candidate cell type for regenerative medicine because of their capacity for self-renewal and multipotent differentiation, as well as the critical role they play in trophic signaling and immunomodulation. However, the key to harnessing the regeneration potential of stem cells residing in connective tissues lies in the design of a cell microenvironment that is conducive to stem cell

lineage commitment, biomimetic tissue regeneration, and ultimately, restoration of physiological function. It is clear that there is significant progress in our understanding of how individual aspects of the microenvironment can guide stem cell differentiation and mediate their regeneration potential.

Still, the frontier of the field resides in elucidating the effects of combined cues from the microenvironment, as well as timing of the delivery of these cues, as current understanding of the biology of connective tissue healing advances. The design of complex matrices capable of providing stem cells with a combination of cues mimetic of those observed within the native connective tissue microenvironment is necessary to guide stem cell response for functional connective tissue regeneration. Guided by these strategies, the studies proposed in this thesis include: 1) the design and optimization of a series of *in vitro* culture models for uncovering the role that MSC play in connective tissue healing and 2) analysis of the effects of matrix alignment and mechanical properties on the healing response using a series of nanofiber-based matrices. Results from these studies will be used for the design and optimization of an engineered matrix for promoting stem cell-guided connective tissue regeneration.

CHAPTER 2: INTERACTIONS BETWEEN FIBROBLASTS AND MACROPHAGES FOLLOWING CONNECTIVE TISSUE INJURY

2.1 Introduction

The first study of this thesis focuses on the development of a platform for studying the cellular communications between native ligament fibroblasts and infiltrating macrophages. Specifically, human ACL fibroblasts and M0 macrophages derived from THP-1, a human monocytic cell line, will be cultured together in order to assess the effects of cellular communications between native ligament fibroblasts and infiltrating macrophages during connective tissue injury and repair. The aim of this chapter is to identify the effects of co-culture on 1) fibroblast fibrotic response and 2) macrophage polarization toward a pro- or anti-inflammatory phenotype.

2.1.1 Background and Motivation

Our goal is to examine the effects of heterotypic interactions between infiltrating macrophages and the native fibroblast population following injury and during healing within an injured ligament. Macrophages are considered to be one of the most important leukocytes for both initiating and resolving the inflammatory response(189). These cells begin to arrive at the injury site within 24-48 hours, and can persist for as long as a few months, until all necrotic debris is cleared and remodeled. While it has been shown that macrophages are capable of modulating the inflammatory response of fibroblasts(91), the mechanisms behind these interactions are not well understood. Therefore, the objective of this study focuses on the development of a co-culture model that is capable of assessing the role of fibroblast-macrophage interactions following injury and during healing on fibroblast inflammatory response, in terms of proliferation, matrix synthesis, and phenotypic response, as well as the mechanisms behind macrophage activation toward pro- and anti-inflammatory phenotypes following accumulation at the injury site.

THP-1 is a human monocytic cell line derived from a patient with acute monocytic leukemia, which are shown to exhibit monocytic properties, including immunological functions(190). This cell line is frequently used as a model of macrophage function, as primary tissue macrophages can be difficult to culture or expand *ex vivo*(191), and isolation of these cells is typically invasive, with low cell yields(192). To this end, THP-1 cells have been used previously in various co-culture studies, including those involving pneumocytes, mast cells, endothelial cells, hepatocytes, astrocytoma cells, and MSC(193-196). This compatibility makes this cell line ideal for studying monocyte and macrophage cell response in co-culture, including design of a model to understand their role in inflammation and healing.

THP-1 can be differentiated from a monocyte-like cell into macrophages in the presence of phorbol 12-myristate 13-acetate (PMA), resulting in an M0, or non-polarized mature phenotype. At this stage, M0 THP-1 are not considered to be pro- or anti-inflammatory, but can be activated *in vitro* toward an M1, or classically activated, pro-inflammatory phenotype, or an M2, or alternatively activated, anti-inflammatory phenotype using chemical stimuli. In this study, PMA-differentiated M0 macrophages were utilized in order to assess the ability of co-culture with fibroblasts to polarize macrophages toward an M1 or M2 phenotype, without the addition of chemical factors.

2.1.2 Objectives

The objective of this study focuses on the development of a co-culture model that is capable of determining the effects of fibroblast-macrophage interactions following injury and during healing on fibroblast fibrotic response, in terms of proliferation, matrix synthesis, and phenotypic changes, as well as the effects on macrophage polarization. It is hypothesized that co-culture of macrophages and fibroblasts will be mimetic of the early inflammatory response following connective tissue injury, resulting in polarization of M0 macrophages toward a pro-inflammatory phenotype, as well as pro-fibrotic response by fibroblasts, as observed through increased proliferation and collagen production.

2.2 Materials and Methods

2.2.1 Cells and Cell Culture

2.2.1.1 Human Anterior Cruciate Ligament Cell Isolation and Culture

Human ACL fibroblasts were derived from explant culture of tissues obtained from a patient (male, aged 21) undergoing ACL reconstruction surgery. Briefly, the tissue samples were rinsed in phosphate-buffered saline (PBS; Sigma-Aldrich), plated in tissue culture dishes, and maintained in Dulbecco's modified Eagle medium (DMEM) supplemented with 10% fetal bovine serum (FBS; Atlanta Biologicals), 1% non-essential amino acids, 1% penicillin-streptomycin (P/S), 0.1% amphotericin-B (Amp-B), and 50 µg/mL gentamicin-sulfate (G/S). Cells were allowed to migrate from the tissue onto tissue culture plastic. The cells from the first migration were subsequently discarded, and the tissue was re-plated in fresh fully supplemented (F/S) medium. Only cells obtained from the second and third migrations were used in this study, as this method has been shown to yield a relatively homogenous fibroblast population.

2.2.1.2 Human THP-1 Culture and Differentiation Toward M0 Macrophages

Human THP-1 cells were obtained commercially (ATCC, TIB-202) and maintained in suspension culture in non-tissue culture treated flasks (25 cm^2, Nunc™) with F/S RPMI-1640 medium containing 10% FBS (Atlanta Biologicals), 1% P/S (Sigma-Aldrich), and 0.05 mM 2-mercaptoethanol (2-ME; Sigma-Aldrich). Medium was replaced every 3-4 days. Briefly, cells suspensions were removed from culture dishes and were centrifuged at 5000 rpm for 5 minutes. Supernatant was aspirated and cells were resuspended in fresh RPMI-1640 medium at a density of $4x10^5$ cells/mL.

For differentiation of THP-1 monocytes toward M0 macrophages, THP-1 in suspension were centrifuged at 5000 rpm for 5 minutes. The supernatant was aspirated and cells were resuspended in F/S RPMI-1640 supplemented with 100 nM PMA (Sigma-Aldrich) at 37°C for 48 hours. After 48 hours, PMA-containing medium (PMA+ medium) was removed, and adherent cells were rinsed with PBS, and medium was replaced with F/S RPMI-1640 medium. Cells were allowed to rest for 72 hours before co-culture, in order to allow for adequate cell spreading and differentiation(191). Prior to all co-culture studies, following this 5-day differentiation period, cells were collected to assess the number of cells attached and the attachment/differentiation efficiency (n=5) using PicoGreen dsDNA assay.

2.2.1.3 Bovine ACL Harvest and Fibroblast Isolation and Culture

Fresh immature bovine knee joints (Green Village Packing Company) were soaked in soapy water followed by 70% ethanol for 20 minutes. To isolate the ACL, a straight midline longitudinal incision extending from the distal femur to the tibia was made in the bovine knee under aseptic conditions. After retraction of skin and subcutaneous fascia, the patellar tendon was removed, and a deeper incision was made into the joint capsule in order to expose the femoral condyle and the tibial plateau. The anterior cruciate ligament was resected from the joint at the insertions and was then soaked in sterile PBS at 37ºC. The ligament sheath was then removed and the ligament tissue was diced into small pieces and plated on tissue culture plastic. Tissue was allowed to adhere to the surface for 15 minutes prior to the addition of F/S DMEM containing 10% FBS, 1% P/S, 1% nonessential amino acids, 0.1% Amp-B and 50 µg/mL G/S. Over two weeks, cells were allowed to migrate from the tissue onto the culture dish. Cells from the first migration were discarded, and only cells obtained from the second and third migrations were used in this study because this method has been shown to yield a relatively homogenous fibroblast population.

2.2.2 Co-Culture Medium Optimization

Prior to co-culture studies, a mixed co-culture of fibroblasts and PMA-differentiated THP-1 were grown in F/S DMEM, F/S RPMI-1640, and a 1:1 mixture of F/S DMEM and F/S RPMI-1640 in order to determine the optimal culture medium for co-culture studies. Single-cultures of fibroblasts only and macrophages only served as controls. All groups were cultured for up to 7 days, and cell proliferation (*n*=5) and viability (*n*=3) were assessed at days 1, 3, and 7 using the PicoGreen dsDNA assay and Live/Dead imaging, respectively.

2.2.3 Macrophage Seeding Density Optimization

In order to ensure a 1:1 ratio of fibroblasts:macrophages in mixed and segregated co-culture, a series of THP-1 seeding density optimization studies were performed in hopes of achieving a final macrophage cell density of $1.5x10^3$ cells/cm^2 in co-culture, or $3x10^4$ cells/cm^2 in single-culture. Briefly, THP-1 monocytes were suspended in PMA+ medium at varying concentrations (1.2, 2.4, and $3.6x10^5$ cells/mL for culture on tissue culture plastic in 48 well plates, and 2.4, 3.6, and $4.8x10^5$ cells/mL for culture on Thermanox coverslips). Samples were incubated at 37°C for 48 hours, at which time, PMA+ medium was removed, samples were rinsed with PBS, and 1 mL F/S RPMI-1640 was added to each well. Samples were allowed to rest for 72 hours prior to collection for assessment of the number of cells attached and the attachment/differentiation efficiency using PicoGreen dsDNA assay.

Additionally, to assess the ratio of fibroblasts:macrophages in mixed co-culture, THP-1-derived M0 macrophages and fibroblasts were stained using CellTracker™ membrane dyes (Invitrogen). Briefly, THP-1 were stained using DiO (green) and fibroblasts were stained with DiD (red) following the manufacturer's protocol. After seeding $1.2x10^5$ THP-1/cm^2, culturing for the 5-day differentiation period, and adding $3x10^4$ fibroblasts/cm^2 at this time, cell sorting was performed using fluorescence-activated cell sorting (FACS) on day 0.

2.2.4 Co-Culture Models

2.2.4.1 Mixed Co-Culture Model

Following co-culture medium optimization, macrophages and fibroblasts were grown in co-culture, with fibroblast-only and macrophage-only single-cultures serving as controls. Briefly, THP-1 monocytes

were seeded at a density of $6x10^4$ for co-culture wells or $1.2x10^5$ cells/well for single-culture controls and incubated in F/S RPMI-1640 medium supplemented with 100 nM PMA at 37°C for 48 hours. After 48 hours, PMA+ medium was removed, samples were rinsed once with PBS, and 1 mL F/S RPMI-1640 was added to each well. Cells were allowed to rest for 72 hours before the addition of fibroblasts. At this time, at a seeding efficiency of ~30%, $1.5x10^4$ cells were observed to adhere to co-culture wells, while $3x10^4$ cells attached to single-culture controls. For co-culture, on day 5, fibroblasts were added to THP-1 culture dishes at a density of $1.5x10^4$ cells/cm^2 for co-culture or $3x10^4$ cells/cm^2 for single-culture. All groups were fed with a 1:1 mixture of F/S DMEM:F/S RPMI-1640.

2.2.4.2 Conditioned Medium Model

To test paracrine effects, fibroblast single-cultures were fed with conditioned medium from macrophage culture and macrophage single-cultures were fed with medium from fibroblast culture. Briefly, for fibroblast-conditioned medium, fibroblasts were seeded at a density of $3x10^4$ cells/cm^2 in a 48-well plate in F/S DMEM for 3 days. On day 3, the medium from these wells was collected and centrifuged at 5000 g for 10 minutes to remove any cells or other debris from the supernatant. The supernatant was then collected and mixed 1:1 with fresh F/S RPMI-1640, and subsequently fed to macrophage single-cultures following the 5-day differentiation period described previously. For macrophage-conditioned medium, THP-1 monocytes were seeded at a density of $1.2x10^5$ cells/cm^2, differentiated in PMA+ medium at 37°C for 48 hours. After 48 hours, PMA+ medium was removed and cells were rinsed one time with PBS. Medium was replaced with F/S RPMI-1640 medium, and cells were cultured for 3 days. On the third day, medium from these wells was collected and centrifuged at 5000 g for 10 minutes to remove any cells or other debris from the supernatant. The supernatant was then collected and mixed 1:1 with fresh F/S DMEM, and subsequently fed to fibroblast single-cultures.

2.2.4.3 Segregated Co-Culture Model

To assess the effects of cellular interactions without direct cell-cell contact, fibroblasts and macrophages were grown in segregated co-culture. Briefly, Thermanox™ coverslips (13mm diameter) were cut in half and halves were placed into 24-well plates. To achieve a final density of $3x10^4$ cells/cm^2 ($2x10^4$ cells/coverslip half), $6x10^4$ fibroblasts or $4.8x10^5$ THP-1 were seeded per well. Following day 5 of the THP-

1 differentiation period, one fibroblast-seeded and one THP-1-seeded coverslip was placed onto either side of a single well in a 24-well plate. 4% agarose VII in PBS was heated to 120°C, allowed to cool, and used as a glue to attach coverslips to the bottom of the well.

2.2.5 In Vitro *Scratch Injury Model*

To assess the effects of fibroblast-macrophage interactions on fibroblast healing response, an *in vitro* scratch model was developed (*n*=6). The injury model utilized in this study replicates the scratch model used as a model of skin wound healing(197;198). Briefly, Thermanox™ coverslips seeded with fibroblasts as described above were scratched along the entire length of the coverslip (6.5 mm, or the radius of the 13-mm coverslip) using a 200 µL micropipette tip. Immediately after scratching, fibroblasts were co-cultured with macrophages in the same manner as described for segregated co-culture. Scratched fibroblasts in single-culture without macrophages were used as a control.

2.2.6 Effects of Fibroblast Injury State on Cell Response

To assess the potential effects of fibroblast injury state on macrophage activation, macrophages were co-cultured with ACL fibroblasts isolated either from torn human ACL tissue collected from a patient undergoing ACL reconstruction (injured fibroblasts) or from a healthy, uninjured bovine ACL collected from a calf knee (healthy fibroblasts). Experimental groups included macrophages in mixed co-culture with healthy or injured fibroblasts, macrophages in segregated co-culture with healthy or injured fibroblasts, and macrophages in fibroblast-conditioned medium collected from culture of either healthy or injured fibroblasts, with macrophage-only single-cultures serving as controls.

2.2.7 Live Cell Tracking

Live cell tracking (*n*=3) was accomplished using CellTracker membrane dyes, following the manufacturer's protocol. Briefly, for fibroblasts, medium was removed from cell culture dishes and cells were incubated in 0.25% trypsin/1 mM ethylenediaminetetraacetate (EDTA) for 3 minutes. Trypsin was neutralized using fresh F/S DMEM and cell suspensions were then collected and centrifuged at 5000 rpm for 10 minutes. For THP-1, cells in suspension were removed from cell culture dishes and the suspension was centrifuged at 5000 g for 5 minutes. For both cell types, supernatant was aspirated from the cell pellets, and cells were resuspended in fresh F/S DMEM for fibroblasts or fresh RPMI-1640 for THP-1. Cells were

counted using a hemocytometer, and resuspended at 1 million cells/mL. A total of 5 µL of CellTracker dye (DiD for fibroblasts or DiO for THP-1) was added per mL of cell suspension, and the suspension was incubated at 37ºC and 5% CO_2 in the dark for 20 minutes. A volume of 10 mL fresh F/S DMEM for fibroblasts or F/S RPMI-1640 for THP-1 was added to cell suspensions and cells were centrifuged at 5000 rpm for 5 minutes. Supernatant was aspirated and cells were resuspended in 5 mL fresh medium. This process was repeated two more times for a total of three washes. Differentiation of THP-1 from monocytes to M0 macrophages using PMA was performed following cell membrane staining, using the protocol described previously.

Prior to imaging, culture medium was removed and replaced with PBS. Samples were imaged using confocal microscopy (Olympus Fluoview FV1000) at excitation wavelengths of 488 nm to visualize macrophages stained with DiO, and 568 nm for fibroblasts stained with DiD.

2.2.8 Live/Dead Cell Viability

Cell viability (*n*=3) was visualized using Live/Dead staining (Molecular Probes). Samples were stained following the manufacturer's suggested protocol, and were subsequently imaged using confocal microscopy (Olympus Fluoview FV1000) at excitation wavelengths of 488 nm (live) and 568 nm (dead).

2.2.9 Cell Proliferation

Cell proliferation (*n*=5) was determined by measuring total DNA content using the PicoGreen dsDNA assay (Invitrogen) following the manufacturer's protocol. Scaffolds were rinsed twice in PBS and stored in 500 µl of 0.1% Triton X (Sigma-Aldrich) at -30°C. Immediately before the analysis, samples were thawed and homogenized, followed by sonication with a cell sonicator (Microson XL-2000) at 5 W for 15 seconds. Fluorescence was measured using a Tecan microplate reader with an excitation wavelength of 485 nm and an emission wavelength of 535 nm. A conversion factor of 8 pg DNA/cell was used to determine cell number.

2.2.10 Collagen Production

Collagen production (*n*=5) was quantified using a modified hydroxyproline assay(199). Samples were digested in a buffered papain solution prior to analysis. For digestion, samples were vacuum dried overnight using the Centrivap concentrator (Labconco). Samples were then digested for 20 hours at 65ºC

with 20 µL/mL papain (Sigma-Aldrich), buffered in 0.1M sodium acetate, 10mM cysteine hydrochloric acid (HCl), and 50M EDTA. For the assay, digested samples were concentrated by drying 125-250 µl of sample overnight in the Centrivap concentrator. Samples were resuspended in 50 µl of 2N sodium hydroxide (NaOH) and autoclaved for 25 minutes. A volume of 450 µl of chloramine T reagent (1.27 g chloramine T in 50% isopropanol brought to 100 mL with acetate-citrate buffer) was added to the samples, which were then allowed to incubate for 25 minutes at room temperature. A volume of 500 µL of Ehrlich's reagent (15 g p-dimethylaminobenzaldehyde in 100 mL (2:1) isopropanol:perchloric acid) was subsequently added, and the samples were incubated at 65ºC for 20 minutes. The absorbance at 555 nm was read using a Tecan microplate reader. Total collagen was determined using a standard curve generated using a collagen standard (Sigma-Aldrich).

The acetate-citrate buffer for the chloramine T solution consisted of 30 g sodium acetate trihydrate, 11.5 g citric acid, 3 mL acetic acid, and 8.5 g NaOH, dissolved in 125 mL of distilled water. The solution was brought to a pH of 6.5 using 1N NaOH or 1N HCl, and then brought to a final volume of 250 mL.

2.2.11 Expression of Ligament-Related Markers

Gene expression was analyzed using quantitative reverse transcriptase polymerase chain reaction (qRT-PCR). Samples were rinsed twice with PBS and stored in Trizol (Invitrogen). RNA was isolated using the chloroform/Trizol extraction method. The extracted RNA pellet was redissolved in 150 µL DEPC H_2O (Ambion). First-strand complementary DNA (cDNA) was synthesized using 50µM oligo$(dT)_{20}$ primer, 10mM dNTP mix, and 8 µL of extracted RNA. cDNA synthesis was accomplished using 5X RT buffer, DTT, 40U/µL RNaseOUT, and 200U/µL SuperScript III RT. The cDNA product was subsequently amplified and quantified through real-time PCR using SYBR Green Supermix (Invitrogen). Glyceraldehyde-3-phosphate dehydrogenase (GAPDH) served as the house-keeping gene. All genes were amplified for 50 cycles in a

Table 2.1: Primer Sequences for Gene Expression

Gene	Sense	Anti-Sense	Blast product Size (bp)
GAPDH	5'- GGCGATGCTGGCGCTGAGTA-3'	5'-ATCCACAGTCTTCTGGGTGG-3'	306
Collagen I	5'-TGGTCCACTTGCTTGAAGAC-3'	5'-ACAGATTTGGGAAGGAGTGG-3'	118
Scleraxis	5'-CAGCGGCACACGGCGAAC-3'	5'-CGTTGCCCAGGTGCGAGATG-3'	163
Tenascin-C	5'-TGCCCATTACAGGAGGTACA-3'	5'-CACTTTCCTCAAAGCCCTTC-3'	132

thermocycler (iCycler iQ Real-Time PCR Detection System, BioRad). See *Table 2.1* for primer sequences used and amplicon sizes. Normalized expression levels were calculated based on the difference between threshold cycles of the gene of interest and GAPDH.

2.2.12 Cytokine Release

Levels of pro- (TNF, IL-1β) and anti-inflammatory (IL-10, TGF-β1) cytokines (*n*=5) were assessed via enzyme-linked immunosorbent assay (ELISA; R&D Systems) according to the manufacturer's protocol. Briefly, supernatants from cell culture were collected after 48 hours and stored at -30°C. On the day of analysis, samples were thawed and added directly to assay diluent in a prepared plate and incubated for two hours at room temperature prior to solution removal. Each well was washed three or four times before incubation with either TNF, IL-1β, or IL-10 conjugate for 1 hour at room temperature, or TGF- β1 conjugate for two hours at room temperature. The conjugate was then removed, the plate was washed three or four times, and the substrate solution was added to each well and allowed to react in the dark. The stop solution was added after 20 minutes for TNF, IL-1β, or IL-10 or 30 minutes for TGF- β1. Sample absorbance was measured using a microplate reader (Tecan) at 450 nm and 570 nm, and the difference was used to calculate cytokine concentration. Base level concentrations of each cytokine in acellular culture medium were used as negative controls.

2.2.13 Statistical Analysis

Results are reported as mean ± standard deviation, with *n* equal to the number of replicates per group. Statistical analyses were performed with JMPIN (4.0.4, SAS Institute, Inc.). Sample sets were checked for normality and equal variance, followed by performance of a corrected t-test. The Tukey-Kramer post-hoc test was used for all pair-wise comparisons, and significance was attained at $p<0.05$.

2.3 Results

2.3.1 Co-Culture Medium Optimization

Results show that for fibroblast single-culture, cell number is significantly lower in F/S RPMI-1640 compared to F/S DMEM by day 3, and is significantly lower than both F/S DMEM and a 1:1 mix of F/S DMEM and F/S RPMI-1640 by day 7 (*Figure 2.2*), suggesting this medium has a negative effect on fibroblast viability. Oppositely, for macrophages, cell number was significantly lower in F/S DMEM than F/S RPMI-

1640 by day 1, and was significantly lower than both F/S RPMI-1640 and a 1:1 mix of F/S DMEM and F/S RPMI-1640 by day 3 (*Figure 2.2*), indicative of a cytotoxic effect of F/S DMEM on THP-1. No effects on cell number in co-culture were observed for any medium type (*Figure 2.2*). Based on these results, a 1:1 mixture of F/S DMEM and F/S RPMI-1640 will be used for all future fibroblast-macrophage co-culture studies. Additionally, to maintain the ratio of DMEM to RPMI-1640 in conditioned medium groups, fibroblasts in macrophage-conditioned medium groups will receive a 1:1 mixture of fresh F/S DMEM and conditioned medium from macrophages cultured in F/S RPMI-1640 only, while macrophages in fibroblast-conditioned medium groups will receive a 1:1 mixture of fresh F/S RPMI-1640 and conditioned medium collected from fibroblasts in F/S DMEM only.

2.3.2 Macrophage Seeding Density Optimization

. Based on these studies, PMA differentiation of THP-1 is observed to result in ~30% cell attachment on tissue culture plastic, regardless of initial seeding density (*Figure 2.3*). In all groups, following day 2, cell number continues to drop, as THP-1 are known to lose viability following differentiation, and are typically only viable for 7 days or less after M0 differentiation. Therefore, to achieve a concentration of $3x10^4$ cells/cm^2 in 48-well plates (($1.5x10^4$ macrophage/cm^2 and $1.5x10^4$ fibroblasts/cm^2) on day 0 of co-culture (or day 5 following initial exposure of THP-1 to PMA), a seeding density of $1.2x10^5$ cells/cm^2 must be used. For segregated co-culture studies on Thermanox™ coverslips, a total of $4.8x10^5$ cells/well is needed to achieve a final cell density of $3x10^4$ cells/cm^2 by day 5 of differentiation, or day 0 of co-culture (*Figure 2.3*). FACS cell sorting results on day 0 of co-culture show that that a 1:1 co-culture of fibroblasts:macrophages was achieved at this time point (*Figure 2.4*).

2.3.3 Cell Proliferation

Total cell number was greater for fibroblast single-culture and fibroblasts in macrophage-conditioned medium compared to all other groups at day 2. Total cell number was greater for fibroblast single-culture and fibroblasts in macrophage-conditioned medium greater than macrophage single-culture and macrophages in fibroblast-conditioned medium at day 7 (*Figure 2.5*). Total cell number increased between days 2 and 7 in co-culture only, with a greater fold change in cell number in co-culture compared to fibroblasts in macrophage-conditioned medium at this time point (*Figure 2.5*). Total cell number in

macrophage single-culture and for macrophages in fibroblast-conditioned medium decreased over time (*Figure 2.5*).

2.3.4 Collagen Production

Total collagen increased over time in co-culture only, with no observed changes in total collagen for any other groups (*Figure 2.6*). Collagen per cell was greater in co-culture compared to fibroblasts in macrophage-conditioned medium at both day 2 and day 7 (*Figure 2.6*).

2.3.5 Expression of Ligament-Related Markers

Type I collagen expression was upregulated for fibroblasts in macrophage-conditioned medium compared to fibroblast single-culture and fibroblast-macrophage co-culture at day 2. This difference was no longer observed by day 7, as type I collagen expression for fibroblasts in macrophage-conditioned medium decreased significantly between days 2 and 7. There were no significant differences in the expression of scleraxis or tenascin-C for any group at either time point (*Figure 2.7*).

2.3.6 Cytokine Secretion

Pro-Inflammatory Cytokines: Total TNF and IL-1β concentrations were greatest for macrophages in fibroblast-conditioned medium compared to all other groups at day 2 (*Figure 2.8*). Total TNF and total IL-1β were greater in co-culture compared to macrophage single-culture and fibroblast single-culture at this time point. Total IL-1β was also greater for fibroblasts in macrophage-conditioned medium compared to fibroblast single-culture (*Figure 2.8*). *Anti-Inflammatory Cytokines*: Total IL-10 was greatest for macrophages in fibroblast-conditioned medium compared to all other groups. Total IL-10 was greater in co-culture compared to macrophage single-culture, fibroblast single-culture, and fibroblasts in macrophage-conditioned medium at day 2 (*Figure 2.8*). Total TGF-β1 was greater for fibroblasts in macrophage-conditioned medium compared to co-culture at this time point (*Figure 2.8*).

2.3.7 Effects of Mode of Cell Contact on Inflammatory Response

Pro-Inflammatory Cytokine Release: Both TNF per cell and IL-1β per cell were greatest for macrophages in fibroblast-conditioned medium compared to all other groups after 48 hours (*Figure 2.9*). TNF per cell was greater in segregated co-culture compared to mixed co-culture at day 2. There were no

observed differences in IL-1β per cell between mixed and segregated co-culture at this time point (*Figure 2.9*). *Anti-Inflammatory Cytokine Release*: IL-10 per cell was greatest for macrophages in fibroblast-conditioned medium compared to all other groups. IL-10 per cell was greater in segregated co-culture compared to mixed co-culture at day 2 (*Figure 2.9*). There were no observed differences in TGF-β1 release per cell between any groups as this time point (*Figure 2.9*).

2.3.8 Effects of Fibroblast-Macrophage Interactions on Fibroblast Healing Response

Use of the scratch model resulted in the formation of reproducible scratch defects that were 362.91 ± 44.30 μm in width and 6.5 mm or 6500 μm in length (*Figure 2.10*). Similar inflammatory cytokine release profiles were observed between segregated co-culture and injury model groups at day 2 (*Figure 2.10*), suggesting that the injury model does not alter fibroblast phenotype toward a pro-inflammatory state. Gap width decreased significantly after 3 hours in culture for scratched fibroblasts in single-culture, with no difference in scratch width over time observed for scratched fibroblasts in segregated co-culture with macrophages. There were no observed differences in total TNF or TGF-β1 release between segregated co-culture and the scratch model after 48 hours (*Figure 2.10*).

2.3.9 Effects of Fibroblast Injury State on Macrophage Polarization

For macrophages co-cultured with fibroblasts isolated from an injured ACL, TNF per cell was lowest for macrophage single-culture controls compared to all other groups (*Figure 2.11*). TNF per cell was greater for macrophages in fibroblast-conditioned medium and in segregated co-culture compared to mixed co-culture. There were no differences in TGF-β1 per cell between groups (*Figure 2.11*). For macrophages co-cultured with fibroblasts isolated from a healthy ACL, TNF per cell was lower in mixed and segregated co-culture compared to macrophage single-culture controls, with no differences in TNF per cell between macrophage single-culture and macrophages in fibroblast-conditioned medium at day 2 (*Figure 2.11*). TGF-β1 per cell was elevated in segregated co-culture compared to all other groups at this time point (*Figure 2.11*).

2.4 Discussion

In this study, an optimized co-culture model was developed for assessing the interactions between native ligament fibroblasts and infiltrating macrophages following connective tissue injury and during

inflammation and repair. It was observed that direct co-culture of these two cell types results in a pro-fibrotic response by fibroblasts, as indicated by increased proliferative activity in co-culture and collagen synthesis in macrophage-conditioned medium. Specifically, total cells increased between days 2 and 7 for mixed co-culture only, with a significantly greater fold change in cell number by day 7 in both mixed and segregated co-culture compared to fibroblasts in macrophage-conditioned medium. As THP-1 have been shown not to proliferate following PMA differentiation(191), it is likely that this observed difference is due to a change in the proliferative response of fibroblasts when in direct contact with macrophages. Additionally, collagen per cell was greater in mixed co-culture compared to fibroblasts in macrophage-conditioned medium at both time points, indicating increased matrix synthesis in this group. Both fibroblast proliferation and increased collagen production are hallmarks of the inflammatory response following injury, and have been shown to result in scar formation in injured ligaments *in vivo*(200).

For fibroblasts in macrophage-conditioned medium, total TGF-β1 was greater than mixed co-culture. Interestingly, there was also an observed increase in the expression of collagen I at day 2 in this group. In mixed co-culture, no differences in fibroblast gene expression were observed, but total TGF-β1 was still elevated compared to macrophage single-culture and macrophages in fibroblast-conditioned medium at day 2. Signaling of TGF-β1 has been reported to promote collagen synthesis by fibroblasts, suggesting that elevation of this cytokine may be responsible, at least in part, for the observed changes in collagen expression in macrophage-conditioned medium, as well as increased collagen production in co-culture(201). Additionally, IL-1β concentrations were elevated for fibroblasts in macrophage-conditioned medium compared to fibroblast single-culture, indicating a pro-inflammatory response, as it has been shown previously that fibroblasts release IL-1β following inflammatory stimulation *in vitro*(202).

In work by Manning *et al*., co-culture of murine tendon fibroblasts with M0 macrophages also resulted in a pro-inflammatory response by fibroblasts, as observed through increased expression of inflammatory markers TNF, IL-1β, and cyclooxygenase (COX)-2, as well as upregulation of matrix metalloproteinases. While the effects of co-culture on fibroblast proliferation were not assessed, collagen I expression was significantly downregulated for co-cultured fibroblasts(91). Works by both Sugarman *et al.* and Battegay *et al*. suggest that this effect may be due in part to TNF released by macrophages in co-culture, as exposure of fibroblasts to recombinant TNF has been shown to enhance cell proliferation *in*

vitro(203;204). Furthermore, findings by Postlethwaite *et al.* indicate that IL-1β released by M1 polarized macrophages may also be responsible for enhanced fibroblast proliferation, as the addition of recombinant human IL-1β to culture medium *in vitro* resulted in increased proliferation by dermal fibroblasts(205). Additionally, it is possible that increased levels of TGF-β1 in co-culture groups led to the observed increase in collagen synthesis, as studies by Find and Goldstein show that TGF-β1 promoted collagen production by human embryonic lung fibroblasts *in vitro*(201). Interestingly, the results observed for fibroblasts in macrophage-conditioned medium suggest that this response is specific to fibroblast contact with polarized M1/M2 macrophages, and not with M0 macrophages. Alternatively, it is also possible that the observed increases in fibroblast proliferation and collagen synthesis are due to direct cell-cell contact, or at least crosstalk between cell types, as these types of communications are not allowed in conditioned medium models.

Co-culture was also observed to result in a heterogeneous activation of macrophages toward both pro- (M1) and anti-inflammatory (M2) phenotypes, as indicated by the enhanced release of TNF and IL-1β, pro-inflammatory cytokines commonly associated with M1 activation, as well as IL-10, a marker of anti-inflammatory macrophage response, for macrophages in mixed co-culture, segregated co-culture, and in fibroblast-conditioned medium. Because it has been previously determined that fibroblasts cannot produce IL-10, it can be assumed that M2 macrophage polarization is responsible for these observed increases in IL-10(206). This is similar to results observed by Manning *et al*., in which co-culture of M0 macrophages with tendon fibroblasts resulted in increased release of IL-1β and IL-10, among other cytokines(91). This response by macrophages seems to be mitigated by direct cell contact, as total concentrations of TNF, IL-1β, and IL-10 are lower in co-culture compared to macrophages in fibroblast-conditioned medium at day 2.

Based on results from co-culture of macrophages with fibroblasts isolated from both healthy and injured ACL tissue, it is possible that macrophage polarization is directly affected by fibroblast injury state, as macrophages in co-culture with fibroblasts that were isolated from an injured ACL secrete greater amounts of TNF than macrophages cultured either in co-culture with healthy ACL fibroblasts or in conditioned medium collected from healthy ACL fibroblasts. It has been shown that injury can result in changes to fibroblast phenotype, as observed through upregulation in the expression of matrix metalloproteinases(207) and release of pro-inflammatory cytokines(208). Interestingly, TNF concentration

per cell is lower in mixed and segregated co-culture with healthy fibroblasts compared to M0 macrophage single-culture controls, suggesting M1 activation of macrophages is minimal in these groups. Additionally, while TGF-β1 levels per cell are not different across co-culture groups for co-culture with injured ACL fibroblasts, levels of this cytokine are greater in mixed and segregated co-culture with healthy fibroblasts compared to macrophage single-culture controls, suggesting macrophages in these groups are undergoing M2 instead of M1 activation. Still, this cannot be definitively stated, as fibroblasts have been shown to release TGF-β1, as well, and could be responsible for the observed increase in these groups.

In summary, the results of this study suggest that macrophage accumulation and subsequent activation at the injury site play an important role in activating a pro-inflammatory and pro-fibrotic response by fibroblasts following injury. Macrophage activation following injury may be due to a change in fibroblast phenotype, resulting in differences in fibroblast gene expression and inflammatory signaling, resulting in polarization of M0 macrophages toward both pro- and anti-inflammatory phenotypes. If the inflammatory signaling observed by injured fibroblasts can be mitigated, it may be possible to reduce macrophage polarization, which in turn could reduce proliferation and slow matrix synthesis by fibroblasts, to minimize scar tissue formation by these cells following injury.

2.5 Conclusion

This study demonstrated that interactions between fibroblasts and macrophages results in heterogeneous inflammatory activation of M0 macrophages, with polarization toward both M1 and M2 macrophage phenotypes observed, as well as a pro-fibrotic response by fibroblasts, as observed via increased fold change in cell number in both mixed and segregated co-culture compared to all other groups, and increased collagen synthesis per cell in mixed co-culture compared to fibroblasts in macrophage-conditioned medium. It is possible that the enhanced inflammatory activation of macrophages in co-culture and conditioned medium is due to fibroblast injury state, as these responses are not observed in co-culture with healthy fibroblasts. Studies performed in *Chapter 3* will seek to assess the role that MSC play in modulating the communications between fibroblasts and macrophages, in order to minimize scar formation in exchange for functional tissue repair.

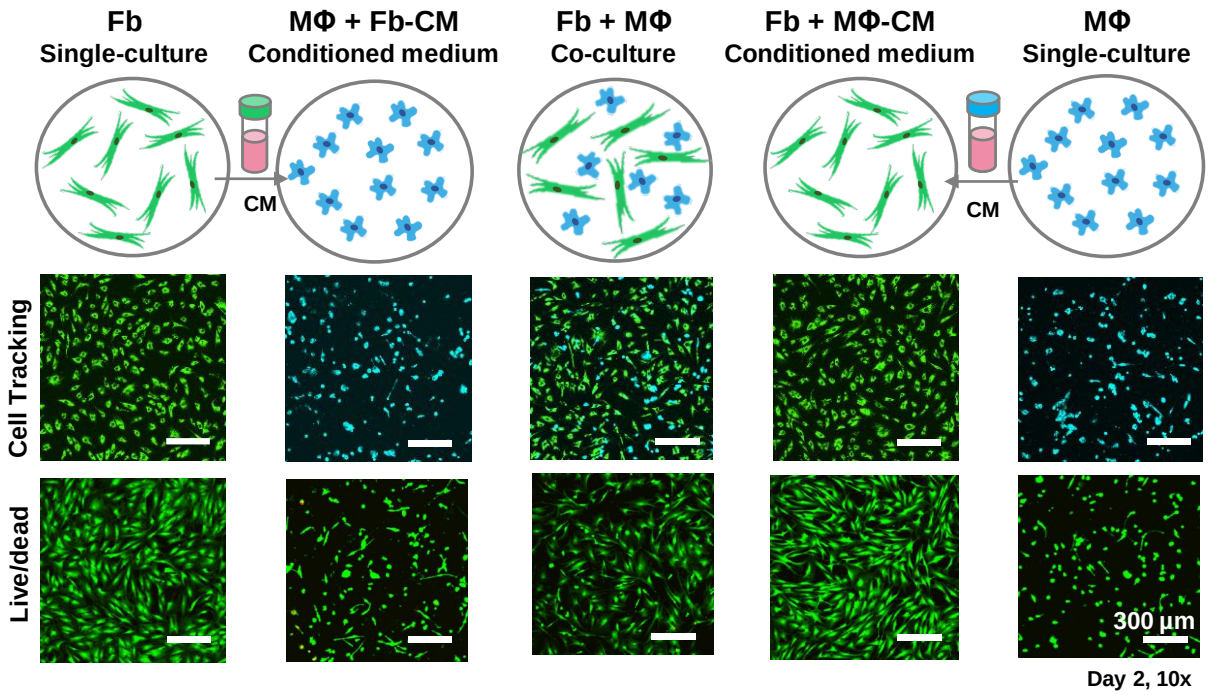

Figure 2.1: Fibroblast-Macrophage Interactions: Co-culture Model. THP-1-derived M0 macrophages (MΦ) and human ACL fibroblasts (Fb) were seeded in co-culture. Conditioned medium groups included fibroblasts in macrophage-conditioned medium and macrophages in fibroblast-conditioned medium with single-cultures of fibroblasts and macrophages serving as controls. *n*=3, Day 2, mag = 10x, scale bar = 300µm.

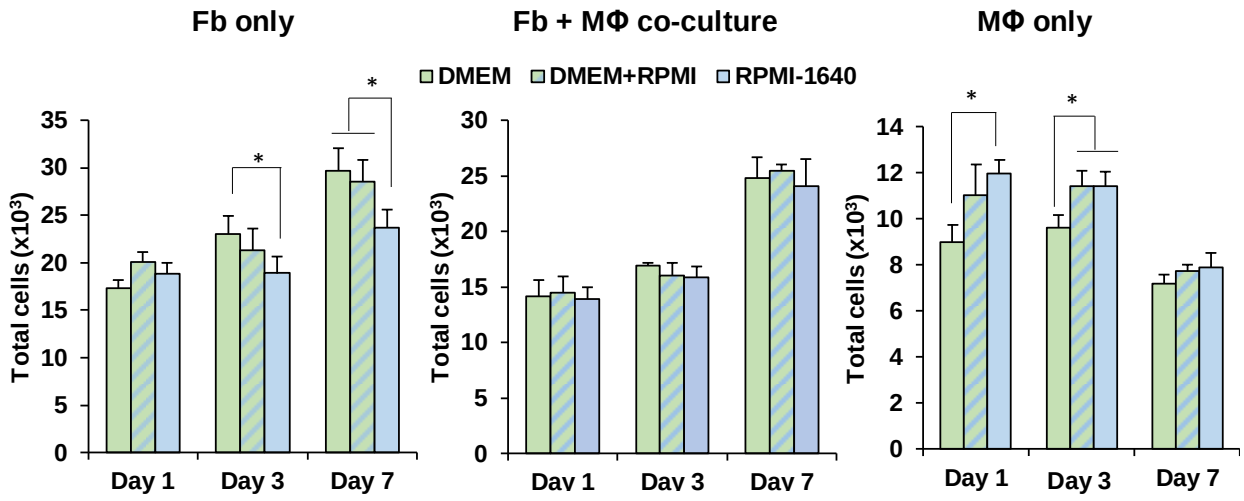

Figure 2.2: Fibroblast-Macrophage Interactions: Co-culture Medium Optimization. For co-culture medium optimization, cell number was lower for fibroblasts in fully-supplemented (F/S) RPMI-1640 compared to F/S DMEM controls at days 3 and 7. Cell number was also lower for macrophages in F/S DMEM compared to F/S RPMI-1640 controls at day 1, and both F/S RPMI-1640 and a 1:1 mix of DMEM:RPMI-1640 at day 3. No effects of medium choice on cell viability was observed in co-culture, suggesting a 1:1 mix of DMEM:RPMI-1640 is suitable for co-culture experiments. *n*=5, significant difference: * between groups, ^ over time ($p<0.05$).

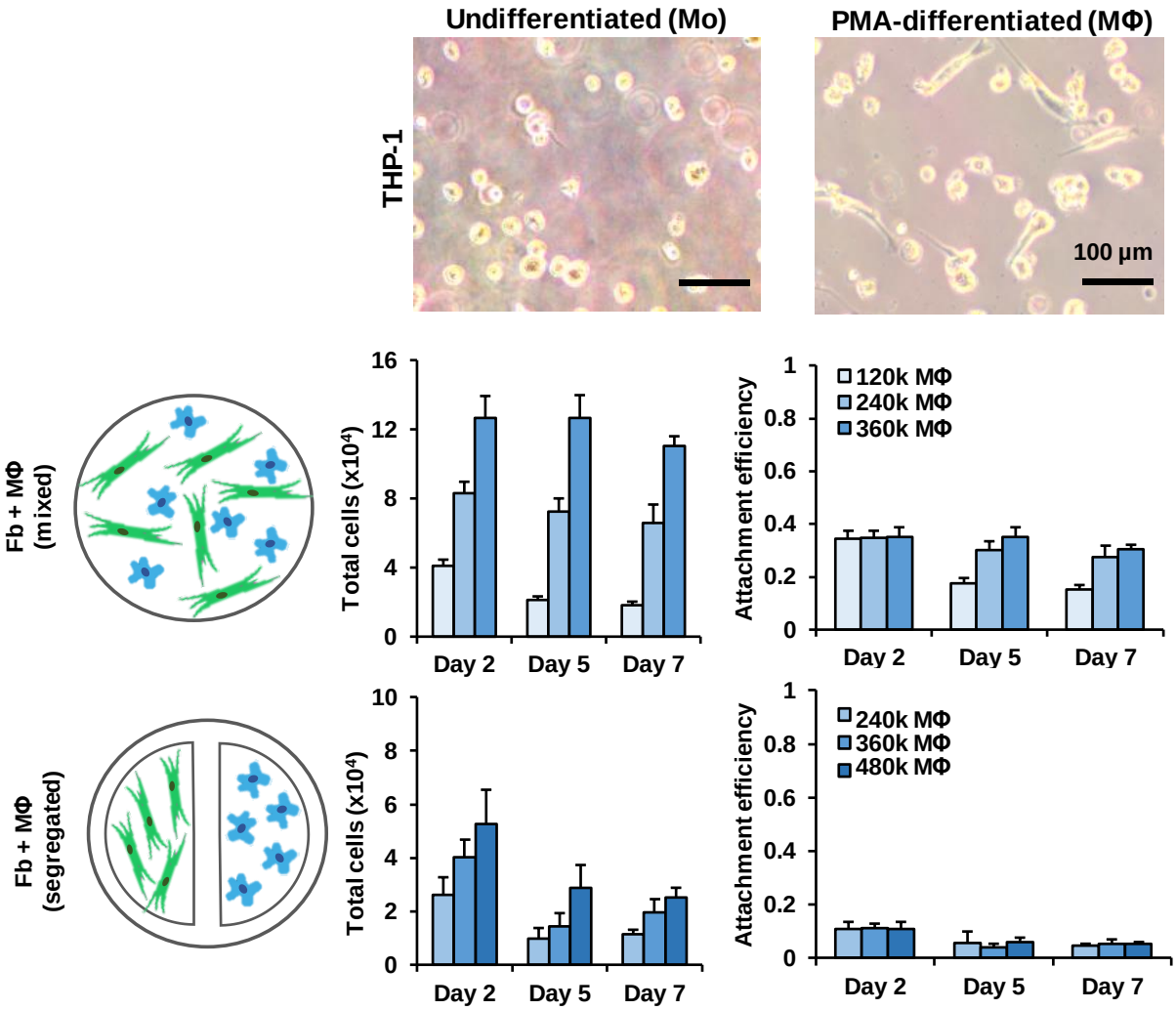

Figure 2.3: Fibroblast-Macrophage Interactions: Macrophage Differentiation Optimization. To achieve a 1:1 ratio of fibroblasts:macrophages in co-culture ($1.5x10^4$ THP-1/cm^2), THP-1 were seeded at varying densities in phorbol-12-myristate-13-acetate (PMA)-containing differentiation medium. Results show about 35% cell adherence following differentiation. Therefore, to achieve a 1:1 ratio of fibroblasts:macrophages in co-culture, $1.2x10^5$ THP-1 must be seeded prior to differentiation. Scale bar = 100 µm, n=5, *p<0.05.

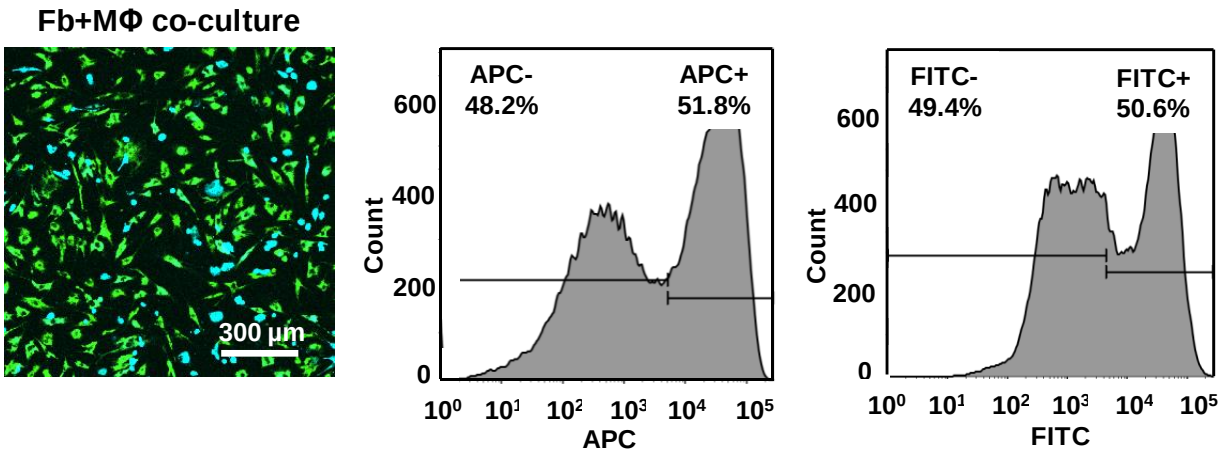

Figure 2.4: Fibroblast-Macrophage Interactions: Co-culture Seeding Optimization. Fluorescence-activated cell sorting (FACS) analysis confirms that a final ratio of 1:1 fibroblasts:macrophages was achieved in co-culture at day 0 when THP-1 are seeded at a density of 1.2×10^5 cells/cm^2 in phorbol-12-myristate-13-acetate (PMA)-containing differentiation medium. Scale bar = 300 µm, $n=5$, $^*p<0.05$.

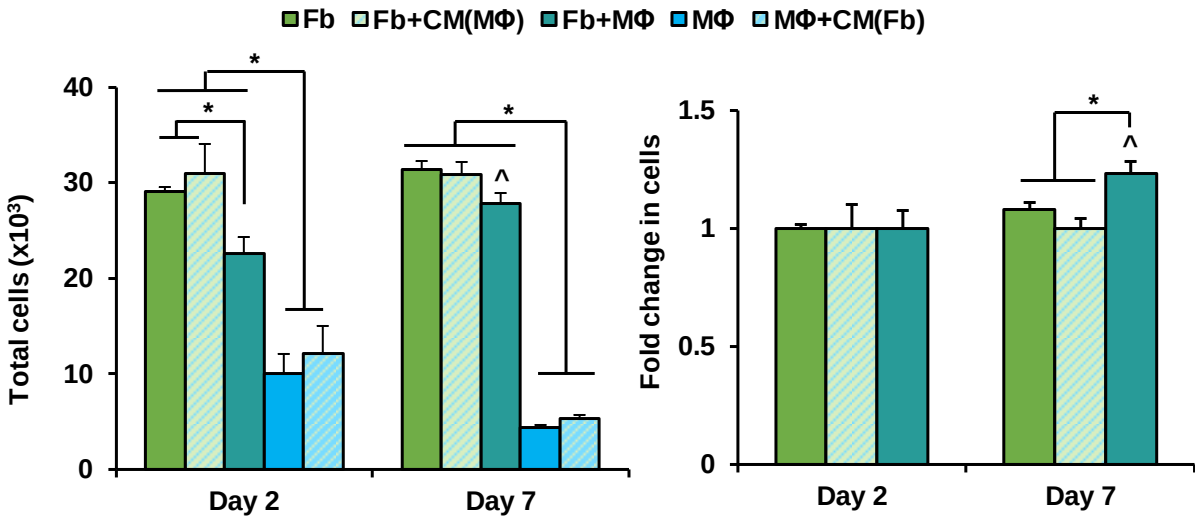

Figure 2.5: Fibroblast-Macrophage Interactions: Fibroblast Proliferation. Total cell number is lower for macrophage single-culture and macrophages in fibroblast-conditioned medium compared to all other groups at day 2, with significantly fewer cells in co-culture compared to fibroblast single-culture and fibroblasts in macrophage-conditioned medium at this time point. Total cells increased over time in co-culture only, with no difference in cell number between fibroblast single-culture, fibroblasts in macrophage-conditioned medium, or co-culture at day 7. Fold change in cell number is significantly greater in co-culture compared to fibroblast single-culture and fibroblasts in macrophage-conditioned medium at day 7. n=5, significant difference: * between groups, ^ over time (p<0.05).

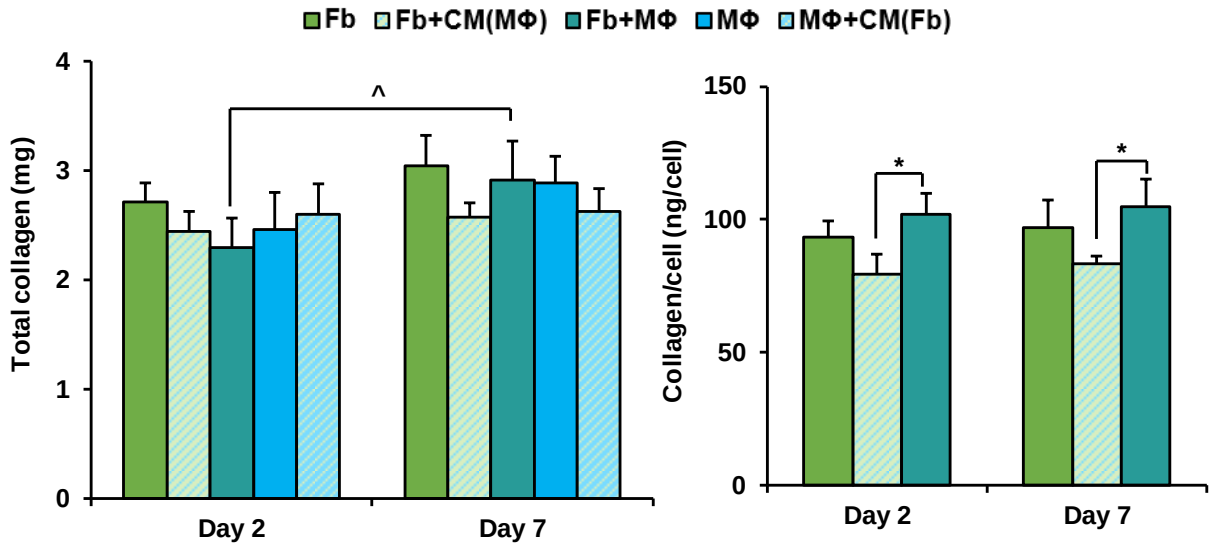

Figure 2.6: Fibroblast-Macrophage Interactions: Collagen Production. Total collagen content increased over time in co-culture only. Collagen per cell was greater in co-culture compared to fibroblasts in conditioned medium at days 2 and 7. *n*=5, significant difference: * between groups, ^ over time ($p<0.05$).

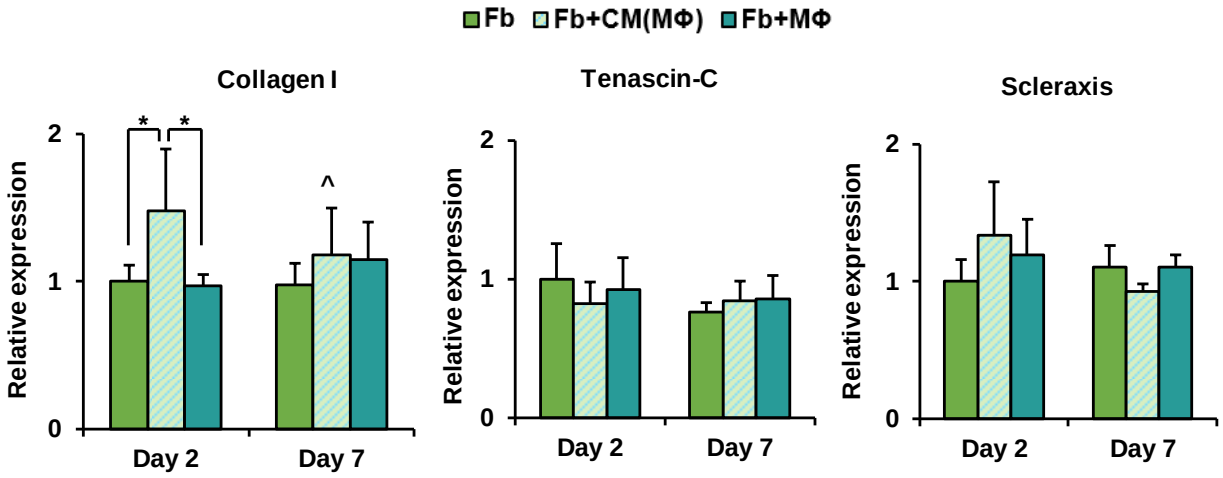

Figure 2.7: Fibroblast-Macrophage Interactions: Expression of Ligament-Related Markers. Type I collagen expression was greater for fibroblasts in macrophage-conditioned medium compared to fibroblast single-culture and co-culture at day 2. Type I collagen expression in this group decreased by day 7, and differences in type I collagen between groups were no longer observed by this time point. There was no significant difference in the expression of tenascin-C or scleraxis between groups at either days 2 or 7, with no changes in expression of these markers over time. n=5, significant difference: * between groups, ^ over time (p<0.05).

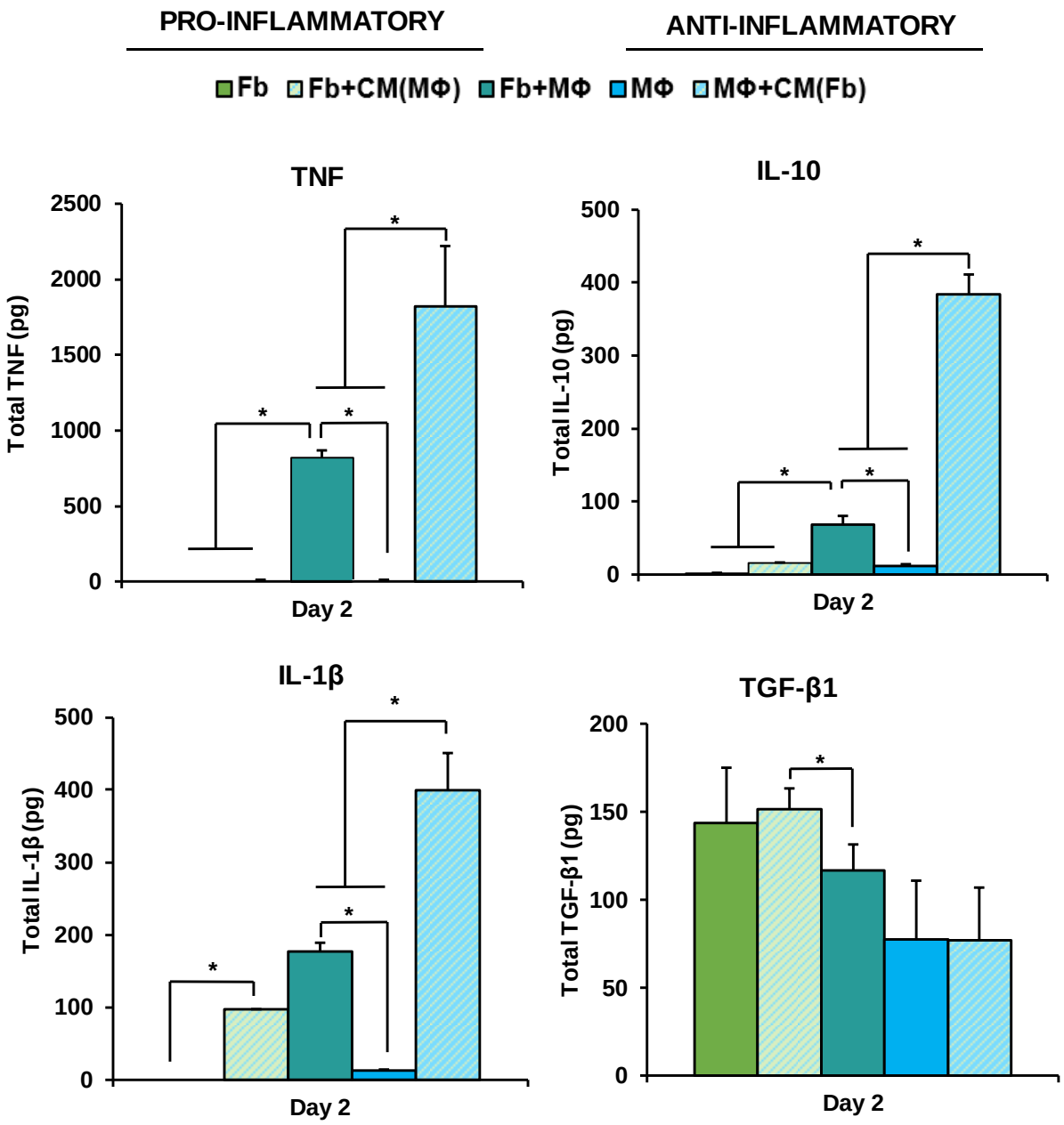

Figure 2.8: Fibroblast-Macrophage Interactions: Release of Pro- and Anti-Inflammatory Cytokines. Total TNF and IL-1β concentrations were greatest for macrophages in fibroblast-conditioned medium. Concentrations of TNF and IL-1β were greater in co-culture than in macrophage and fibroblast single-culture controls. Total IL-1β was greater for fibroblasts in macrophage-conditioned medium compared to fibroblast single-culture. Total TGF-β1 was greater for fibroblasts in macrophage-conditioned medium compared to co-culture. Total IL-10 was greatest for macrophages in fibroblast-conditioned medium, and concentrations of IL-10 were greater in co-culture than in macrophage and fibroblast single-culture controls. n=5, p<0.05.

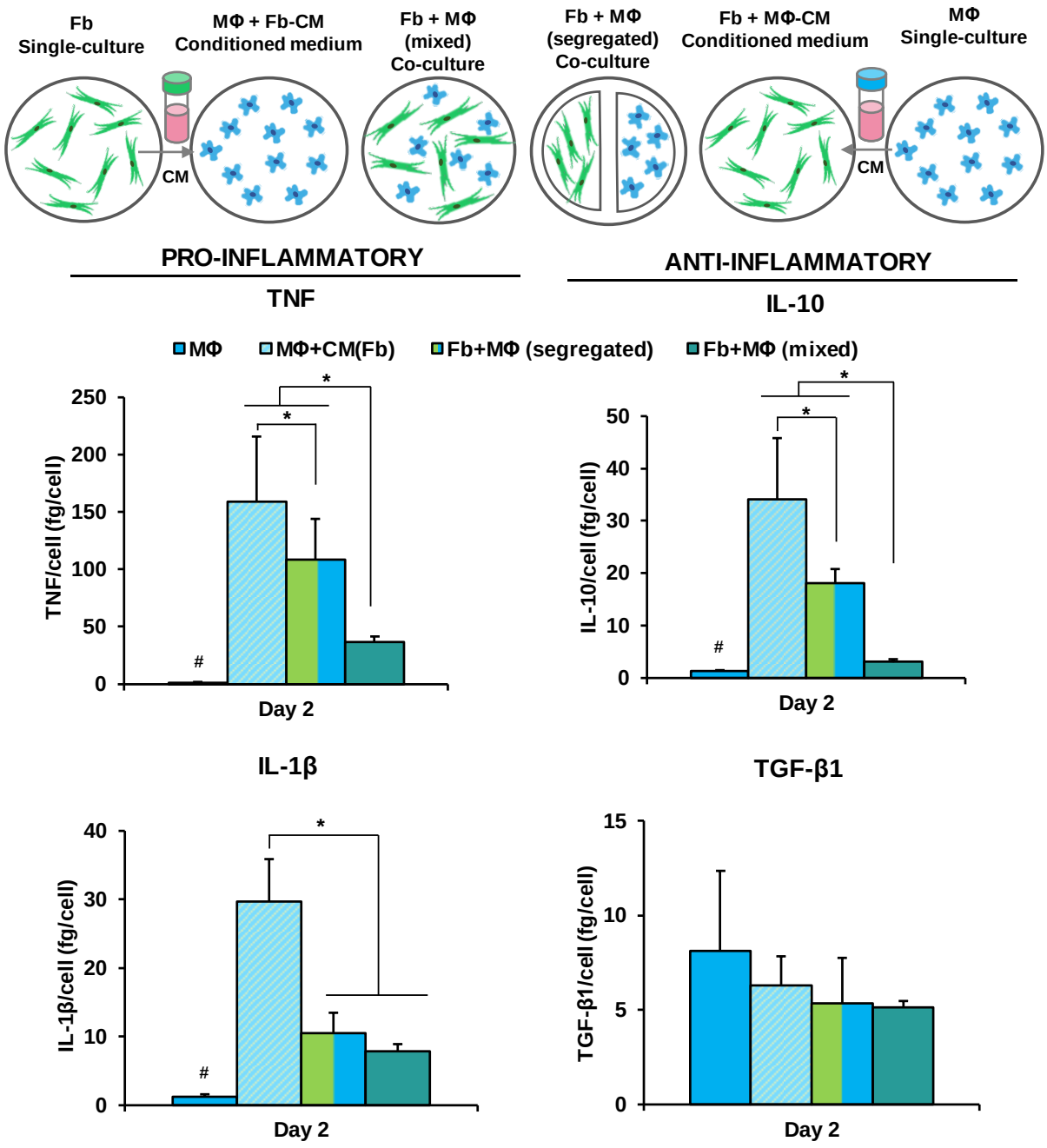

Figure 2.9: Fibroblast-Macrophage Interactions: Effects of Mode of Contact on Macrophage Polarization. To assess the effects of direct cell contact and paracrine signaling on macrophage response, a segregated co-culture model was developed, in which ACL fibroblasts (Fb) and THP-1-derived M0 macrophages (MΦ) were seeded on individual Thermanox coverslips and cultured in the same well. Release of TNF per cell, IL-1β per cell, and IL-10 per cell were greatest for macrophages in fibroblast-conditioned medium compared to all other groups after 48 hours. TNF per cell and IL-10 per cell were greater in segregated co-culture compared to mixed co-culture, with no differences in IL-1β per cell between mixed and segregated co-cultures at this time point. There were no observed differences in TGF-β1 per cell between groups. n=5, * significant difference between groups, # significantly different from all groups (p<0.05).

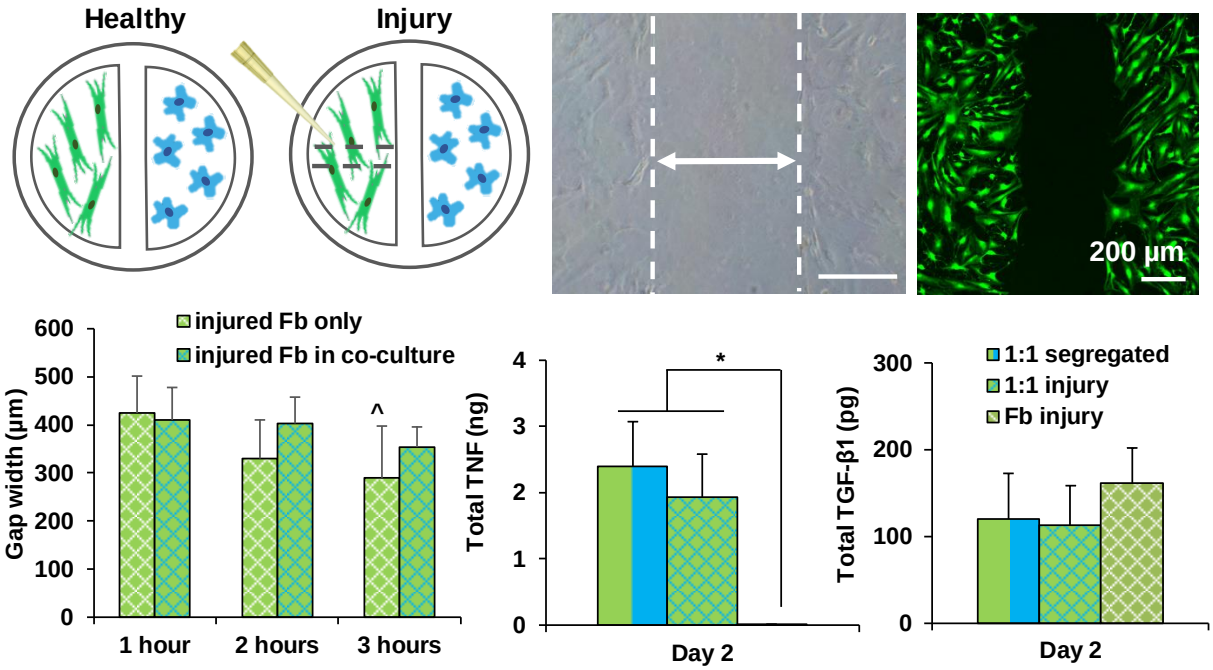

Figure 2.10: Fibroblast-Macrophage Interactions: Fibroblast Injury Scratch Model. Schematic of healthy vs. injury co-culture models. To injure the fibroblasts, a 200 µL yellow pipette tip was manually dragged across the center of the Thermanox coverslip seeded with a confluent layer of fibroblasts. Bright field and confocal images show that scratching the surface leads to a uniform scratch along the midsection of coverslips, with an average width of 362.91 ± 44.30 µm and an average length of 6.5 mm or 6500 µm. Gap width decreased significantly after 3 hours in culture for scratched fibroblasts in single-culture, with no difference in scratch width over time observed for scratched fibroblasts in segregated co-culture with macrophages. There were no observed differences in total TNF or TGF-β1 release between segregated co-culture and the scratch model after 48 hours. n=6, significant difference: * between groups, ^ over time, (p<0.05); Bright field: 5x, Fluorescence: 10x, Day 2, Scale bars = 200 µm.

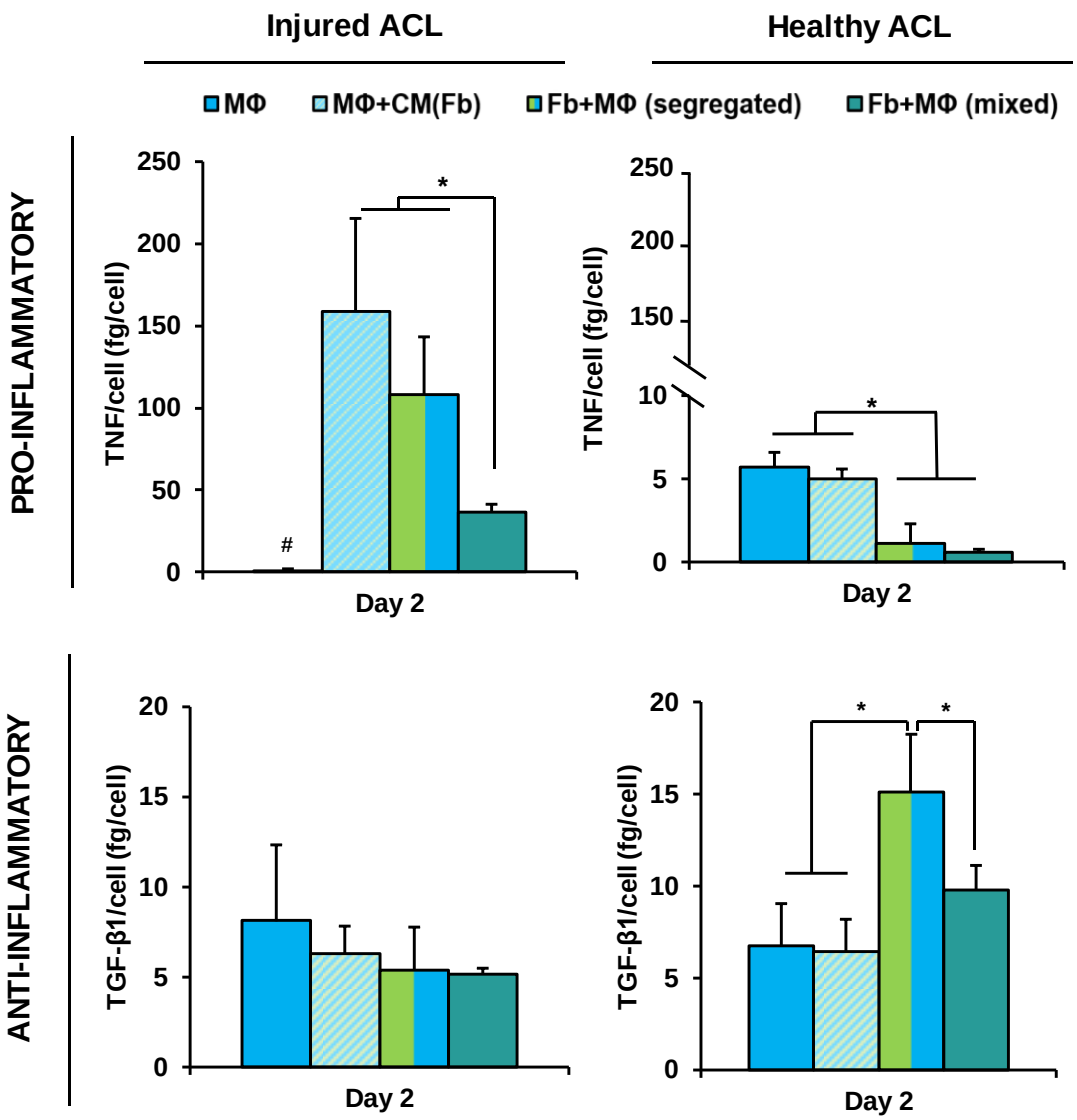

Figure 2.11: Fibroblast-Macrophage Interactions: Effects of Fibroblast Injury State on Macrophage Response. For macrophages co-cultured with fibroblasts isolated from an injured ACL, TNF per cell was lowest for macrophage single-culture controls compared to all other groups. TNF per cell was greater for macrophages in fibroblast-conditioned medium and in segregated co-culture compared to mixed co-culture. There were no differences in TGF-β1 per cell between groups. For macrophages co-cultured with fibroblasts isolated from a healthy ACL, TNF per cell was lower in mixed and segregated co-culture compared to macrophage single-culture controls, with no differences in TNF per cell between macrophage single-culture and macrophages in fibroblast-conditioned medium. TGF-β1 per cell was elevated in segregated co-culture compared to all other groups at this time point. n=5, * significant difference between groups, # significantly different from all groups, p<0.05.

CHAPTER 3: THE ROLE OF MESENCHYMAL STEM CELLS IN CONNECTIVE TISSUE INJURY

3.1 Introduction

In *Chapter 2*, the interactions between native tissue fibroblasts and infiltrating macrophages following connective tissue injury were assessed. The goal of this chapter is to identify the role that MSC play following injury and during connective tissue healing. To this end, three studies were performed. In study 1, the interactions between native ligament fibroblasts and MSC during both early- and late-stage healing were studied. In study 2, the interactions between MSC and macrophages to assess the immunomodulatory role that MSC play during inflammation and tissue healing were examined. In study 3, the heterotypic interactions between MSC, macrophages, and fibroblasts in tri-culture were assessed, in order to better understand the interactions between all three cell types throughout the healing process, and to elucidate the role of MSC in promoting repair and regeneration.

3.1.1 Background and Motivation

During healing, MSC are observed to naturally home, or migrate, to injured tissue to help with tissue regeneration. While MSC are capable of differentiating into a variety of mesenchymal lineages, research has shown that these cells are valuable during healing due to their capacity for trophic signaling, which serves to enhance the cell response and promote healing activities by native tissue cells. The goal of the first study in this chapter is to examine the effects of cellular interactions between ligament fibroblasts and MSC on the response of each cell type, in terms of proliferation, matrix synthesis, and phenotypic response. The ideal co-culture model for understanding the cellular communications between these two cell types must be able to recapitulate the homotypic and heterotypic interactions that these cells experience *in vivo* following the migration of MSC to the injury site. Toward this goal, a co-culture system will be developed for studying the effects of direct cell contact, as well as paracrine signaling, on stem cell behavior. Additionally, physiologically relevant cell ratios will be utilized to mimic the cell population at the injury site over time, by imitating both early-stage ligament healing, when the concentration of MSC is lower, and late-stage repair, as the total number of MSC present at the injury site increases.

While macrophage-driven inflammation is important during connective tissue repair, an excessive inflammatory response can be associated with poor clinical outcomes, and can result in impaired wound healing, as well as non-healing wounds(209). Therefore, it is important that this process is modulated, to improve connective tissue healing and allow for functional tissue repair. As mentioned previously, MSC are

believed to play an important role in the wound healing process following homing to the injury site. One possible mechanism through which MSC aid in healing could be through modulation of the inflammatory response. Multiple studies have shown that MSC demonstrate immunomodulatory properties, both *in vitro* and *in vivo*(5). Early studies on the immunosuppressive potential of MSC show that cells derived from human(54-57), baboons(58), and mice(59;60) are all capable of suppressing T cell proliferation and inflammatory cytokine secretion, as well as the proliferation and cytokine release of other inflammatory cell types, including B cells, antigen-presenting cells, and natural killer cells. Our goal is to determine the effects of MSC on the inflammatory response caused by infiltrating macrophages during connective tissue healing, and to uncover the mechanisms behind MSC immunomodulation. Therefore, the objective of the second study in this chapter is to utilize a co-culture model to examine the effects of heterotypic interactions between macrophages and MSC on macrophage inflammatory response and activation in terms of cytokine secretion and phenotype, as well as MSC response in terms of proliferation, matrix synthesis, and phenotypic response.

While the previous three studies discussed in **Aim 1** are intended to identify the heterotypic cellular interactions between 1) macrophages and fibroblasts, 2) MSC and fibroblasts, and 3) MSC and macrophages, these models do not take into account the cross-talk that may occur among all three cell types during the inflammatory and repair process *in vivo*. Therefore, it is important to expose all three cell types to one another in order to better mimic the physiological cellular environment. In previous work by Manning *et al*., it was observed that, while exposure of murine tendon fibroblasts to pro-inflammatory cytokines released by M1 macrophages resulted in an upregulation of pro-inflammatory factors and matrix degradation factors, the addition of adipose-derived MSC to the co-culture model was able to suppress the effects of M1 macrophages on fibroblast inflammatory response(210). This study suggests the importance of tri-culture models in more fully understanding the heterotypic cellular interactions that take place in the complex cellular environment *in vivo*. The goal of the third study in this chapter is to examine the roles that MSC play in both modulating fibroblast-macrophage interactions, through development of a tri-culture model that better mimics the complex spatial and temporal interactions that occur *in vivo* following injury, compared to the co-culture models used in the previous three studies.

3.1.2 Objectives

The objective of this study is to assess the interactions between MSC and both native ligament fibroblasts and infiltrating macrophages to better understand the role of MSC in modulating the cellular microenvironment following connective tissue injury and promoting tissue repair and regeneration. It is hypothesized that 1) MSC-fibroblast interactions will result in increased proliferation during co-culture models of early-stage healing, while late-stage healing models will result in increased matrix synthesis, and 2) interactions between macrophages and MSC will suppress macrophage activation in both co-culture and tri-culture.

3.2 Materials and Methods

3.2.1 Cells and Cell Culture

3.2.1.1 Human Mesenchymal Stem Cell Isolation and Culture

Human mesenchymal stem cells were isolated from bone marrow aspirate of a 21 y/o male donor, obtained commercially (Lonza). Briefly, the aspirate was centrifuged on a discontinuous Percoll gradient to remove blood cells. Supernatant was then removed and mixed with F/S DMEM and plated on tissue culture plastic. Medium was changed the following day to remove non-adherent cells. Adherent cells were assumed to be MSC and were passaged once prior to use or cryopreservation. For cryopreservation, cells were frozen in cryomedium containing F/S DMEM, 20% FBS, and 10% DMSO (Sigma-Aldrich). Cells were thawed at P2 and maintained in culture with F/S DMEM containing 10% FBS and 1% P/S, without other antibiotics.

3.2.1.2 Human Anterior Cruciate Ligament Cell Isolation and Culture

Human ACL fibroblasts were derived from explant culture of tissues obtained from a patient (male, aged 21) undergoing ACL reconstruction surgery. Briefly, the tissue samples were rinsed in PBS, plated in tissue culture dishes, and maintained in DMEM supplemented with 10% FBS, 1% non-essential amino acids, 1% P/S, 0.1% Amp-B and 50 µg/mL G/S. The cells from the first migration were subsequently discarded, and the tissue was re-plated in fresh fully supplemented medium. Only cells obtained from the second and third migrations were used in this study because this method has been shown to yield a relatively homogenous fibroblast population.

3.2.1.3 Human THP-1 Culture and Differentiation Toward M0 Macrophages

Human THP-1 cells were obtained commercially (ATCC, TIB202) and maintained in continuous culture in non-tissue culture treated flasks (25 cm^2, Nunc™) with F/S RPMI-1640 containing 10% FBS, 1% P/S, and 0.05 mM 2-ME. Medium was replaced every 3-4 days. Briefly, cells suspensions were removed from culture dishes once every 3-4 days and cells were centrifuged at 5000 rpm for 5 minutes. Supernatant was aspirated and cells were resuspended in fresh RPMI-1640 at a density of $4x10^5$ cells/mL.

For differentiation of THP-1 monocytes into M0 macrophages, THP-1 in suspension were centrifuged at 5000 rpm for 5 minutes. The supernatant was aspirated and cells were resuspended in F/S RPMI-1640 supplemented with 100 nM PMA at 37°C for 48 hours. After 48 hours, PMA+ medium was removed, cells were rinsed one time with PBS, and medium was replaced with F/S RPMI-1640. Cells were allowed to rest for 72 hours before co-culture, in order to allow for adequate cell spreading and differentiation(191).

3.2.2 Fibroblast-MSC Co-Culture

3.2.2.1 Effects of Fibroblast-MSC Co-Culture Ratio on Cell Response

In order to mimic the cell ratios of native ligament cells and infiltrating stem/progenitor cells during early- and late-stage healing, fibroblasts and MSC were mixed at a 10:1 (91,000:9,100) or 1:1 (50,000:50,000) ratio and seeded at a density of $1x10^4$ cells/cm^2 in 6-well plates in 1 mL of F/S DMEM ($1x10^5$ cells/well total). After seeding, an additional 2 mL of fresh F/S DMEM was added to each well. Fibroblast single-culture and MSC-single culture groups were seeded as controls for comparison. Medium was changed every 2-3 days.

3.2.2.2 Effects of Paracrine Signaling on Cell Response

To assess the role of paracrine signaling on each cell type individually, MSC and fibroblast single-cultures were fed conditioned medium collected from fibroblast-MSC co-culture. Briefly, 1:1 co-culture samples were grown in tandem with fibroblast-only and MSC-only single-cultures. On feeding days, medium was collected from 1:1 co-culture samples, centrifuged at 500 g to remove any potential cells or cell debris, and mixed with an equal amount of fresh F/S DMEM. 3 mL of the co-culture-conditioned medium was added

to each well, and medium was changed every 2-3 days. Single-cultures of MSC only and fibroblasts only in fresh F/S DMEM served as controls.

3.2.2.3 Live Cell Tracking

Live cell tracking (*n*=3) was accomplished using CellTracker membrane dyes, following the manufacturer's protocol. Briefly, medium was removed from cell culture dishes and cells were incubated in 0.25% trypsin/1 mM EDTA for 3 minutes. Trypsin was neutralized using fresh F/S DMEM and cell suspensions were then collected and centrifuged at 5000 rpm for 10 minutes. For both cell types, supernatant was aspirated from the cell pellets, and cells were resuspended in fresh F/S DMEM. Cells were counted using a hemocytometer, and resuspended at 1 million cells/mL. A total of 5 µL of CellTracker dye (DiO for fibroblasts or DiD for MSC) was added per mL of cell suspension, and the suspension was incubated at 37ºC and 5% CO_2 in the dark for 20 minutes. A volume of 10 mL fresh F/S DMEM was added to cell suspensions and cells were centrifuged at 5000 rpm for 5 minutes. Supernatant was aspirated and cells were resuspended in 5 mL fresh medium. This process was repeated two more times for a total of three washes.

Prior to imaging, culture medium was removed and replaced with 1X PBS. Samples were imaged using confocal microscopy (Olympus Fluoview FV1000) at excitation wavelengths of 488 nm to visualize fibroblasts stained with DiO (green), and 568 nm for MSC stained with DiD (red).

3.2.3 Macrophage-MSC Co-Culture

3.2.3.1 Co-Culture Medium Optimization

Prior to co-culture studies, a mixed co-culture of MSC and THP-1-derived M0 macrophages were grown in F/S DMEM, F/S RPMI-1640, and a 1:1 mixture of F/S DMEM and F/S RPMI-1640. Single-cultures of MSC only and macrophages only served as controls. All groups were cultured for up to 7 days, and cell proliferation and viability were assessed using the PicoGreen dsDNA assay at days 1, 3, and 7.

3.2.3.2 Mixed Co-Culture Model

Following co-culture medium optimization, THP-1-derived M0 macrophages and MSC were grown in co-culture, with single-cultures of MSC only and macrophages only serving as controls. Briefly, THP-1 monocytes were seeded at a density of $6x10^4$ for co-culture wells or $1.2x10^5$ cells/well for single-culture

controls and incubated in F/S RPMI-1640 supplemented with 100 nM PMA (PMA+ medium) at 37°C for 48 hours. After 48 hours, PMA+ medium was removed and replaced with F/S RPMI-1640. Cells were allowed to rest for 72 hours before co-culture. Following 72 hours, at a seeding efficiency of ~30%, $1.5x10^4$ cells were observed to adhere to co-culture wells, while $3x10^4$ cells attached to single-culture control wells. For co-culture, on day 5, MSC were added to macrophage culture at a density of $1.5x10^4$ cells/cm^2 for co-culture, with $3x10^4$ cells/cm^2 seeded per well for single-culture controls. All groups were fed with a 1:1 mixture of F/S DMEM:F/S RPMI-1640, which was determined to be the optimal co-culture medium from optimization studies.

3.2.3.3 Conditioned Medium Model

To test paracrine effects, MSC were fed a 1:1 mixture of F/S DMEM and medium from macrophage single-culture, while macrophages were fed a 1:1 mixture of F/S RPMI-1640 and medium from MSC. Briefly, for MSC-conditioned medium, MSC were seeded at a density of $3x10^4$ cells/cm^2 in a 48-well plate in F/S DMEM for 3 days. On day 3, the medium from these wells was collected and centrifuged at 5000 g for 10 minutes to remove any cells or other debris from the supernatant. The supernatant was then collected and mixed 1:1 with fresh F/S RPMI-1640. This medium was immediately used to feed macrophage single-cultures following the 5-day differentiation period described previously. For macrophage-conditioned medium, THP-1 monocytes were seeded at a density of $1.2x10^5$ cells/well in 48-well plates and differentiated in PMA+ RPMI-1640 at 37°C for 48 hours. After 48 hours, PMA+ medium was removed and cells were rinsed one time with PBS. Medium was replaced with F/S RPMI-1640 medium, and cells were cultured for 3 days. On the third day, medium from these wells was collected and centrifuged at 500 g for 10 minutes to remove any cells or other debris from the supernatant. The supernatant was then collected and mixed 1:1 with fresh F/S DMEM. Medium was then immediately used to feed MSC single-cultures.

3.2.3.4 Segregated Co-culture Model

To assess the effects of paracrine signaling, MSC and macrophages were grown in segregated co-culture. Briefly, Thermanox™ coverslips (13-mm diameter) were cut in half and halves were placed into individual wells of 24-well plates. To achieve a final density of $3x10^4$ cells/cm^2 ($2 x10^4$ cells/coverslip half), $6x10^4$ MSC or $4.8x10^5$ THP-1 were seeded per well. Following day 5 of the THP-1 differentiation period,

one MSC-seeded and one macrophage-seeded coverslip were placed opposite one another in a single well in a 24-well plate. A solution of 4% agarose VII in PBS was heated to 120°C, allowed to cool, and used as a glue to attach coverslips to the bottom of the well. Following gelation of agarose, 1 mL of a 1:1 mixture of F/S DMEM and F/S RPMI-1640 was added to each well.

3.2.4 Tri-Culture

3.2.4.1 Tri-Culture Model

For tri-culture studies, Thermanox™ coverslips (13 mm diameter) were cut in half and halves were placed into individual wells of 24-well plates. To achieve a final density of $3x10^4$ cells/cm^2 ($2x10^4$ cells/coverslip half), $6x10^4$ fibroblasts, $6x10^4$ MSC, or $4.8x10^5$ THP-1 were seeded per well. Following day 5 of the THP-1 differentiation period, one MSC-seeded, one Fb-seeded, and one THP-1-seeded coverslip were placed within a single well of a 12-well plate. A solution of 4% agarose VII in PBS was heated to 120°C, allowed to cool, and used as a glue to attach coverslips to the bottom of the well. Following gelation of agarose, 1 mL of a 1:1 mixture of F/S DMEM and F/S RPMI-1640 was added to each well. Fibroblast-macrophage segregated co-culture samples served as a positive control, while single-cultures of fibroblasts only, MSC only, and macrophages only were used as negative controls.

3.2.4.2 Effects of Timing of MSC Delivery on Cell Response

To assess the effects of the timing of MSC delivery on macrophage response and fibroblast activity, MSC were added to tri-culture on either day 0 or day 2 of tri-culture. Briefly, using the tri-culture model described above, MSC, fibroblasts, and THP-1-derived macrophages were cultured on Thermanox™ coverslips, and were either all added to the same well on day 0, or fibroblasts and macrophages were added to the same well on day 0, with MSC added on day 2.

3.2.5 Live/Dead Cell Viability

Cell viability (n=3) was visualized using Live/Dead staining (Molecular Probes), following the manufacturer's suggested protocol. Samples were imaged using confocal microscopy (Olympus Fluoview FV1000) at excitation wavelengths of 488 nm (live) and 568 nm (dead).

3.2.6 Cell Proliferation

Cell proliferation (*n*=5) was determined by measuring total DNA content using the PicoGreen dsDNA assay (Invitrogen) following the manufacturer's protocol. Samples were rinsed twice in PBS and stored in 500 µl of 0.1% Triton X (Sigma-Aldrich) at -30°C. Immediately before the analysis, samples were thawed and homogenized followed by sonication with a cell sonicator (Microson XL-2000) at 5 W for 15 seconds. Fluorescence was measured using a Tecan microplate reader with an excitation wavelength of 485 nm and an emission wavelength of 535 nm. A conversion factor of 8 pg DNA/cell was used to determine cell number.

3.2.7 Collagen Production

Collagen production (*n*=5) was quantified using a modified hydroxyproline assay(199). Samples were digested in a buffered papain solution prior to analysis. For digestion, samples were vacuum dried overnight using the Centrivap concentrator (Labconco). Samples were then digested for 20 hours at 65ºC with 20 µL/mL papain (Sigma-Aldrich), buffered in 0.1 M sodium acetate, 10 mM cysteine HCl, and 50 M EDTA. For the assay, digested samples were concentrated by drying 125-250 µL of sample overnight in the Centrivap concentrator. Samples were resuspended in 50 µL of 2 N NaOH and autoclaved for 25 minutes. 450 µL of Chloramine T Reagent (1.27 g chloramine T in 50% isopropanol brought to 100 mL with acetate-citrate buffer) was added to the samples, which were then allowed to incubate for 25 minutes at room temperature. 500 µL of Ehrlich's reagent (15g p-dimethylaminobenzaldehyde in 100 mL (2:1) isopropanol:perchloric acid) was subsequently added, and the samples incubated at 65ºC for 20 minutes. The absorbance at 555 nm was read using a Tecan microplate reader. Total collagen was determined using a standard curve generated using a collagen standard (Sigma-Aldrich).

The acetate-citrate buffer for the chloramine T solution consisted of 30 g sodium acetate trihydrate, 11.5 g citric acid, 3 mL acetic acid, and 8.5 g NaOH, dissolved in 125 mL of distilled water. The solution was brought to a pH of 6.5 using 1N NaOH or 1N HCl, and then brought to a final volume of 250 mL.

3.2.8 Expression of Ligament-Related Markers

Gene expression (*n*=5) was analyzed using qRT-PCR. Samples were rinsed twice with PBS and stored in Trizol (Invitrogen). RNA was isolated using the chloroform/Trizol extraction method. The extracted RNA pellet was dissolved in 150 µL DEPC H_2O (Ambion). First-strand cDNA was synthesized using 50 µM oligo$(dT)_{20}$ primer, 10 mM dNTP mix, and 8 µL of extracted RNA. cDNA synthesis was accomplished using 5X RT buffer, DTT, 40 U/µL RNaseOUT, and 200 U/µL SuperScript III RT. The cDNA product was subsequently amplified and quantified through real-time PCR using SYBR Green Supermix (Invitrogen). GAPDH served as the house-keeping gene. All genes were amplified for 50 cycles in a thermocycler (iCycler iQ Real-Time PCR Detection System, BioRad). See *Table 3.1* for primer sequences used and amplicon sizes. Normalized expression levels were calculated based on the difference between threshold cycles of the gene of interest and GAPDH.

Table 3.1: Primer Sequences for Gene Expression

Gene	Sense	Anti-Sense	Blast product Size (bp)
GAPDH	5'- GGCGATGCTGGCGCTGAGTA-3'	5'-ATCCACAGTCTTCTGGGTGG-3'	306
Collagen I	5'-TGGTCCACTTGCTTGAAGAC-3'	5'-ACAGATTTGGGAAGGAGTGG-3'	118
Collagen III	5'-GGCTACTTCTCGCTCTGCTT-3'	5'-CATATTTGGCATGGTTCTGG-3'	130
Fibronectin	5'-TTGAACCAACCTACGGATGA-3'	5'-AAATGACCACTTCCAAAGCC-3'	137
Scleraxis	5'-CAGCGGCACACGGCGAAC-3'	5'-CGTTGCCCAGGTGCGAGATG-3'	163
Tenascin-C	5'-TGCCCATTACAGGAGGTACA-3'	5'-CACTTTCCTCAAAGCCCTTC-3'	132

3.2.9 Cytokine Release

Levels of pro- (TNF, IL-1β) and anti-inflammatory (IL-10, TGF-β1) cytokines (*n*=5) were assessed via ELISA (R&D Systems) according to the manufacturer's protocol. Briefly, supernatants from cell culture were collected after 48 hours and stored at -30°C. On the day of analysis, samples were thawed and added directly to assay diluent in a prepared plate and incubated for two hours at room temperature prior to solution removal. Each well was washed three or four times before incubation with either TNF, IL-1β, or IL-10 conjugate for 1 hour at room temperature, or TGF-β1 conjugate for two hours at room temperature. The conjugate was then removed, the plate was washed three or four times, and the substrate solution was added to each well and allowed to react in the dark. The stop solution was added after 20 minutes for TNF, IL-1β, or IL-10 or 30 minutes for TGF-β1, and the absorbance was measured using a microplate reader

Sample absorbance was measured using a microplate reader (Tecan) at 450 nm and 570 nm, and the difference was used to calculate cytokine concentration. Base level concentrations of each cytokine in acellular culture medium were used as negative controls.

3.2.10 Statistical Analysis

Results are reported as mean ± standard deviation, with n equal to the number of replicates per group. Statistical analyses were performed with JMPIN (4.0.4, SAS Institute, Inc.). Sample sets were checked for normality and equal variance, followed by performance of a corrected t-test. The Tukey-Kramer post-hoc test was used for all pair-wise comparisons, and significance was attained at $p<0.05$.

3.3 Results

3.3.1 Fibroblast-MSC Co-Culture: Cell Tracking, Viability, and Proliferation

Live Cell Tracking: Fluorescent images in *Figure 3.1* show that cells can be imaged and tracked over time, with fibroblasts shown in green and MSC shown in red. By day 14 in the 10:1 and 1:1 co-culture groups, a population of yellow-stained cells is visible. FACS results show that this color is due to a double-positive staining on these cells, which appear to have both DiO and DiD staining on their membranes, indicative of cell-cell contact over time (*Figure 3.2*). *Cell Viability:* Live/dead images show that cells remain viable in all groups over 21 days (*Figure 3.2*). *Cell Proliferation:* Total cell number is greater in 1:1 fibroblast:MSC co-culture compared to 10:1 co-culture and fibroblast-only single-culture at day 21 (*Figure 3.3*). Fold change in cell number is greatest in 10:1 co-culture compared to all other groups at this time point, and fold change is greater in 1:1 co-culture compared to MSC single-culture at day 21 (*Figure 3.3*).

3.3.2 Fibroblast-MSC Co-Culture: Collagen Production

Total collagen increased over time in all groups except for fibroblast-only controls (*Figure 3.4*). Total collagen is greater for fibroblast single-culture compared to all other groups at day 7 and is greater than both 10:1 and 1:1 co-culture groups at day 14. These differences are no longer observed by day 21 (*Figure 3.4*). Collagen per cell was greatest for fibroblast single-culture at days 1 and 7 compared to all other groups, with no observed differences between groups at days 14 (*Figure 3.4*). Collagen synthesis per cell was greater in the 10:1 fibroblast:MSC co-culture group compared to 1:1 co-culture by day 21 (*Figure 3.4*).

3.3.3 Fibroblast-MSC Co-Culture: Expression of Ligament-Related Markers

There were no observed differences in the expression of ligament-related markers in co-culture when compared to single-culture controls after 14 days (*Figure 3.5*).

3.3.4 Fibroblast-MSC Co-Culture: Effects of Paracrine Signaling on Individual Cell Response

Cell Viability: Cells remain viable in all groups over the 21-day study (*Figure 3.7*). *Cell Proliferation:* Total cell number was significantly lower for fibroblasts in co-culture-conditioned medium compared to fibroblast single-culture at days 14 and 21, with a significantly lower fold change in cell number at day 21 (*Figure 3.8*). Similar results were observed for MSC, with significantly fewer total MSC in co-culture-conditioned medium compared to MSC single-culture by day 21, and a significantly lower fold change in cell number for MSC in co-culture-conditioned medium at day 21 compared to MSC single-culture (*Figure 3.8*). *Collagen Production:* Total collagen was significantly lower for fibroblasts in co-culture-conditioned medium compared to fibroblast single-culture controls at days 7 and 14 (*Figure 3.9*). This difference was no longer observed by day 21. Conversely, greater total collagen was observed for MSC in co-culture-conditioned medium at days 7 and 21 compared to MSC single-culture. Collagen per cell was also greater for MSC in co-culture-conditioned medium compared to MSC single-culture at day 21 (*Figure 3.9*). *Expression of Ligament-Related Markers:* There were no observed differences in the expression of ligament-related markers between groups after 14 days (*Figure 3.10*).

3.3.5 Macrophage-MSC Co-Culture: Co-Culture Medium Optimization

Analysis of cell proliferation over 7 days shows that the choice of culture medium has no effect on cell proliferation or viability for any group, as there were no significant differences in cell number between groups at any time point (*Figure 3.12*). Therefore, for comparison to the results in *Chapter 2*, as well as for ease of translation to tri-culture, a 1:1 mixture of F/S DMEM and F/S RPMI-1640 was used for all groups.

3.3.6 Macrophage-MSC Co-Culture: Cell Proliferation

Cell number significantly increased over time for MSC single-culture and mixed co-culture groups only *(Figure 3.13*). By day 7, cell number was significantly lower for MSC in macrophage-conditioned medium compared to both MSC single-culture and mixed co-culture (*Figure 3.13*). Analysis of fold change in cell number reveals that, while there were no differences in fold change between MSC in macrophage-

conditioned medium and MSC single-culture controls, fold change in cell number was significantly greater in mixed co-culture compared to all other groups (*Figure 3.13*). Cell number for macrophages in MSC-conditioned medium, as well as macrophage single-culture were significantly lower than all other groups at day 7 (*Figure 3.13*), which is expected because of the short lifespan of THP-1 following PMA differentiation(191).

3.3.7 Macrophage-MSC Co-Culture: Collagen Production

There was no significant difference in total collagen between MSC single-culture, MSC in macrophage-conditioned medium, and mixed co-culture at either day 2 or day 7. Total collagen in these groups did not change over time (*Figure 3.14*). Total collagen was greatest in segregated co-culture at day 2 compared to all other groups, but this difference was no longer observed by day 7 (*Figure 3.14*). Total collagen in this group did not change over time. Total collagen and collagen per cell were significantly greater for macrophages in MSC-conditioned medium compared to macrophage single-culture by day 7 (*Figure 3.14*).

3.3.8 Macrophage-MSC Co-Culture: Cytokine Secretion

Pro-Inflammatory Cytokines: TNF per cell was lower in segregated co-culture compared to macrophage single-culture and macrophages in MSC-conditioned medium at day 2 (*Figure 3.15*). IL-1β release per cell was greatest for macrophages in MSC-conditioned medium compared to all other groups, with no difference in IL-1β per cell between mixed and segregated co-cultures and macrophage single-culture controls (*Figure 3.15*). *Anti-Inflammatory Cytokines:* IL-10 per cell was greater for macrophages in MSC-conditioned medium and in mixed co-culture groups compared to macrophage single-culture (*Figure 3.15*). At day 2, IL-10 per cell was greater for MSC in macrophage-conditioned medium compared to MSC single-culture (*Figure 3.15*). IL-10 per cell was also higher in mixed co-culture compared to segregated co-culture. TGF-β1 per cell was lower for macrophage single-culture and macrophages in MSC-conditioned medium compared to all other groups at day 2, with no observed difference in TGF- β1 per cell between co-culture groups, MSC single-culture, and MSC in macrophage-conditioned medium (*Figure 3.15*).

3.3.9 Tri-Culture: Cytokine Secretion

Pro-Inflammatory Cytokines: Total TNF and TNF per cell were lower in tri-culture compared to fibroblast-macrophage co-culture at day 2, with no significant difference in either total TNF or TNF per cell between tri-culture and M0 macrophage single-culture controls on day 2 (*Figure 3.17*). Total IL-1β release was similar between tri-culture, fibroblast-macrophage co-culture, and macrophage single-culture. Total IL-1β in all three groups was significantly greater than total IL-1β for fibroblast and MSC single-cultures. However, on a per cell basis, IL-1β per cell was lower in tri-culture compared to fibroblast-macrophage co-culture at day 2 (*Figure 3.17*). *Anti-Inflammatory Cytokines*: There were no observed differences in total TGF-β1 between groups. However, TGF-β1 per cell was lower in tri-culture compared to macrophage single-culture at day 2, with no differences observed between co-culture and tri-culture at this time point (*Figure 3.17*). Total IL-10 was significantly greater in fibroblast-macrophage co-culture and tri-culture compared to macrophage single-culture at day 2. Levels of IL-10 per cell was greater in co-culture compared to macrophage single-culture and tri-culture at this time point (*Figure 3.17*).

3.3.10 Tri-Culture: Effects of Timing of MSC Delivery on Cell Response

Pro-Inflammatory Cytokines: Total TNF and TNF per cell were lower in delayed tri-culture groups compared to tri-culture after 2 days. There were no differences observed in total IL-1β or IL-1β per cell between tri-culture and delayed tri-culture groups (*Figure 3.19*). *Anti-Inflammatory Cytokines*: Total IL-10 and IL-10 per cell were lower in delayed tri-culture groups compared to tri-culture after 2 days. There were no observed differences in the total release of TGF-β1 or TGF-β1 per cell between tri-culture and delayed tri-culture (*Figure 3.19*).

3.4 Discussion

In this chapter, a series of co-culture models, as well as a tri-culture model, were developed for assessment of the interactions between 1) fibroblasts and MSC during early and late-stage connective tissue healing, 2) MSC and macrophages during inflammation and repair, and 3) all three cell types throughout connective tissue injury and the healing process. Through this series of studies, it was determined that MSC interactions with fibroblasts and macrophages following injury play a number of important roles in the healing microenvironment.

In fibroblast-MSC co-culture, while there was an observed increase in total cell number in 1:1 co-culture compared to all other groups by day 21, assessment of fold change in cell number over time indicates that cell proliferation rate is enhanced in both 10:1 and 1:1 co-culture compared to fibroblast and MSC single-cultures at this time point. Cell sorting data from FACS analysis at day 21 reveals that close to two thirds of the cells in 1:1 co-culture are fibroblasts by this time point, suggesting that increased cell numbers in co-culture are likely a result of enhanced fibroblast proliferation rate when these cells are in direct contact with MSC. Similar results were observed by Proffen *et al*., which show that ACL fibroblast proliferation rate is increased when in contact with porcine MSC isolated from the retropatellar fat pad(62). Still, this effect was not seen for fibroblasts in co-culture with PBMC in this same study, suggesting that this response may be dependent on the tissue source of MSC.

Total collagen synthesis was lower in co-culture compared to fibroblast single-culture at all time points. Based on conditioned medium studies, this may be due to decreased fibroblast collagen synthesis when in contact with MSC. This is different than results described by Proffen *et al*., which show that procollagen synthesis by fibroblasts is enhanced when co-cultured with ADSC. These observed differences could however be due to MSC cell source, as results from this study also show that for fibroblasts in co-culture with PBMC, no effect on collagen synthesis is observed. Interestingly, while fibroblast collagen synthesis is lower in MSC-conditioned medium, total collagen produced by MSC in fibroblast-conditioned medium is greater that MSC single-culture controls at days 7 and 21, suggesting that co-culture may lead to enhanced collagen synthesis by MSC. In work by Proffen *et al*., they observed a similar increase in collagen synthesis and collagen I gene expression by ADSC in co-culture with ACL fibroblasts, supporting these findings(62).

In terms of the immunoregulatory role that MSC play in the connective tissue injury microenvironment, MSC-macrophage co-culture studies show that the secretion of pro-inflammatory cytokines, including TNF and IL-1β, in MSC-macrophage co-culture is similar to cytokine release profiles observed for M0 macrophage single-culture controls. This is true in both the mixed and segregated co-culture groups, as well as for macrophages in MSC-conditioned medium, suggesting that MSC-macrophage interactions via direct cell contact, paracrine signaling, or unidirectional signaling do not result in M1 activation by macrophages. Alternatively, for macrophages in mixed co-culture and macrophages in

MSC-conditioned medium, IL-10 secretion per cell is enhanced compared to macrophage single-culture, indicative of M2 polarization by a population of these cells. These results are supported by findings by Manning *et al*., which show that MSC are able to promote a switch of macrophages from an M1 to an M2 phenotype in co-culture(91). Also, paracrine signaling by MSC resulted in increased collagen production by macrophages in MSC-conditioned medium. It has been shown previously that macrophages are capable of secreting extracellular matrix components, including fibronectin, types VI and VIII collagen(211). As type VI collagen secretion serves as a marker for a non-destructive, matrix-conserving macrophage phenotype, the increased collagen production observed in MSC-conditioned medium further supports a shift of M0 macrophages toward an M2 phenotype in this group.

Interestingly, in addition to enhanced macrophage secretion of IL-10 in co-culture and in MSC-conditioned medium, IL-10 release by MSC in macrophage-conditioned medium is increased compared to MSC single-culture controls. Previous work by Choi *et al*. suggests that IL-10 expression by MSC can have an immunomodulatory role in an inflammatory microenvironment(212). Additionally, Qu *et al*. have shown that secretion of IL-10 by MSC may be the mechanism through which MSC modulate immune response, as it was shown that IL-10 secretion by MSC resulted in decreased differentiation of Th17 cells(213).

Further, total cells in mixed co-culture were greater than MSC in macrophage-conditioned medium and segregated co-culture at day 7. This corresponds to a greater fold change in cell number in mixed co-culture compared to all other MSC-containing groups at day 7. As THP-1 have been shown not to proliferate following PMA differentiation(191), it is likely that this observed difference is due to a change in the proliferative response of MSC in direct contact with macrophages. Therefore, these results suggest that macrophage-driven inflammation results in enhanced proliferation by MSC, and this response is cell contact-dependent, as the increased fold change in cell number was observed in mixed co-culture and not segregated co-culture. While studies have not yet been performed which assess the interactions between MSC and M0 macrophages in co-culture, work by Freytes *et al*. shows that MSC proliferation is enhanced by M2-activated macrophages(196), while MSC viability was decreased in co-culture with M1 macrophages. These results provide further evidence that M0 macrophages in co-culture do indeed differentiate toward an M2, anti-inflammatory phenotype, resulting in enhanced MSC proliferation over 7 days in co-culture. Still, this proliferative effect is not observed in segregated co-culture, suggesting that

direct cell contact is necessary in order to observe this effect. Alternatively, it may be possible that the effect of M2 polarized macrophages on MSC proliferation is slowed in segregated co-culture, and might be observed over longer culture periods.

Finally, in tri-culture, it was observed that the addition of MSC to macrophage-fibroblast co-culture results in a significant decrease in the release of both pro- and anti-inflammatory cytokines. Specifically, total TNF, as well as TNF, IL-1β, TGF-β1 and IL-10 per cell were significantly lower in tri-culture compared to macrophage-fibroblast co-culture after 48 hours. This suggests that macrophage activation is inhibited by the presence of MSC, resulting in fewer M1 and M2 polarized macrophages in tri-culture compared to co-culture. In tri-culture studies by Manning *et al*., in which murine macrophages, tendon fibroblasts, and MSC are grown in a combination mixed and segregated model, MSC are able to promote a switch of macrophages from an M1 to an M2 phenotype(91).

Interestingly, the time at which MSC are added to fibroblast-macrophage co-culture also affects macrophage response, suggesting that MSC delivery following connective tissue injury may still be effective, even if the delivery is delayed beyond the first few days of tissue injury. Total TNF and TNF per cell, as well as IL-10 and IL-10 per cell, were significantly lower following delayed addition of MSC compared to immediate addition of MSC. This could be due to suppressed activation of both M1 and M2 macrophages or reversion of macrophages back toward an M0 phenotype, following the addition of MSC. Still, it cannot be ruled out that this could be due to decreased activation of macrophages over time, regardless of co- or tri-culture conditions. Further studies will be necessary to assess the cause of these differences.

In summary, the findings of this chapter highlight the important roles that MSC play during the inflammatory and healing response following connective tissue injury. During healing, MSC promote fibroblast proliferation, with a greater effect observed in early- compared to late-stage healing, when the population of MSC present at the injury site is smaller. Additionally, co-culture with MSC led to less collagen production by fibroblasts, while MSC collagen synthesis increased at all time points. This suggests that MSC contribute to the healing response by modulating scar tissue formation by native tissue fibroblasts. Additionally, MSC trophic signaling plays an important role in modulating the inflammatory response, by suppressing macrophage polarization toward both M1 and M2 phenotypes. Toward development of an MSC-based therapy for promoting functional connective tissue regeneration following injury, an MSC

delivery method would be valuable in 1) promoting the proliferative phase of connective tissue healing, 2) minimizing the inflammatory phase, and 3) promoting new tissue formation through synthesis of collagen matrix. Additionally, it may be beneficial to deliver these cells a few days after injury, rather than immediately, as MSC are still effective in mitigating the inflammatory response even during delayed delivery.

3.5 Conclusion

In this chapter, the interactions between MSC and native ligament fibroblasts, as well as macrophages, following connective tissue injury and during inflammation and repair were assessed. Through these studies, it was observed that MSC promote fibroblast proliferation and contribute to tissue repair through enhanced collagen synthesis. Additionally, MSC are capable of modulating the inflammatory response by minimizing M1 polarization and promoting M2 activation of M0 macrophages. Based on the analysis of the release of IL-10 by MSC in macrophage-conditioned medium, it is possible that IL-10 secretion is an underlying mechanism for the anti-inflammatory immune response of macrophages promoted by MSC. In later chapters of this thesis, the role of MSC and MSC-cell interactions on cell response in a more physiologically relevant 3D microenvironment will be assessed.

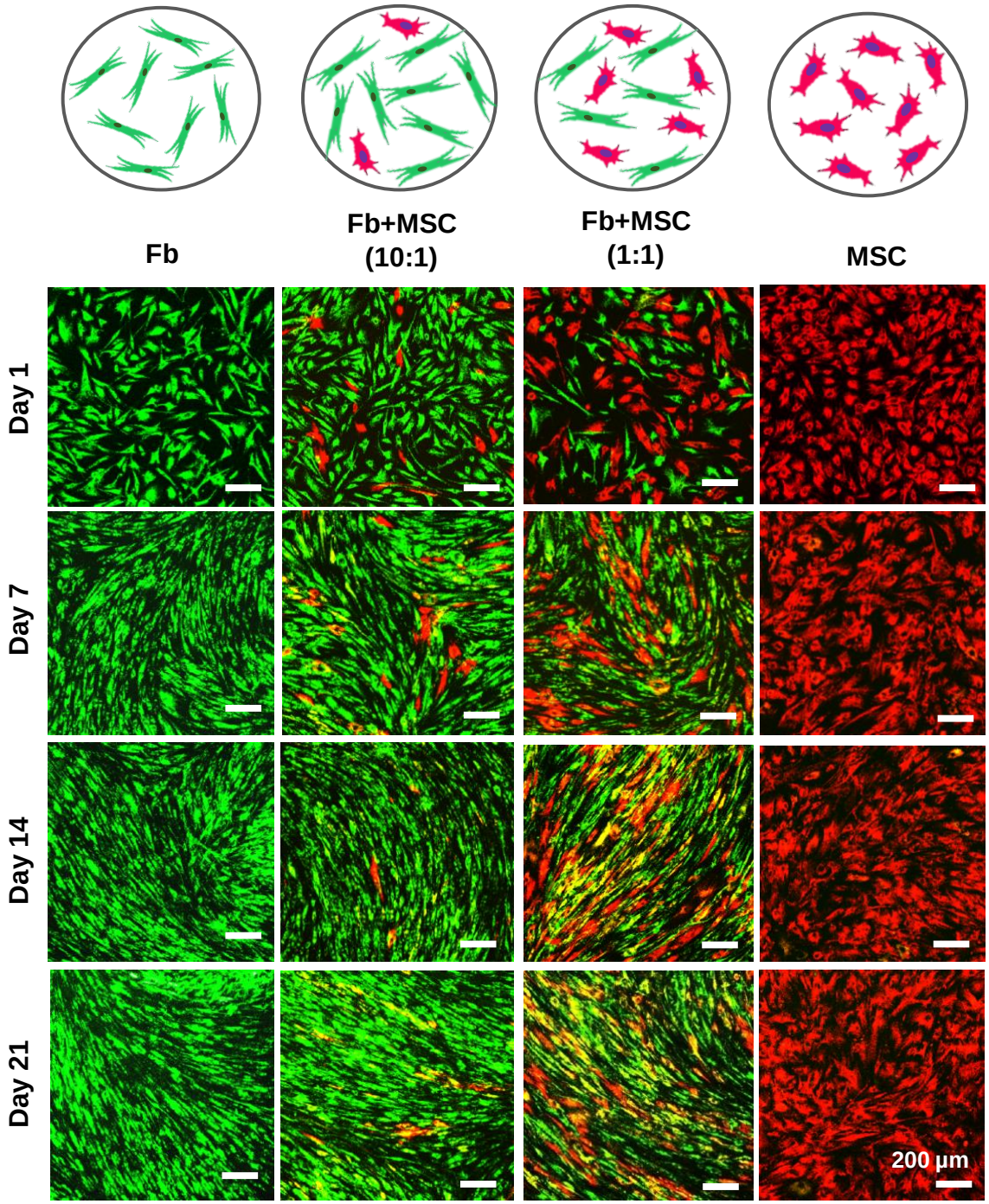

Figure 3.1: Fibroblast-MSC Interactions: Co-Culture Model. Human ACL fibroblasts (Fb) and MSC were seeded in co-culture at 10:1 and 1:1 ratios, mimetic of early- vs. late-stage healing. Single-cultures of fibroblasts and MSC served as controls. Cell membranes were stained using lipophilic membrane dyes, with fibroblasts stained in DiO (green) and MSC stained with DiD (red). *n*=3, scale bar = 200 µm.

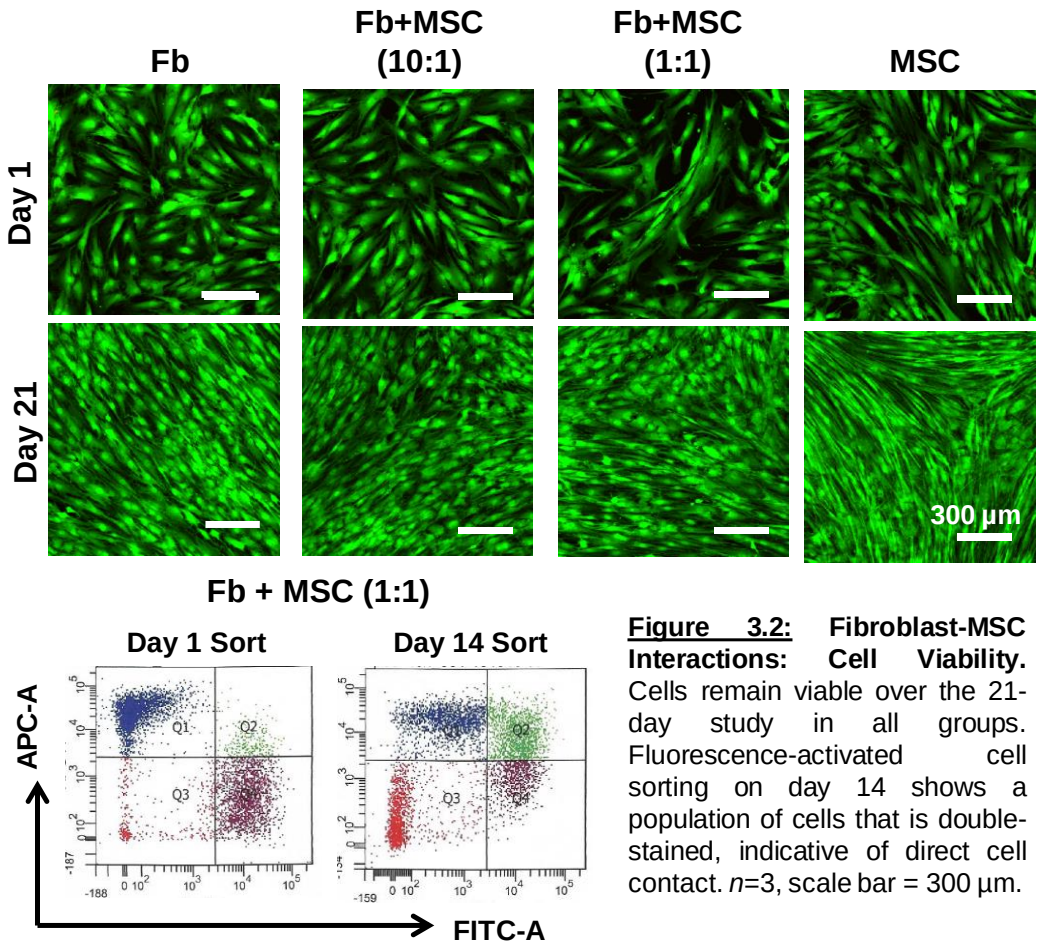

Figure 3.2: Fibroblast-MSC Interactions: Cell Viability. Cells remain viable over the 21-day study in all groups. Fluorescence-activated cell sorting on day 14 shows a population of cells that is double-stained, indicative of direct cell contact. *n*=3, scale bar = 300 µm.

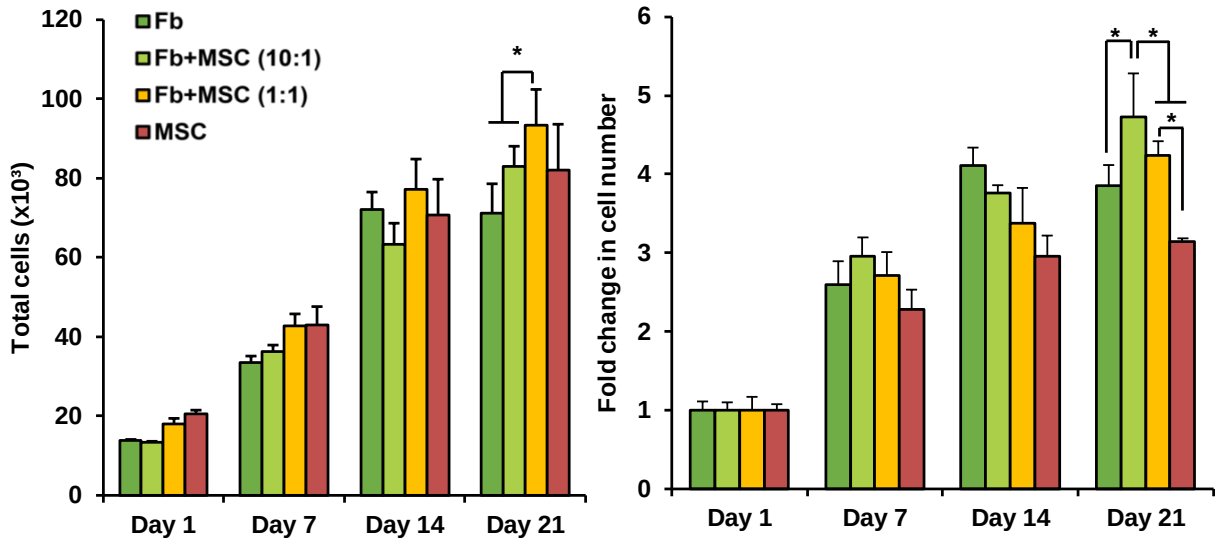

Figure 3.3: Fibroblast-MSC Interactions: Cell Proliferation. Total cell number is greater in 1:1 Fb:MSC co-culture compared to 10:1 co-culture and fibroblast-only single-culture at day 21. Fold change in cell number from day 1 is greatest in 10:1 co-culture, and fold change is greater in 1:1 co-culture compared to MSC single-culture at day 21. n=5, significant difference: * between groups, ^ over time (p<0.05).

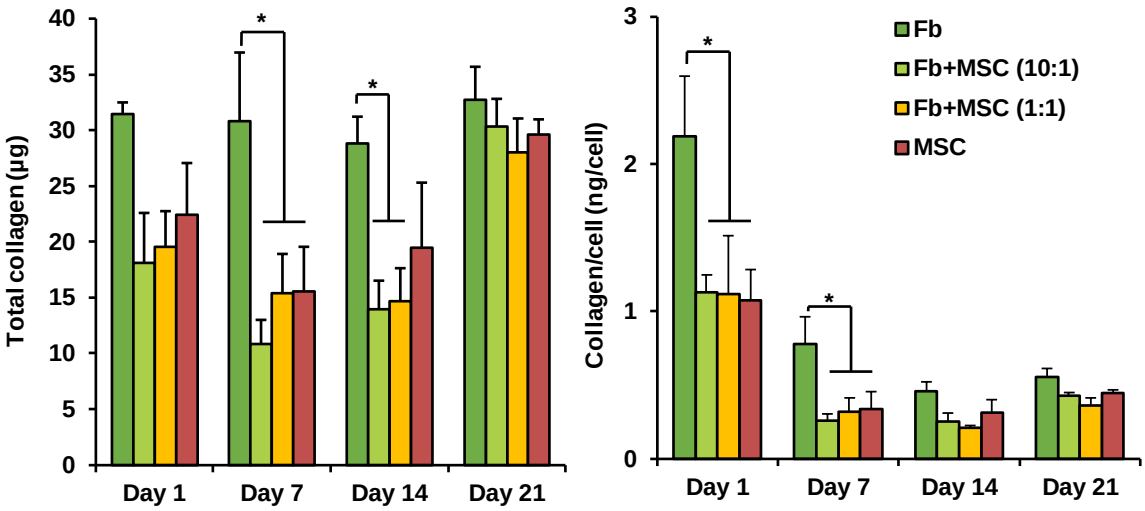

Figure 3.4. Fibroblast-MSC Interactions: Collagen Production. Total collagen is greater for fibroblast single-culture compared to all other groups at day 7 and is greater than both co-culture groups at day 14. These differences are no longer observed by day 21. Collagen per cell was greatest for fibroblast single-culture at day 1 and 7 compared to all other groups, with no observed differences between groups at days 14 and 21. *n*=5, significant difference: * between groups, ^ over time ($p<0.05$).

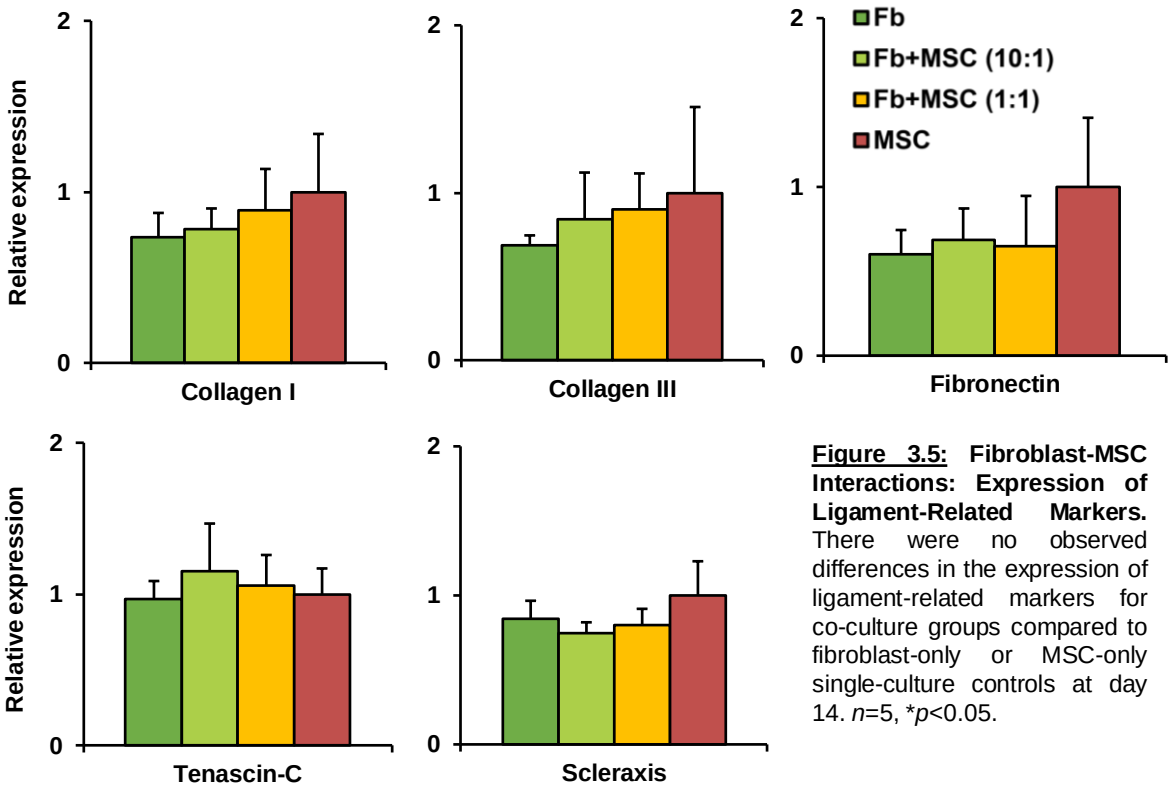

Figure 3.5: Fibroblast-MSC Interactions: Expression of Ligament-Related Markers. There were no observed differences in the expression of ligament-related markers for co-culture groups compared to fibroblast-only or MSC-only single-culture controls at day 14. *n*=5, **p*<0.05.

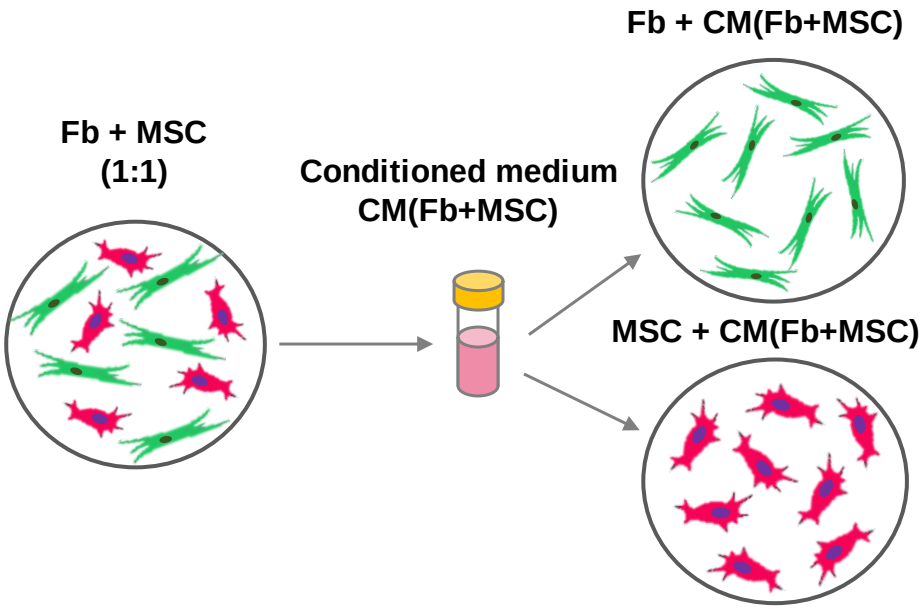

Figure 3.6. Fibroblast-MSC Interactions: Conditioned Medium Model. A 1:1 co-culture of fibroblasts and MSC was grown in tandem with single-cultures of fibroblasts and MSC. Fibroblasts and MSC were fed with 1:1 co-culture medium every 2-3 days.

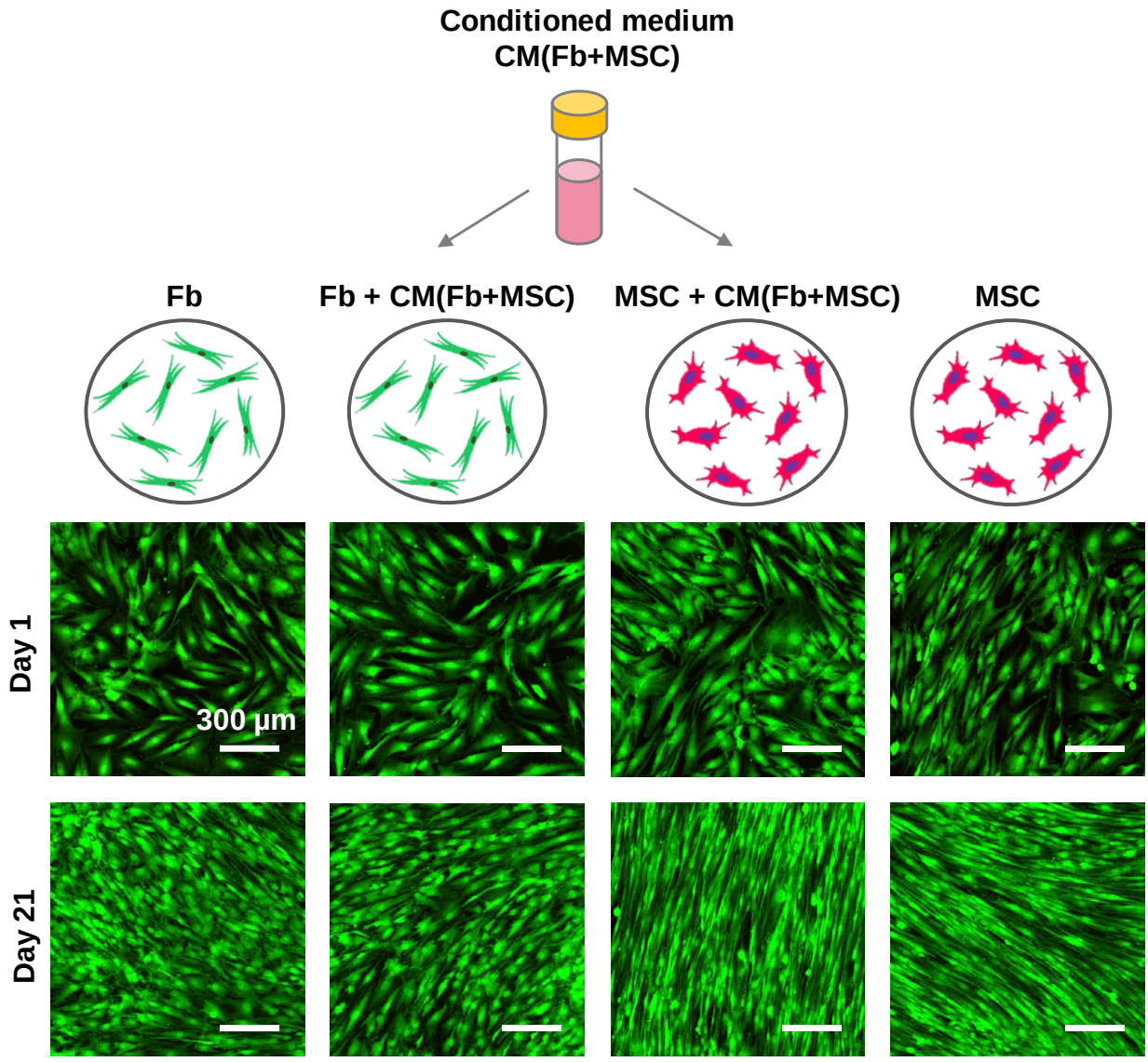

Figure 3.7: Fibroblast-MSC Interactions – Conditioned Medium Model: Cell Viability. Cells remain viable in all groups over 21 days. *n*=3, mag = 20x, scale bar = 300 µm.

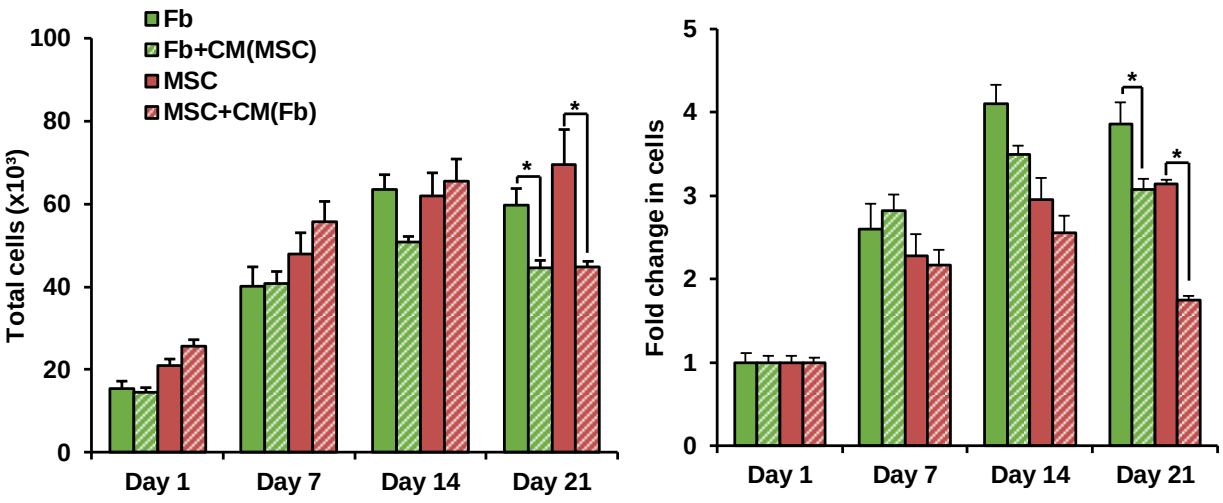

Figure 3.8: Fibroblast-MSC Interactions – Conditioned Medium Model: Cell Proliferation. Total cell number and fold change in cell number are lower for fibroblasts in co-culture-conditioned medium compared to fibroblast-single culture at day 21. Total cell number and fold change in cell number are also lower for MSC in co-culture-conditioned medium compared to MSC single-culture at this time point. n=5, significant difference: * between groups, ^ over time (p<0.05).

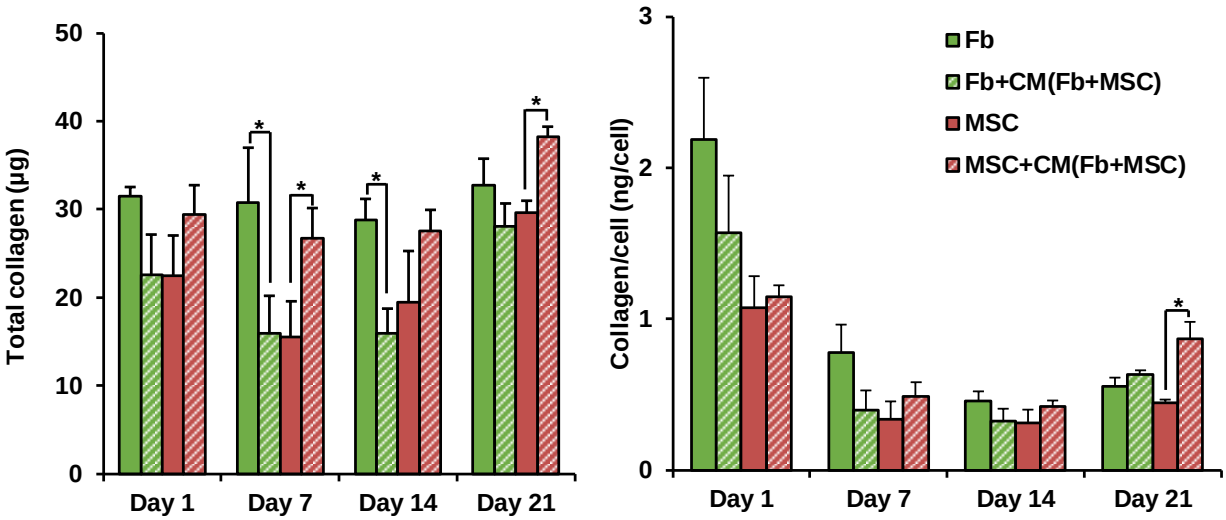

Figure 3.9: Fibroblast-MSC Interactions – Conditioned Medium Model: Collagen Production. Total collagen is lower for fibroblasts in co-culture-conditioned medium compared to fibroblast single-culture at days 7 and 14. This difference is no longer observed by day 21. Total collagen is greater for MSC in co-culture-conditioned medium compared to MSC single-culture at day 7, with greater total collagen and collagen per cell for MSC in co-culture-conditioned medium compared to MSC single-culture at 21. n=5, significant difference: * between groups, ^ over time (p<0.05).

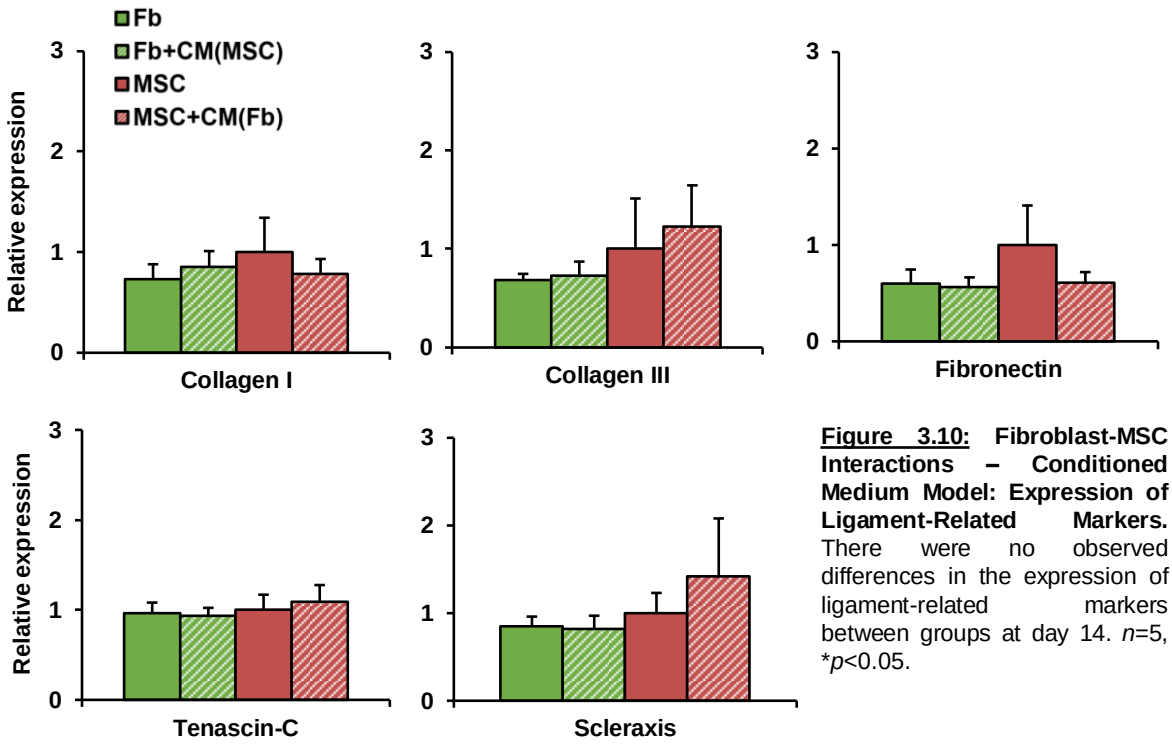

Figure 3.10: Fibroblast-MSC Interactions – Conditioned Medium Model: Expression of Ligament-Related Markers. There were no observed differences in the expression of ligament-related markers between groups at day 14. n=5, *p<0.05.

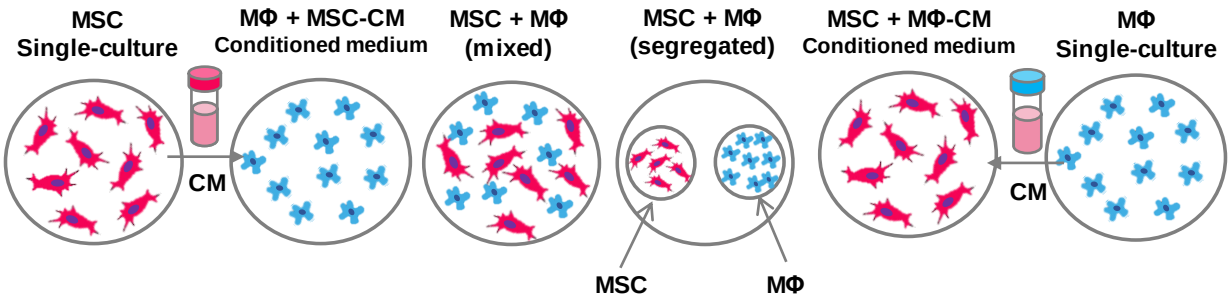

Figure 3.11: Stem Cell-Macrophage Interactions: Co-Culture Model. Human mesenchymal stem cells (MSC) and THP-1-derived M0 macrophages (MΦ) were seeded in co-culture. Conditioned medium groups included MSC in macrophage-conditioned medium and macrophages in MSC-conditioned medium, with single-cultures of macrophages and MSC serving as controls.

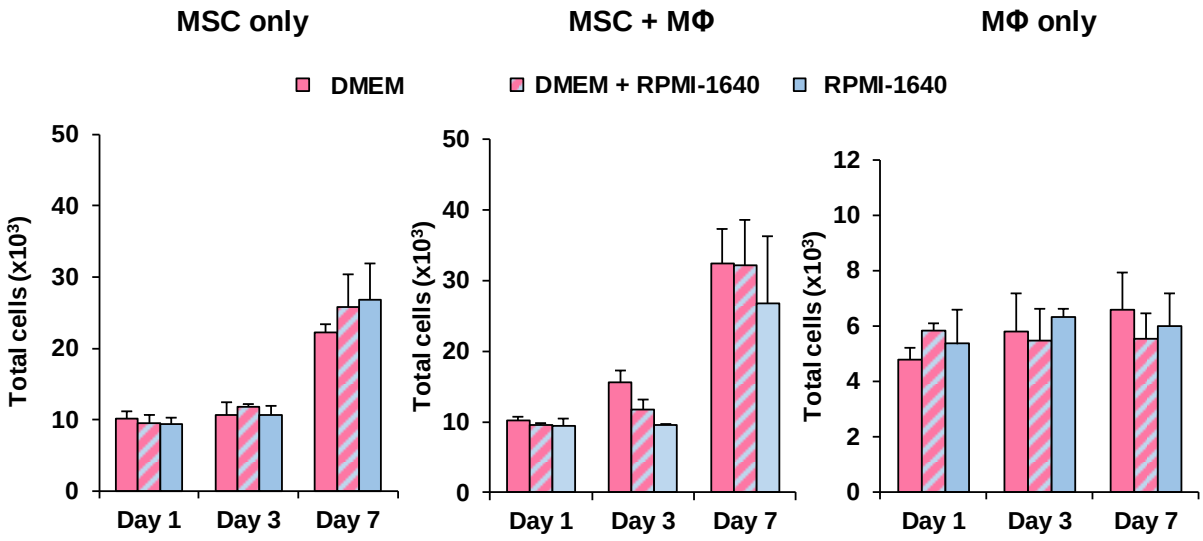

Figure 3.12: Stem Cell-Macrophage Interactions: Co-Culture Medium Optimization. For co-culture medium optimization, cell number was lower for fibroblasts in fully-supplemented (F/S) RPMI-1640 compared to F/S DMEM controls at days 3 and 7. Cell number was also lower for macrophages in F/S DMEM compared to F/S RPMI-1640 controls at day 1, and both F/S RPMI-1640 and a 1:1 mix of DMEM:RPMI-1640 at day 3. No effects of medium choice on cell viability was observed in co-culture, suggesting a 1:1 mix of DMEM:RPMI-1640 is suitable for co-culture experiments. n=5, *p<0.05.

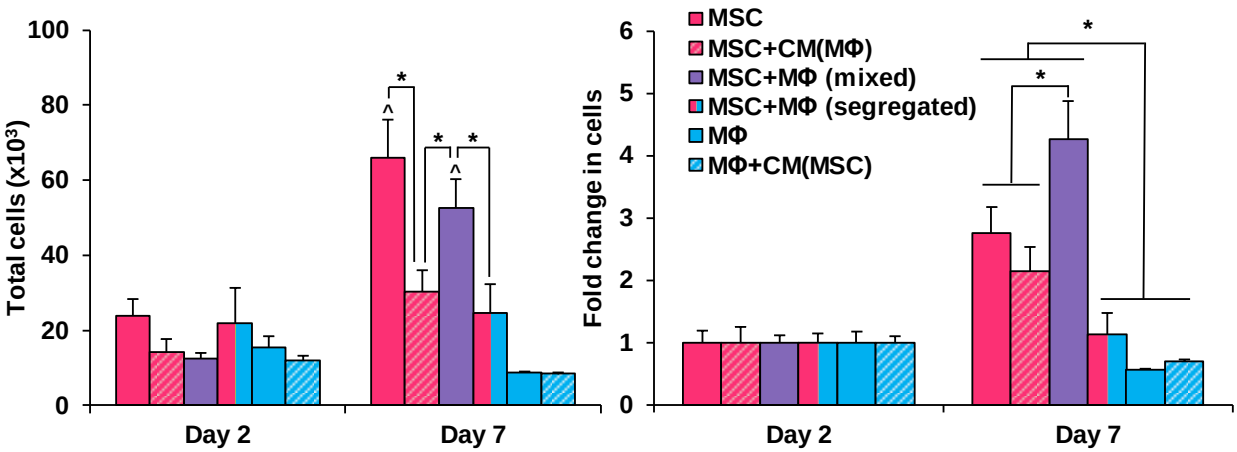

Figure 3.13: Stem Cell-Macrophage Interactions: Cell Proliferation. Total cell number is lowest for macrophage single-culture and macrophages in MSC-conditioned medium at day 7. Total cell number is greater for MSC single-culture and mixed co-culture compared to MSC in macrophage-conditioned medium and segregated co-culture at day 7. Fold change in cell number is greatest in mixed co-culture at day 7 compared to all other groups. n=5, significant difference: * between groups, ^ over time (p<0.05).

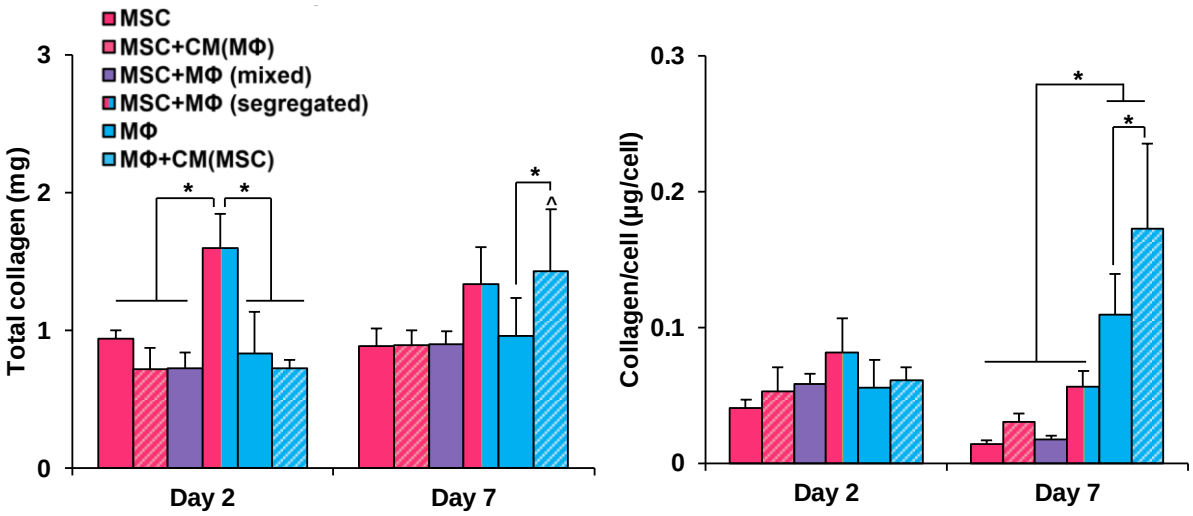

Figure 3.14: Stem Cell-Macrophage Interactions: Collagen Production. Total collagen content increased for macrophages in MSC-conditioned medium only between days 2 and 7, with no observed differences in total collagen over time for any other group. Total collagen was greatest in segregated co-culture compared to all other groups at day 2, but this difference was no longer observed by day 7. Collagen per cell was greater for macrophages in MSC-conditioned medium compared to macrophage single-culture at day 7. Collagen per cell was greater for macrophage single-culture and macrophages in MSC-conditioned medium compared to all other groups at day 7. n=5, significant difference: * between groups, ^ over time (p<0.05).

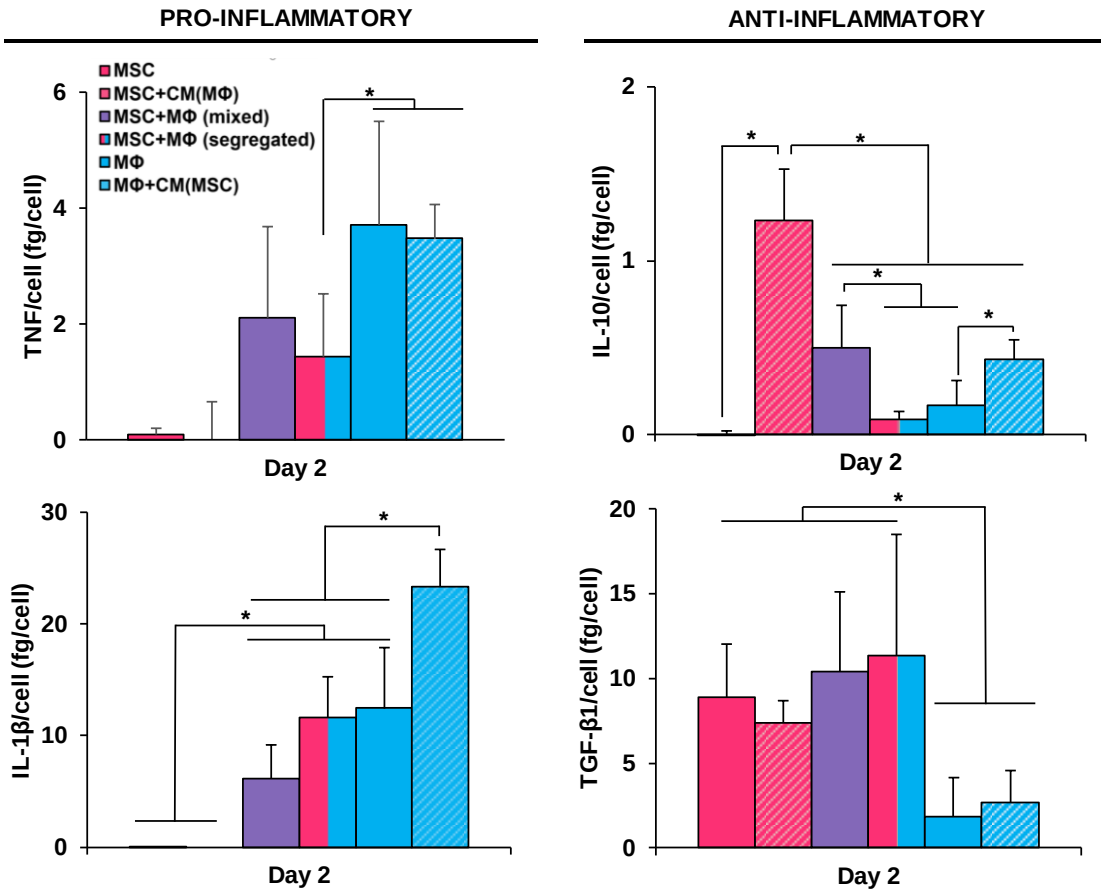

Figure 3.15: Stem Cell-Macrophage Interactions: Release of Pro- and Anti-Inflammatory Cytokines. At day 2, TNF per cell was lower in segregated co-culture than macrophage single-culture and macrophages in MSC-conditioned medium. IL-1β per cell was greater for macrophages in MSC-conditioned medium compared to all other groups. In terms of anti-inflammatory cytokine secretion, IL-10 per cell was greater for MSC in macrophage-conditioned medium compared to MSC single-culture, and IL-10 per cell was greater in mixed co-culture than segregated co-culture and macrophage single-culture. IL-10 per cell was elevated for macrophages in MSC-conditioned medium compared to macrophage single-culture at day 2. TGF-β1 per cell was greater in all MSC-containing groups compared to macrophage single-cultures. n=5, *p<0.05.

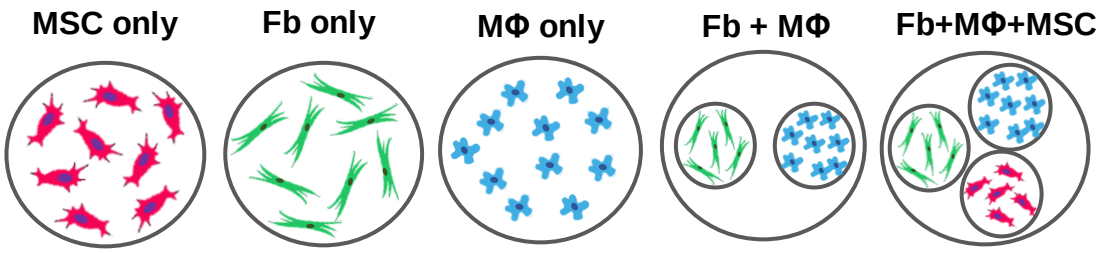

Figure 3.16: Tri-culture model. For tri-culture, human mesenchymal stem cells (MSC), fibroblasts (Fb), and THP-1-derived M0 macrophages (MΦ) were seeded on Thermanox coverslips and placed into the same well on day 0. Single-cultures of MSC, Fb, and MΦ served as negative controls while segregated co-culture of Fb + MΦ served as a positive control.

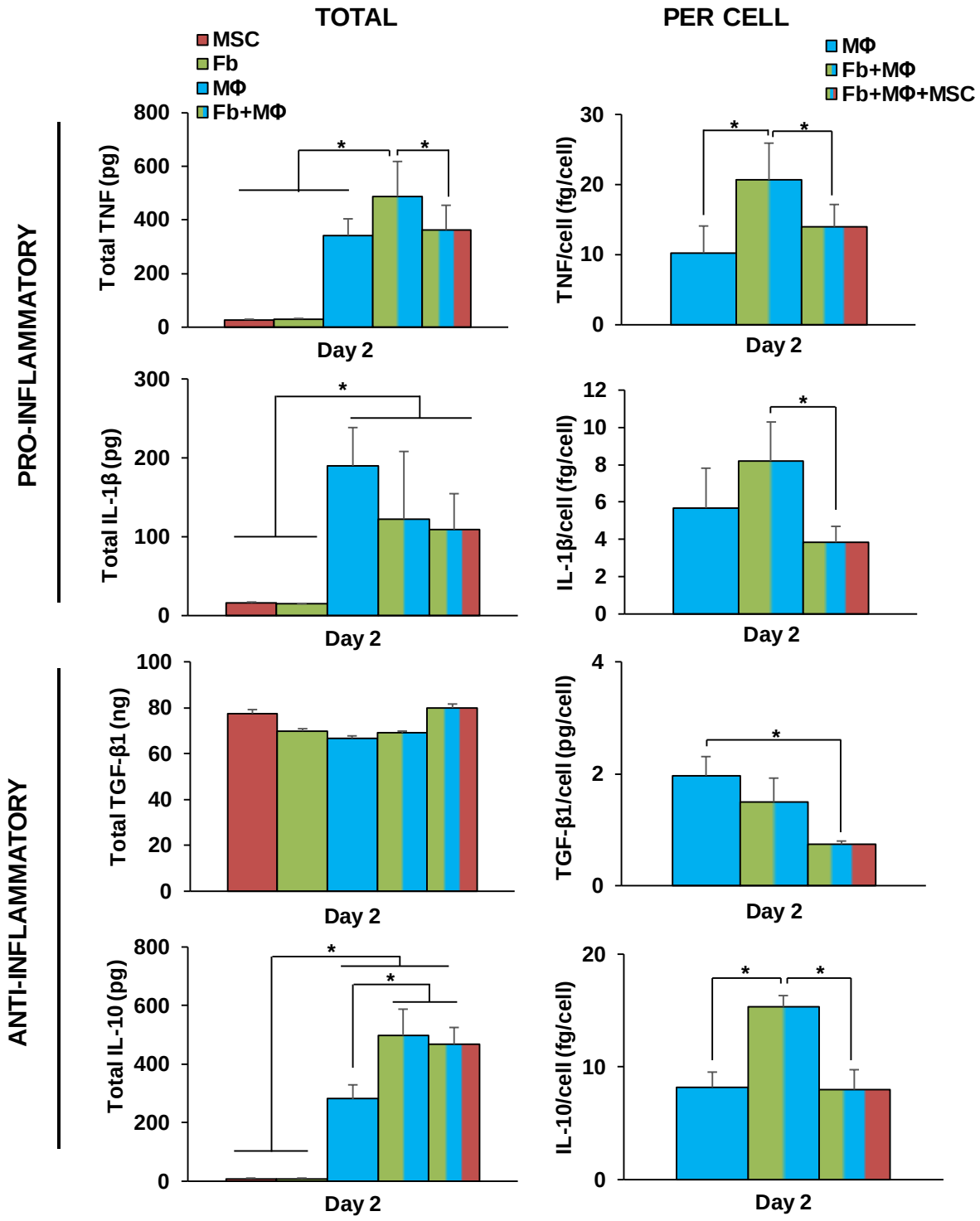

Figure 3.17: Tri-Culture: Release of Pro- and Anti-Inflammatory Cytokines. Total TNF and TNF per cell were lower in tri-culture than fibroblast-macrophage co-culture at day 2. There were no differences in total IL-1β or total TGF-β1 between macrophage single-culture, fibroblast-macrophage co-culture, and tri-culture, but IL-1β per cell was lower in tri-culture than fibroblast-macrophage co-culture, TGF-β1 per cell was lower in tri-culture than macrophage single-culture at day 2. Total IL-10 was greater in fibroblast-macrophage co-culture and tri-culture than macrophage single-culture, while IL-10 per cell was lower in tri-culture than fibroblast-macrophage single-culture at this time. n=5, *p<0.05.

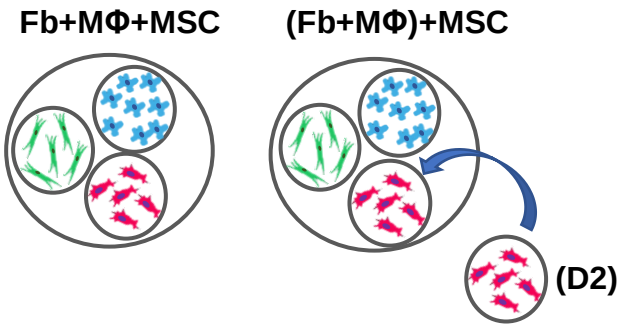

Figure 3.18: Tri-Culture: Delayed Tri-Culture Model. For tri-culture (Fb+MΦ+MSC), MSC, THP-1-derived M0 macrophages, and fibroblasts were seeded on Thermanox coverslips and placed into the same well on day 0. For delayed tri-culture ((Fb+MΦ)+MSC), M0 macrophages, fibroblasts, and MSC were seeded on Thermanox coverslips. Fb and MΦ were added on day 0 while MSC were added later, on day 2.

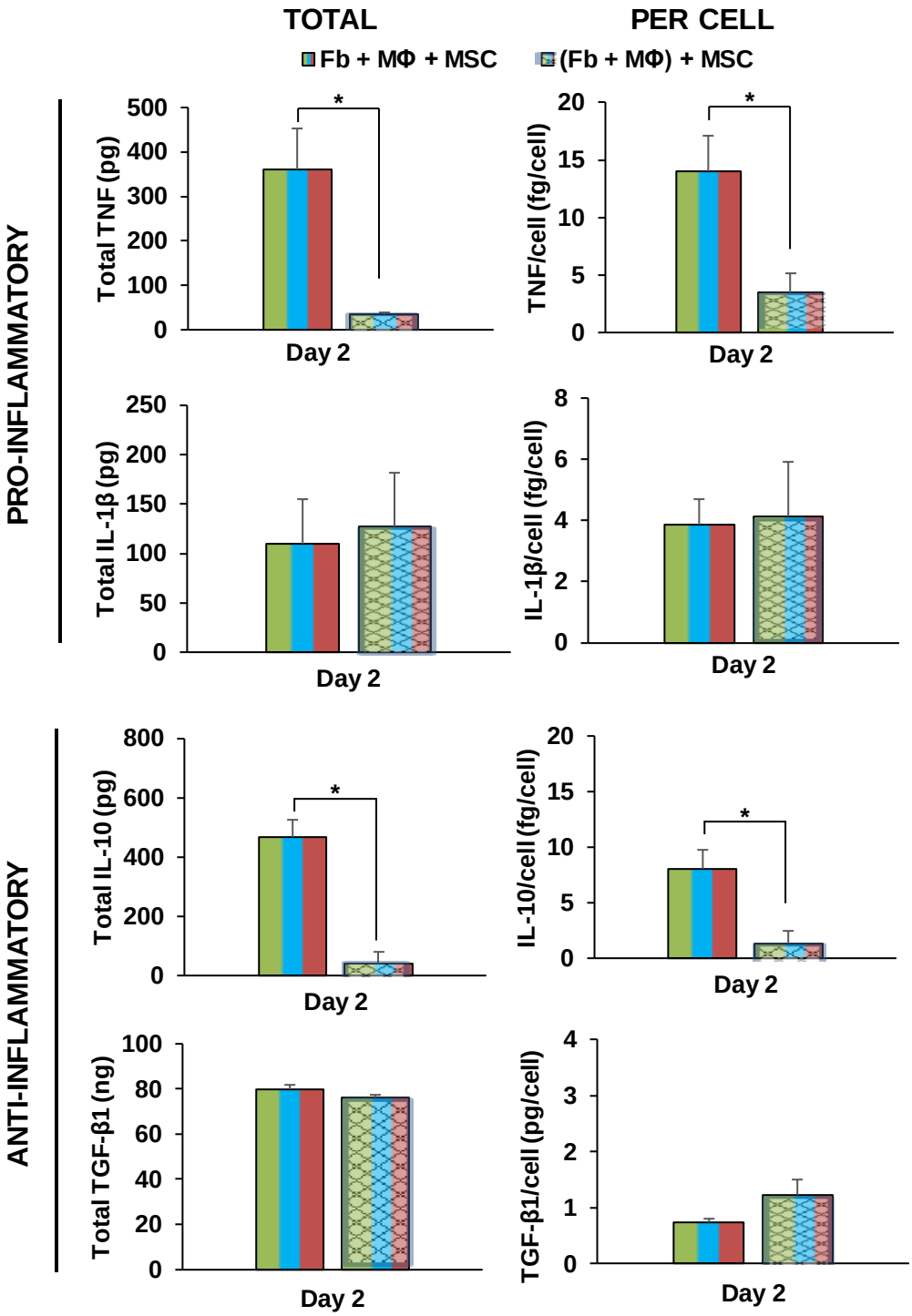

<u>Figure 3.19:</u> Delayed Tri-Culture: Release of Pro- and Anti-Inflammatory Cytokines. Total TNF and TNF per cell, as well as total IL-10 and IL-10 per cell were lower in delayed tri-culture groups compared to tri-culture after 2 days. There were no differences observed in total IL-1β or IL-1β per cell between tri-culture and delayed tri-culture. There were no observed differences in the total release of TGF-β1 or TGF-β1 per cell between tri-culture and delayed tri-culture. n=5, *p<0.05.

CHAPTER 4: DEVELOPMENT OF A NANOFIBER MATRIX-BASED PLATFORM FOR STUDYING CELL-MATRIX AND CELL-CELL INTERACTIONS IN CONNECTIVE TISSUE

4.1 Introduction

In *Chapters 2* and *3*, the heterotypic cellular interactions between native fibroblasts, infiltrating macrophages, and homed or exogenously delivered MSC during connective tissue injury and repair were evaluated. *Chapter 4* focuses on the development and optimization of an electrospun nanofiber matrix-based platform for assessing the impact of matrix alignment and mechanical properties on the behavior of each of these three cell types, as well as interactions between each cell type, in a physiologically relevant, 3D fibrous microenvironment mimetic of connective tissue.

4.1.1 Background and Motivation

This study is focused on the development of a series of nanofiber matrices for assessing the effects of matrix alignment and mechanical properties on cell response. Electrospun nanofibers have been used to recapitulate the native architecture of fibrous connective tissues in the body, including bone(214;215), skeletal muscle(12;216), tendon(217;218), ligament(11;219-221), and fibrocartilage(222;223), as they provide a means of mimicking fibrous tissue structure at the nanoscale. Additionally, nanofiber-based meshes can be electrospun in both aligned and unaligned fiber orientations, accurately modeling the differences in fiber alignment that are observed during healing and remodeling(224). To this end, four meshes will be fabricated to assess the effects of changes in matrix alignment and mechanical properties on cell response. These meshes will assess cell response to 1) unaligned vs. aligned fibers and 2) soft vs. stiff fibers.

Still, methods for controlling the mechanical properties of nanofiber matrices to study the effects of changes in both fiber alignment and mechanical properties on cell response have not yet been developed. The aim of this chapter is to engineer nanofibers comprised of PDMS, a flexible polymer with a controllable range of elastic properties, which has been used extensively for studying the effects of matrix elasticity on the behavior of cells in 2D, including stem cells(15-19). Previous work shows that PDMS is difficult to electrospin, due to the relatively low molecular weight of the pre-cured polymer solution(225;226). In order to overcome this limitation, PCL, a biodegradable polyester previously used in electrospinning for regeneration of fibrous tissues such as bone, fibrous cartilage, meniscus, intervertebral disk, tendons, and ligaments(32;223;227-230), will be utilized as a carrier polymer to aid in PDMS electrospinning.

4.1.2 Objectives

The goal of this study is to develop and optimize an electrospun nanofiber matrix-based platform to serve as a physiologically relevant in vitro model of fibrous connective tissues, in order to assess the effects of changes in matrix alignment and mechanical properties on the response of the cell types utilized in *Chapters 2* and *3* – fibroblasts, MSC, and macrophages – as well as the interactions between these cell types. Specifically, nanofiber meshes comprised of either PCL alone or a blend of PDMS and PCL will be fabricated in both aligned and unaligned fiber orientations, and meshes will be characterized in terms of fiber alignment and mechanical properties, as well as fiber diameter, surface chemistry, and surface energy. Fibers will be optimized such that significant differences in alignment and mechanical properties between meshes are achieved, without altering fiber diameter or any other parameters. It is hypothesized that 1) PCL will serve as an adequate carrier polymer for electrospinning PDMS-containing meshes, resulting in formation of PDMS-PCL blend nanofibers, and 2) PDMS-PCL blend fibers will exhibit decreased mechanical properties compared to PCL-only fibers in both unaligned and aligned fiber orientations.

4.2 Materials and Methods

4.2.1 Nanofiber Mesh Fabrication

4.2.1.1 Unaligned PCL Meshes

A 16% (w/v) PCL solution was prepared by dissolving PCL (M_n = 70,000-90,000, Sigma-Aldrich) into 3:1 solution of dichloromethane (DCM, Sigma-Aldrich):N,N-dimethylformamide (DMF, Sigma-Aldrich). The solution was mixed overnight, vortexed for 1 hour prior to electrospinning, and then loaded into a 5 mL syringe attached with a 23-gauge stainless steel blunt-tip needle. A voltage of 7-9 kV was applied to the needle tip and a pump flow rate of 1 mL/hr was used. Fibers were collected on a grounded stationary plate placed 15 cm from the needle tip. Approximately 2 mL of polymer solution was electrospun to fabricate scaffolds of thickness ranging from 0.09-0.14 mm as measured with a digital caliper.

4.2.1.2 Aligned PCL Meshes

An 18% (w/v) PCL solution was prepared by dissolving PCL into 3:2 mixture of DCM:DMF. The solution was mixed overnight, vortexed for 1 hour prior to electrospinning, and loaded into a 5 mL syringe with a 23-gauge stainless steel blunt-tip needle. A voltage of 9-10 kV was applied to the needle tip and a

pump flow rate of 1 mL/hr was used. Fibers were collected on a grounded rotating mandrel (2500 rpm), 13 cm from the needle tip.

4.2.1.3 Unaligned PDMS-PCL Blend Meshes

Methods utilized for fabricating unaligned PDMS-PCL fibers are outlined in *Figure 4.1.* Unaligned PDMS-PCL blend meshes were fabricated by adding a 1:1 mixture of PDMS (Sylgard 184, 50:1 base:crosslinker, Dow Corning) and PCL to a 3:1 solution of DCM:DMF to achieve varying polymer concentrations in solution, ranging from 15 wt.% polymer to 50 wt.% polymer. Solutions were vortexed for 4 hours prior to electrospinning, and then loaded into a 5 mL syringe attached with a 23-gauge stainless steel blunt-tip needle. A voltage of 10-11 kV was applied to the needle tip and a pump flow rate of 1 mL/hr was used. Fibers were collected on a grounded stationary plate placed 12 cm from the needle tip. Approximately 3 mL of polymer solution was electrospun to fabricate scaffolds of thickness ranging from 0.07-0.14 mm as measured with a digital caliper.

4.2.1.4 Aligned PDMS-PCL Blend Meshes

Methods utilized for fabricating aligned PDMS-PCL fibers are outlined in *Figure 4.1.* Aligned PDMS-PCL blend meshes were fabricated by adding a 1:1 mixture of PDMS and PCL to a 3:1 solution of DCM:DMF to achieve varying polymer concentrations in solution, ranging from 15 wt.% polymer to 50 wt.% polymer. Solutions were vortexed for 4 hours prior to electrospinning, and then loaded into a 5 mL syringe attached with a 23-gauge stainless steel blunt-tip needle. A voltage of 10-11 kV was applied to the needle tip and a pump flow rate of 1 mL/hr was used. Fibers were collected on a grounded rotating mandrel (2100 rpm), 12 cm from the needle tip.

4.2.2 Nanofiber Mesh Characterization

4.2.2.1 Fiber Diameter and Alignment

Fiber morphology and diameter of as-fabricated meshes were determined using scanning electron microscopy (SEM; 5 kV, 10 µA, Hitachi 4700). Prior to imaging, a conductive gold-palladium (AuPd) coating was applied to the scaffold surface via sputter coating (Cressington 108). Fiber diameter was measured using ImageJ (National Institutes of Health). Fiber diameter values are an average of measurements taken

from 6 independent regions of the mesh imaged at 1000x and 2500x magnification (*n*=6 images/group), with 20 measurements per image.

Fiber alignment of unaligned and aligned meshes was quantified following the methods of Costa *et al.* Briefly, confocal images (*n*=6/group) of cell-seeded meshes were analyzed using circular statistics software customized for evaluating fiber alignment (Fiber 3)(231). The circular statistics parameters determined included mean vector angle (MA), which represents the average fiber alignment in the matrix ($-90^{o} < \theta < 90^{o}$; 0^{o} indicates horizontal orientation); mean vector length (MVL), which ranges from zero for a randomly distributed sample to unity for an aligned sample ($0 < r < 1$); and angular deviation (AD), which characterizes the dispersion of the non-Gaussian angle distribution of the nanofibers (0-40.5º). Specifically, an angular deviation of 0^{o} represents an aligned sample, and 40.5^{o} is indicative of random distribution.

4.2.2.2 Fourier Transform Infrared Spectroscopy

Chemistry of as-fabricated polymer nanofiber meshes (*n*=6/group) was assessed using Fourier transform infrared (FTIR) spectroscopy (Digilab FTS 3000MX, Agilent). Spectra were collected in attenuated total reflectance (ATR) mode from 400-4000 cm^{-1} using 300 scans with a resolution of 2 cm^{-1}.

4.2.2.3 Contact Angle Measurement

Contact angle (*n*=6/group) between a water droplet and as-fabricated nanofiber meshes were measured using a contact angle goniometer (ramé-hart). Briefly, 10 µL of deionized water was pipetted onto the surface of fibers, and the angle between the formed droplet and the surface of the mesh was assessed and recorded. Measurements were performed on six different regions of mesh for each mesh type. Following initial measurements on as-fabricated meshes, the surface of each sample was air plasma treated (Harrick Plasma PDC-32G) at high radiofrequency (RF) setting for 30 seconds. Contact angle measurements were repeated on treated samples within 30 minutes of plasma treatment.

4.2.2.4 Uniaxial Tensile Mechanical Testing

The uniaxial tensile mechanical properties of as-fabricated meshes (*n*=6/group) were evaluated following the American Society for Testing and Materials (ASTM) standard for plastic tensile properties testing (ASTM D638), which tests the tensile properties of materials using standard “dog-bone-” or “dumbbell-” shaped testing specimens. Briefly, meshes were cut using a custom-built cutter to create dog-

bone-shaped samples. The average thickness of each sample was measured using digital calipers and meshes were secured with custom clamps and mounted on a custom mechanical testing device with an average gauge length of 20-30 mm. The samples were pre-loaded with 0.1 N, and were loaded at a strain rate of 5 mm/min until failure. Local strains within the dog bone region were assessed by spraying samples with waterproof India ink, allowing for local displacement and strain measurements via Vic-2D (Correlated Solutions Inc.). The elastic modulus was calculated using the linear portion of the stress-strain curve, and the stress and strain at failure were used to calculate the ultimate tensile strength and ductility, respectively.

4.2.2.5 Atomic Force Microscopy

Surface topography and mechanical properties of as-fabricated meshes were evaluating via atomic force microscopy (AFM; Bioscope Catalyst, Veeco). Samples were cut into 1 cm^2 squares and were adhered to double-sided tape and UV-treated in a UV ozone cleaner (ProCleaner; Bioforce Nanosciences), for 60 seconds. Samples were then individually loaded atop the 20x objective of a confocal microscope (Axio Observer A1; Zeiss) and positioned beneath the Catalyst Bioscope AFM system, loaded with an HMX-10 (Bruker) pyramidal tipped probe with a 10 nm diameter tip, and a spring constant of ~4 N/m and resonant frequency of ~60 Hz. Samples were imaged in tapping mode within a 65 µm x 65 µm imaging space, or smaller. Calculation of elastic modulus values from the torsional vibration signals is performed with a personal computer equipped with two processors (3.2 GHz, 2 GB shared memory)(232).

Previously described mathematical procedures were used to reconstruct the tip–sample force waveform from the raw deflection signals(232;233). The elements of this procedure are: averaging vibration waveforms over several consecutive oscillation cycles to reduce noise, correcting the effect of the torsional frequency response, and eliminating the cross-talk from large vertical signals. The calculations are carried out in the form of matrix multiplication in Labview. Elements of this matrix are calculated once at the beginning of the imaging process. The same procedure was followed for cross-talk elimination(232;233), where a linear curve fitting procedure is used. After these linear steps, the waveform still remains in voltage units. Calibration of this signal (i.e. volts to Newtons conversion) is performed according to Sahin *et al.*, 2007(233). For this study, voltage is converted to force by the equation $E_{mod} = (10^V) * x$, where E_{mod} is the elastic modulus, V is the observed voltage, and x is the conversion factor. The conversion factor here is equal to 0.5263805.

Stiffness calculations could then be used to analyze nanofibers for spring constant and elastic modulus. All data was further processed in Gwyddion, a free and open-source software covered by GNU General Public License and available at gwyddion.net, to analyze mechanical properties along distinct fibers, as well as to create topographical maps of each mesh. To plot the elastic modulus along the length of entire fibers, data was imported into Matlab and plotted using the xlsread tool. Mechanical data was further analyzed using Excel to calculate elastic modulus and spring constant from raw voltage data. Following data acquisition and calculation of stiffness and elastic modulus, samples were then quantitatively analyzed (n=60 fibers/group, attained from 6 images per group) for elastic modulus and fiber diameter. Elastic modulus was compared for PDMS-PCL vs. PCL-only meshes, aligned vs. unaligned meshes, and data was also assessed for potential impacts of fiber diameter and fiber packing on modulus.

4.2.2.6 Statistical Analysis

Results are reported as mean ± standard deviation, with n equal to the number of replicates per group. Statistical analyses were performed with JMPIN (4.0.4, SAS Institute, Inc.). One-way analysis of variance (ANOVA) was used to determine differences between PDMS-PCL and PCL-only fibers in terms of diameter, pore size, contact angle, and alignment, while a two-way ANOVA was used to assess the effects of nanofiber alignment and composition on matrix bulk and local mechanical properties. The Tukey-Kramer post-hoc test was used for all pair-wise comparisons, and significance was attained at $p<0.05$.

4.3 Results

4.3.1 PDMS-PCL Blend Optimization

Following initial testing, PDMS-PCL nanofiber meshes were successfully fabricated using 20, 25, 30, and 35 wt.% polymer in solution. Solutions with a polymer content greater than 35 wt.% were too viscous to spin, and did not result in the formation of a steady jet during the spinning process, while those solutions with polymer concentrations lower than 20 wt.% did not form distinct fibers, but rather a 2D polymer mat similar to that observed during electrospraying techniques, as complete evaporation of solvent was not possible during the electrospinning process. Scanning electron micrographs reveal that a 35 wt.% polymer solution resulted in the most uniform fibers in both the aligned and unaligned fiber orientations. In both the unaligned and aligned fiber orientations, 20 wt.% and 25 wt.% polymer concentrations resulted in the

formation of junctions or solders, as described by Yang *et al.* during PMMA-PDMS electrospinning(234), and in some cases, such as the unaligned 20 wt.% solution, resulted in the formation of a non-porous mat with fibrous topography, rather than a 3D fiber mesh. Electrospinning of 30 wt.% polymer solutions resulted in the formation of distinct fibers, but with smaller than desired fiber diameters, and a non-uniform fiber shape and a large deviation in fiber diameter.

Following SEM analysis, a 35 wt.% polymer solution was chosen for PDMS-PCL electrospinning. Fibers spun using this formulation are similar in morphology to PCL-only meshes (*Figure 4.2*). FTIR analysis of aligned and unaligned fibers fabricated using this formulation shows that both PDMS and PCL were successfully incorporated into PDMS-PCL blend fibers, as observed by the characteristic peaks for both polymers (*Figure 4.3*).

4.3.2 Nanofiber Mesh Characterization

4.3.2.1 Fiber Diameter, Alignment, and Surface Properties

Effects of Matrix Alignment: There were no significant differences in fiber diameter between unaligned and aligned nanofiber meshes composed of either PCL-only or PDMS-PCL (*Table 4.1*). Pore sizes were larger for unaligned meshes compared to aligned meshes for both fiber compositions, as is expected due to effects of fiber alignment on fiber packing density (*Table 4.1*). Aligned fibers were significantly more aligned than unaligned fibers (decreased MVA and AD, increased MVL) for both PCL-only and PDMS-PCL compositions (*Table 4.1*). There were no observed differences in FTIR spectra (*Figure 4.3*) or contact angle measurements between unaligned and aligned fibers comprised of either PCL alone or PDMS-PCL blends (*Table 4.1*). *Effects of Matrix Composition*: There were no significant differences in fiber diameter or pore size between PCL-only and PDMS-PCL matrices in either aligned or unaligned fiber orientations (*Table 4.1*). For aligned meshes, alignment (MVA, AD, MVL) is similar for PCL-only and PDMS-PCL meshes, with the majority of fibers at or close to 0º from the horizontal, representing alignment in the horizontal direction. For unaligned fibers, fiber orientation appears random for both PCL-only and PDMS-PCL meshes, as indicated by similarly low frequencies (~10%) of fibers oriented in all directions (*Figure 4.2*). FTIR spectra of PDMS-PCL unaligned and aligned meshes contain the characteristic peaks for both PCL (solid lines) and PDMS (dotted lines) (*Figure 4.3*). Contact angle measurements of as-fabricated samples reveal that both PDMS-PCL and PCL-only fibers are hydrophobic, with contact angles exceeding

90º. Contact angles for unaligned and aligned PDMS-PCL fibers were significantly greater than PCL-only fibers (*Table 4.1*). Wettability of all four meshes was significantly increased via plasma treatment, which resulted in absorption of water droplets into meshes for all four mesh types.

4.3.2.2 Uniaxial Tensile Mechanical Properties

Characteristic stress-strain curves for unaligned and aligned PCL-only and PDMS-PCL meshes are shown in *Figure 4.4*. *Effects of Matrix Alignment*: Uniaxial tensile testing results show that aligned fibers have a significantly greater Young's modulus, ultimate tensile strength, and yield strength than unaligned meshes, regardless of composition (*Table 4.2*). *Effects of Matrix Composition:* The Young's modulus, ultimate tensile strength, and yield strength of PCL-only meshes are significantly greater than those for PDMS-PCL in both the unaligned and aligned fiber orientations, indicating that the addition of PDMS does result in lower mechanical properties than meshes comprised of PCL alone (*Table 4.2*).

4.3.2.3 Local Mechanical Properties

Local mechanical properties as determined via AFM are at least an order of magnitude lower than bulk mechanical properties as determined via uniaxial tensile testing. For all meshes, a range of moduli were observed, as depicted in the histograms in *Figure 4.5.* Still, elastic modulus along the length of individual fibers was relatively consistent, as shown in *Figure 4.6*. *Effects of Matrix Alignment*: No significant differences in local modulus were observed between unaligned and aligned meshes of PCL-only fibers and there was no significant difference between unaligned or aligned fibers for either fiber composition (*Table 4.2*). *Effects of Matrix Composition:* The local elastic modulus of PDMS-PCL, as determined via AFM, is significantly lower than the local modulus of PCL-only fibers, for both unaligned and aligned fiber orientations (*Table 4.2*). The local moduli of unaligned and aligned PCL-only meshes were 16.28 ± 10.58 MPa and 19.35 ± 12.05 MPa, respectively, while the moduli of PDMS-PCL fibers were more than ten-fold lower, with moduli of 1.26 ± 0.81 and 1.28 ± 0.77 MPa for unaligned and aligned fibers, respectively.

4.4 Discussion

This study explores the addition of PDMS to PCL-only nanofibers as a means of decreasing nanofiber mechanical properties. While PDMS has been used extensively as a 2D substrate for studying

the effects of matrix stiffness on the behavior of cells, including stem cells(15-19), it has not been commonly used in 3D fibrous matrices, as it is difficult to electrospin.

Current methods for electrospinning PDMS blend fibers include the introduction of a carrier polymer to the PDMS prepolymer solution prior to electrospinning, to aid in entangling of PDMS chains for fiber creation and stabilization of the PDMS prepolymer. In work done by Yang *et al.*, poly(methyl methacrylate) (PMMA) and PDMS (Sylgard 184, 10:1 base:crosslinker) were solubilized in DMF and tetrahydrofuran (THF), at various PDMS/PMMA weight ratios (0:1, 1:2, 1:1, 2:1, 3:1, 4:1 PDMS:PMMA)(225). Still, for PDMS-PMMA blends, composite fibers tended to aggregate and form what look like junctions or solders between fibers. Moreover, at weight ratios greater than 4:1, the electrospun fibers no longer kept their individual shape and fused to one another.

By utilizing Sylgard 184 (Dow Corning), a commercially available PDMS that is provided as a two-part solution (base and crosslinker) by the manufacturer, the ratio of base to crosslinker can be altered to form PDMS with a variety of elasticities(235). Specifically, the higher the degree of the PDMS network's crosslinking (by increasing the volume of crosslinker, or decreasing the ratio of base to crosslinker), the higher its stiffness(235). Here, a ratio of 50:1 PDMS base:crosslinker was utilized, as it has been shown that this ratio is the upper limit for Sylgard 184, resulting in the most compliant form of PDMS possible(236). Following base-crosslinker mixing, PDMS and PCL were combined at a 1:1 ratio in a solution containing 3:1 DCM:DMF at a range of polymer weight ratios (20, 25, 30, 35wt.%) and electrospun into aligned and unaligned fiber orientations. Results show that a 35 wt.% polymer solution is optimal for spinning both unaligned and aligned fibers with morphologies and fiber diameters similar to PCL-only meshes.

At both the bulk and local level, PDMS-PCL meshes are observed to have lower mechanical properties than PCL-only meshes, with a bulk elastic modulus that is about one half that of PCL-only, and a local elastic modulus one-tenth the modulus of PCL-only. Interestingly, the local modulus of PDMS-PCL fibers as determined via AFM is similar to the local mechanical properties of PDMS film (Sylgard; 10:1 base:crosslinker), which served as a control group in this study, and was the same order of magnitude as measurements previously made by others(237). This may be due to segregation of the PDMS polymer to the surface of fibers due to its lower surface tension(238). This phenomenon has been observed previously

in work by Rutledge and coworkers, during electrospinning of PDMS-polystyrene block copolymers blended with polystyrene homopolymer(239).

Meshes composed of PDMS-PCL are shown to have similar fiber diameter and pore size to PCL-only meshes, with similar degrees of alignment between aligned PDMS-PCL and PCL-only fibers. Differences in contact angle between as-fabricated PCL-only and PDMS-PCL meshes were observed, likely due to the inherent hydrophobicity of PDMS. In order to eliminate this variable between fiber compositions for future cell studies, as will be performed in *Chapters 5-8*, all meshes will be plasma treated to promote surface reactivity, as this method has been shown to increase mesh wettability(240;241), minimizing differences in mesh hydrophobicity/surface energy between PCL-only and PDMS-PCL blend fibers.

Therefore, unaligned and aligned meshes composed of PCL-only and PDMS-PCL will serve as a platform for assessing the synergistic effects of matrix alignment and mechanical properties on cell response following connective tissue injury and during tissue healing. These meshes will be utilized throughout the remainder of this thesis to determine the effects of changes in fiber alignment and mechanical properties on 1) stem cell response, 2) fibroblast activity, 3) macrophage polarization, and 4) the heterotypic cellular interactions between these three cell types in tri-culture as they relate to connective tissue injury and healing response.

4.5 Conclusion

Through this study, a series of electrospun nanofiber-based meshes were successfully fabricated to serve as a platform for studying the effects of matrix alignment and mechanical properties on cell-matrix and cell-cell interactions in connective tissue. This study demonstrated that the addition of PDMS to PCL-only nanofibers results in fibers with lower mechanical properties than PCL alone. These differences in mechanical properties were observed not only at the bulk level, as shown through uniaxial tensile testing, but also at the cellular level, as measured via atomic force microscopy. In *Chapter 5-8*, these meshes will be used as a platform for studying the effects of differences in both matrix alignment and mechanical properties on cell-matrix and cell-cell interactions in connective tissue following injury and during, in order to determine the optimal matrix topography and mechanical properties to modulate inflammation as well as promote stem cell-guided tissue regeneration.

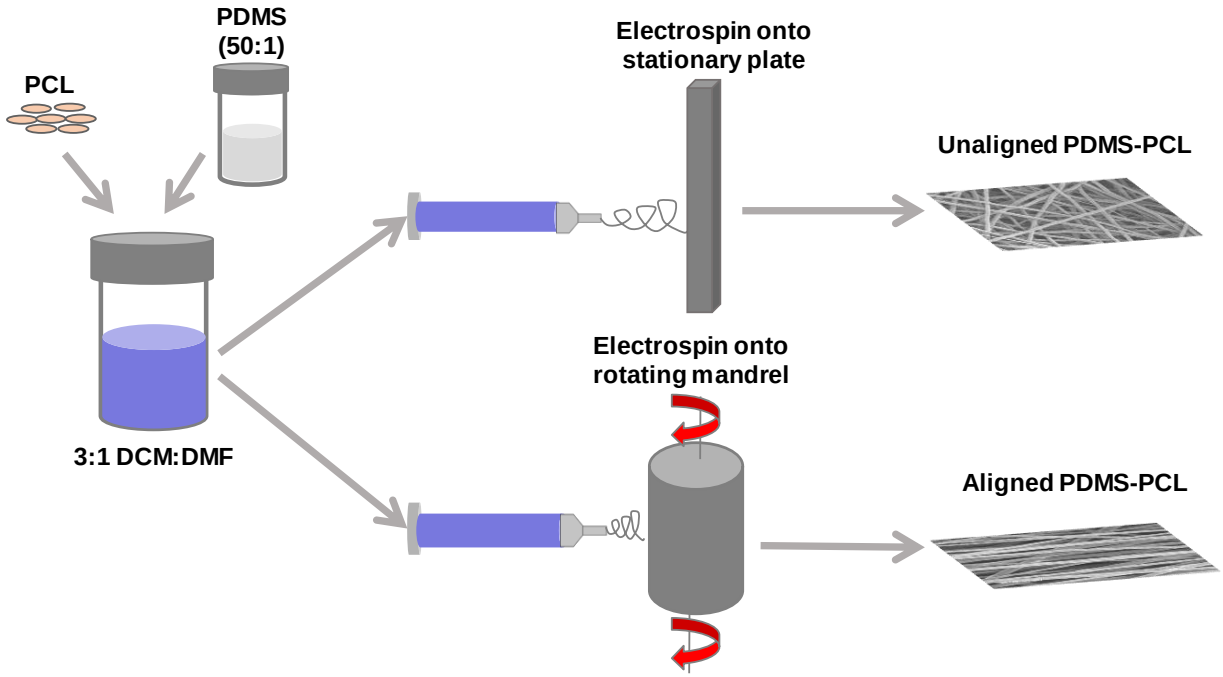

Figure 4.1: Electrospinning Unaligned and Aligned PDMS-PCL Blend Nanofiber Meshes. For PDMS-PCL blends, PCL and PDMS (50:1 base:crosslinker) were mixed at a 1:1 ratio (w/w) in a 3:1 solution of DCM:DMF and electrospun onto a stationary plate or a rotating mandrel for unaligned and aligned fibers, respectively.

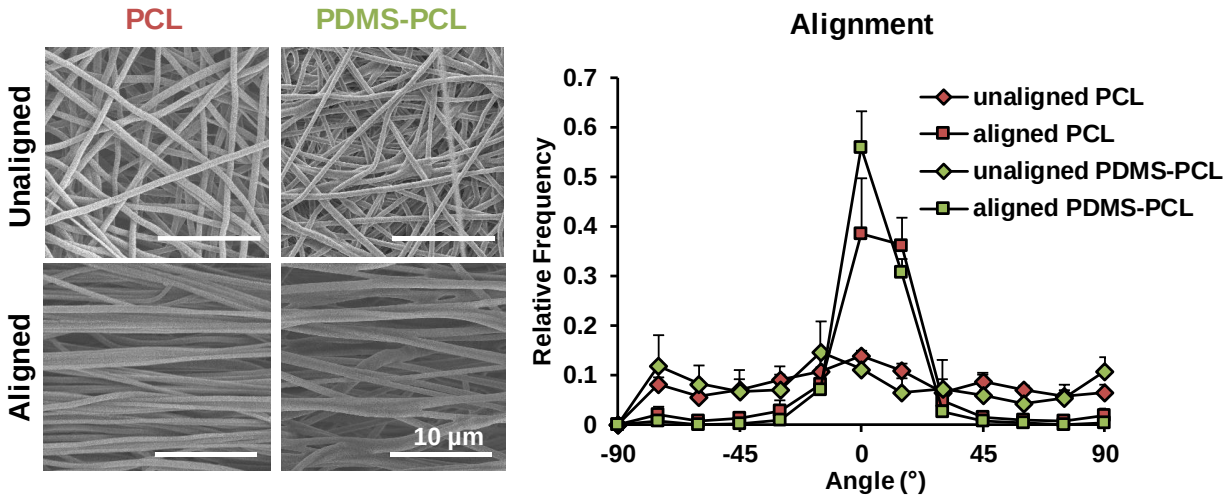

Figure 4.2: Characterization of PDMS-PCL and PCL-Only Nanofiber Meshes: Morphology and Alignment. Scanning electron micrographs (SEM) at left show that PCL-only and PDMS-PCL fibers are similar in morphology, and optimized electrospinning protocols result in the formation of smooth, distinct fibers for all groups. Quantitative analysis of fiber angular deviation shows that fiber alignment was similar between PDMS-PCL and PCL-only for both aligned and unaligned fiber orientations. *n*=6 independent regions imaged at 1000x and 2500x magnification, 20 measurements per image.

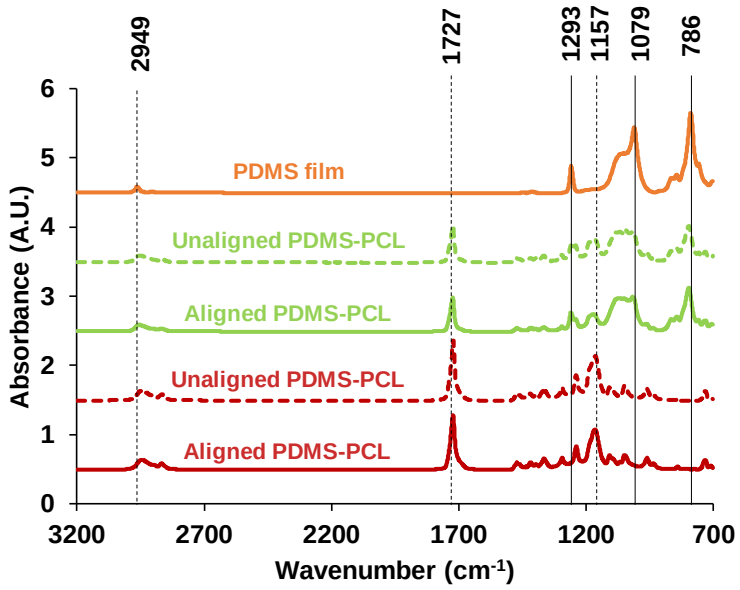

Figure 4.3: Characterization of PDMS-PCL and PCL-Only Nanofiber Meshes: Chemical Composition. Fourier transform infrared (FTIR) analysis shows that PDMS and PCL were both successfully incorporated into PDMS-PCL blends. *n*=6 independent regions per group. Dotted lines indicate PCL chemical groups, solid lines indicate PDMS chemical groups.

Table 4.1: Characterization of PDMS-PCL and PCL-Only Nanofiber Meshes: Fiber Diameter, Alignment, and Surface Energy. There were no differences in fiber diameter between any group. Contact angle was greater for PDMS-PCL fibers compared to PCL-only fibers, with no differences in contact angle due to fiber alignment for either PCL-only or PDMS-PCL fibers. Mean vector angle (MA) was significantly lower for aligned fibers compared to unaligned fibers for both PCL-only and PDMS-PCL fibers, while mean vector length was significantly greater for aligned vs. unaligned fibers for both fiber compositions, indicating that aligned fibers are significantly more aligned than unaligned meshes. Fiber diameter values are an average of measurements taken from SEM images, n=6 independent regions imaged at 1000x and 2500x magnification, 20 measurements per image. Significant difference between: * PCL-only and PDMS-PCL fiber compositions, ^ aligned and unaligned fiber orientations (p<0.05).

Alignment	Composition	Fiber diameter (nm)	Contact angle (º)	MA ± AD (°)	MVL
unaligned	PCL	710.94 ± 188.28	118.9 ± 4.6	19.25 ± 36.10	0.20 ± 0.09
unaligned	PDMS-PCL	760.09 ± 167.87	142.3 ± 1.2 *	36.60 ± 35.20	0.24 ± 0.07
aligned	PCL	664.20 ± 64.96	125.9 ± 9.1	2.00 ± 13.16 ^	0.89 ± 0.03 ^
aligned	PDMS-PCL	656.18 ± 50.24	141.8 ± 0.6 *	2.28 ± 11.93 ^	0.91 ± 0.03 ^

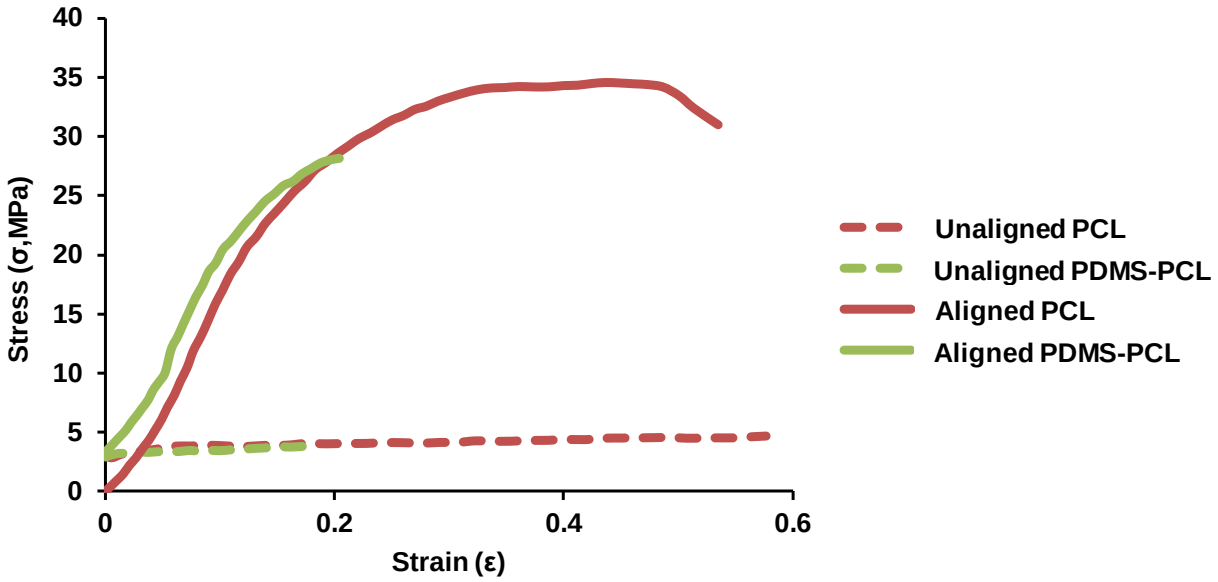

Figure 4.4. Characterization of PCL-Only and PDMS-PCL Blend Nanofiber Meshes: Uniaxial Tensile Testing. Characteristic stress-strain curves for unaligned and aligned PCL-only and PDMS-PCL blend nanofiber meshes, as assessed via uniaxial tensile testing. *n*=6 samples per group.

Table 4.2: Characterization of PCL-Only and PDMS-PCL Blend Nanofiber Meshes: Mechanical Properties. Local elastic modulus (E_{local}) is greater for PCL-only fibers compared to PDMS-PCL fibers for both unaligned and aligned fiber orientations, with no differences due to fiber alignment. Bulk elastic modulus (E_{bulk}) is also greater for PCL-only fibers compared to PDMS-PCL fibers, with increased bulk elastic modulus for aligned fibers compared to unaligned fibers for both PCL-only and PDMS-PCL fiber compositions. The ultimate tensile strength (UTS) of PCL-only fibers is greater than PDMS-PCL fibers, with increased UTS for aligned fibers compared to unaligned fibers for both PCL-only and PDMS-PCL fiber compositions. Yield strength was also enhanced for aligned compared to unaligned fibers for both PCL-only and PDMS-PCL meshes. There were no observed differences in ductility between groups. n=6, significant difference between: * PCL-only and PDMS-PCL fiber compositions, ^ aligned and unaligned fiber orientations (p<0.05).

Alignment	Composition	E_{local} (MPa)	E_{bulk} (MPa)	UTS (MPa)	Y (MPa)	Ductility (%)
unaligned	PCL	16.28 ± 10.58 *	24.63 ± 6.71 *,^	5.20 ± 1.50 *,^	1.22 ± 0.49 ^	212.34 ± 45.93
unaligned	PDMS-PCL	1.26 ± 0.81 *	11.53 ± 2.94 *,^	2.78 ± 0.62 *,^	1.93 ± 0.70 ^	146.34 ± 66.78
aligned	PCL	19.35 ± 12.05 *	131.12 ± 24.81 *,^	66.27 ± 6.36 *,^	9.24 ± 2.96 ^	228.83 ± 18.96
aligned	PDMS-PCL	1.28 ± 0.77 *	90.98 ± 13.42 *,^	33.48 ± 6.27 *,^	6.66 ± 1.35 ^	162.89 ± 6.44

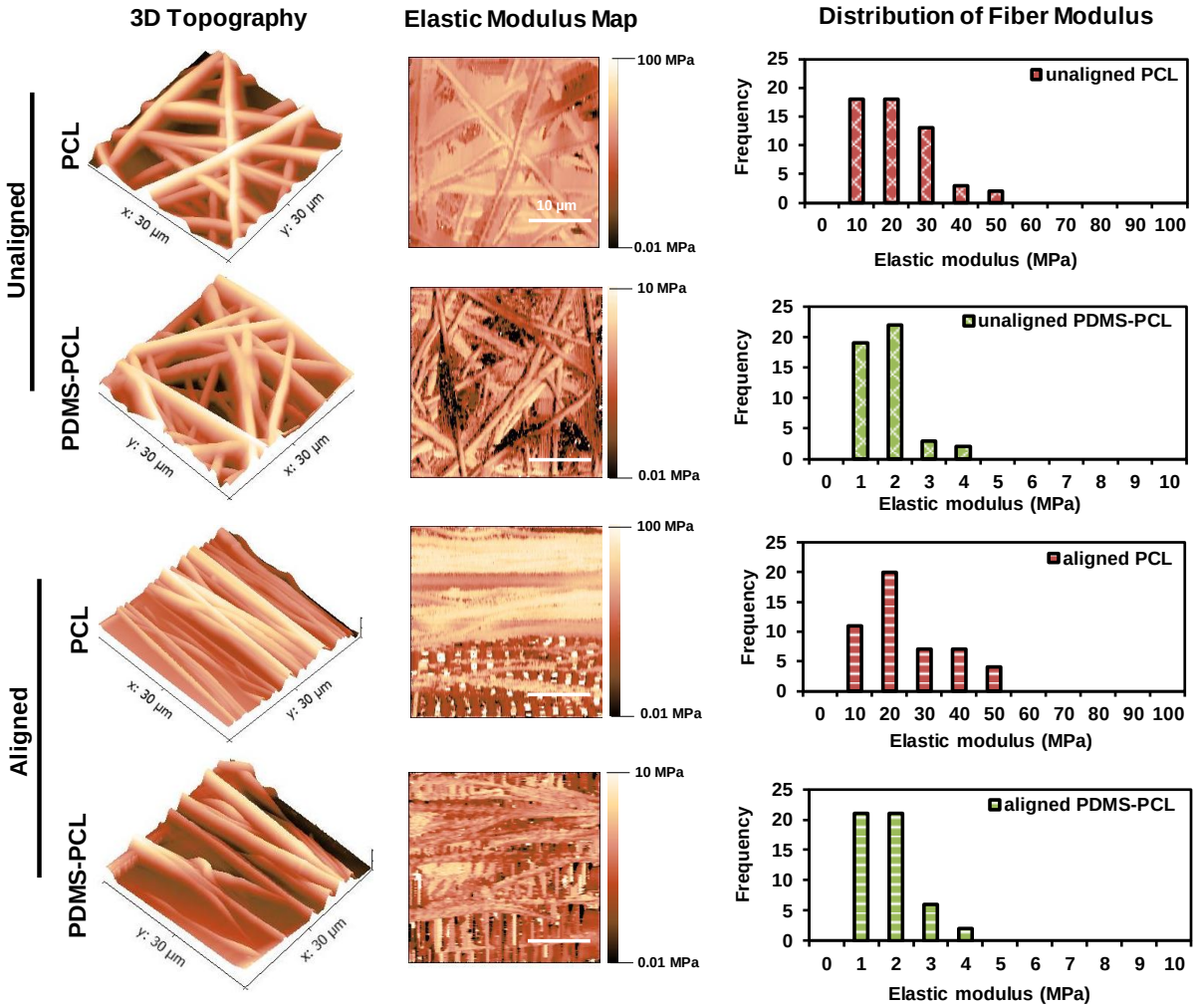

Figure 4.5: AFM Analysis of Unaligned and Aligned PCL-Only and PDMS-PCL Blend Nanofiber Meshes. For PCL-only meshes, fiber moduli range from 10-50 MPa, while for PDMS-PCL meshes, fiber moduli are ten-fold lower, and range from 1-4 MPa. There are no observed differences between unaligned and aligned fiber orientations for either PCL-only or PDMS-PCL meshes. *n*=6 independent regions per mesh, 10 measurements per image.

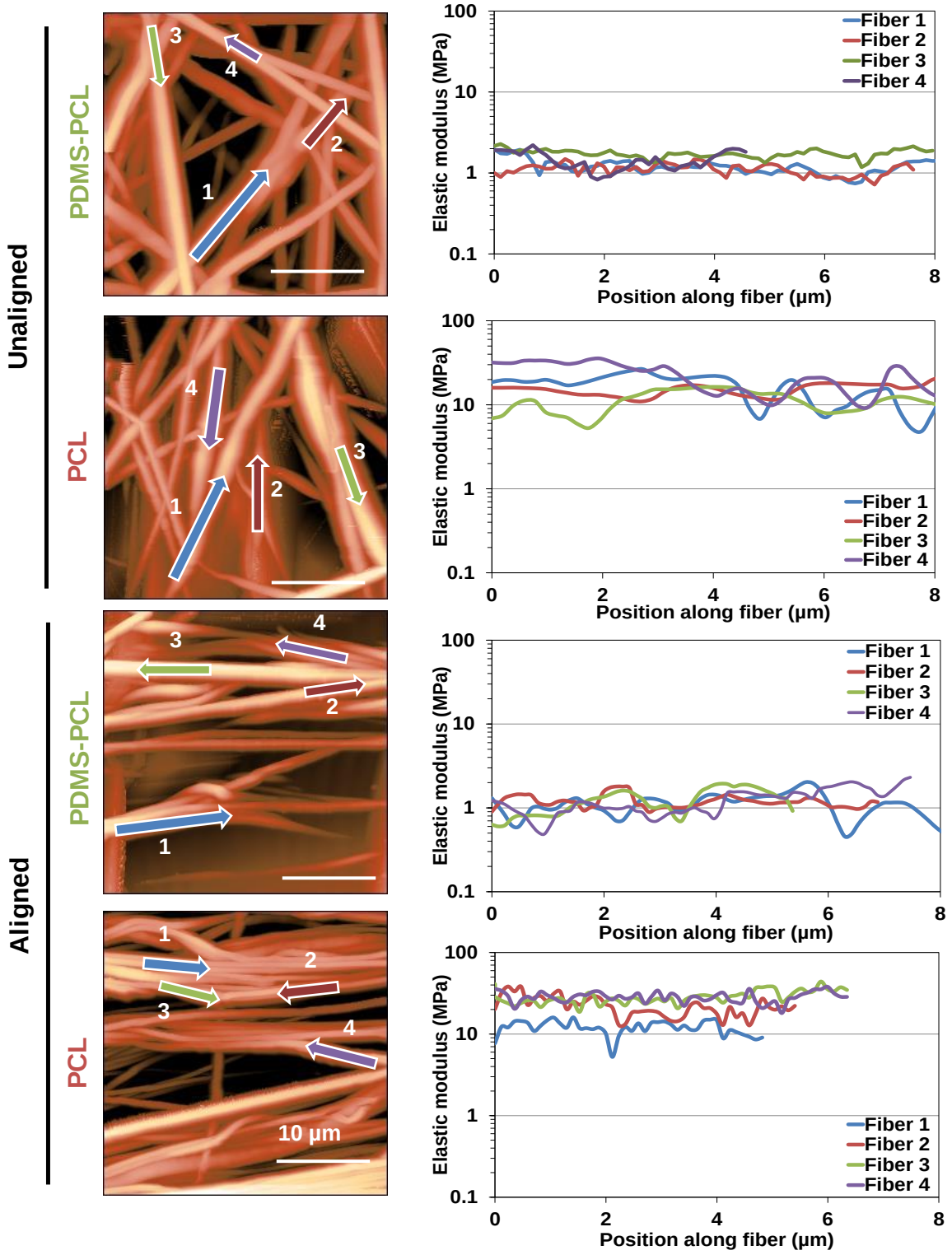

<u>Figure 4.6:</u> Sample Profiles Of Elastic Modulus Along Individual Fibers of PCL-Only and PDMS-PCL Blends in Unaligned and Aligned Fiber Orientations, as Determined via Atomic Force Microscopy. Elastic modulus was observed to be similar along the length of individual fibers for all groups. Some variation between fibers was observed. *n* = 6 independent images per group, 10 fibers per image.

CHAPTER 5: EFFECTS OF MATRIX ALIGNMENT AND MECHANICAL PROPERTIES ON MESENCHYMAL STEM CELL RESPONSE

5.1 Introduction

In *Chapter 4*, a nanofiber matrix-based platform was developed and optimized for assessing the effects of changes in matrix alignment and mechanical properties on cell response within the connective tissue cell microenvironment. In this chapter, the effects of these matrix-based differences on the response of mesenchymal stem cells, in terms of initial cell attachment, spreading, and alignment, as well as changes in cell proliferation, matrix synthesis, and differentiation potential were assessed.

5.1.1 Background and Motivation

Our goal is to examine the effects of matrix alignment and mechanical properties on MSC response, in order to determine the matrix-based cues which are critical to promoting stem cell-mediated tissue regeneration. Given their similarity to the native extracellular matrix (ECM), nanofiber-based scaffolds have been used to promote MSC response and differentiation. Early work by Baker *et al*. reported that for bovine MSC on PCL nanofibers, increased matrix mechanical properties were measured for aligned meshes after 10 weeks *in vitro* compared to unaligned meshes, when coupled with chondrogenic induction media(229). Notably, the majority of these studies have employed chemical factors along with scaffold cues, making it difficult to decouple the effects of these distinct stimuli. Still, more recent studies by Schofer *et al*.(242) and Jiang *et al*.(243) suggest that nanofiber alignment alone may guide MSC differentiation. Additionally, Subramony *et al*. has shown through culture of human MSC on unaligned and aligned PLGA that fiber alignment alone or paired with mechanical stimulation can result in MSC differentiation and enhanced proliferation and collagen synthesis(20).

In addition to the role that matrix architecture plays in determining stem cell lineage commitment and response, extensive work has been done to elucidate the effects of substrate stiffness on MSC behavior(22;23). Results show that at physiological elasticities, MSC are able to sense and respond their environment. In work by Engler *et al*., a series of polyacrylamide gels with elasticities ranging from 0.1-40 kPa were capable of modulating MSC shape, ultimately guiding stem cell differentiation. While soft substrates resulted in neuronal differentiation, stiffer substrates led to MSC differentiation toward a myogenic lineage(22). Finally, rigid substrates resulted in osteogenic differentiation. Building upon these findings, Zemel *et al*. determined that there is a mechanical coupling between cell shape and the

organization of the cytoskeleton with rigidity of the surroundings, and this is what modulates stem cell differentiation toward muscle cells(23).

5.1.2 Objectives

The objective of this study is to assess the effects of changes in matrix alignment and mechanical properties on stem cell response. Following gaining a better understanding of the role that these matrix properties play on modulating stem cell activation, in terms of proliferation, matrix synthesis, and differentiation, an ideal mesh may be chosen for design of a stem cell delivery vehicle for aiding in tissue regeneration following connective tissue injury. It is hypothesized that fiber alignment and mechanical properties will have a synergistic effect on MSC attachment, spreading, and alignment, resulting in enhanced MSC proliferation, matrix synthesis, and expression of ligament-related markers.

5.2 Materials and Methods

5.2.1 Human Mesenchymal Stem Cell Isolation and Culture

Human MSC were isolated from bone marrow aspirate of a 21 y/o male donor, obtained commercially (Lonza). Briefly, the aspirate was centrifuged on a discontinuous Percoll gradient to remove blood cells. Supernatant was then removed and mixed with F/S DMEM and plated on tissue culture plastic. Media was changed the following day to remove non-adherent cells. Adherent cells were assumed to be MSC and were passaged once prior to use or cryopreservation. For cryopreservation, cells were frozen in cryomedia containing F/S DMEM, 20% FBS, and 10% DMSO. Cells were thawed at P2 and maintained in culture with F/S DMEM containing 10% FBS (Atlanta Biologicals) and 1% P/S, without other antibiotics. Cells were passaged once prior to use in all studies.

5.2.2 Nanofiber Mesh Fabrication

5.2.2.1 Unaligned PCL

A 16% (w/v) PCL solution was prepared by dissolving PCL (M_n = 70,000-90,000, Sigma-Aldrich) into 3:1 solution of DCM (Sigma-Aldrich):DMF (Sigma-Aldrich). The solution was mixed overnight, vortexed for 1 hour prior to electrospinning, and then loaded into a 5 mL syringe attached with a 23-gauge stainless steel blunt-tip needle. A voltage of 7-9 kV was applied to the needle tip and a pump flow rate of 1 mL/hr was used. Fibers were collected on a grounded stationary plate placed 15 cm from the needle tip.

Approximately 2 mL of polymer solution was electrospun to fabricate scaffolds of thickness ranging from 0.09-0.14 mm as measured with a digital caliper.

5.2.2.2 Aligned PCL

An 18% (w/v) PCL solution was prepared by dissolving PCL (M_n = 70,000-90,000) into 3:2 mixture of DCM:DMF. The solution was mixed overnight, vortexed for 1 hour prior to electrospinning, and the entire solution loaded into a 5 mL syringe with a 23-gauge stainless steel blunt-tip needle. A voltage of 9-10 kV was applied to the needle tip and a pump flow rate of 1 mL/hr was used. Fibers were collected on a grounded rotating mandrel (2500 rpm), 13 cm from the needle tip. Approximately 5 mL of polymer solution was electrospun to fabricate scaffolds of thickness ranging from 0.07-0.14 mm as measured with a digital caliper.

5.2.2.3 Unaligned PDMS-PCL Blend

A 35% (w/v) PDMS-PCL solution was prepared by dissolving a 1:1 mixture of PDMS (Sylgard 184, 50:1 base:crosslinker, Dow Corning) and PCL (M_n = 70,000-90,000) in a 3:1 solution of DCM:DMF. The solution was vortexed for 4 hours prior to electrospinning, and then loaded into a 5 mL syringe attached with a 23-gauge stainless steel blunt-tip needle. A voltage of 10-11 kV was applied to the needle tip and a pump flow rate of 1 mL/hr was used. Fibers were collected on a grounded stationary plate placed 12 cm from the needle tip. Approximately 3 mL of polymer solution was electrospun to fabricate scaffolds of thickness ranging from 0.07-0.14 mm as measured with a digital caliper.

5.2.2.4 Aligned PDMS-PCL Blend

A 35% (w/v) PDMS-PCL solution was prepared by dissolving a 1:1 mixture of PDMS (50:1 base:crosslinker) and PCL (M_n = 70,000-90,000) in a 3:1 solution of DCM:DMF. The solution was vortexed for 4 hours prior to electrospinning, and then loaded into a 5 mL syringe attached with a 23-gauge stainless steel blunt-tip needle. A voltage of 10-11 kV was applied to the needle tip and a pump flow rate of 1 mL/hr was used. Fibers were collected on a grounded rotating mandrel (2100 rpm), 12 cm from the needle tip. Approximately 3.5 mL of polymer solution was electrospun to fabricate scaffolds of thickness ranging from 0.07-0.14 mm as measured with a digital caliper.

5.2.3 Cell Seeding on Nanofiber Meshes

Electrospun meshes were cut to 1 cm x 1.8 cm and secured to custom-made backings with tape, resulting in a cell culture surface area of 1 cm^2. To enhance surface reactivity and eliminate observed differences in fiber surface energy, PCL-only and PDMS-PCL fibers were then air plasma treated (Harrick Plasma PDC-32G) at high radiofrequency (RF) setting for 30 seconds. Meshes were then immediately UV sterilized (both sides, 15 minutes each) at 365 nm and incubated at 37ºC and 5% CO_2 overnight in F/S DMEM with 20% FBS to promote cell attachment.

After the overnight soak, media was removed and MSC were seeded on meshes at a density of $1x10^4$ cells/cm^2 (1 M cells/mL, 10 µl) and allowed to attach for 15 minutes under humidified conditions at 37ºC, 5% CO_2 before the addition of F/S DMEM. Monolayer culture seeded at $1x10^4$ cells/well on a 48 well (1 cm^2) plate served as controls. Cells were maintained at 37°C, 5% CO_2 and media was exchanged every 2-3 days.

5.2.4 Cell Viability

Cell viability (*n*=3) was visualized using Live/Dead staining (Molecular Probes). Cells on both monolayer and nanofiber meshes were stained following the manufacturer's suggested protocol. Samples were imaged using confocal microscopy (Olympus Fluoview FV1000) at excitation wavelengths of 488 nm (live) and 568 nm (dead).

5.2.5 Cell Proliferation

Cell proliferation (*n*=5) was determined by measuring total DNA content using the PicoGreen dsDNA assay (Invitrogen) following the manufacturer's protocol. Samples were rinsed twice in PBS and stored in 500 µL of 0.1% Triton X (Sigma-Aldrich) at -30°C. Immediately before the analysis, samples were thawed and homogenized and subjected to ultrasonication at 5W (Microson XL-2000) for 15 seconds. Fluorescence was measured using a microplate reader (Tecan, Research Triangle Park, NC) at an excitation wavelength of 485 nm and an emission wavelength of 535 nm. A standard curve was derived and used to correlate DNA concentration to fluorescence intensity, and cell number was determined based on a conversion factor of 8 pg DNA/cell(244).

Results from the dsDNA assay were also used to assess fold change in cell number, doubling time(245), and total population doublings(246) of MSC on fibers over time. Briefly, fold change in cell number was calculated using the equation: $FC = N / N_0$, where N is the total cells at that time point and N_0 is the average number of cells for the same group at day 1. Doubling time was calculated using the equation: $DT = (T - T_0) \log 2 / (\log N - \log N_0)$, where $(T - T_0)$ is the incubation period between the current time point and the previous time point (in hours), N is the number of cells at the time point of interest, and N_0 is the number of cells at the previous time point. Total population doubling was calculated using the equation: $PD = \log FC / \log 2$, where FC is the fold change as calculated above.

5.2.6 Cell Attachment and Spreading

Early cytoskeletal organization and formation of focal adhesions (*n*=3) was analyzed using immunohistochemistry. After 30 minutes, 1 hour, 3 hours, and 24 hours in culture, samples were rinsed twice in PBS and fixed in a 4% paraformaldehyde in PBS (pH 7.2) solution (preheated to 37°C) for 10 minutes. After fixation, samples were rinsed three times in PBS for 5 minutes each and then permeabilized with 0.1% Triton-X in PBS for 10 minutes. After one rinse in PBS, samples were blocked by the addition of a solution containing 1% bovine serum albumin (BSA) and 5% Goat Serum in an Immunostaining Buffer (20 mM Tris, 155 mM sodium chloride (NaCl), 2 mM ethylene glycol-bis(β-aminoethyl ether)-N,N,N',N'-tetraacetic acid (EGTA), 2 mM magnesium chloride ($MgCl_2$) (pH 7.4)) for 1 hr. Samples were then incubated with the primary antibody (Paxillin 1:500) for 1 hour in a humidified chamber at room temperature. The primary antibody was removed and samples were rinsed three times in PBS. The secondary antibody was added (Alexa Fluor 488 1:300), along with phalloidin conjugated to Alexa Fluor 647 (1:100), and samples were incubated for 1 hour at room temperature in the dark. After removal of this solution, samples were rinsed three times in PBS and counter-stained with DAPI for 30 minutes. Samples were rinsed three times in PBS and mounted on glass slides for visualization via confocal microscopy. All antibody dilutions were performed in the Immunostaining Buffer + 1% BSA solution.

Cell morphology (*n*=3) was also assessed after 1 day, 3 days, and 7 days of culture on nanofibers using SEM. At each time point, samples were rinsed twice in PBS and fixed in 10% NBF with 1% CPC overnight at 4ºC. After fixation, samples were dehydrated via ethanol series and allowed to dry overnight

before storage under vacuum in a desiccator. Prior to imaging, samples were sputter coated with AuPd. Nanofibers were then imaged using SEM (5 kV, 10 μA).

5.2.7 Cell Alignment

For cell alignment analysis, cell viability micrographs (*n*=6) were determined using circular statistics customized for evaluating alignment (Fiber3)(231). Circular statistics parameters include: the MA, which represents the average fiber alignment in the matrix ($|\theta| \leq 90°$), 0° representing a horizontal orientation; the MVL ($0 \leq r \leq 1$), 0 indicates a random and 1 indicates an aligned morphology; and AD which characterizes the dispersion of the non-Gaussian angle distribution of the nanofibers ($0° \leq \theta \leq 40.5°$), 0° represents aligned while 40.5° represents a random distribution.

5.2.8 Effects of Blebbistatin on Cell Proliferation

To determine whether observed differences in cell proliferation are a result of differences in cell spreading and actin stress fiber formation on meshes, blebbistatin was used in order to inhibit myosin II. For these studies, unaligned PCL-only or PDMS-PCL meshes were cut to 1 cm x 1.8 cm and secured to custom-made backings with tape, resulting in a cell culture surface area of 1 cm^2. To enhance surface reactivity and eliminate observed differences in fiber surface energy, PCL-only and PDMS-PCL fibers were then air plasma treated (Harrick Plasma PDC-32G) at high radiofrequency (RF) setting for 30 seconds. Meshes were then immediately UV sterilized (both sides, 15 minutes each) at 365 nm and incubated at 37ºC and 5% CO_2 overnight in F/S DMEM with 20% FBS to promote cell attachment.

After the overnight soak, medium was removed and MSC were seeded on meshes at a density of $1x10^4$ cells/cm^2 (1 M cells/mL, 10 μL) and allowed to attach for 15 minutes under humidified conditions at 37ºC, 5% CO_2 before the addition of F/S DMEM. Cells were also seeded in monolayer at a density of $1x10^4$ cells/well on a 48 well (1 cm^2) plate. Cells were maintained at 37°C, 5% CO_2. For experimental groups, 50 μM blebbistatin in 90% DMSO was added to each well in the dark. For control groups, an equal amount of 90% DMSO without blebbistatin was added to each well. Medium was replaced every 48 hours and samples were cultured for 14 days. Samples were collected at 1 and 14 days for quantification of cell number, suing the protocol described in *Section 5.2.5*.

5.2.9 Primary Cilium Staining

Unaligned PCL-only or PDMS-PCL meshes were cut to 1 cm x 1.8 cm and secured to custom-made backings with tape, resulting in a cell culture surface area of 1 cm^2. To enhance surface reactivity and eliminate observed differences in fiber surface energy, PCL-only and PDMS-PCL fibers were then air plasma treated (Harrick Plasma PDC-32G) at high radiofrequency (RF) setting for 30 seconds. Meshes were then immediately UV sterilized (both sides, 15 minutes each) at 365 nm and incubated at 37ºC and 5% CO_2 overnight in F/S DMEM with 20% FBS to promote cell attachment. After the overnight soak, medium was removed and MSC were seeded on meshes at a density of $1x10^5$ cells/cm^2 (10 M cells/mL, 10 µL) and allowed to attach for 15 minutes under humidified conditions at 37ºC, 5% CO_2 before the addition of F/S DMEM. Cells were cultured up to 7 days, and culture medium was changed every 2-3 days.

On day 7, cells were fixed in 10% neutral buffer formalin for 10 minutes. Fixed cells were rinsed three times with PBS, permeabilized with 0.1% Triton X-100 in PBS for 5 minutes, followed by a blocking wash consisting of 10% Goat Serum in PBS for 1 hour. Cells were then incubated in monoclonal murine anti-acetylated α tubulin (C3B9, gifted from Jacobs lab) diluted 1:10 in PBS for 1 hour at room temperature, followed by AlexaFluor 488 goat anti-mouse IgG diluted 1:1000 in PBS for 1 hour at room temperature. Nuclei were counterstained with DAPI (0.5 mg/ml) diluted 1:100 in PBS for 7 minutes. Cells were then washed three times with PBS and imaged immediately.

Confocal micrographs were used to determine the incidence of primary cilia for cells on both unaligned PCL-only and PDMS-PCL (*n*=5 images/group). Images were collected from regions with similar cell densities and total cell number, at a magnification of 40x. Using ImageJ software (NIH), the number of nuclei and the number of primary cilia in each image were counted manually and the incidence of primary cilia was calculated by dividing the total number of observed cilia by the total number of cell nuclei in each image.

5.2.10 Collagen Production

Collagen production (*n*=5) was quantified using a modified hydroxyproline assay(199). Samples were digested in a buffered papain solution prior to analysis. For digestion, samples were vacuum dried overnight using a Centrivap concentrator (Labconco). Samples were then digested for 18 hours at 65ºC with 20 µL/mL papain (Sigma-Aldrich), buffered in 0.1 M sodium acetate, 10 mM cysteine HCl, and 50 M

EDTA. For the assay, digested samples were concentrated by drying 125-250 µL of sample overnight in the Centrivap concentrator. Samples were resuspended in 50 µL of 2 N NaOH and autoclaved for 25 minutes. 450 µL of Chloramine T Reagent (1.27 g chloramine T in 50% isopropanol brought to 100 mL with acetate-citrate buffer) was added to the samples, which were then allowed to incubate for 25 minutes at room temperature. 500 µL of Ehrlich's reagent (15 g p-dimethylaminobenzaldehyde in 100 mL (2:1) isopropanol:perchloric acid) was subsequently added, and the samples incubated at 65ºC for 20 minutes. The absorbance at 555 nm was read using a Tecan microplate reader. Total collagen was determined using a standard curve generated using a collagen standard (Sigma).

The acetate-citrate buffer for the chloramine T solution consisted of 30 g sodium acetate trihydrate, 11.5 g citric acid, 3 mL acetic acid, and 8.5 g NaOH, dissolved in 125 mL of distilled water. The solution was brought to a pH of 6.5 using 1 N NaOH or 1 N HCl, and then brought to a final volume of 250 mL.

5.2.11 Alkaline Phosphatase Activity

After sample homogenization, samples were assayed for alkaline phosphatase (ALP) activity. On ice, 50 µL of sample was added to a 96-well plate and 50 µL of 0.1 M Na_2CO_3:2 mM $MgCl_2$ with 10 mM pNP-PO_4 was subsequently added. The plate was incubated at 37°C until a color change was noted. The absorbance at 405 nm was then read using a Tecan microplate reader. ALP activity is reported normalized to incubation time and post-sonication cell number.

5.2.12 Expression of Ligament- and Bone-Related Markers

Gene expression was analyzed using qRT-PCR. Samples were rinsed twice with PBS and stored in Trizol (Invitrogen). RNA was isolated using the chloroform/Trizol extraction method. The extracted RNA pellet was redissolved in 150 µL DEPC H_2O (Ambion). First-strand cDNA was synthesized using 50 µM oligo$(dT)_{20}$ primer, 10 mM dNTP mix, and 8 µL of extracted RNA. cDNA synthesis was accomplished using 5X RT buffer, DTT, 40 U/µL RNaseOUT, and 200U/µL SuperScript III RT. The cDNA product was subsequently amplified and quantified through real-time PCR using SYBR Green Supermix (Invitrogen). GAPDH served as the house-keeping gene. All genes were amplified for 50 cycles in a thermocycler (iCycler iQ Real-Time PCR Detection System, BioRad). See *Table 5.1* for primer sequences used and

amplicon sizes. Normalized expression levels were calculated based on the difference between threshold cycles of the gene of interest and GAPDH.

Table 5.1: Primer Sequences for Gene Expression

Gene	Sense	Anti-Sense	Blast product Size (bp)
GAPDH	5'- GGCGATGCTGGCGCTGAGTA-3'	5'-ATCCACAGTCTTCTGGGTGG-3'	306
Collagen I	5'-TGGTCCACTTGCTTGAAGAC-3'	5'-ACAGATTTGGGAAGGAGTGG-3'	118
Collagen III	5'-GGCTACTTCTCGCTCTGCTT-3'	5'-CATATTTGGCATGGTTCTGG-3'	130
Fibronectin	5'-TTGAACCAACCTACGGATGA-3'	5'-AAATGACCACTTCCAAAGCC-3'	137
Osteocalcin	5'-AGGGCAGTAAGGTGGTGAAT-3'	5'-CTAAACGGTGGTGCCATAGA-3'	135
Osteopontin	5'-TGTGTCCTCTGAAGAAACGG-3'	5'-AGAATCCTCGCTCTCTGCAT-3'	82

5.2.13 Statistical Analysis

Results are reported as mean ± standard deviation, with n equal to the number of replicates per group. Statistical analyses were performed with JMPIN (4.0.4, SAS Institute, Inc.). Two-way ANOVA was used to determine the effects of nanofiber alignment and composition on cell response (cell alignment, proliferation, matrix deposition, ALP activity, gene expression). To determine the effects of matrix composition on the incidence of primary cilia, sample sets were checked for normality and equal variance, followed by performance of a corrected t-test. The Tukey-Kramer post-hoc test was used for all pair-wise comparisons, and significance was attained at $p<0.05$.

5.3 Results

5.3.1 Cell Viability and Proliferation

Cells remain viable and proliferate on all meshes and in monolayer over the three-week study (*Figure 5.1*). *Effects of Fiber Alignment*: There were no observed differences in cell number or fold change in cell number between unaligned and aligned fibers for either PCL-only or PDMS-PCL meshes (*Figure 5.2*). *Effects of Fiber Mechanical Properties:* For unaligned meshes, total cell number and fold change in cell number were significantly greater on PDMS-PCL compared to PCL-only on days 14 and 21. For aligned meshes, total cell number and fold change in cell number over time were greater on PDMS-PCL compared to PCL-only at day 21 (*Figure 5.2*). Total population doublings and doubling time over the three-week study appear similar for all groups (*Figure 5.2*).

5.3.2 Cell Organization and Morphology

Immunohistochemical staining for F-actin and focal adhesions shows cell attachment and spreading within 30 minutes on all groups (*Figure 5.3). Effects of Fiber Alignment*: There appears to be a higher incidence of projections and increased stress fiber formation on aligned fibers compared to unaligned fibers for both PCL-only and PDMS-PCL meshes within 30 minutes (*Figure 5.3*). By day 1 on aligned fibers, cells appear aligned on both PCL-only and PDMS-PCL meshes, with actin stress fibers formed parallel to polymer fibers (*Figure 5.3*). *Effects of Fiber Mechanical Properties:* After 30 minutes on meshes, there are no observable differences between cell spreading on PDMS-PCL and PCL-only for either fiber orientation at this time point. After 24 hours on unaligned fibers, cells on PDMS-PCL fibers appear to form small projections in all directions, while stress fiber formation and polarization can be observed on PCL-only meshes (*Figure 5.3*). Additionally, focal adhesions, as indicated by paxillin staining, appear more prominent on PCL-only fibers after 24 hours compared to PDMS-PCL fibers in both unaligned and aligned fiber orientations (*Figure 5.3*). Scanning electron microscopy images after 24 hours confirm these results, as MSC on unaligned PCL and PDMS-PCL fibers appear more spread, with no inherent alignment, while MSC on aligned meshes appear aligned along the direction of nanofiber alignment. By day 7, MSC spreading is enhanced on all groups, with a greater degree of alignment and a more spindle-shaped cell morphology than was observed on day 1 (data not shown).

5.3.3 Cell Alignment

Cellular alignment was quantified, as shown in *Figure 5.4*. *Effects of Fiber Alignment*: Assessment of cellular AD shows that cells remain randomly oriented on unaligned fibers over time. Cells are significantly more aligned on aligned meshes compared to unaligned groups by day 1, as shown by a significantly decreased AD and increased MVL (*Figure 5.4*). *Effects of Fiber Mechanical Properties:* For cells on unaligned meshes, MSC remain randomly oriented throughout the 21-day study on both PCL-only and PDMS-PCL meshes, with minor increases in alignment (as observed by a decrease in AD from ~30º at day 1 to ~20º by day 21) over time. Alignment on both unaligned PCL and PDMS-PCL meshes is similar to cell alignment in monolayer at all time points. For aligned meshes, MSC appear aligned (AD ~5º) on PCL-only fibers by day 1, while MSC on PDMS-PCL fibers were significantly less aligned (AD ~15º) at this

time point (*Figure 5.4*). By day 7, this difference was no longer observed, and cells remain aligned through the remainder of the 21-day study.

5.3.4 Mechanism of Cell Mechanotransduction

For MSC in monolayer, the addition of 50 μM blebbistatin to culture medium results in decreased MSC proliferation at all time points compared to controls (*Figure 5.5)*. On unaligned PCL-only and PDMS-PCL, cell number was significantly lower for blebbistatin-treated groups compared to untreated controls by day 14 (*Figure 5.5*). Still, fold change in cell number was greater on PDMS-PCL fibers compared to PCL-only in both blebbistatin-treated groups and untreated controls by day 14, suggesting that differences in non-muscle myosin II are not responsible for the observed differences in cell proliferation on PDMS-PCL and PCL-only fibers (*Figure 5.5*).

The incidence of primary cilia on MSC seeded on unaligned PCL-only and PDMS-PCL was determined on day 7. Results show that a significantly greater concentration of primary cilia was observed on PC-only fibers compared to PDMS-PCL, with a 33.7 ± 9.8% incidence on PCL-only and only 20.3 ± 2.7% of cells staining for the presence of primary cilia on PDMS-PCL meshes (*Figure 5.6*).

5.3.5 Mineralization Potential

Alkaline phosphatase activity normalized to cell number and reaction time is reported in *Figure 5.7* for nanofiber groups and monolayer. ALP activity showed similar trends over time for all nanofiber groups and monolayer, with an initial peak in activity at days 1 and 3, and decreasing ALP activity per cell over time for the remainder of the study (*Figure 5.7*). *Effects of Fiber Alignment*: There was no significant difference in ALP activity at any time point between unaligned and aligned fibers for PCL-only or PDMS-PCL groups (*Figure 5.7*). *Effects of Fiber Mechanical Properties:* There was no significant difference in ALP activity at any time point between PCL-only and PDMS-PCL meshes in either unaligned or aligned fiber orientations (*Figure 5.7*).

5.3.6 Stem Cell Differentiation

Effects of Fiber Alignment: There were no differences in MSC gene expression at days 1 or 14 between unaligned and aligned fibers for PCL-only or PDMS-PCL groups (*Figure 5.8*). *Effects of Fiber Mechanical Properties:* There were no major differences observed in the expression of tendon-related

(fibronectin, type I collagen, type III collagen) or bone-related (osteocalcin, osteopontin) genetic markers on days 1 or 14 between unaligned PDMS-PCL and PCL-only fibers (*Figure 5.8*). For aligned meshes, similar gene expression was observed for MSC on PDMS-PCL and PCL-only fibers, as well (*Figure 5.8*).

5.4 Discussion

In this chapter, the effects of matrix alignment and mechanical properties on stem cell response were assessed using four distinct meshes (unaligned vs. aligned fibers and PDMS-PCL vs. PCL-only fibers), in terms of cell attachment, spreading, and alignment, as well as effects of cell-matrix interactions on stem cell response in terms of proliferation and differentiation. While matrix alignment and mechanical properties did not have a significant effect on stem cell differentiation toward a ligament or bone lineage, matrix mechanical properties resulted in differences in MSC proliferation *in vitro*.

With respect to the effects of matrix alignment on stem cell response, initial cell alignment was guided by scaffold fiber organization, with MSC displaying an elongated and organized morphology on the aligned fibers only, regardless of polymer type. This is expected as cells attach and interact with their substrates through focal adhesions which are associated with cytoskeletal actin stress fibers and thus control cell shape(247;248). Interestingly, cells in all groups, including unaligned fibers and monolayer, became more aligned and organized with time, in which no significant differences of cell alignment parameters were observed after 4 weeks of culture. This phenomenon may be mimetic of the maturation and remodeling phase of connective tissue repair, in which scar tissue generated during the proliferative phase is disorganized and cells on this matrix are randomly oriented, but as cells begin to remodel the scar tissue to improve matrix alignment and mechanical properties, cells begin to align and deposit aligned collagen, as well.

Over the 21-day study, cell proliferation was greater on all meshes compared to tissue culture plastic. This is similar to findings observed by Jahani *et al.,* who observed increased proliferation by rat MSC seeded on unaligned and aligned plasma-treated PCL fibers than tissue culture plastic over 5 days(249). This is potentially due to the increased surface area of nanofiber meshes compared to 2D substrates, offering more space for cells to divide. Still, there were no observed differences in cell number between cells on unaligned and aligned fibers for either fiber composition at day 21, suggesting that fiber alignment does not impact cell proliferative rate. Previous findings on the effects of fiber alignment on stem

cell proliferation are mixed, as Subramony *et al*. observed increased proliferation by human MSC on aligned PLGA fibers compared to unaligned fibers *in vitro*(20), while Jahani *et al.* observed the opposite effect, with increased cell number on unaligned PCL fibers compared to aligned PCL fibers after 5 days(249).

No effects of matrix alignment on the expression of tendon-/ligament-related markers were observed at days 1 or 14. This is similar to the results observed by Subramony *et al*., which suggest that fiber alignment alone is not sufficient to promote tenogenic differentiation of MSC(32). These findings suggest that fiber alignment alone is not sufficient to promote MSC differentiation toward a fibroblastic phenotype. Still, by pairing fiber alignment with other cues, such as mechanical stimulation or chemical supplementation, it may be possible that fiber alignment plays a role in promoting differentiation, and it is likely that an aligned matrix mimetic of healthy fibrous connective tissue may aid in tenogenic differentiation.

With respect to the effects of matrix mechanical properties on cell response, fiber modulus affects cell spreading and cytoskeletal organization as early as 30 minutes after cell seeding, as cells on unaligned, mechanically stiffer PCL-only fibers appear larger and more spread than MSC on unaligned PDMS-PCL at this time point. This difference in cell spreading is even more apparent on aligned fibers, as cells on PCL-only meshes appear more spread with longer actin stress fibers, as compared to MSC on aligned PDMS-PCL, which appear mostly rounded at this time. After 24 hours, MSC on unaligned PCL-only appear to undergo stress fiber polarization, with actin fibers aligned along the length of polymer fibers, while on PDMS-PCL, cells remain rounded with many tiny projections forming in all directions. Cell spreading on unaligned PDMS-PCL meshes within 24 hours is similar to what has been described by Engler *et al.,* in which MSC were seeded on soft collagen-coated gels(22). At low matrix elasticities similar to the elasticity observed in brain tissue, MSC were observed to exhibit branched, filopodia-rich morphologies. Alternatively, in other works, Engler *et al.* seeded MSC on ten-fold stiffer substrates mimetic of muscle stiffnesses and observed more spindle-shaped cells(114), similar to the morphology of MSC on unaligned PCL-only fibers.

Additionally, cell proliferation is greater on softer PDMS-PCL fibers compared to PCL-only fibers at days 14 and 21, for both unaligned and aligned meshes. According to work by Chen *et al*., it has been shown that substrate stiffness and its initial effects on cell adhesion can have long-term effects on cell

proliferation and apoptosis, due to changes in integrin signaling(250). There were no observed effects of matrix mechanical properties on the expression of ligament-related markers, however, at days 1 or 14.

In an attempt to elucidate the mechanism by which matrix mechanical properties affect stem cell proliferative rate, the role of non-muscle myosin and primary cilia were assessed. In order to isolate the effects of non-muscle myosin on stem cell proliferative rate, blebbistatin was added to the culture medium of MSC cultured on unaligned PDMS-PCL and PCL-only meshes. Blebbistatin is a small molecule inhibitor of non-muscle myosin II, and has been shown to block branching, elongation, and spreading on MSC in 2D, resulting in differences in stem cell lineage commitment(22;251). Here, the effects of blebbistatin on stem cell proliferative rate were assessed, and it was observed that blebbistatin significantly reduced cell proliferation on both 2D and 3D substrates. Still, for MSC cultured with and without blebbistatin, fold change in cell number was greater on unaligned PDMS-PCL compared to PCL-only by day 14, suggesting that differences in proliferative rate for MSC on these two matrices are not related to non-muscle myosin II.

Primary cilia are sensory organelles(252) that have been shown to contribute to cell mechanotransduction and lineage commitment in human MSC(253;254). In this study, the incidence of cilia on MSC seeded on unaligned PCL-only and PDMS-PCL fibers was assessed, and it was found that there is a lower incidence of cilia on PDMS-PCL fibers compared to PCL-only. This may be correlated to observed differences in MSC proliferative rate on PDMS-PCL vs. PCL-only fibers, as primary cilia have previously been shown to regulate the proliferation of human MSC *in vitro*(254). That is, it has been observed that the incidence of cilia is enhanced for cells in the G_0 resting phase of the cell cycle compared to cells in the active phases of the cell cycle. This suggests that mechanotransduction via the primary cilium may be a mechanism via which stem cells sense their surrounding microenvironment. Specific to the ACL, this sensing ability may be further enhanced *in vivo* in the join capsule, when fluid flow occurs during movement, resulting in further mechanosensing capabilities of the primary cilia.

Results from this study show that stem cell survival and growth are supported on both unaligned and aligned meshes comprised of PDMS-PCL and PCL-only. In choosing an optimal matrix organization and composition for an engineered cellular microenvironment for promoting stem cell-guided tissue regeneration, it is worth noting that PCL-only fibers, especially in aligned fiber orientations, may be beneficial for promoting collagen synthesis by MSC, while PDMS-PCL may serve as a valuable matrix for

promoting stem cell proliferation. Additionally, MSC are not observed to undergo differentiation toward a fibroblast phenotype on any mesh over time. Therefore, if stem cell differentiation toward a ligament or tendon lineage is desired, additional stimuli, such as mechanical stimulation or chemical supplementation may be necessary in order to achieve this outcome. These observations will be taken into account when choosing the ideal fiber alignment and composition for delivery of stem cells to promote connective tissue regeneration.

5.5 Conclusion

In this chapter, the effects of changes in matrix alignment and mechanical properties on stem cell response were determined. In terms of the effects of fiber alignment on stem cell response, it was observed that MSC spread more quickly on aligned fibers, as cells appear larger on aligned fibers within 30 minutes compared to cells on unaligned fibers, and a greater incidence of focal adhesions on these substrates were observed compared to unaligned fibers by day 1. Additionally, cells are more aligned on aligned fibers within 30 minutes, as observed by the presence of stress fibers at this early time point, and cells remain significantly more aligned over 21 days. Still, no effects of fiber alignment on cell proliferation, matrix synthesis, or gene expression were observed. As for the effects of matrix mechanical properties, fiber modulus appears to impact cytoskeletal organization, as cells on unaligned, stiffer PCL-only fibers contain organized actin fibers within 24 hours, while cells on unaligned PDMS-PCL appear more rounded with randomly oriented projections. Cell proliferation was also significantly increased over time on both unaligned and aligned PDMS-PCL fibers compared to PCL-only fibers, suggesting initial cell attachment may have an impact on cell cycle. In *Chapter 8*, the effects of matrix topography and mechanics on the healing response of MSC will be assessed.

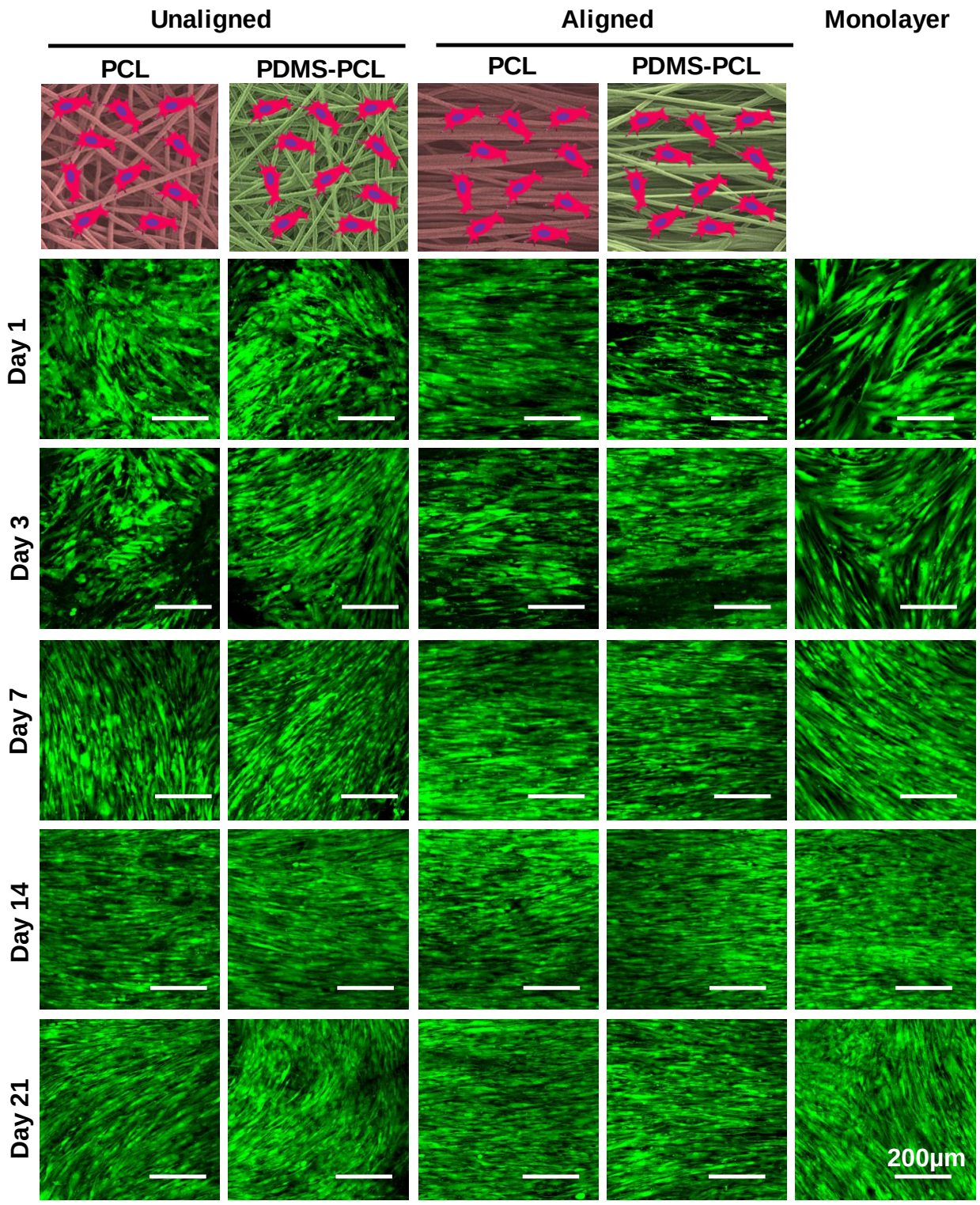

Figure 5.1: Effects of Matrix Alignment and Mechanical Properties on MSC Response: Cell Viability. Cells remain viable on all meshes, as well as in monolayer, over 21 days. *n*=3, mag = 20x, scale bar = 200 µm.

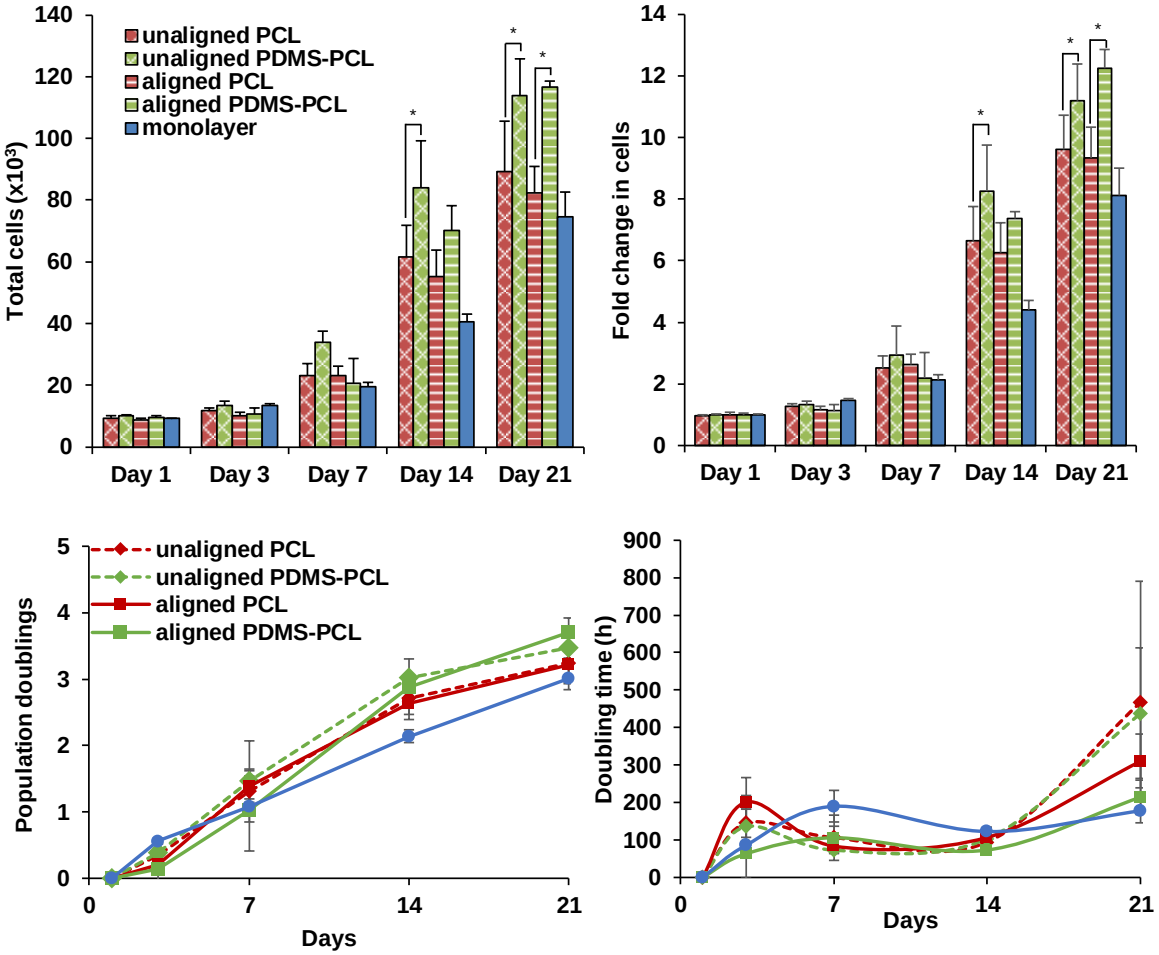

<u>Figure 5.2:</u> Effects of Matrix Alignment and Mechanical Properties on MSC Response: Cell Proliferation. Cell number was greater on all meshes compared to monolayer at days 14 and 21. Cell number and fold chance in cell number is greater for MSC on unaligned PDMS-PCL fibers compared to PCL-only fibers at days 14 and 21. Total cells and fold change in cell number were greater on aligned PDMS-PCL compared to PCL-only by day 21, as well. n=5. Significant difference between: * PCL-only and PDMS-PCL fiber compositions, ^ aligned and unaligned fiber orientations (p<0.05).

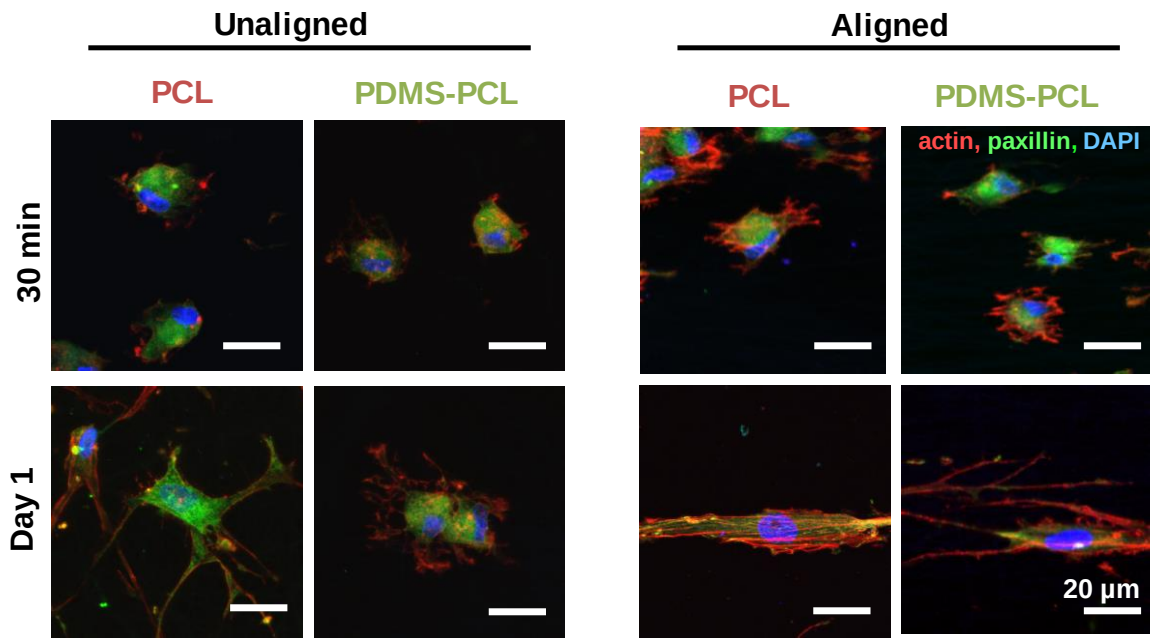

Figure 5.3: Effects of Matrix Alignment and Mechanical Properties on MSC Response: Cell Attachment and Spreading. Cells appear more spread out on PCL-only fibers compared to PDMS-PCL after 30 minutes of attachment, with more intense staining for actin stress fiber polarization by day 1 on both aligned and unaligned PCL-only fibers compared to PDMS-PCL. Stress fibers are visible on aligned fibers within 30 minutes, and are more visible on aligned fibers than unaligned fibers at both 30 minutes and 24 hours after cell seeding. Focal adhesions, observed via paxillin staining, appear more prominently on MSC seeded on PCL-only compared to PDMS-PCL fibers. Mag = 40x, *n*=3, scale bar = 20 µm.

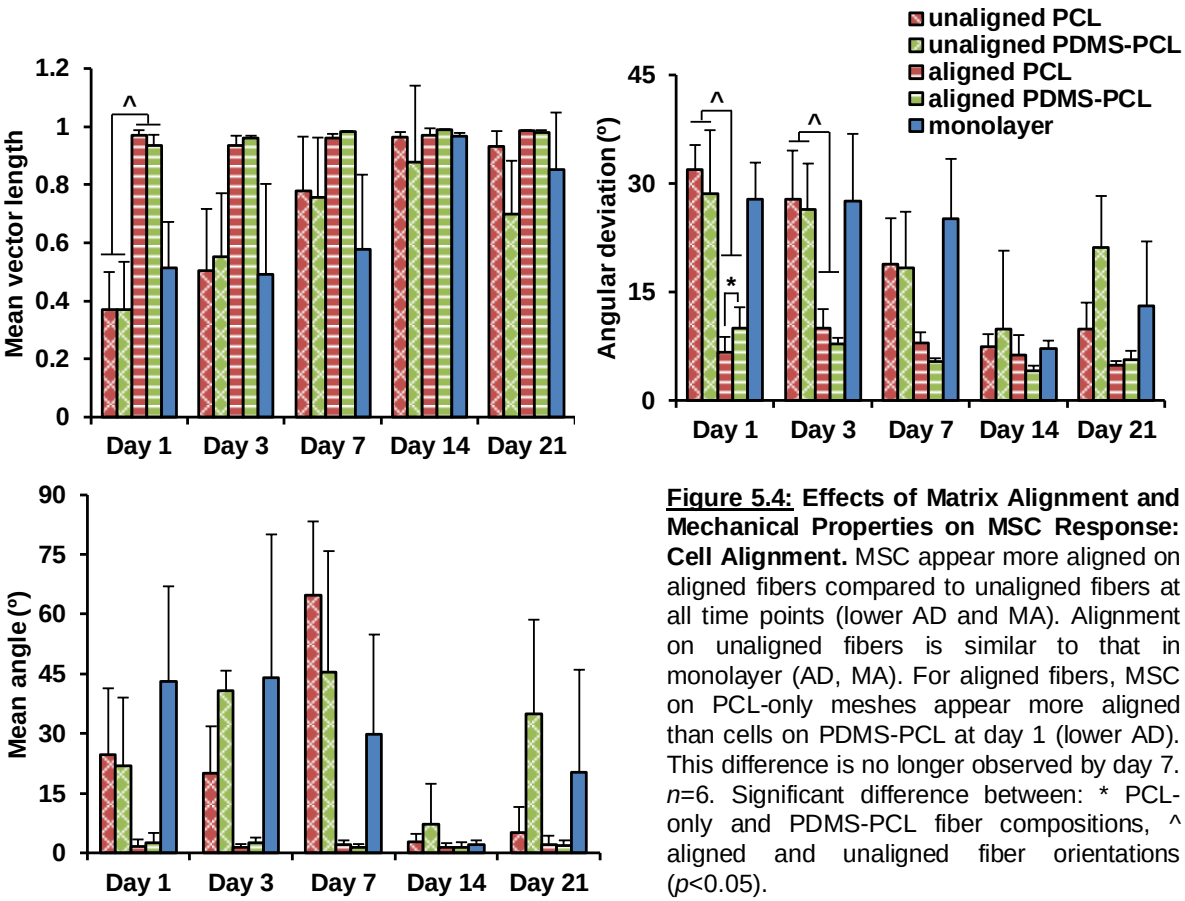

Figure 5.4: Effects of Matrix Alignment and Mechanical Properties on MSC Response: Cell Alignment. MSC appear more aligned on aligned fibers compared to unaligned fibers at all time points (lower AD and MA). Alignment on unaligned fibers is similar to that in monolayer (AD, MA). For aligned fibers, MSC on PCL-only meshes appear more aligned than cells on PDMS-PCL at day 1 (lower AD). This difference is no longer observed by day 7. *n*=6. Significant difference between: * PCL-only and PDMS-PCL fiber compositions, ^ aligned and unaligned fiber orientations ($p<0.05$).

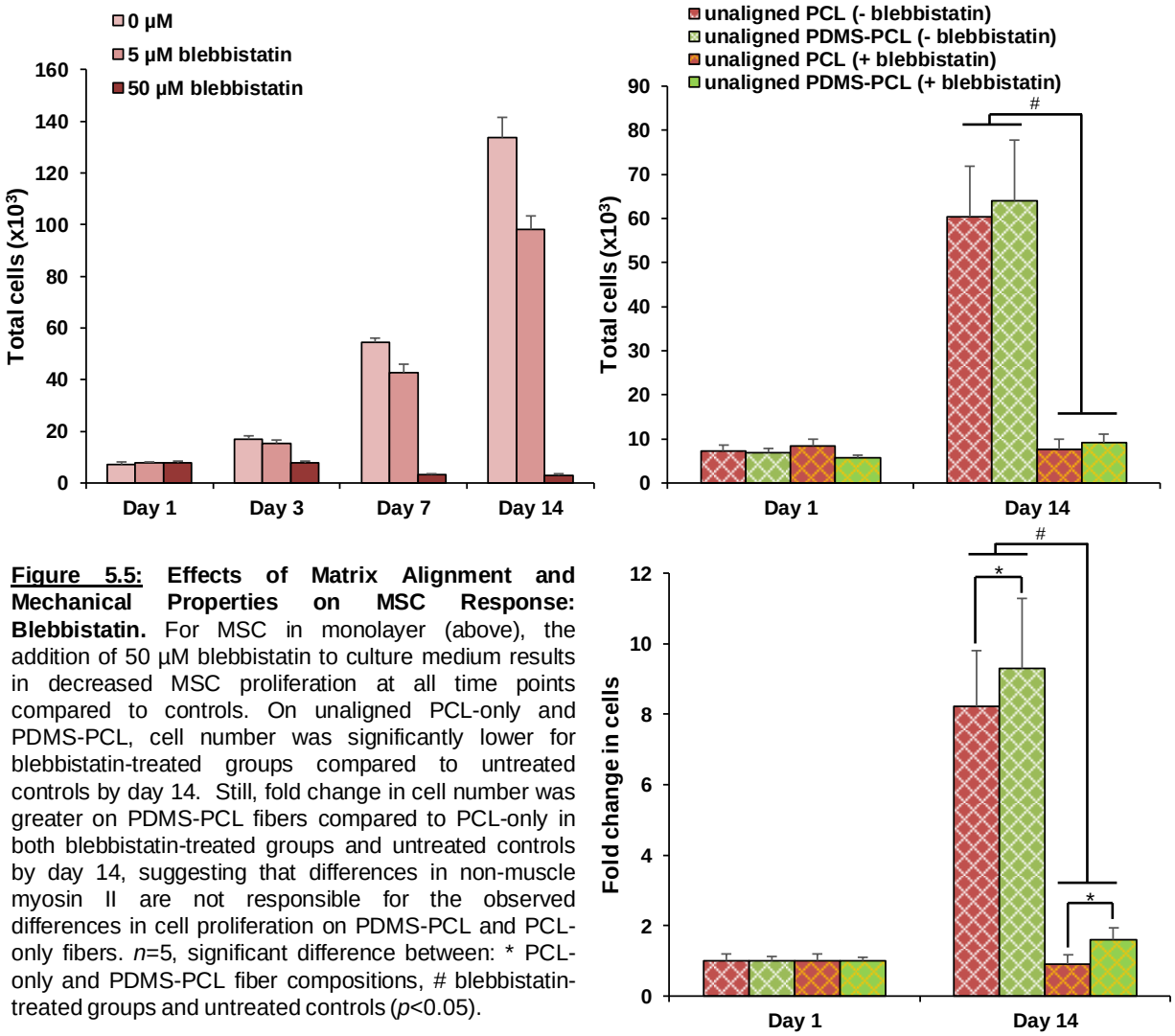

Figure 5.5: Effects of Matrix Alignment and Mechanical Properties on MSC Response: Blebbistatin. For MSC in monolayer (above), the addition of 50 µM blebbistatin to culture medium results in decreased MSC proliferation at all time points compared to controls. On unaligned PCL-only and PDMS-PCL, cell number was significantly lower for blebbistatin-treated groups compared to untreated controls by day 14. Still, fold change in cell number was greater on PDMS-PCL fibers compared to PCL-only in both blebbistatin-treated groups and untreated controls by day 14, suggesting that differences in non-muscle myosin II are not responsible for the observed differences in cell proliferation on PDMS-PCL and PCL-only fibers. *n*=5, significant difference between: * PCL-only and PDMS-PCL fiber compositions, # blebbistatin-treated groups and untreated controls ($p<0.05$).

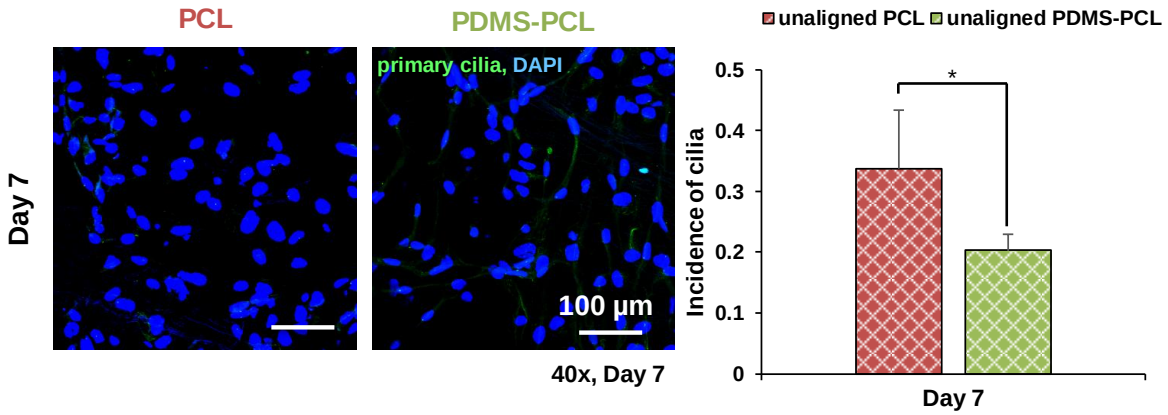

Figure 5.6: Effects of Matrix Alignment and Mechanical Properties on MSC Response: Incidence of Primary Cilia. The incidence of primary cilia on MSC seeded on unaligned PCL-only and PDMS-PCL was determined on day 7. Results show that a significantly greater concentration of primary cilia was observed on PCL-only fibers compared to PDMS-PCL, with a 33.7 ± 9.8% incidence on PCL-only and 20.3 ± 2.7% of cells staining for the presence of primary cilia on PDMS-PCL meshes. n=5, significant difference between: * PCL-only and PDMS-PCL fiber compositions (p<0.05).

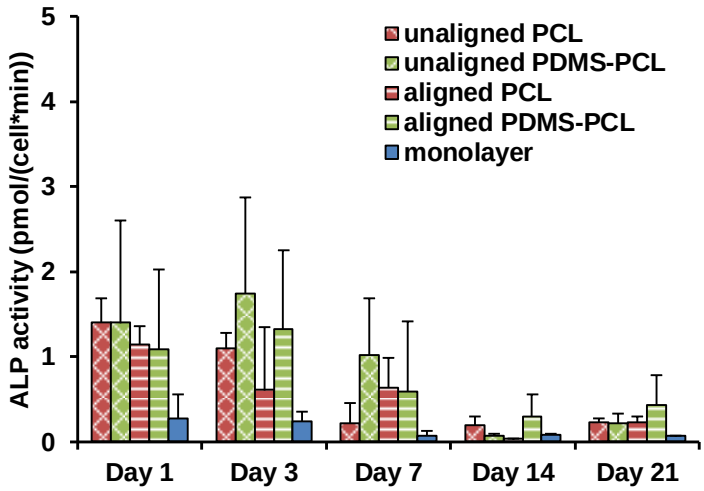

Figure 5.7: Effects of Matrix Alignment and Mechanical Properties on MSC Response: Alkaline Phosphatase Activity. There were no major differences in alkaline phosphatase (ALP) activity between groups at any time point over the 21-day study. n=5, significant difference between: * PCL-only and PDMS-PCL fiber compositions, ^ aligned and unaligned fiber orientations (p<0.05).

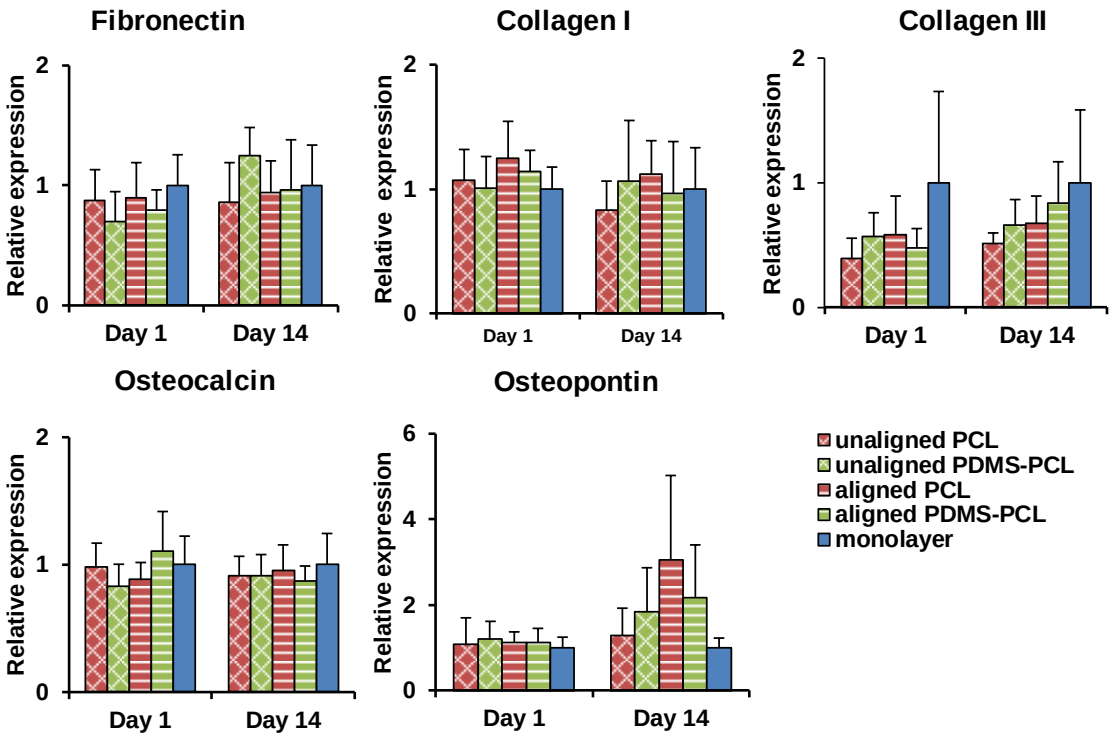

Figure 5.8: Effects of Matrix Alignment and Mechanical Properties on MSC Response: Gene Expression. There were no differences in the expression of any of the genes analyzed between unaligned and aligned fiber orientations, for either PCL-only or PDMS-PCL fiber compositions, at days 1 or 14. There were also no differences in the expression of any of the genes analyzed between PCL-only and PDMS-PCL meshes in either unaligned or aligned fiber orientations at either time point. n=5, significant difference between: * PCL-only and PDMS-PCL fiber compositions, ^ aligned and unaligned fiber orientations (p<0.05).

CHAPTER 6: EFFECTS OF MATRIX ALIGNMENT AND MECHANICAL PROPERTIES ON FIBROBLAST ACTIVITY

6.1 Introduction

In *Chapter 5*, the effects of matrix alignment and mechanical properties on MSC was assessed. It was found that fiber mechanical properties resulted in initial differences in cell attachment, spreading, and cytoskeletal organization at early time points, and differences in proliferative rate at later time points. *Chapter 6* focuses on assessing the impacts of changes in matrix topography and mechanical properties on the response of ligament fibroblasts during connective tissue healing.

6.1.1 Background and Motivation

With respect to differences in matrix mechanical properties, it has been shown previously that differentiated cells are able to adhere, contract and crawl on soft and stiff tissues, and variation in tissue elasticity has an effect on the focal adhesion structure and cytoskeleton of adherent cells, affecting cell morphology and associated phenotype(21;22;255). Specific to fibroblasts, previous work studying the NIH-3T3 cell line on polyacrylamide gels with elasticities close to that of connective tissue shows that these cells are capable of actively contracting their cytoskeleton to modulate their internal stiffness, in order to match the stiffness of the underlying substrate(256). However, because these studies examined the response of cells on gels or films, differences in substrate elasticity often result in undesired differences in substrate topography and porosity, as well. These additional variables may interfere with elucidating the contribution of substrate stiffness to the observed cell responses.

More recently, Palchesko *et al*. assessed the response of C2C12 myoblasts to PDMS substrates with a range of elastic moduli, and was able to control surface topography, surface energy, and protein adhesion across all elasticities. Results from this study show that myotube formation was enhanced on stiffer substrates, while myotubes on softer substrates appeared shorter, suggesting these cells' ability to sense environmental differences in stiffness(15). Still, culture of fibroblasts on 2D substrates is not necessarily indicative of fibroblast response *in vivo*, as it does not account for the effects of the 3D fibrous nature of the surrounding microenvironment on cell response. Our objective is to assess the effects of changes in matrix elasticity on fibroblast behavior on a physiologically relevant fibrous substrate using the PDMS-PCL nanofiber-based scaffolds designed and optimized in *Chapter 4*. These meshes have a similar topography (i.e. fiber diameter and porosity) to PCL-only scaffolds, eliminating the potential contributions of surface morphology to the observed cell response.

Nanofibrous matrices have been used to recapitulate the fibrillar structure of a variety of fibrous connective tissues, including the ligament(11), skeletal muscle(12), and skin(13). Additionally, fiber topography can be used to mimic the architecture of healthy connective tissue vs. scar tissue, and has been used as a platform for studying the effects of connective tissue healing phase on fibroblast response(224). Previous studies assessing the effects of fiber alignment on fibroblast response have found that matrix alignment affects cell attachment, spreading, and integrin expression(24), resulting in differences in cell migration(257) and matrix organization(219). Still the combined effects of matrix alignment and mechanical properties on fibroblast response on a physiologically relevant fibrous substrate have not yet been assessed, and therefore will be the focus of this chapter.

6.1.2 Objectives

The objective of this study is to assess the effects of changes in matrix alignment and mechanical properties on the response of ligament fibroblasts. It is hypothesized that fiber alignment and mechanical properties will affect fibroblast spreading and alignment, resulting in differences in cell proliferation and matrix synthesis.

6.2 Materials and Methods

6.2.1 Human Anterior Cruciate Ligament Fibroblast Isolation and Culture

Human ACL fibroblasts were derived from explant culture of tissues obtained from a patient (male, aged 21) undergoing ACL reconstruction surgery. Briefly, the tissue samples were rinsed in PBS (Sigma-Aldrich), plated in tissue culture dishes, and maintained in DMEM supplemented with 10% FBS, 1% non-essential amino acids, 1% P/S, 0.1% Amp-B and 50 µg/mL G/S. The cells from the first migration were subsequently discarded, and the tissue was re-plated in fresh fully supplemented medium. Only cells obtained from the second and third migrations were used in this study because this method has been shown to yield a relatively homogenous fibroblast population.

6.2.2 Nanofiber Mesh Fabrication

6.2.2.1 Unaligned PCL

A 16% (w/v) PCL solution was prepared by dissolving PCL (M_n = 70,000-90,000) into 3:1 solution of DCM:DMF. The solution was mixed overnight, vortexed for 1 hour prior to electrospinning, and then

loaded into a 5 mL syringe attached with a 23-gauge stainless steel blunt-tip needle. A voltage of 7-9 kV was applied to the needle tip and a pump flow rate of 1 mL/hr was used. Fibers were collected on a grounded stationary plate placed 15 cm from the needle tip. Approximately 3.5 mL of polymer solution was electrospun to fabricate scaffolds of thickness ranging from 0.09-0.14 mm as measured with a digital caliper.

6.2.2.2 Aligned PCL

An 18% (w/v) PCL solution was prepared by dissolving PCL into 3:2 mixture of DCM:DMF. The solution was mixed overnight, vortexed for 1 hour prior to electrospinning, and the entire solution loaded into a 5 mL syringe with a 23-gauge stainless steel blunt-tip needle. A voltage of 9-10 kV was applied to the needle tip and a pump flow rate of 1 mL/hr was used. Fibers were collected on a grounded rotating mandrel (2500 rpm), 13 cm from the needle tip. Approximately 5 mL of polymer solution was electrospun to fabricate scaffolds of thickness ranging from 0.07-0.14 mm as measured with a digital caliper.

6.2.2.3 Unaligned PDMS-PCL Blend

A 35% (w/v) PDMS-PCL solution was prepared by dissolving a 1:1 mixture of PDMS (Sylgard 184, 50:1 base:crosslinker) and PCL (M_n = 70,000-90,000) in a 3:1 solution of DCM:DMF. The solution was vortexed for 4 hours prior to electrospinning, and then loaded into a 5 mL syringe attached with a 23-gauge stainless steel blunt-tip needle. A voltage of 10-11 kV was applied to the needle tip and a pump flow rate of 1 mL/hr was used. Fibers were collected on a grounded stationary plate placed 12 cm from the needle tip. Approximately 3 mL of polymer solution was electrospun to fabricate scaffolds of thickness ranging from 0.07-0.14 mm as measured with a digital caliper.

6.2.2.4 Aligned PDMS-PCL Blend

A 35% (w/v) PDMS-PCL solution was prepared by dissolving a 1:1 mixture of PDMS (50:1 base:crosslinker) and PCL (M_n = 70,000-90,000) in a 3:1 solution of DCM:DMF. The solution was vortexed for 4 hours prior to electrospinning, and then loaded into a 5 mL syringe attached with a 23-gauge stainless steel blunt-tip needle. A voltage of 10-11 kV was applied to the needle tip and a pump flow rate of 1 mL/hr was used. Fibers were collected on a grounded rotating mandrel (2100 rpm), 12 cm from the needle tip.

Approximately 3.5 mL of polymer solution was electrospun to fabricate scaffolds of thickness ranging from 0.07-0.14 mm as measured with a digital caliper.

6.2.3 Cell Seeding on Nanofiber Meshes

Electrospun polymer scaffolds were cut to 1 cm x 1.8 cm and secured to custom-made backings with tape, resulting in a cell culture surface area of 1 cm^2. To enhance surface reactivity, PCL-only and PDMS-PCL fibers were then air plasma treated (Harrick Plasma PDC-32G) at high radiofrequency (RF) setting for 30 seconds. Meshes were then immediately UV sterilized (both sides, 15 minutes each) at 365 nm and incubated at 37ºC, 5% CO_2 overnight in F/S DMEM with 20% FBS to promote cell attachment.

After the overnight soak, media was removed and fibroblasts were seeded on meshes at a density of $3x10^4$ cells/cm^2 (3 M cells/mL, 10 µL) and allowed to attach for 15 minutes under humidified conditions at 37ºC, 5% CO_2 before the addition of F/S DMEM. Monolayer culture seeded at $3x10^4$ cells/well in a 48-well plate (1 cm^2) served as controls. Cells were maintained at 37°C, 5% CO_2 and media was exchanged every 2-3 days.

6.2.4 Cell Viability and Alignment

Cell viability (*n*=3) was visualized using Live/Dead staining (Molecular Probes). Both monolayer and nanofiber mesh groups were stained following the manufacturer's suggested protocol. Samples were imaged using confocal microscopy (Olympus Fluoview FV1000) at excitation wavelengths of 488 nm and 568 nm.

For cell alignment analysis, cell viability micrographs (*n*=6) were evaluated using circular statistics customized for quantifying alignment (Fiber3)(231). Circular statistics parameters include: the MA, which represents the average fiber alignment in the matrix ($|\theta| \leq 90°$), 0° representing a horizontal orientation; the MVL ($0 \leq r \leq 1$), 0 indicates a random and 1 indicates an aligned/elongated morphology; and AD which characterizes the dispersion of the non-Gaussian angle distribution of the nanofibers ($0° \leq \theta \leq 40.5°$), 0° represents aligned and 40.5° a random distribution.

6.2.5 Cell Proliferation

Cell proliferation (*n*=5) was determined by measuring total DNA content using the PicoGreen dsDNA assay (Invitrogen) following the manufacturer's protocol. Samples were rinsed twice in PBS and

stored in 500 µL of 0.1% Triton-X (Sigma-Aldrich) at -30°C. Immediately before the analysis, samples were thawed and homogenized and subjected to ultrasonication at 5W (Microson XL-2000) for 15 seconds. Fluorescence was measured using a microplate reader (Tecan, Research Triangle Park, NC) at an excitation wavelength of 485 nm and an emission wavelength of 535 nm. A standard curve was derived and used to correlate DNA concentration to fluorescence intensity, and cell number was determined based on a conversion factor of 8 pg DNA/cell(244). Results from the dsDNA assay were also used to assess fold change in cell number, doubling time(245), and total population doublings(246) over time.

6.2.6 Collagen Production

Collagen production (*n*=5) was quantified using a modified hydroxyproline assay(199). Samples were digested in a buffered papain solution prior to analysis. For digestion, samples were vacuum dried overnight using the Centrivap concentrator (Labconco). Samples were then digested for 20 hours at 65ºC with 20 µL/mL papain (Sigma-Aldrich), buffered in 0.1M sodium acetate, 10 mM cysteine HCl, and 50 M EDTA. For the assay, digested samples were concentrated by drying 125-250 µL of sample overnight in the Centrivap concentrator. Samples were resuspended in 50 µL of 2 N NaOH and autoclaved for 25 minutes. 450 µL of Chloramine T Reagent (1.27 g chloramine T in 50% isopropanol brought to 100 mL with acetate-citrate buffer) was added to the samples, which were then allowed to incubate for 25 minutes at room temperature. 500 µL of Ehrlich's reagent (15 g p-dimethylaminobenzaldehyde in 100 mL (2:1) isopropanol:perchloric acid) was subsequently added, and the samples incubated at 65ºC for 20 minutes. The absorbance at 555 nm was read using a Tecan microplate reader. Total collagen was determined using a standard curve generated using a collagen standard (Sigma-Aldrich).

The acetate-citrate buffer for the chloramine T solution consisted of 30 g sodium acetate trihydrate, 11.5 g citric acid, 3 mL acetic acid, and 8.5 g NaOH, dissolved in 125 mL of distilled water. The solution was brought to a pH of 6.5 using 1 N NaOH or 1 N HCl, and then brought to a final volume of 250 mL.

6.2.7 Alkaline Phosphatase Activity

After sample homogenization as described in *Section 6.2.5*, samples were assayed for ALP activity. On ice, 50 µL of sample was added to a 96-well plate and 50 µL of 0.1 M Na_2CO_3:2 mM $MgCl_2$ with 10 mM pNP-PO_4 was subsequently added. The plate was incubated at 37°C until a color change was noted. The

absorbance at 405 nm was then read using a Tecan microplate reader. ALP activity is reported in picomoles, normalized to incubation time and post-sonication cell number.

6.2.8 Statistical Analysis

Results are reported as mean ± standard deviation, with n equal to the number of replicates per group. Statistical analyses were performed with JMPIN (4.0.4, SAS Institute, Inc.). Two-way ANOVA was used to determine the effects of nanofiber alignment and composition on cell response (cell alignment, proliferation, matrix deposition, ALP activity). The Tukey-Kramer post-hoc test was used for all pair-wise comparisons, and significance was attained at $p<0.05$.

6.3 Results

6.3.1 Cell Viability and Alignment

Cells remain viable and proliferate on all groups over the two-week study (*Figure 6.1*). Cell alignment, including MA, AD, and MVL, were quantified as shown in *Figure 6.3*. *Effect of Fiber Alignment*: Fibroblasts are significantly more aligned on aligned meshes by day 1 compared to cells on unaligned meshes, and alignment is greater on aligned meshes compared to unaligned meshes throughout the two-week study (*Figure 6.2)*. *Effect of Fiber Mechanical Properties*: Quantitative analysis of cell alignment over time shows that, for unaligned meshes, fibroblasts remain randomly oriented on unaligned fibers composed of both PCL-only and PDMS-PCL over the 14-day study, with a significant increase in regional alignment over time on both meshes (*Figure 6.2)*. For aligned meshes, fibroblasts are aligned along the direction of fiber alignment on both PCL-only and PDMS-PCL fibers by day 1, and remain oriented in this direction over 14 days (*Figure 6.2)*. There are no observed differences alignment between cells on PCL-only and PDMS-PCL for unaligned or aligned fiber orientations at any time point (*Figure 6.2)*.

6.3.2 Cell Proliferation

Total cell number was greater on all meshes compared to monolayer at day 14 (*Figure 6.3*). *Effect of Fiber Alignment*: There were no observed differences in cell number or fold change in cell number between unaligned and aligned fibers for either PCL-only or PDMS-PCL fiber compositions (*Figure 6.3*). *Effect of Fiber Mechanical Properties*: For unaligned meshes, total cell number and fold change in cell number were significantly greater on PDMS-PCL compared to PCL-only on day 14 (*Figure 6.3*). For aligned

meshes, total cell number and fold change in cell number were significantly greater on PDMS-PCL compared to PCL-only on day 14, as well (*Figure 6.3*). Total population doublings and doubling time over the two-week study appear similar for all groups (*Figure 6.3*).

6.3.3 Matrix Synthesis

Total collagen and collagen per cell at days 1, 3, 7, and 14 are shown in *Figure 6.4.* Total collagen content increased over time for all groups, except for unaligned PDMS-PCL and monolayer groups. *Effect of Fiber Alignment*: For fibroblasts on PCL-only fibers, total collagen is greater on aligned meshes compared to unaligned meshes at day 7. This difference is no longer observed by day 14. For MSC on PDMS-PCL fibers, total collagen is greater on aligned PDMS-PCL compared to unaligned PDMS-PCL at day 14 (*Figure 6.4)*. *Effect of Fiber Mechanical Properties*: For unaligned meshes, there is significantly more collagen for fibroblasts on unaligned PCL-only compared to fibroblasts on PDMS-PCL at day 14. For aligned meshes, there is significantly more collagen on PCL-only compared to PDMS-PCL meshes at day 7. This difference is no longer observed by day 14 (*Figure 6.4)*.

6.3.4 Mineralization Potential

Fibroblast ALP activity normalized to cell number and reaction time is reported in *Figure 6.4* for fibroblasts on nanofiber mesh groups and in monolayer. Alkaline phosphatase activity decreased over time for all groups, and was significantly lower for monolayer controls than nanofiber mesh groups at day 1 (*Figure 6.4)*. *Effects of Fiber Alignment:* There were no differences in ALP activity between fibroblasts on unaligned vs. aligned fibers at any time point, for either fiber composition (*Figure 6.4)*. *Effects of Fiber Mechanical Properties*: For unaligned fibers, there was no difference in ALP activity over time for fibroblasts on PCL-only and PDMS-PCL fibers (*Figure 6.4)*. For aligned fibers, ALP activity decreased significantly for PCL-only samples between day 1 and day 3, while ALP activity remained elevated on PDMS-PCL groups until day 7. Therefore, ALP activity was significantly lower on PCL-only meshes compared to PDMS-PCL at day 3 (*Figure 6.4)*.

6.4 Discussion

In this chapter, the effects of fiber alignment and mechanical properties on the response of native ligament fibroblasts were assessed, as it relates to connective tissue injury and healing. Degree of cell

alignment was observed to be lower for fibroblasts on unaligned compared to aligned meshes, regardless of composition, over the 21-day study. Specifically, fibroblasts were observed to align along the direction of fiber orientation on aligned fibers by day 1. This is similar to results observed by Park *et al*., in which dermal fibroblasts were found to align along the direction of aligned PCL fibers, so long as fiber spacing was similar to or smaller than cell size(258). Similarly, Fee *et al*. seeded NIH3T3 fibroblasts on PCL/gelatin fibers and observed cell alignment along the direction of fibers on aligned fibers(259). Alternatively, cells on unaligned fibers appear randomly oriented on unaligned fibers at day 1. Still, cells on unaligned meshes become more aligned and elongated over time, as observed via increasing mean vector length and decreasing angular deviation, for cells on both unaligned PDMS-PCL and PCL-only, as well as in monolayer, by day 21 compared to day 1. This is similar to the findings of Lee *et al.,* in which the alignment of human rotator cuff fibroblasts cultured on unaligned PLGA fibers was observed to increase over time(224). This phenomenon may be mimetic of the connective tissue repair process, in which fibroblasts initially are unaligned and deposit randomly oriented matrix following injury in order to rapidly fill the tissue void, and cells orient themselves and deposit organized matrix over time to reorganize and strengthen the new tissue.

Fibroblasts remained viable and proliferated on all nanofiber meshes over time. While proliferation was greater on all meshes than in monolayer culture, there were no observed effects of fiber alignment on fibroblast proliferation for either mesh composition over 14 days. These results echo those observed by Chen *et al*., in which proliferation of NIH3T3 fibroblasts seeded on unaligned and aligned electrospun PLGA was similar over time. Additionally, recent work by Fee *et al*. examined the growth of the same fibroblast cell line on PCL fibers and observed no difference in cell growth on unaligned vs. aligned fibers, though culture was only performed up to 4 days(259). In work by Lee *et al.,* human rotator cuff fibroblast proliferation was greater on unaligned PLGA nanofibers than aligned PLGA nanofibers, but this effect was only observed after 21 days in culture, and not at earlier time points(224). Therefore, it is possible that differences in proliferation due to alignment would be observed between ACL fibroblasts on unaligned and aligned PCL-only or PDMS-PCL meshes over longer periods of *in vitro* culture.

With respect to the effects of matrix mechanical properties on fibroblast response, cell alignment was similar on aligned PDMS-PCL and PCL-only meshes at all time points, while increases in fibroblast

alignment on unaligned meshes were similar between unaligned PDMS-PCL and PCL-only, as well. Similar to results observed for MSC on PDMS-PCL vs. PCL-only meshes in *Chapter 5*, cell number and fold change in cell number were greater on PDMS-PCL fibers compared to PCL-only fibers, in both unaligned and aligned fiber orientations, at day 14. This may be mimetic of the proliferative phase of the wound healing process, which takes place during early tissue repair, following tissue injury and inflammation. During this phase of healing, cell proliferation, and subsequently cell density, increase rapidly during the first 7-10 days of injury, largely due to an increase in fibroblast proliferation. Specifically, granulation tissue, as formed by fibroblasts following injury, is typically weaker and softer than the aligned fibrous collagenous matrix observed in healthy connective tissue. This is similar to the PDMS-PCL fibers utilized in this study, which are softer than PCL-only fibers.

In summary, these results show that PDMS-PCL meshes serve as an early-stage repair model of connective tissue, resulting in enhanced proliferation by fibroblasts over 14 days in culture. Alternatively, collagen production occurred more quickly on unaligned and aligned PCL-only meshes compared to PDMS-PCL meshes, which may be mimetic of the remodeling phase of connective tissue healing. While fiber alignment resulted in differences in fibroblast alignment on meshes, there were no observed differences in collagen synthesis between aligned and unaligned meshes. In choosing an optimal matrix for promoting stem cell-guided tissue regeneration following connective tissue injury, it is important to choose a substrate that balances the growth and biosynthesis of native tissue fibroblasts following implantation. These findings will be considered when choosing an ideal matrix at the culmination of this thesis.

6.5 Conclusion

In this chapter, the effects of matrix alignment and mechanical properties on fibroblast response were assessed. Fiber alignment was shown to affect initial cell spreading and alignment, while matrix mechanical properties affected cell proliferation and matrix synthesis, as PDMS-PCL fibers enhanced fibroblast proliferation while PCL-only fibers resulted in enhanced collagen synthesis per cell. In designing an optimal matrix for connective tissue regeneration, it is important to choose a matrix that supports fibroblast healing response. Future studies will focus on assessing the effects of matrix properties on fibroblast response in the presence of both macrophages and MSC as a means of predicting cell response *in vivo* following connective tissue injury.

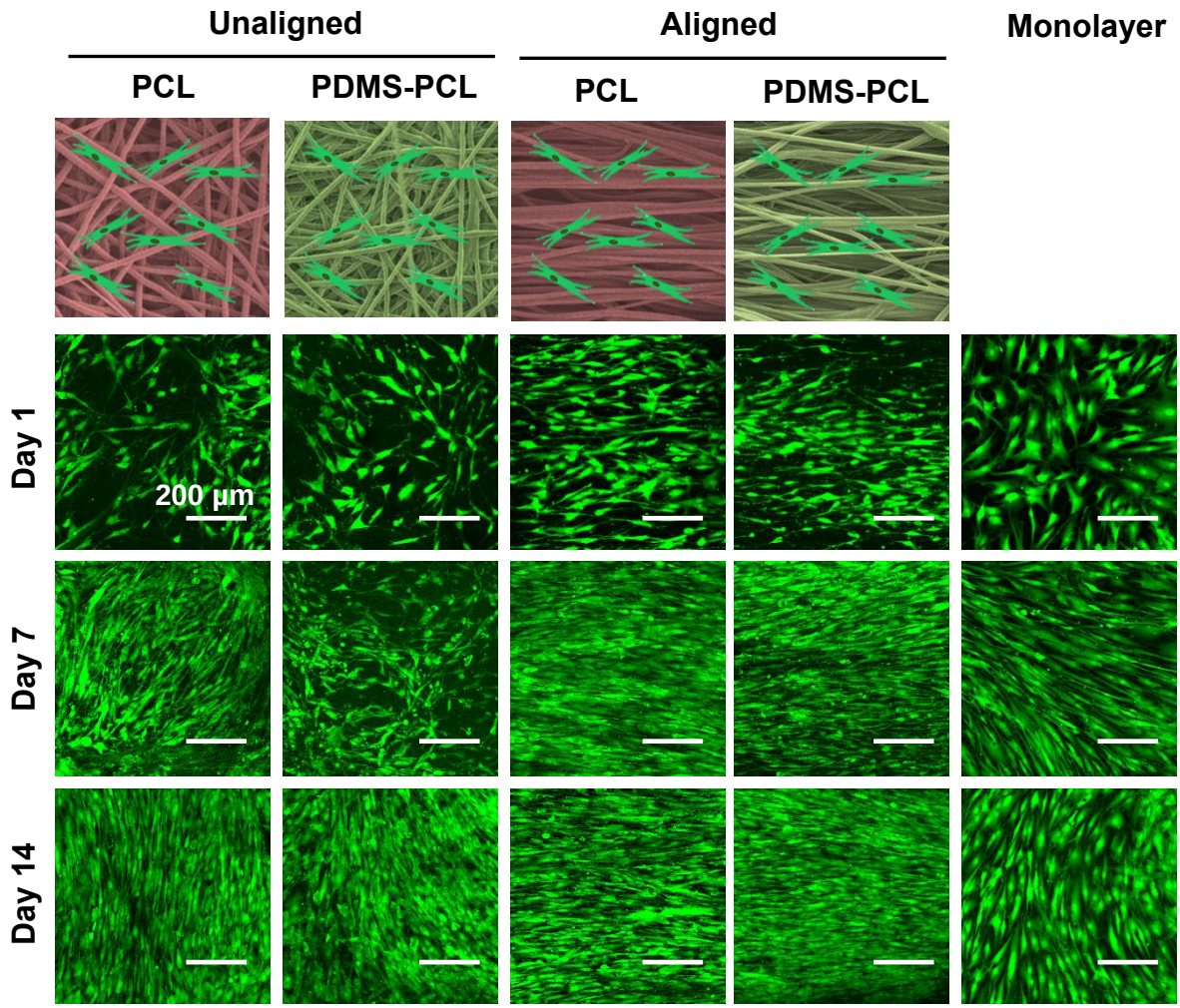

Figure 6.1: Effects of Matrix Alignment and Mechanical Properties on Fibroblast Response: Cell Viability. Cells remain viable on all meshes, as well as in monolayer, over 21 days. *n*=3, mag = 20x, scale bar = 200 µm.

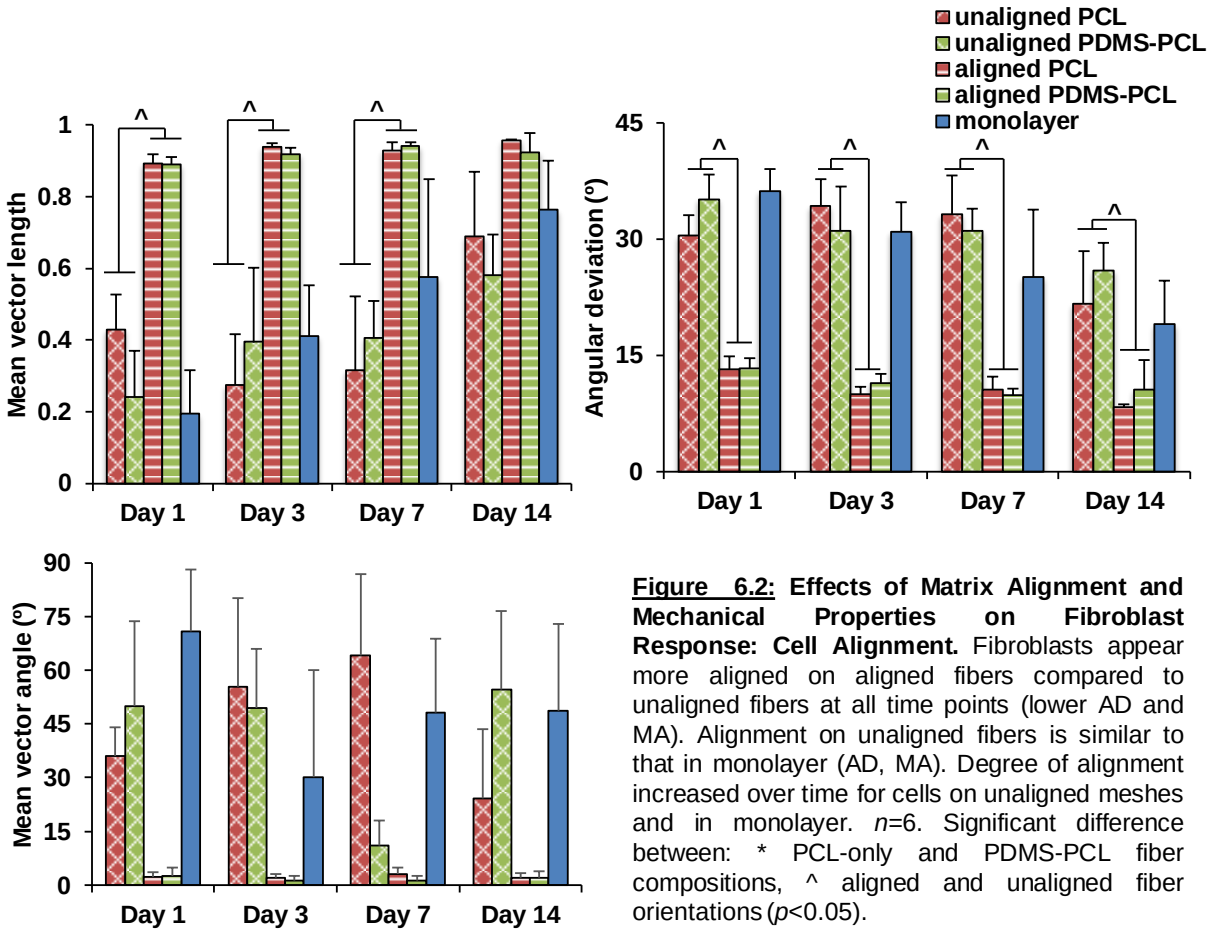

Figure 6.2: Effects of Matrix Alignment and Mechanical Properties on Fibroblast Response: Cell Alignment. Fibroblasts appear more aligned on aligned fibers compared to unaligned fibers at all time points (lower AD and MA). Alignment on unaligned fibers is similar to that in monolayer (AD, MA). Degree of alignment increased over time for cells on unaligned meshes and in monolayer. *n*=6. Significant difference between: * PCL-only and PDMS-PCL fiber compositions, ^ aligned and unaligned fiber orientations ($p<0.05$).

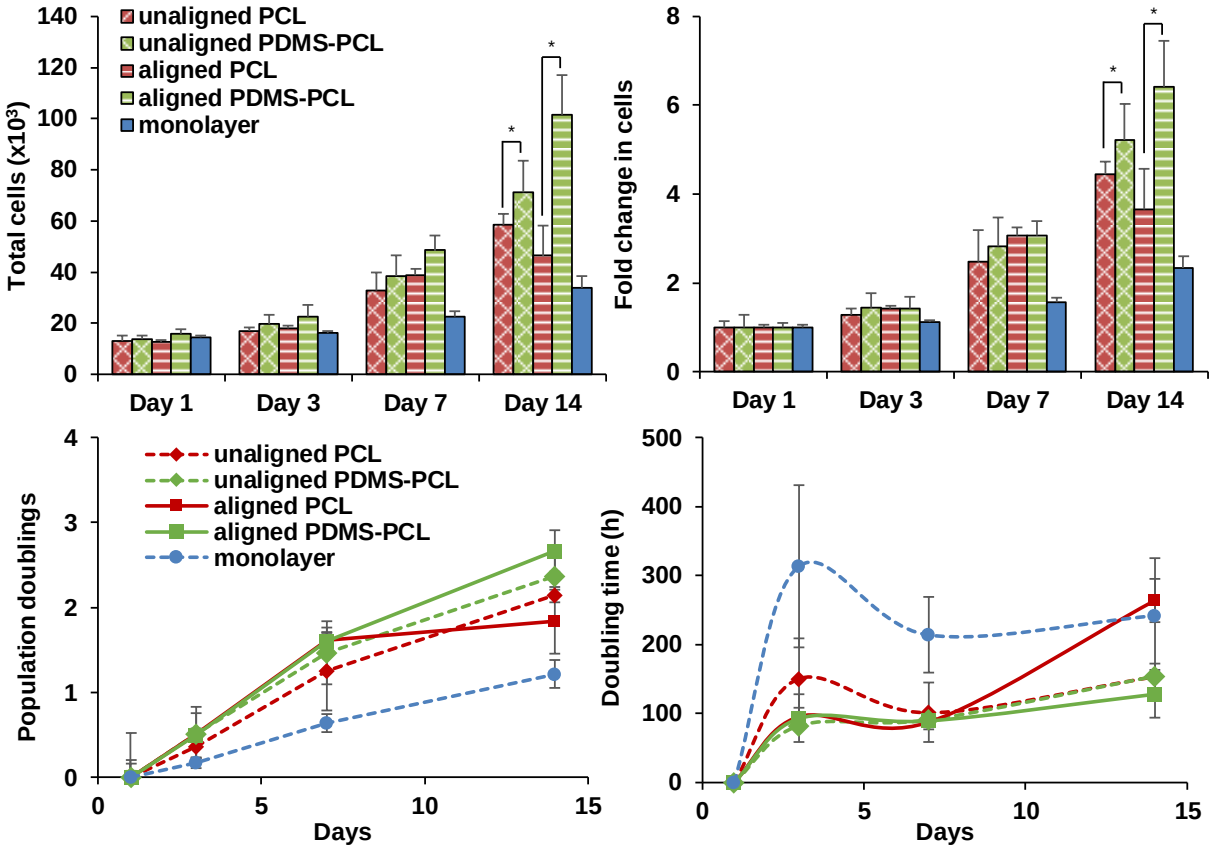

Figure 6.3: Effects of Matrix Alignment and Mechanical Properties on Fibroblast Response: Proliferation. Cell number was greater on all meshes compared to monolayer at days 7 and 14. Cell number and fold change in cell number were greater for fibroblasts on PDMS-PCL fibers compared to PCL-only fibers in both unaligned and aligned fiber orientations at day 14. There were no differences due to cell alignment on total cells or fold change in cell number at any time point. n=5, significant difference between: * PCL-only and PDMS-PCL fiber compositions, ^ aligned and unaligned fiber orientations (p<0.05).

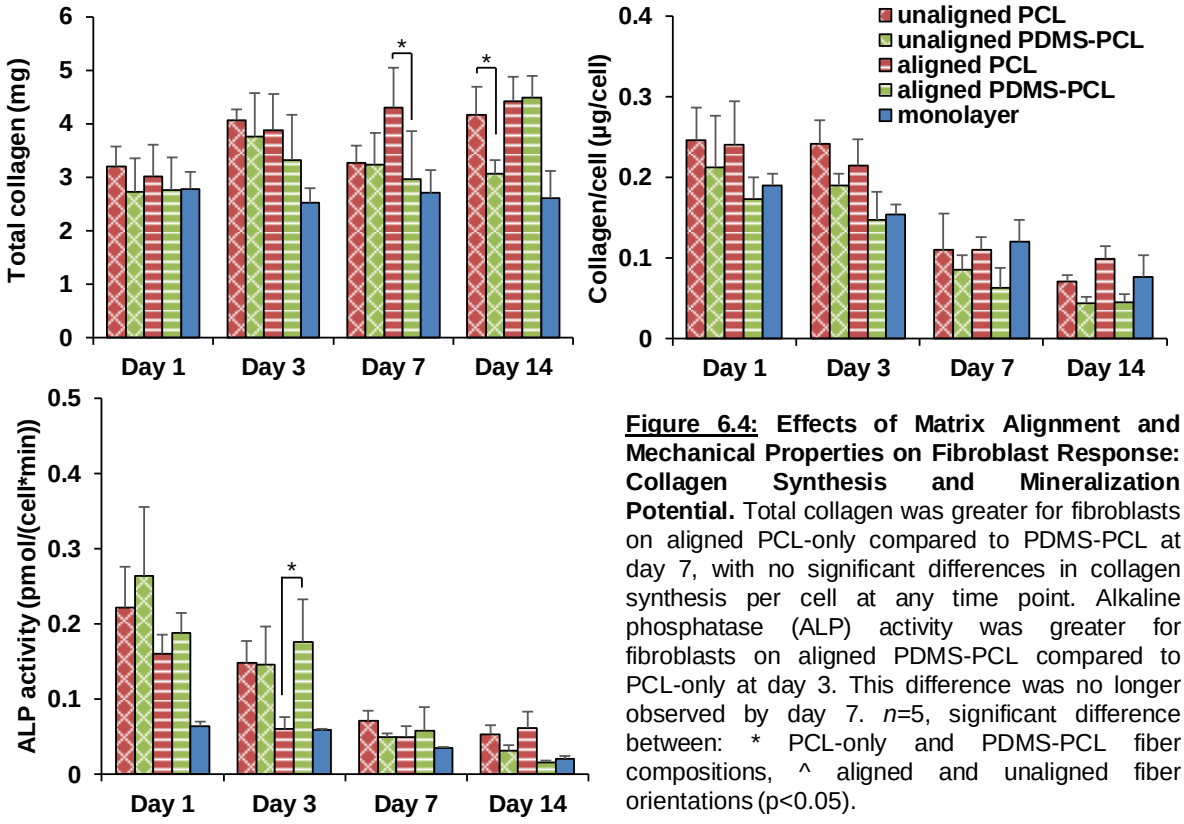

Figure 6.4: Effects of Matrix Alignment and Mechanical Properties on Fibroblast Response: Collagen Synthesis and Mineralization Potential. Total collagen was greater for fibroblasts on aligned PCL-only compared to PDMS-PCL at day 7, with no significant differences in collagen synthesis per cell at any time point. Alkaline phosphatase (ALP) activity was greater for fibroblasts on aligned PDMS-PCL compared to PCL-only at day 3. This difference was no longer observed by day 7. *n*=5, significant difference between: * PCL-only and PDMS-PCL fiber compositions, ^ aligned and unaligned fiber orientations ($p<0.05$).

CHAPTER 7: EFFECTS OF MATRIX ALIGNMENT AND MECHANICAL PROPERTIES ON MACROPHAGE ACTIVATION

7.1 Introduction

In *Chapters 5* and *6*, the effects of matrix alignment and mechanical properties on MSC and fibroblasts were assessed. It was observed that the mechanical properties of fibrous matrices impact initial cell attachment and spreading, resulting in observed changes in cell proliferative response by both fibroblasts and MSC, with no major differences in matrix synthesis or gene expression. *Chapter 7* focuses on the effects of these matrix properties on the response of M0 macrophages, in terms of pro- or anti-inflammatory polarization.

7.1.1 Background and Motivation

Toward the design of a nanofiber mesh for promoting stem cell-guided tissue regeneration, the ideal implantable matrix should 1) at least not elicit a heightened immune reaction by immune cells which are migrating to the injury site, and also 2) potentially minimize the inflammatory response in order to minimize scar tissue formation and allow for functional tissue regeneration.

Thus far, because of the interest in using electrospun nanofiber-based scaffolds for use in tissue engineering and regenerative medicine applications, investigation into the native immune response fibrous scaffolds has been performed. To this end, Bowlin *et al*. assessed the immune response of macrophages to electrospun nylon, poly(glycolic acid), poly(lactic acid), polydioxanone (PDO), and PDO blended with other materials *in vitro*(260-262). Results of a study which assessed the response of peripheral blood monocyte-derived macrophages on nanofibers comprised of PDO, elastin, or a combination of PDO and elastin showed that macrophage growth factor secretion on all three fibrous substrates was similar to that of macrophages on tissue culture plastic(260), suggesting that a fibrous topography alone does not elicit an immune response by macrophages *in vitro*.

With respect to the effects of fiber alignment on macrophage behavior, Cao *et al.* analyzed the attachment and spreading of human primary monocytes on unaligned and aligned PCL nanofibers, as well as PCL films and arginylglycylaspartic acid (RGD)-coated glass *in vitro*, and found that monocyte adhere less to aligned nanofibers compared to unaligned fibers(266). *In vivo* results from this study also show that, while cells were able to infiltrate aligned meshes, a fibrous capsule was formed on the surface of unaligned fibers. In combination, these results are indicative of a minimized host response on aligned fibers compared to unaligned fibers(266). Interestingly, these findings are contradicted by work by Saino *et al*., in which

attachment of the murine macrophage-like RAW 264.7 cell line is enhanced on aligned PLLA fibers compared to unaligned PLLA (25). These inconsistent outcomes suggest that either other characteristics of the fibrous matrix microenvironment besides fiber alignment, such as fiber chemistry, surface energy, or mechanical properties, play a role in macrophage attachment, or attachment is affected by macrophage species or cell source.

In terms of macrophage response due to matrix mechanical properties, a number of studies have shown that macrophages are sensitive to the elasticity of the underlying matrix both *in vitro* and *in vivo*, and differences in matrix mechanical properties affect macrophages in terms of attachment, spreading, proliferation, phagocytosis, and vulnerability to inflammatory stimuli(267-269). Specific to inflammatory activation of macrophages *in vitro*, Blakey *et al.* analyzed the activation of murine RAW 264.7 macrophages on RGD-modified PEG hydrogels with varying compressive moduli (130-840 kPa) and found that macrophage attachment is enhanced on stiffer gels compared to softer gels, with increased expression of M1 markers, including TNF, IL-1β, and IL-6, after stimulation with lipopolysaccharide (LPS) at day 1(267). It was determined through this work that differences in macrophage vulnerability to inflammatory stimulation with LPS may be due to differences in cell spreading on stiff versus soft matrices, as cells appeared more spread on gels with higher compressive modulus compared to lower modulus gels(267). Though these findings suggest that matrix mechanical properties can have an effect on macrophage response to surrounding stimuli, there is much work to be done in order to determine the effects of matrix-based cues without additional stimulation on macrophage response as it relates to the injured microenvironment.

7.1.2 Objectives

The objective of this study is to assess the effects of matrix alignment and mechanical properties on macrophage response and activation, through assessment of macrophage adhesion to fibers, as well as subsequent release of pro- and anti-inflammatory cytokines. It is hypothesized that fiber alignment and mechanical properties will have a combined effect on macrophage inflammatory activation, in terms of initial cell attachment and the release of pro- and anti-inflammatory cytokines.

7.2 Materials and Methods

7.2.1 Human THP-1 Cell Culture

Human THP-1 cells were obtained commercially (ATCC, TIB202) and maintained in continuous culture in non-tissue culture treated flasks (25 cm^2, Nunc™) with F/S RPMI-1640 containing 10% FBS, 1% P/S, and 0.05 mM 2-ME. Media was replaced every 3-4 days. Briefly, cells suspensions were removed from culture dishes once every 3-4 days and cells were centrifuged at 5000 rpm for 5 minutes. Supernatant was aspirated and cells were resuspended in fresh RPMI-1640 at a density of $4x10^5$ cells/mL.

7.2.2 Nanofiber Mesh Fabrication

7.2.2.1 Unaligned PCL

A 16% (w/v) PCL solution was prepared by dissolving PCL (M_n = 70,000-90,000, Sigma-Aldrich) into 3:1 solution of DCM (Sigma-Aldrich):DMF (Sigma-Aldrich). The solution was mixed overnight, vortexed for 1 hour prior to electrospinning, and then loaded into a 5 mL syringe attached with a 23-gauge stainless steel blunt-tip needle. A voltage of 7-9 kV was applied to the needle tip and a pump flow rate of 1 mL/hr was used. Fibers were collected on a grounded stationary plate placed 15 cm from the needle tip. Approximately 3.5 mL of polymer solution was electrospun to fabricate scaffolds of thickness ranging from 0.09-0.14 mm as measured with a digital caliper.

7.2.2.2 Aligned PCL

An 18% (w/v) PCL solution was prepared by dissolving PCL into 3:2 mixture of DCM:DMF. The solution was mixed overnight, vortexed for ~1 hour prior to electrospinning, and the entire solution loaded into a 5 mL syringe with a 23-gauge stainless steel blunt-tip needle. A voltage of 9-10 kV was applied to the needle tip and a pump flow rate of 1 mL/hr was used. Fibers were collected on a grounded rotating mandrel (2500 rpm), 13 cm from the needle tip. Approximately 5 mL of polymer solution was electrospun to fabricate scaffolds of thickness ranging from 0.07-0.14 mm as measured with a digital caliper.

7.2.2.3 Unaligned PDMS-PCL Blend

A 35% (w/v) PDMS-PCL solution was prepared by dissolving a 1:1 mixture of PDMS (Sylgard 184, 50:1 base:crosslinker) and PCL (M_n = 70,000-90,000) in a 3:1 solution of DCM:DMF. The solution was vortexed for 4 hours prior to electrospinning, and then loaded into a 5 mL syringe attached with a 23-gauge

stainless steel blunt-tip needle. A voltage of 10-11 kV was applied to the needle tip and a pump flow rate of 1 mL/hr was used. Fibers were collected on a grounded stationary plate placed 12 cm from the needle tip. Approximately 3 mL of polymer solution was electrospun to fabricate scaffolds of thickness ranging from 0.07-0.14 mm as measured with a digital caliper.

7.2.2.4 Aligned PDMS-PCL Blend

A 35% (w/v) PDMS-PCL solution was prepared by dissolving a 1:1 mixture of PDMS (50:1 base:crosslinker) and PCL (M_n = 70,000-90,000) in a 3:1 solution of DCM:DMF. The solution was vortexed for 4 hours prior to electrospinning, and then loaded into a 5 mL syringe attached with a 23-gauge stainless steel blunt-tip needle. A voltage of 10-11 kV was applied to the needle tip and a pump flow rate of 1 mL/hr was used. Fibers were collected on a grounded rotating mandrel (2100 rpm), 12 cm from the needle tip. Approximately 3.5 mL of polymer solution was electrospun to fabricate scaffolds of thickness ranging from 0.07-0.14 mm as measured with a digital caliper.

7.2.3 Cell Seeding on Nanofiber Meshes

Electrospun polymer meshes were cut to 1 x 1.8 cm and secured to custom backings using tape, resulting in a cell culture surface area of 1 cm^2. To enhance surface reactivity, PCL-only and PDMS-PCL fibers were then air plasma treated (Harrick Plasma PDC-32G) at high radiofrequency (RF) setting for 30 seconds. Meshes were then immediately UV sterilized (both sides, 15 minutes each) at 365 nm and press-fit into the bottom of 12-well plates. Samples were then incubated at 37ºC, 5% CO_2 overnight in F/S RPMI-1640 with 20% FBS (2 ml/well) to promote cell attachment.

After the overnight soak, THP-1 monocytes were suspended in F/S RPMI-1640 supplemented with 100 nM PMA at a density of $1x10^6$ cells/mL. At the time of seeding, soaking medium was removed from meshes and 2 mL of cell suspension (2 M cells total) was added per well. Cells were allowed to attach for 48 hours, at which point PMA+ medium was removed and samples were transferred to a new 12-well plate. Samples were then soaked in PBS for 1 minute to rinse away any remaining PMA, at which point the PBS was aspirates and replaced with 2 mL of fresh F/S RPMI-1640. Monolayer culture in a 48-well (1 cm^2) plate served as a control. Cells were maintained at 37°C, 5% CO_2.

7.2.4 Cell Attachment

Cell attachment (*n*=5) was determined by measuring total DNA content using the PicoGreen dsDNA assay (Invitrogen) following the manufacturer's protocol. Samples were rinsed twice in PBS and stored in 500 µL of 0.1% Triton-X (Sigma-Aldrich) at -30°C. Immediately before analysis, samples were thawed and homogenized and subjected to ultrasonication at 5W (Microson XL-2000) for 15 seconds. Fluorescence was measured using a microplate reader (Tecan, Research Triangle Park, NC) at an excitation wavelength of 485 nm and an emission wavelength of 535 nm. A standard curve was derived and used to correlate DNA concentration to fluorescence intensity, and cell number was determined based on a conversion factor of 8 pg DNA/cell(244).

7.2.5 Cell Spreading on Fiber Meshes

Cell spreading on nanofiber meshes (*n*=3) was assessed via AFM. Following the five-day differentiation protocol described above (48 hours in PMA+ medium, followed by 72 hours of rest), samples were rinsed twice in PBS and fixed in 10% NBF with 1% CPC overnight at 4ºC. After fixation, samples were dehydrated via ethanol series and allowed to dry overnight before storage under vacuum in a desiccator. Prior to imaging, samples were sputter coated with AuPd. Meshes were then imaged using SEM (5 kV, 10 µA).

7.2.6 Cytokine Secretion

Levels of pro- (TNF, IL-1β) and anti-inflammatory (IL-10, TGF-β1) cytokines (*n*=5) for macrophages on all nanofiber meshes, as well as in monolayer, were assessed via ELISA according to the manufacturer's protocol. Briefly, supernatants from cell culture were collected after 48 hours and stored at -30°C. On the day of analysis, samples were thawed and added directly to assay diluent in a prepared plate and incubated for two hours at room temperature prior to solution removal. Each well was washed three or four times before incubation with either TNF, IL-1β, or IL-10 conjugate for 1 hour at room temperature, or TGF-β1 conjugate for two hours at room temperature. The conjugate was then removed, the plate was washed three or four times, and the substrate solution was added to each well and allowed to react in the dark. The stop solution was added after 20 minutes for TNF, IL-1β, or IL-10 ELISAs or 30 minutes for TGF-β1 ELISA, and the absorbance was measured using a microplate reader Sample absorbance was measured using a

microplate reader (Tecan) at 450 nm and 570 nm, and the difference was used to calculate cytokine concentration. Base level concentrations of each cytokine in acellular culture medium were used as negative controls.

7.2.7 Statistical Analysis

Results are reported as mean ± standard deviation, with *n* equal to the number of replicates per group. Statistical analyses were performed with JMPIN (4.0.4, SAS Institute, Inc.). Two-way ANOVA was used to determine the effects of nanofiber alignment and mechanical properties on cell response (cell attachment, cytokine release). The Tukey-Kramer post-hoc test was used for all pair-wise comparisons, and significance was attained at $p<0.05$.

7.3 Results

7.3.1 Cell Attachment

Total cells on nanofiber meshes increased with increasing seeding density (*Figure 7.2*). To achieve a final cell density of $3x10^4$ cells/mesh, 1 million cells/mL in PMA+ medium was determined to be optimal seeding density for unaligned PCL-only nanofiber meshes (*Figure 7.2*). *Effects of Matrix Alignment:* For PCL-only fibers, there is no difference in cell attachment between unaligned and aligned fibers (*Figure 7.3*). For PDMS-PCL fibers, cell attachment is significantly lower on aligned fibers compared to unaligned fibers (*Figure 7.3*). *Effects of Matrix Mechanical Properties:* For unaligned fibers, there was no difference in attachment on PCL-only and PDMS-PCL fibers. For aligned meshes, there were significantly more cells on aligned PCL-only compared to PDMS-PCL after 48 hours (*Figure 7.3*). In order to achieve a cell density on aligned PDMS-PCL fibers that is similar to cell numbers observed on unaligned PCL-only and PDMS-PCL meshes, as well as aligned PCL-only meshes, the seeding density must be increased three-fold.

In terms of attachment efficiency, cell attachment was significantly lower on all nanofiber mesh groups compared to monolayer (*Figure 7.3)*. A total of 6% of seeded macrophages were observed to adhere to unaligned PCL-only and unaligned PDMS-PCL meshes, as well as aligned PCL-only meshes (*Figure 7.3*). Attachment efficiency was significantly lower on aligned PDMS-PCL fibers, with an attachment efficiency as low as 2% on aligned PDMS-PCL. In order to compensate for differences in cell attachment efficiency, and its effect on the final cell density on meshes, cell seeding density was increased from 1

million cells/mL to 3 million cells/mL on aligned PDMS-PCL fibers. This resulted in a similar final cell number on all meshes prior to cytokine release analysis (*Figure 7.3*).

7.3.2 Cytokine Secretion

Levels of IL-1β per cell were lower on all nanofiber meshes compared to monolayer, and levels of IL-10 per cell and TGF-β1 per cell were higher on nanofibers than in monolayer at day 2 (*Figure 7.4*). Concentrations of TNF per cell were also lower for macrophages on unaligned PCL-only, unaligned PDMS-PCL meshes, and aligned PCL-only meshes compared to monolayer at this time point, with no differences in TNF per cell between macrophages on aligned PDMS-PCL and in monolayer (*Figure 7.4*). *Effects of Matrix Alignment*: For PCL-only meshes, there were no observed differences in the secretion of pro- or anti-inflammatory cytokines per cell between unaligned and aligned fibers. For PDMS-PCL meshes, there was significantly more TNF, IL-1β, and IL-10 per cell on aligned fibers compared to unaligned fibers (*Figure 7.4*). There were no observed differences in TGF-β1 secretion for any group (*Figure 7.4*). *Effects of Matrix Mechanical Properties:* For macrophages on unaligned fibers, there were no observed differences in the secretion of any of the pro- or anti-inflammatory cytokines analyzed (*Figure 7.4*). For aligned meshes, IL-1β, TNF, and IL-10 per cell were all greater for macrophages on aligned PDMS-PCL compared to aligned PCL-only after 48 hours in culture (*Figure 7.4*).

7.4 Discussion

In this study, macrophages were successfully seeded on nanofiber meshes, and results from this study suggest that the nanofiber matrix can play an immunomodulatory role on macrophage activation. Initial cell attachment studies show that cell attachment is lower on all nanofiber meshes compared to tissue culture plastic after the five-day differentiation period. Macrophage attachment has been shown to be a necessary precursor for macrophage activation toward a pro- or anti-inflammatory phenotype(25;263;264). Therefore, lower attachment to nanofiber matrices compared to tissue culture plastic is indicative of decreased potential for macrophage activation on fiber mesh groups compared to monolayer controls. This suggests that a fibrous matrix may be beneficial for minimizing the inflammatory response *in vivo* compared to smooth matrices. Additionally, for the population of macrophages which did adhere to the surface of meshes, compared to macrophages on tissue culture plastic, cells on nanofibers release significantly less

TNF and IL-1β per cell, as well as significantly more IL-10 and TGF-β1 per cell, indicating that cells on nanofibers are polarized toward an anti-inflammatory phenotype, while cells on tissue culture plastic exhibit a pro-inflammatory phenotype.

Further, while there were no observed differences in macrophage attachment on unaligned and aligned PCL-only meshes, significantly fewer cells attached to aligned PDMS-PCL compared to unaligned PDMS-PCL. This is similar to results observed by Cao *et al*., who investigated the effects of fiber alignment on the foreign body response both *in vivo* and *in vitro*(265;266). *In vitro* results show that human primary monocytes adhere less to aligned nanofibers compared to unaligned fibers. And while cells were able to infiltrate aligned meshes, a fibrous capsule was formed on the surface of unaligned fibers, suggesting a minimized host response on aligned fibers compared to unaligned fibers(266). It is possible, under these circumstances, that macrophages recognize aligned fibers as a healthy fibrous tissue, while unaligned fibers may represent a scar-like tissue.

Alternatively, in previous work by Saino *et al*. using the murine macrophage-like RAW 264.7 cell line, the opposite effect was observed, with increased macrophage attachment to aligned PLLA fibers compared to unaligned PLLA (25). And while the release of pro-inflammatory cytokines, including granulocyte colony-stimulating factor (G-CSF), interferon-γ (INF-γ), macrophage inflammatory protein-1α (MIP-1α), and TNF, was enhanced on both aligned and unaligned PLLA fibers compared to PLLA films, results studying the differences in response to aligned and unaligned fibers were inconclusive. Therefore, it is possible that the effects of matrix alignment on cell attachment is unique to the fiber material composition. Indeed, there is still much left to be discovered in order to understand the interactions between macrophages and fibrous matrices, especially as they apply to the wound healing environment.

With respect to the role of matrix mechanical properties on macrophage activation and inflammatory response following connective tissue injury and during tissue repair and remodeling, results from this chapter show that, for aligned fibers, cell attachment is significantly greater on PCL-only meshes compared to PDMS-PCL blends. Previous work assessing RAW 264.7 macrophage response on RGD-modified PEG hydrogels of varying mechanical properties revealed that macrophage attachment is enhanced on stiffer substrates, and increased substrate stiffness results in increased cell spreading after 24 hours, leading to the classically activated, or M1, phenotype, as observed through increased expression

of pro-inflammatory markers including TNF, IL-1β, and IL-6 at day 1(267). Still, little is known concerning the mechanisms with which macrophages are capable of sensing their environment. Previous work has shown that, while substrate stiffness can affect macrophage spreading, this change is not due to an increase in internal tension caused by actin stress fiber polarization, indicated by the absence of visible actin during immunostaining(267;268). But more recent work shows that stress fibers do form within macrophages, especially on stiffer surfaces, and the length and alignment of these fibers increases with increasing stiffness(269).

To this end, results of this chapter indicate that a fibrous mesh is a suitable substrate to serve as an implantable matrix to modulate the inflammatory response following connective tissue injury. As mentioned previously, an optimal implantable matrix for the delivery of MSC 1) must not elicit an inflammatory response by inflammatory cells present at the site of injury, and 2) should modulate polarization of macrophages toward an anti-inflammatory phenotype instead of a pro-inflammatory phenotype. Overall cell attachment and pro-inflammatory activation of cells on all meshes was minimal compared to monolayer culture, suggesting that a fiber-based implant may serve to minimize the inflammatory reaction by infiltrating macrophages, as well as promote anti-inflammatory polarization of activated macrophages, following implantation compared to an implant with a smooth surface. In choosing an ideal mesh from the series of samples tested (unaligned vs. aligned and PCL-only vs. PDMS-PCL), cell attachment was lowest on aligned PDMS-PCL, resulting in the lowest levels of both pro- and anti-inflammatory cytokine secretion compared to all other meshes. Still, for the cells which did attach, cytokine release per cell was greater than other fibers, suggesting macrophage activation toward both M1 and M2 phenotypes are enhanced on this substrate. The studies performed in *Chapter 8* will shed more light on macrophage response in the presence of relevant cell types in order to better assess the effects of matrix alignment and mechanical properties on macrophage activation.

7.5 Conclusion

This study demonstrated that macrophages can be cultured on unaligned and aligned nanofibers composed of either PCL alone or PDMS-PCL blends, and macrophage phenotype and activation on these substrates in the absence of other stimuli is different than macrophage response on tissue culture plastic. To this end, fibrous matrices minimize macrophage release of pro-inflammatory cytokines and cause

increased release of anti-inflammatory cytokines compared to macrophages seeded in 2D, indicating that cells on 3D fibrous matrices exhibit decreased pro-inflammatory response and increased anti-inflammatory behavior compared to response on tissue culture plastic. This also suggests that use of an implantable fibrous matrix rather than a smooth, flat substrate may in itself improve macrophage inflammatory response after injury. Further, as no differences in cell response on unaligned versus aligned PCL-only meshes were observed, this suggests that fiber alignment alone does not modulate macrophage activation. However, with observed decreases in cell attachment on aligned PDMS-PCL fibers, as well as increased release of IL-10 and IL-1β per cell on aligned PDMS-PCL compared to all other meshes, it seems that by tuning both matrix alignment and mechanical properties together, these matrix-based cues have a combined effect on macrophage response.

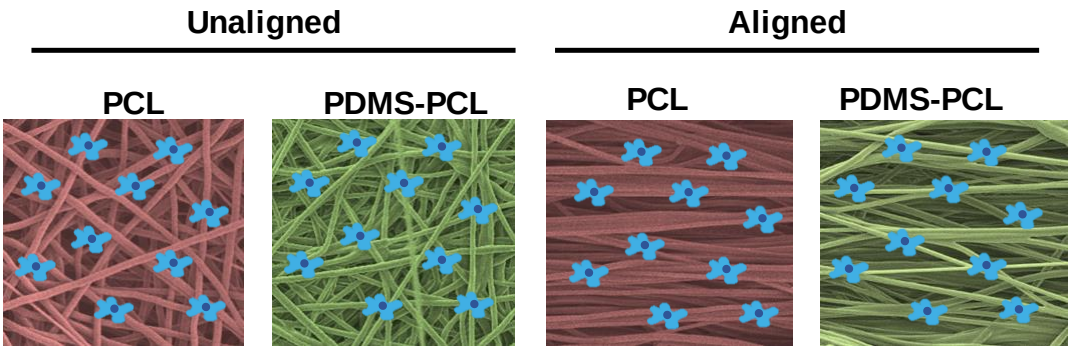

Figure 7.1: Effects of Matrix Alignment and Mechanical Properties on Macrophage Response: Schematic of Groups. Macrophages were seeded on unaligned and aligned PDMS-PCL and PCL-only meshes, as well as in monolayer.

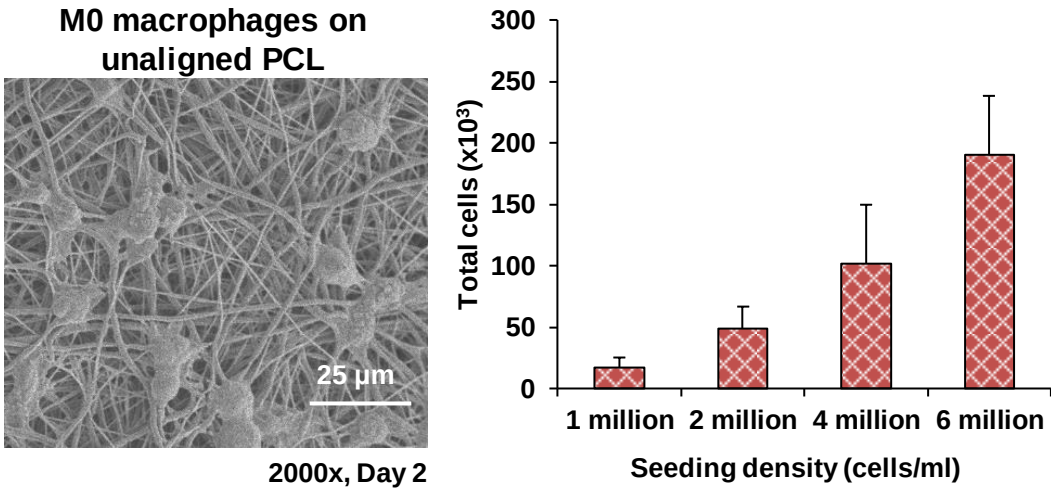

Figure 7.2: Effects of Matrix Alignment and Mechanical Properties on Macrophage Response: Seeding Density Optimization. To seed cells, THP-1 monocytes were suspended in PMA+ medium at varying densities (1 million-6 million cells/ml) and 2 ml of cell suspension was added per well. Cell were allowed 48 hours to attach. Cell density on meshes increases in a concentration-dependent manner As seeding density is increased, total cells on scaffolds increased linearly. SEM: *n*=3, day 2, mag = 2000x, scale bar = 25 µm. Cell attachment: *n*=5.

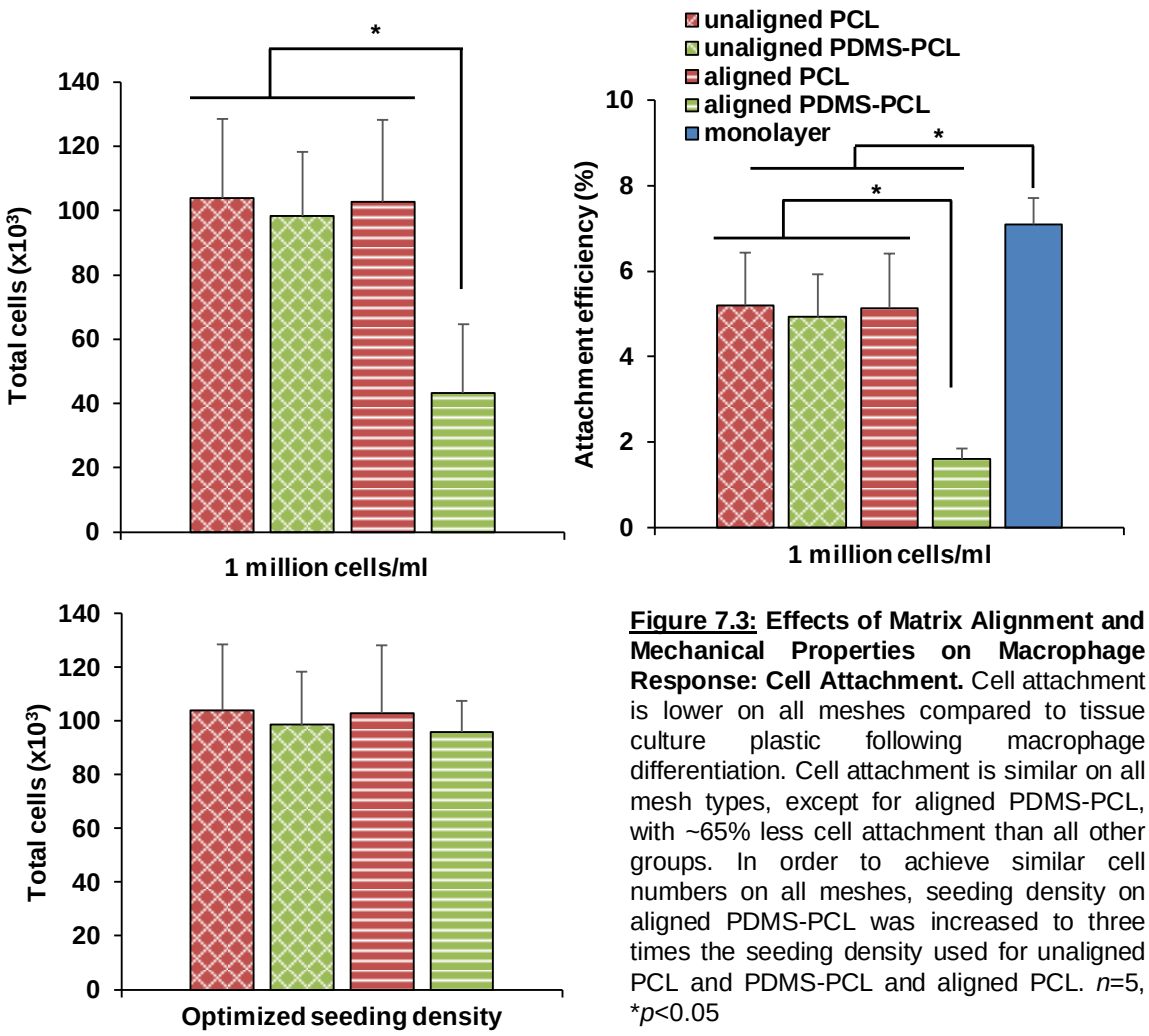

<u>Figure 7.3:</u> Effects of Matrix Alignment and Mechanical Properties on Macrophage Response: Cell Attachment. Cell attachment is lower on all meshes compared to tissue culture plastic following macrophage differentiation. Cell attachment is similar on all mesh types, except for aligned PDMS-PCL, with ~65% less cell attachment than all other groups. In order to achieve similar cell numbers on all meshes, seeding density on aligned PDMS-PCL was increased to three times the seeding density used for unaligned PCL and PDMS-PCL and aligned PCL. n=5, *p<0.05

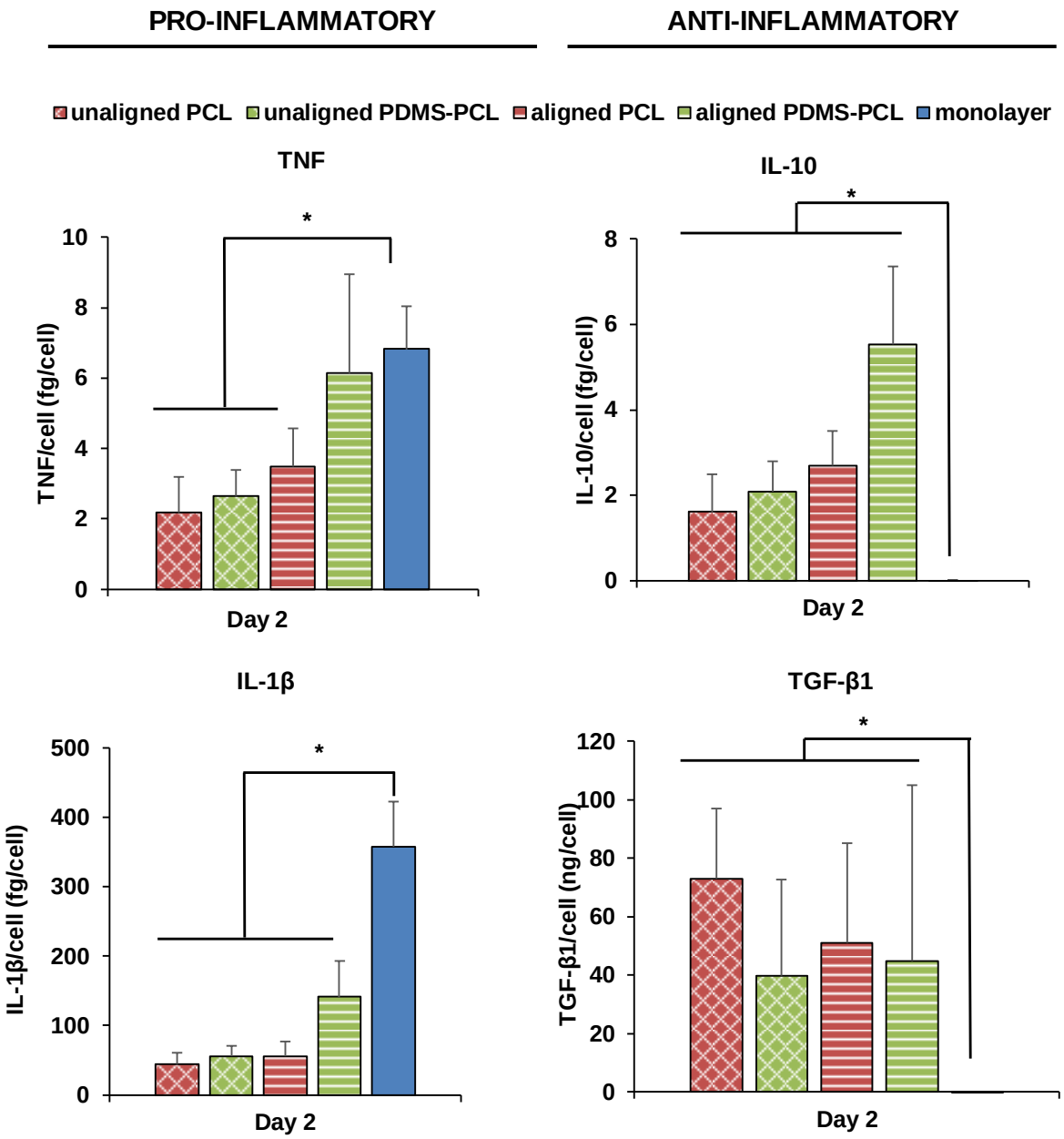

Figure 7.4: Effects of Matrix Alignment and Mechanical Properties on Macrophage Response: Release of Pro- and Anti-inflammatory Cytokines. There was significantly lower concentrations of IL-1β in all nanofiber groups compared to monolayer at day 2. TNF levels were also lower for macrophages on unaligned PDMS-PCL and PCL-only meshes, as well as on aligned PCL-only meshes compared to monolayer at day 2. IL-10 and TGF-β1 release were greater on nanofibers than in monolayer, with significantly more IL-10 release on aligned PDMS-PCL compared to other meshes. n=5, *p<0.05

CHAPTER 8: EFFECTS OF MATRIX ALIGNMENT AND MECHANICAL PROPERTIES ON HETEROTYPIC CELLULAR INTERACTIONS

8.1 Introduction

In *Chapters 5-7*, the effects of matrix alignment and mechanical properties on the response of MSC, ligament fibroblasts, and macrophages in single-culture were determined. Results from these studies show that matrix elasticity affects initial cell attachment and spreading of both MSC and fibroblasts, resulting in differences in cell proliferative rate over time, while matrix alignment and mechanical properties have a combined effect on modulating the inflammatory response of M0 macrophages. In this chapter, the effects of matrix alignment and mechanical properties on the heterotypic interactions between these cell types were determined using a physiologically relevant 3D tri-culture model that combines the tri-culture model developed in *Chapter 3*, as well as the nanofiber matrix platform devised in *Chapter 4*.

8.1.1 Background and Motivation

Mesenchymal stem cells have been shown to modulate the inflammatory microenvironment following injury, improving healing response. Work by Thomopoulos and coworkers has shown that the ability of MSC to modulate the inflammatory response and promote tissue healing by fibroblasts stems from the ability of MSC to modulate macrophage activation state(91). In this work, it was observed that the addition of ADSC to a co-culture of tendon fibroblasts and M1 macrophages resulted in a shift of macrophages from a pro-inflammatory, M1 phenotype toward an anti-inflammatory, M2 phenotype *in vitro*. In turn, this shift protects tendon fibroblasts from the harmful effects of pro-inflammatory cytokines, such as IL-1β and TNF. These results are further supported by the results obtained in *Chapter 3* of this thesis, in which the addition of MSC to fibroblast-macrophage co-culture results in decreased pro- and anti-inflammatory activation of M0 macrophages compared to fibroblast-macrophage co-culture. While these results illustrate the potential value of MSC for controlling the inflammatory microenvironment, in order to minimize prolonged inflammation and associated scar tissue formation, little work has been done to assess these cellular interactions in a 3D matrix microenvironment.

In *Chapter 7*, it was determined that matrix-based cues play an important role in controlling macrophage phenotype. Specifically, macrophage attachment, a precursor for macrophage activation, was decreased on fibrous matrices compared to flat 2D substrates. Additionally, for cells that did attach, pro-inflammatory activation of M0 macrophages was downregulated by anti-inflammatory activation was upregulated compared to macrophages on tissue culture plastic. These results suggest that a fibrous

microenvironment, similar to that observed at the native injury site, plays an immunomodulatory role in macrophage response. Furthermore, this effect was further enhanced on aligned PDMS-PCL fibers compared to unaligned matrices and matrices with higher elastic modulus, suggesting that fiber alignment and mechanical properties can be optimized to improve the inflammatory response to an even greater extent. Still, a better understanding of the role that matrix-based cues play in guiding macrophage response in a more complex cellular microenvironment that recapitulates the interactions between these cells and the other cell types observed at the injury site is necessary to fully understand these effects during the native repair response is it occurs *in vivo*.

8.1.2 Objectives

The objectives of this study are to 1) determine the role that matrix-based cues (matrix alignment and mechanical properties) play in modulating the interactions between native ligament fibroblasts, MSC, and macrophages following connective tissue injury and during repair, and 2) determine the optimal combination of matrix alignment and mechanical properties for mitigating macrophage-driven inflammation and promoting a healing response by ligament fibroblasts and MSC. Toward these goals, fibroblasts, MSC, and macrophages will be tri-cultured on the unaligned and aligned PCL-only and PDMS-PCL fibers developed and utilized in *Chapters 4-7*. It is hypothesized that 1) matrix-based cues will have an effect on the interactions between macrophages, fibroblasts, and MSC, resulting in differences in macrophage inflammatory activation, fibroblast proliferation and matrix synthesis, and matrix production by MSC, and 2) the aligned, PDMS-PCL matrix will be optimal for minimizing macrophage inflammatory activation, resulting in promotion of matrix synthesis by fibroblasts and MSC.

8.2 Materials and Methods

8.2.1 Cells and Cell Culture

8.2.1.1 Human Mesenchymal Stem Cell Isolation and Culture

Human MSC were isolated from bone marrow aspirate of a 21 y/o male donor, obtained commercially (Lonza). Briefly, the aspirate was centrifuged on a discontinuous Percoll gradient to remove blood cells. Supernatant was then removed and mixed with F/S DMEM and plated on tissue culture plastic. Media was changed the following day to remove non-adherent cells. Adherent cells were assumed to be

MSC and were passaged once prior to use or cryopreservation. For cryopreservation, cells were frozen in cryomedia containing F/S DMEM, 20% FBS, and 10% DMSO. Cells were thawed at P2 and maintained in culture with F/S DMEM containing 10% FBS and 1% P/S, without other antibiotics.

8.2.1.2 Human Anterior Cruciate Ligament Cell Isolation and Culture

Human ACL fibroblasts were derived from explant culture of tissues obtained from a patient (male, aged 21) undergoing ACL reconstruction surgery. Briefly, the tissue samples were rinsed in PBS, plated in tissue culture dishes, and maintained in DMEM supplemented with 10% FBS, 1% non-essential amino acids, 1% P/S, 0.1% Amp-B and 50 µg/mL G/S. The cells from the first migration were subsequently discarded, and the tissue was re-plated in fresh fully supplemented medium. Only cells obtained from the second and third migrations were used in this study because this method has been shown to yield a relatively homogenous fibroblast population.

8.2.1.3 Human THP-1 Culture

Human THP-1 cells were obtained commercially (ATCC, TIB202) and maintained in continuous culture in non-tissue culture treated flasks (25 cm^2) with F/S RPMI-1640 containing 10% FBS, 1% P/S, and 0.05 mM 2-ME. Media was replaced every 3-4 days. Briefly, cells suspensions were removed from culture dishes once every 3-4 days and cells were centrifuged at 5000 rpm for 5 minutes. Supernatant was aspirated and cells were resuspended in fresh RPMI-1640 at a density of $4x10^5$ cells/mL.

8.2.2 Nanofiber Mesh Fabrication

8.2.2.1 Unaligned PCL

A 16% (w/v) PCL solution was prepared by dissolving PCL (M_n = 70,000-90,000) into 3:1 solution of DCM:DMF. The solution was mixed overnight, vortexed for ~1 hour prior to electrospinning, and then loaded into a 5 mL syringe attached with a 23-gauge stainless steel blunt-tip needle. A voltage of 7-9 kV was applied to the needle tip and a pump flow rate of 1 mL/hr was used. Fibers were collected on a grounded stationary plate placed 15 cm from the needle tip. Approximately 3.5 mL of polymer solution was electrospun in order to fabricate meshes with thicknesses ranging from 0.09-0.14 mm as measured with a digital caliper.

8.2.2.2 Aligned PCL

An 18% (w/v) PCL solution was prepared by dissolving PCL into 3:2 mixture of DCM:DMF. The solution was mixed overnight, vortexed for ~1 hour prior to electrospinning, and the entire solution loaded into a 5 mL syringe with a 23-gauge stainless steel blunt-tip needle. A voltage of 9-10 kV was applied to the needle tip and a pump flow rate of 1 mL/hr was used. Fibers were collected on a grounded rotating mandrel (2500 rpm), 13 cm from the needle tip. Approximately 5 mL of polymer solution was electrospun in order to fabricate meshes with thicknesses ranging from 0.07-0.14 mm as measured with a digital caliper.

8.2.2.3 Unaligned PDMS-PCL Blend

A 35% (w/v) PDMS-PCL solution was prepared by dissolving a 1:1 mixture of PDMS (Sylgard 184, 50:1 base:crosslinker) and PCL (M_n = 70,000-90,000) in a 3:1 solution of DCM:DMF. The solution was vortexed for 4 hours prior to electrospinning, and then loaded into a 5 mL syringe attached with a 23-gauge stainless steel blunt-tip needle. A voltage of 10-11 kV was applied to the needle tip and a pump flow rate of 1 mL/hr was used. Fibers were collected on a grounded stationary plate placed 12 cm from the needle tip. Approximately 3 mL of polymer solution was electrospun in order to fabricate meshes with thicknesses ranging from 0.07-0.14 mm as measured with a digital caliper.

8.2.2.4 Aligned PDMS-PCL Blend

A 35% (w/v) PDMS-PCL solution was prepared by dissolving a 1:1 mixture of PDMS (50:1 base:crosslinker) and PCL (M_n = 70,000-90,000) in a 3:1 solution of DCM:DMF. The solution was vortexed for 4 hours prior to electrospinning, and then loaded into a 5 mL syringe attached with a 23-gauge stainless steel blunt-tip needle. A voltage of 10-11 kV was applied to the needle tip and a pump flow rate of 1 mL/hr was used. Fibers were collected on a grounded rotating mandrel (2100 rpm), 12 cm from the needle tip. Approximately 3.5 mL of polymer solution was electrospun in order to fabricate meshes with thicknesses ranging from 0.07-0.14 mm as measured with a digital caliper.

8.2.3 Cell Seeding on Nanofiber Meshes

Electrospun polymer meshes were cut to 1 x 1.8 cm and secured to custom-made backings using tape, resulting in a cell culture surface area of 1 cm^2. To enhance surface reactivity, PCL-only and PDMS-PCL fibers were then air plasma treated (Harrick Plasma PDC-32G) at RF setting for 30 seconds. Meshes

were then immediately UV sterilized (both sides, 15 minutes each) at 365 nm and incubated overnight at 37ºC, 5% CO_2 in either F/S DMEM with 20% FBS for fibroblast-seeded and MSC-seeded meshes, or F/S RPMI-1640 with 20% FBS for macrophage-seeded meshes to promote cell attachment.

After the overnight soak, medium was removed and cells were seeded as described in *Chapters 5-7*. Briefly, for macrophage-seeded meshes, THP-1 monocytes were suspended in F/S RPMI-1640 supplemented with 100 nM PMA at a density of $5x10^5$ cells/mL. Cells were allowed to attach for 48 hours, at which point PMA+ medium was removed and samples were rinsed one time in PBS. Meshes seeded with THP-1 were allowed to soak for 1 minute in PBS prior to aspiration and the addition of 2 mL of fresh F/S RPMI-1640. Macrophage-seeded meshes were then allowed to rest for 72 hours prior to tri-culture.

On the same day that PMA+ medium was removed from macrophage-seeded meshes, MSC and fibroblasts were seeded on nanofiber meshes. For MSC-seeded meshes, MSC were seeded on meshes at a density of $3x10^4$ cells/cm^2 (3 M cells/mL, 10 µL) and allowed to attach for 15 minutes under humidified conditions at 37ºC, 5% CO_2 before the addition of F/S DMEM. For fibroblast-seeded meshes, fibroblasts were seeded on meshes at a density of $3x10^4$ cells/cm^2 (3 M cells/mL, 10 µL) and allowed to attach for 15 minutes under humidified conditions at 37ºC, 5% CO_2 before the addition of F/S DMEM. Cells were cultured on meshes for the remainder of the five-day macrophage differentiation period prior to tri-culture. All samples were maintained at 37°C, 5% CO_2.

8.2.4 Tri-Culture Model

Following cell seeding on nanofiber meshes, one MSC-seeded, one fibroblast-seeded, and one macrophage-seeded mesh were placed within a single well of a 6-well plate, and 2 mL of a 1:1 mixture of F/S DMEM and F/S RPMI-1640 was added to each well. Fibroblast-macrophage co-culture, fibroblast-MSC co-culture, and MSC-macrophage co-culture, as well as single-cultures of fibroblasts, MSC, and macrophages were used as controls.

8.2.4.1 Delayed Tri-Culture Model

To assess the effects of the timing of MSC delivery on macrophage response and fibroblast activity, MSC were added to tri-culture on either day 0 or day 2 of tri-culture. Briefly, using the tri-culture model described above, MSC, fibroblasts, and THP-1-derived macrophages were cultured on nanofiber meshes,

and were either all added to the same well on day 0, or fibroblasts and macrophages were added to the same well on day 0, with MSC added on day 2.

8.2.5 Cytokine Secretion

Levels of pro- (TNF, IL-1β) and anti-inflammatory (IL-10, TGF-β1) cytokines (*n*=5) were evaluated for all tri-culture conditions via ELISA according to the manufacturer's protocol. Briefly, supernatants from cell culture were collected after 48 hours and stored at -30°C. On the day of analysis, samples were thawed and added directly to assay diluent in a prepared plate and incubated for two hours at room temperature prior to solution removal. Each well was washed three or four times before incubation with either TNF, IL-1β, or IL-10 conjugate for 1 hour at room temperature, or TGF-β1 conjugate for two hours at room temperature. The conjugate was then removed, the plate was washed three or four times, and the substrate solution was added to each well and allowed to react in the dark. The stop solution was added after 20 minutes for TNF, IL-1β, or IL-10 ELISAs or 30 minutes for TGF-β1 ELISA, and the absorbance was measured using a microplate reader Sample absorbance was measured using a microplate reader (Tecan) at 450 nm and 570 nm, and the difference was used to calculate cytokine concentration. Base level concentrations of each cytokine in acellular culture medium were used as negative controls.

8.2.6 Cell Proliferation

Cell proliferation (*n*=5) was determined by measuring total DNA content using the PicoGreen dsDNA assay (Invitrogen) following the manufacturer's protocol. Samples were rinsed twice in PBS and stored in 500 µL of 0.1% Triton X (Sigma-Aldrich) at -30°C. Immediately before the analysis, samples were thawed and homogenized followed by ultrasonication at 5W (Microson XL-2000) for 15 seconds. Fluorescence was measured using a Tecan microplate reader with an excitation wavelength of 485 nm and an emission wavelength of 535 nm. A conversion factor of 8 pg DNA/cell was used to determine cell number.

8.2.7 Collagen Production

Collagen production (*n*=5) was quantified using a modified hydroxyproline assay(199). Samples were digested in a buffered papain solution prior to analysis. For digestion, samples were vacuum dried overnight using the Centrivap concentrator (Labconco). Samples were then digested for 20 hours at 65ºC

with 20 µL/mL papain (Sigma-Aldrich), buffered in 0.1 M sodium acetate, 10 mM cysteine HCl, and 50 M EDTA. For the assay, digested samples were concentrated by drying 125-250 µL of sample overnight in the Centrivap concentrator. Samples were resuspended in 50 µL of 2N NaOH and autoclaved for 25 minutes. 450 µL of Chloramine T Reagent (1.27 g chloramine T in 50% isopropanol brought to 100 mL with acetate-citrate buffer) was added to the samples, which were then allowed to incubate for 25 minutes at room temperature. 500 µL of Ehrlich's reagent (15 g p-dimethylaminobenzaldehyde in 100 mL (2:1) isopropanol:perchloric acid) was subsequently added, and the samples were incubated at 65ºC for 20 minutes. The absorbance at 555 nm was read using a Tecan microplate reader. Total collagen was determined using a standard curve generated using a collagen standard (Sigma-Aldrich).

The acetate-citrate buffer for the chloramine T solution consisted of 30 g sodium acetate trihydrate, 11.5 g citric acid, 3 mL acetic acid, and 8.5 g NaOH, dissolved in 125 mL of distilled water. The solution was brought to a pH of 6.5 using 1 N NaOH or 1 N HCl, and then brought to a final volume of 250 mL.

8.2.8 Exosome Isolation

In an attempt to uncover the mode of communications between cell types in tri-culture, optimization of a protocol for exosome isolation was performed. In this study, as a proof-of-concept, exosomes were isolated from MSC single-culture (*n*=5) using protocols developed by Théry *et al*.(270) and analyzed using a zetasizer to determine particle size. Briefly, MSC were cultured in monolayer for 7 days, and culture media was collected immediately centrifuged in 50 mL conical tubes at 300 g for 10 minutes to remove any cells. The supernatant was then collected and transferred to 1.5 mL Eppendorf tubes and centrifuged at 10,000 g in a microcentrifuge at 4ºC for 30 minutes to remove any cellular debris from the supernatant. Medium was again collected in 36 mL polypropylene tubes and centrifuged in an ultracentrifuge (Optima XPN-80, Beckman-Coulter) with a Type 70 Ti rotor at 100,000 g for 90 minutes at 4ºC to collect exosomes. The supernatant was removed and the pellet was saved and resuspended in 10 mL PBS, followed by ultracentrifugation at 100,000 g for 90 minutes at 4ºC once more. The supernatant was removed and the pellet was resuspended in 1 mL PBS and filtered through a sterile filter with 0.22 µm pores. Size distribution of exosomes was measured using dynamic light scattering (*n*=5; Malvern Zetasizer Nano ZS).

8.2.9 Statistical Analysis

Results are reported as mean ± standard deviation, with *n* equal to the number of replicates per group. Statistical analyses were performed with JMPIN (4.0.4, SAS Institute, Inc.). Two-way ANOVA was used to determine the effects of nanofiber alignment and mechanical properties on cytokine release, while multi-way ANOVA was used to determine the effects of nanofiber alignment and mechanical properties on cell proliferation and collagen synthesis over time. The Tukey-Kramer post-hoc test was used for all pair-wise comparisons, and significance was attained at $p<0.05$.

8.3 Results

8.3.1 Cytokine Secretion

Effects of Heterotypic Interactions in 3D: On both unaligned and aligned meshes, TNF release is significantly greater in fibroblast-macrophage co-culture than MSC-macrophage co-culture and delayed tri-culture. It was also greater than tri-culture on unaligned fibers only (*Figure 8.2*). IL-1β secretion was also lower in MSC-macrophage co-culture than fibroblast-macrophage co-culture and tri-culture on both unaligned and aligned fibers (*Figure 8.2*). Total IL-10 release was greater in fibroblast-macrophage co-culture and in tri-culture compared to MSC-macrophage co-culture on both unaligned and aligned fibers (*Figure 8.3*). *Effects of Fiber Alignment in Tri-Culture:* In delayed tri-culture, there was significantly more TNF for tri-culture on unaligned PCL-only fibers compared to aligned PCL-only, with no observed effect on IL-1β release (*Figure 8.4*). Total IL-10 was also greater for tri-culture on unaligned PCL-only fibers compared to aligned PCL-only, with no effect on the release of TGF-β1 at 48 hours (*Figure 8.5*). For PDMS-PCL fibers, there were no major differences in the release of either pro- or anti-inflammatory cytokines after 48 hours of tri-culture (*Figures 8.4 and 8.5)*. *Effects of Fiber Mechanical Properties in Tri-Culture*: There were no observed differences in cytokine secretion in tri-culture on PCL-only vs. PDMS-PCL fibers in either unaligned or aligned fiber orientations (*Figures 8.4 and 8.5*). However, for delayed tri-culture, total IL-10 release was greater for tri-culture on unaligned PCL-only compared to tri-culture on unaligned PDMS-PCL fibers (*Figure 8.5*). *Combined Effects of Fiber Alignment and Mechanical Properties in Tri-Culture:* In tri-culture, total IL-1β release was greater on unaligned PCL-only fibers compared to aligned PDMS-PCL fibers, with no effect on TNF (*Figure 8.4*). In delayed tri-culture, TNF release was elevated on unaligned PCL-only fibers compared to both unaligned and aligned PDMS-PCL fibers (*Figure 8.4*). Total IL-10 was

also greater for tri-culture on unaligned PCL-only fibers compared to aligned PDMS-PCL fibers after 48 hours (*Figure 8.5*), with no effect on TGF-β1 release. In delayed tri-culture, total IL-10 was greater on unaligned PCL-only fibers compared to all other groups at this time point (*Figure 8.5*).

8.3.2 Effects of Timing of MSC Delivery on Cell Response

Total TNF release was lower for all groups in delayed tri-culture compared to day 0 tri-culture (*Figure 8.4*). There were no effects of delayed tri-culture on the release of IL-1β for any group. In terms of anti-inflammatory cytokine release, there no differences in the release of either IL-10 or TGF-β1 after 48 hours between delayed tri-culture and day 0 tri-culture groups on any matrix type (*Figure 8.5*).

8.3.3 Fibroblast Proliferation

Fibroblast proliferation over time is shown in *Figure 8.6*. *Effects of Fiber Alignment:* There were no observed differences in cell number at days 2 or 7 between fibroblasts on unaligned and aligned nanofiber meshes for either PCL-only or PDMS-PCL compositions (*Figure 8.6*). Cell number did not change significantly over time for any group (*Figure 8.6*). *Effects of Fiber Mechanical Properties*: There were no observed differences in cell number at days 2 or 7 between fibroblasts on PCL-only and PDMS-PCL meshes, regardless of fiber alignment (*Figure 8.6*). Cell number did not change significantly over time for any group (*Figure 8.6*).

8.3.4 Fibroblast Collagen Production

Total collagen production for fibroblasts on nanofiber meshes is shown in *Figure 8.7*. *Effects of Fiber Alignment:* Total collagen increased over time on aligned meshes only, with no differences in total collagen between days 2 and 7 on unaligned meshes composed of either PCL-only or PDMS-PCL (*Figure 8.7). Effects of Fiber Mechanical Properties*: Total collagen was greater on PCL-only meshes compared to PDMS-PCL meshes at day 7 (*Figure 8.7)*.

8.3.5 Stem Cell Collagen Production

Total collagen was greater for MSC on unaligned PCL-only compared to aligned PCL-only fibers at day 2. This difference was no longer observed by day 7. Total collagen decreased over time on unaligned PCL-only fibers, with no difference in total collagen over time on aligned PCL-only fibers (*Figure 8.8*). There

were no observed differences in total collagen for MSC on unaligned and aligned PDMS-PCL fibers at days 2 or 7 (*Figure 8.8*).

8.3.6 Exosome Isolation

After completion of the exosome isolation protocol for MSC single-cultures, the presence of and size distribution of particles in solution were determined via dynamic light scattering. Results show that particles in suspension had diameters of d= 92.62 ± 28.30 nm. It has been previously shown that exosomes range in size from 40-100 nm, suggesting that these particles may indeed be exosomes isolated from MSC single-culture (*Figure 8.9)*.

8.4 Discussion

In this chapter, a 3D tri-culture model was designed that is capable of assessing the interactions between MSC, fibroblasts, and macrophages during connective tissue injury and repair. All three cell types were cultured on either PDMS-PCL or PCL-only fibers in unaligned or aligned orientations to determine the combined effects of matrix-based cues and heterotypic cellular interactions on the response of each individual cell type. Using this model, MSC, fibroblasts, and macrophages were each cultured on individual matrices and then cultured in tri-culture in order to analyze the effects of paracrine signaling among all three cell types on the response of each cell type. Additionally, MSC were added to tri-culture on day 0, at the same time as fibroblasts and macrophages, as well as on day 2 following co-culture of fibroblasts and macrophages for 48 hours. This highlights the flexibility of this model for studying the effects of 1) mode of cell-cell contact and 2) timing of cell-cell contact, among other variables, in tri-culture.

Results of this study show that matrix-based cues not only play a critical role in controlling the response of individual cell types, but can also modulate the interactions between cell types *in vitro*. With respect to fibroblast activity, fibroblasts produced more collagen by day 7 in tri-culture on aligned fibers compared to unaligned fibers. This is similar to the day 7 results observed for fibroblast single-culture studied in *Chapter 6*, in which total collagen was greater on aligned PCL-only fibers compared to unaligned fibers at this time point. And while there were no observed differences in MSC collagen production on unaligned and aligned fibers in tri-culture at days 2 or 7 for PCL-only or PDMS-PCL fibers, it is possible that

differences may be observed if later time points are assessed, as it has been observed in other studies that increases in MSC collagen synthesis can take up to 14 days *in vitro*(20).

Also, the release of both pro- and anti-inflammatory cytokines was decreased on aligned fibers with a local elastic modulus of ~1 MPa (aligned PDMS-PCL matrices), compared to unaligned fibers and fibers with greater local and bulk elastic moduli. These results indicate that matrices with elastic moduli similar to the elastic modulus observed for native healthy connective tissues, as is typically utilized for tissue engineering applications for connective tissue repair, are not necessarily the ideal substrates for promoting functional connective tissue healing after injury. Furthermore, the starkest difference in inflammatory activation by macrophages is observed between unaligned PCL-only and aligned PDMS-PCL meshes, for both immediate and delayed delivery of MSC in tri-culture, suggesting that matrix alignment and mechanical properties have a combined effect on regulating the inflammatory response, which is not observed when either of these matrix-based cues is altered individually. It is possible that an aligned matrix with mechanical properties similar to those observed for PDMS-PCL fibers serves to mimic the native connective tissue microenvironment during embryonic development, prompting a healing response by cells, rather than a fibrotic response. This was true in tri-culture, as well as for fibroblast-macrophage co-culture. Therefore, even in the absence of MSC, an optimal matrix that provides critical cues may be beneficial in modulating the inflammatory response following injury, even without the addition of stem cells.

Release of cytokines was further decreased when MSC were added to tri-culture on day 2, rather than day 0, which suggests that timing of MSC delivery is an important parameter to consider when developing a stem cell-based regenerative therapy for the treatment of connective tissue injury. To this end, it may be beneficial to deliver a cell-laden matrix a few days after injury, once inflammation has already begun, rather than immediately following injury. Because macrophages are capable of switching between activation states (i.e. M1 macrophages can be polarized toward an M2 phenotype), MSC delivery may still be valuable later in repair, even if a pro-inflammatory reaction has already mounted at the injury site. Still, it cannot be definitively determined from this study whether this observed difference in cytokine release profile is due to the delayed addition of MSC or due to changes in macrophage phenotype and cytokine *release in vitro* over time. Further assessment of macrophage response in co- and tri-culture at later time points beyond 48 hours is necessary to better understand this cell response. Also, proof-of-concept studies

for exosome isolation show that exosomes can be isolated from culture medium, providing an additional avenue for future tri-culture studies in order to assess the mode of communication between cell types in this model.

8.5 Conclusion

This study demonstrates the design of a 3D tri-culture model which can be used to assess the effects of matrix-based cues on heterotypic interactions between fibroblasts, MSC, and macrophages in a physiologically relevant fibrous matrix microenvironment. Results from this study suggest that matrix alignment and mechanical properties play a combined role in modulating the inflammatory response that is observed following connective tissue injury, while matrix alignment guides matrix elaboration by fibroblasts in tri-culture. Specifically, macrophage activation toward pro- and anti-inflammatory phenotypes in minimized on aligned PDMS-PCL fibers compared to unaligned PCL-only fibers, while fibroblast matrix synthesis is greater on aligned vs. unaligned meshes. Therefore, an aligned matrix with local and bulk elastic moduli similar to those of connective tissues during embryonic development may be suitable for promoting functional tissue healing and minimizing the formation of scar tissue following injury. Additionally, the tri-culture model designed in this chapter could serve as a platform for studying heterotypic cellular interactions under a variety of conditions, as this model can be tuned for studying the effects of 1) mode of cell-cell contact and 2) timing of cell-cell contact on the response of each cell type, among other variables. This model could also easily be expanded to study cellular interactions between other cell types relevant to the repair and regeneration of a variety of other fibrous tissues.

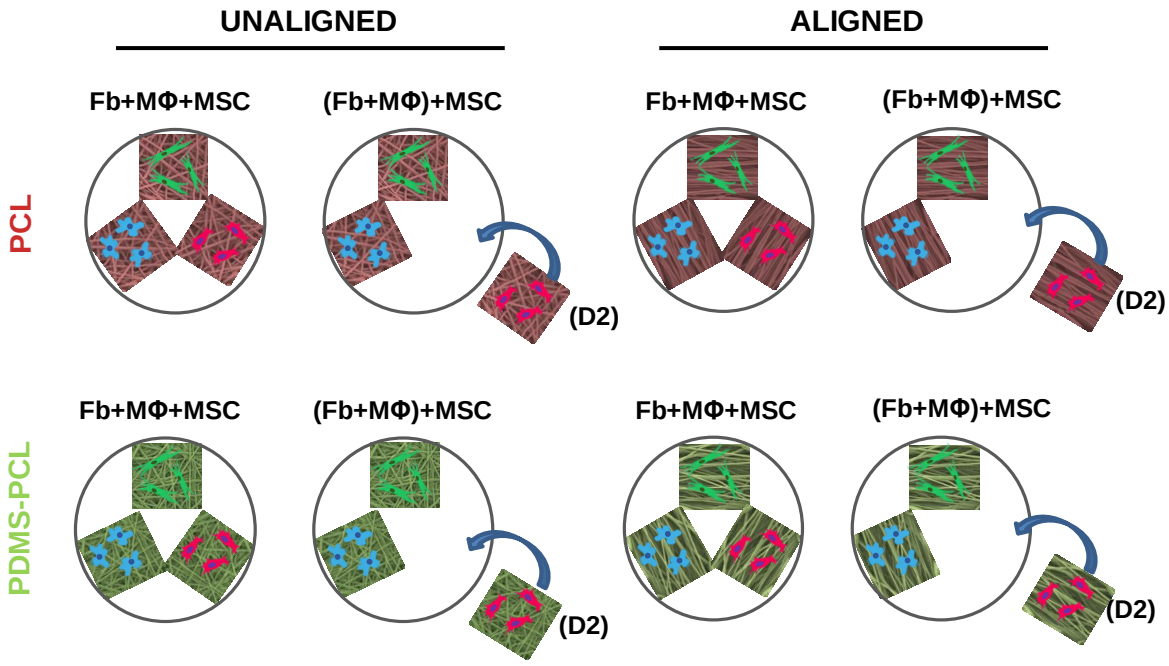

Figure 8.1: Effects of Matrix Alignment and Mechanical Properties on Heterotypic Cellular Interactions: Schematic of Study Design. For tri-culture, human mesenchymal stem cells (MSC), fibroblasts (Fb), and THP-1-derived M0 macrophages (MΦ) were seeded on either unaligned or aligned PCL nanofiber meshes and placed into the same well on day 0. Co-culture and single-cultures of MSC, Fb, and MΦ served as controls.

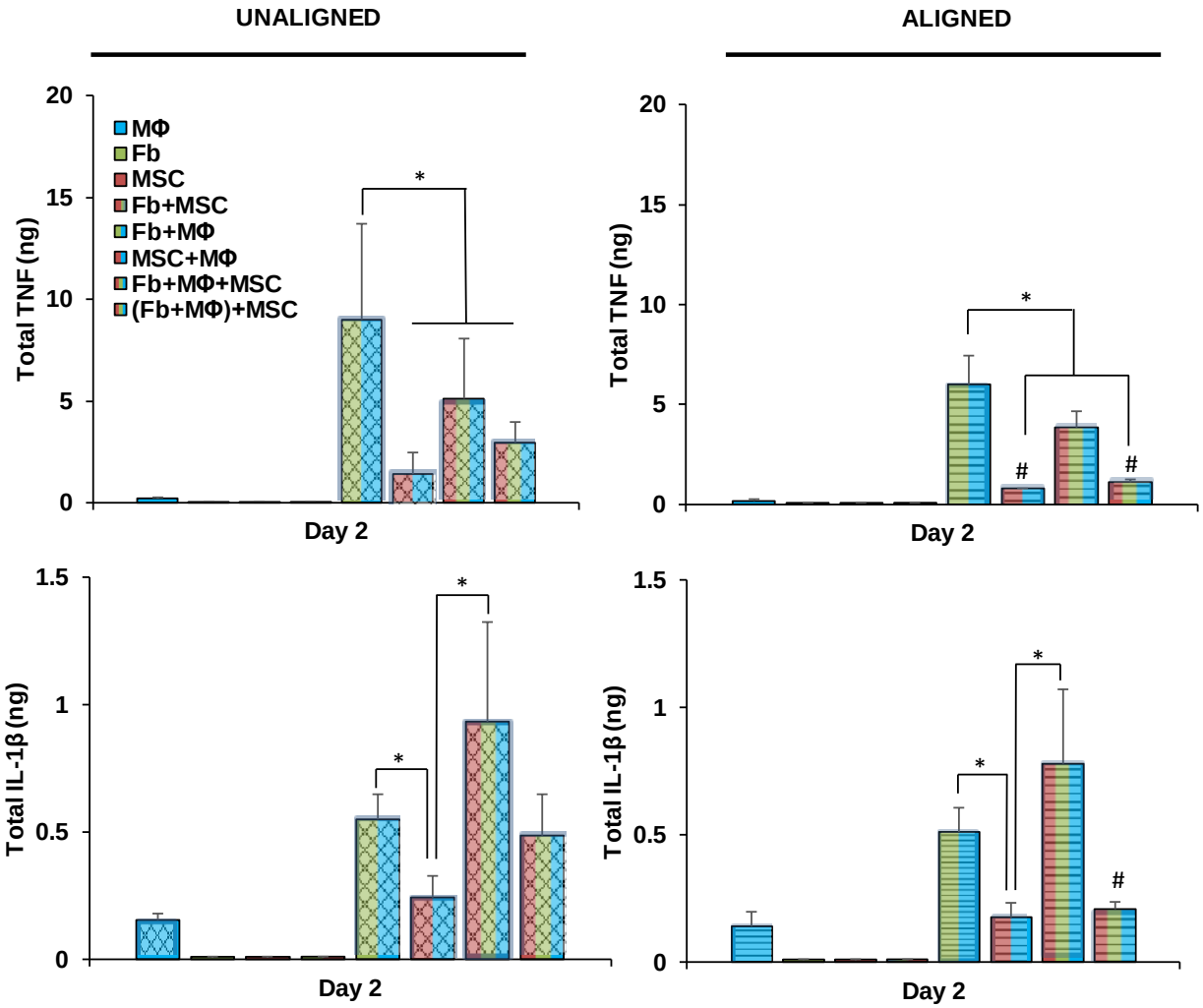

Figure 8.2: Effects of Matrix Alignment and Mechanical Properties on Heterotypic Cellular Interactions: Release of Pro-Inflammatory Cytokines. Total release of TNF was lower in MSC-macrophage (MSC-MΦ) co-culture and tri-culture than fibroblast-macrophage (Fb-MΦ) co-culture on both unaligned and aligned fibers. Secretion of TNF was lower for MSC-MΦ co-culture and delayed tri-culture on aligned fibers compared to unaligned fibers. IL-1β secretion was lower in MSC-MΦ co-culture than Fb-MΦ co-culture and tri-culture on both unaligned and aligned fibers. *n*=5, Significant difference: * between groups on the same fiber orientation, # between unaligned and aligned fiber orientations ($p<0.05$).

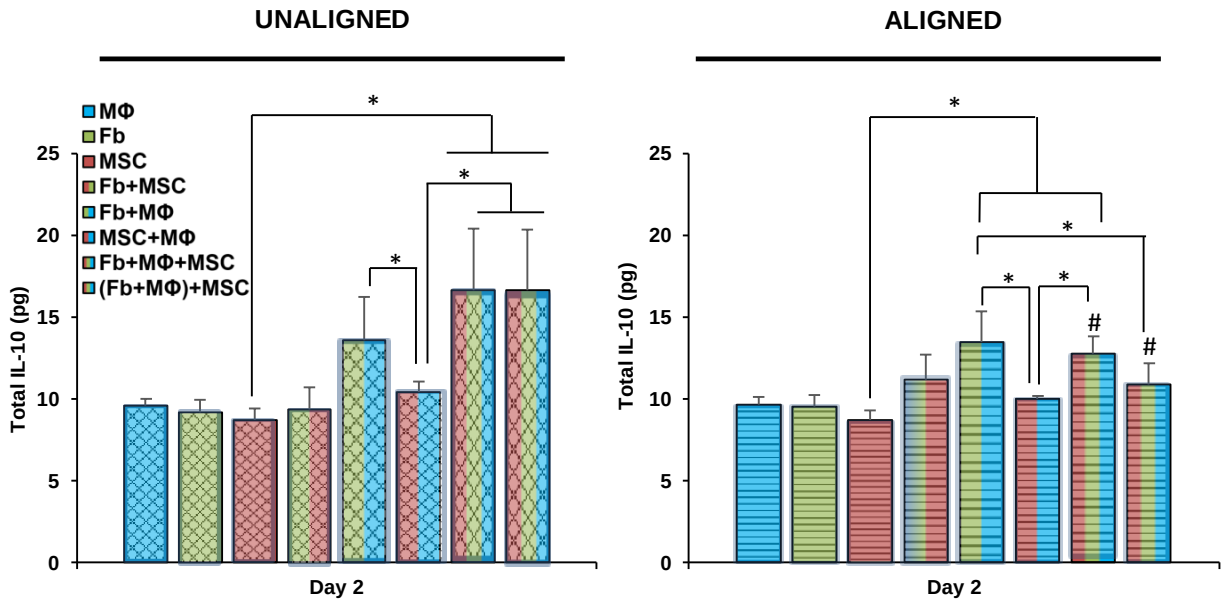

Figure 8.3: Effects of Matrix Alignment and Mechanical Properties on Heterotypic Cellular Interactions: Release of Anti-Inflammatory Cytokines. Total IL-10 release was greater in fibroblast-macrophage (Fb-MΦ) co-culture and in tri-culture compared to MSC-macrophage (MSC-MΦ) co-culture on both unaligned and aligned fibers. IL-10 secretion was lower in tri-culture and delayed tri-culture on aligned fibers compared to unaligned fibers**.** n=5, significant difference: * between groups on the same fiber orientation, # between unaligned and aligned fiber orientations (p<0.05).

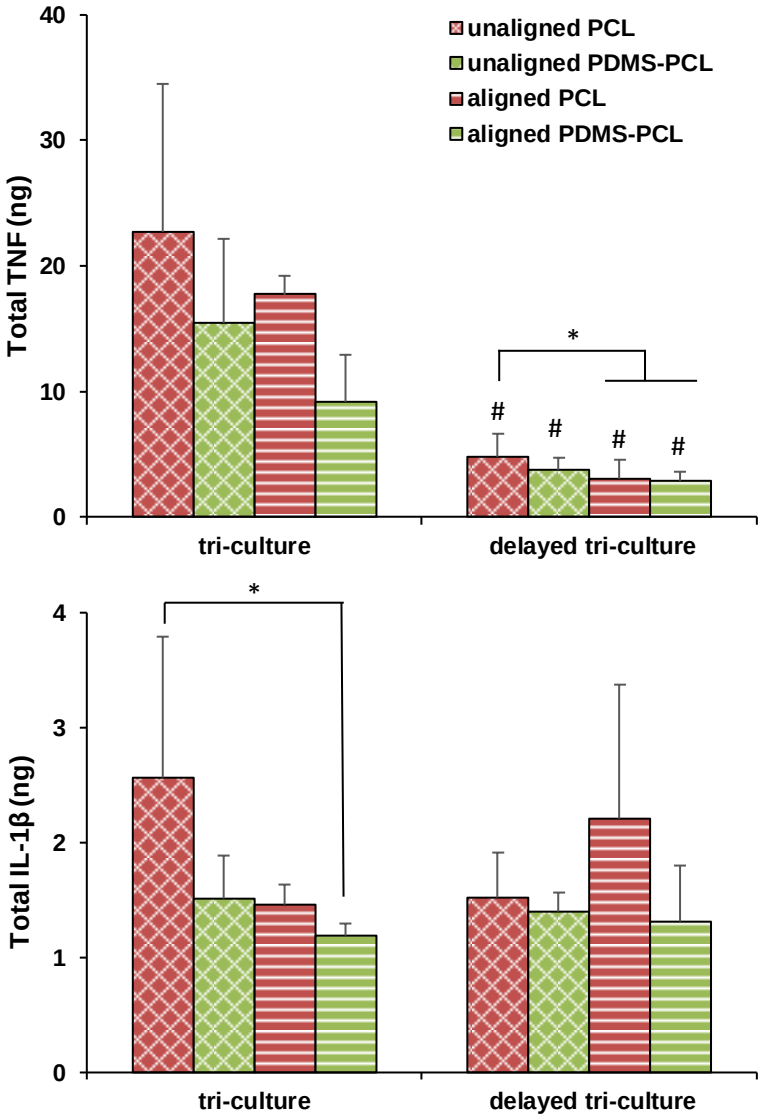

<u>Figure 8.4:</u> Effects of Matrix Alignment and Mechanical Properties on Heterotypic Cellular Interactions: Pro-Inflammatory Cytokine Release. There were no observed differences in TNF levels for any tri-culture group. TNF release was lower with delayed tri-culture than in D0 tri-culture. Total TNF was lower for delayed tri-culture on aligned PCL-only and PDMS-PCL compared to unaligned PCL-only. Total IL-1β release was greater in tri-culture on unaligned PCL-only compared to aligned PDMS-PCL, with no differences in IL-1β due to delayed tri-culture. *n*=5, significant difference: * between groups, # between tri-culture and delayed tri-culture. ($p<0.05$).

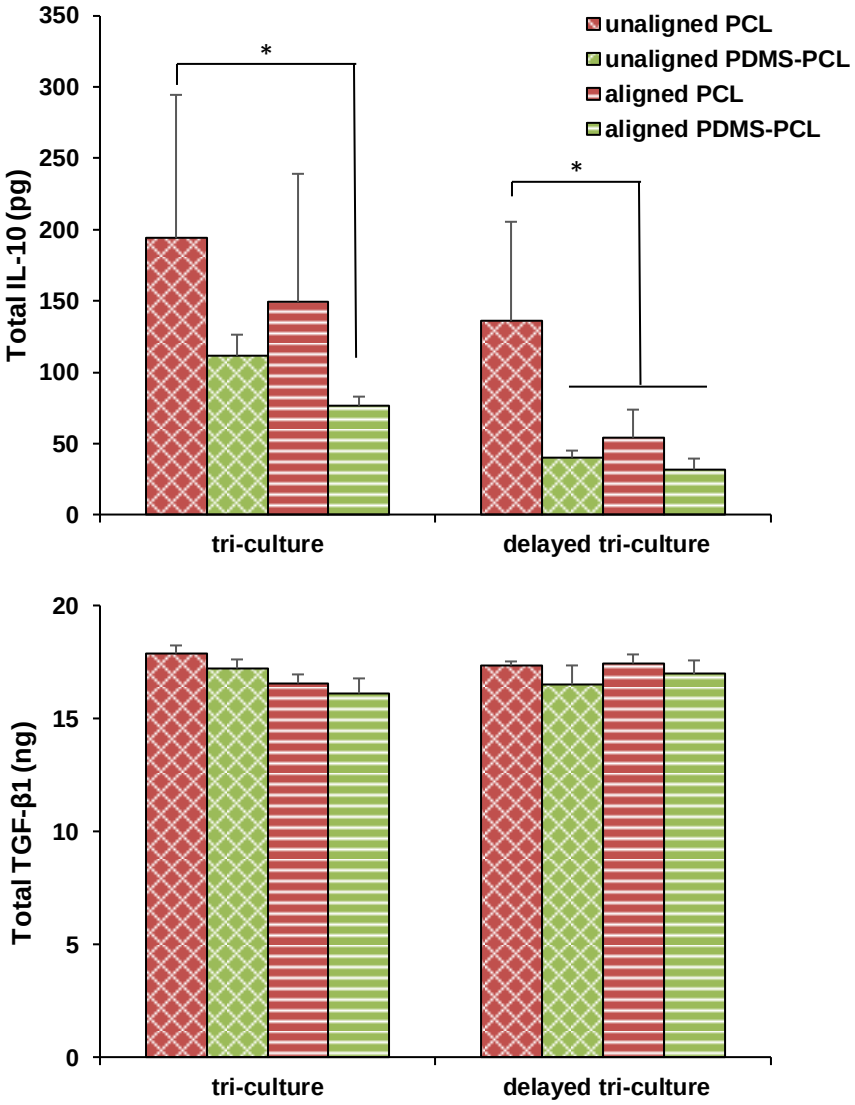

<u>Figure 8.5:</u> Effects of Matrix Alignment and Mechanical Properties on Heterotypic Cellular Interactions: Anti-Inflammatory Cytokine Release. Total IL-10 was lower for tri-culture on aligned PDMS-PCL compared to unaligned PCL-only. In delayed tri-culture, IL-10 release was greater on unaligned PCL-only meshes compared to all other groups. There were no observed differences in TGF-β1 secretion between groups, due to delayed tri-culture. n=5, significant difference: * between groups, # between tri-culture and delayed tri-culture. (p<0.05).

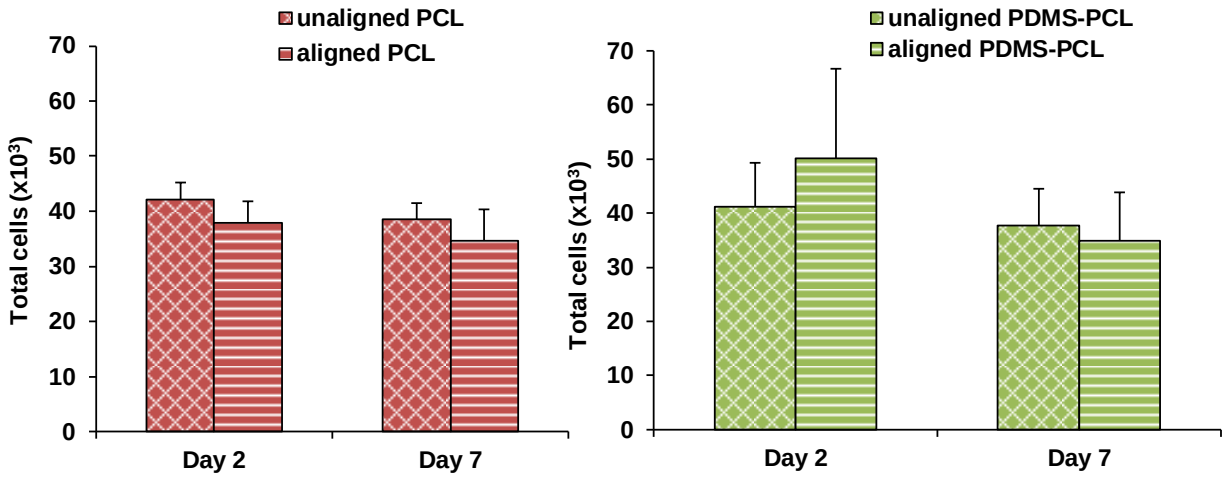

Figure 8.6: Effects of Matrix Alignment and Mechanical Properties on Heterotypic Cellular Interactions: Fibroblast Proliferation. There were no observed differences in cell number on fibroblast-seeded meshes in tri-culture over the 7-day study. n=5, significant difference: * between groups, ^ over time. (p<0.05).

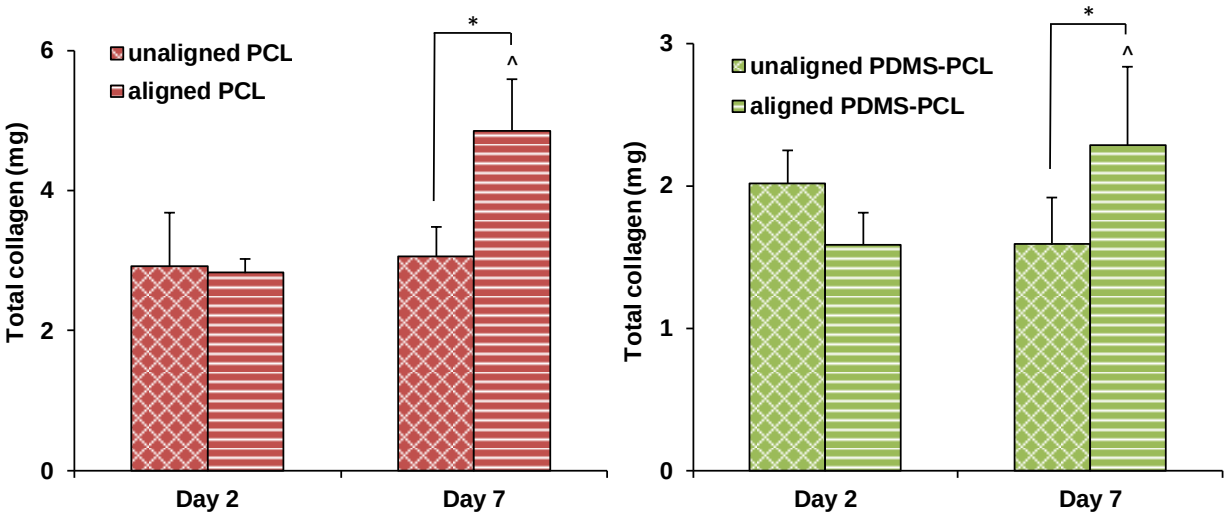

Figure 8.7: Effects of Matrix Alignment and Mechanical Properties on Heterotypic Cellular Interactions: Fibroblast Collagen Synthesis. Total collagen increased over time on aligned PCL-only and PDMS-PCL meshes only, with greater total collagen on aligned fibers compared to unaligned fibers for both PCL-only and PDMS-PCL fiber compositions. n=5, significant difference: * between groups, ^ over time (p<0.05).

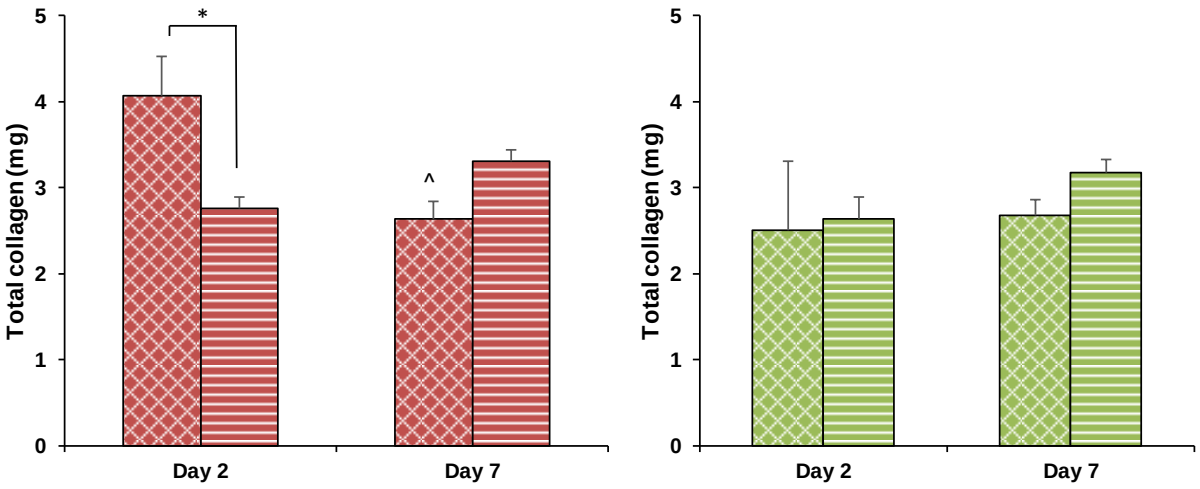

<u>Figure 8.8:</u> Effects of Matrix Alignment and Mechanical Properties on Heterotypic Cellular Interactions: Stem Cell Collagen Synthesis. Total collagen was greater on unaligned PCL-only fibers compared to aligned fibers at day 2. This difference was no longer observed by day 7. There were no differences in total collagen between MSC on unaligned and aligned PDMS-PCL . *n*=5, significant difference: * between groups, ^ over time ($p<0.05$).

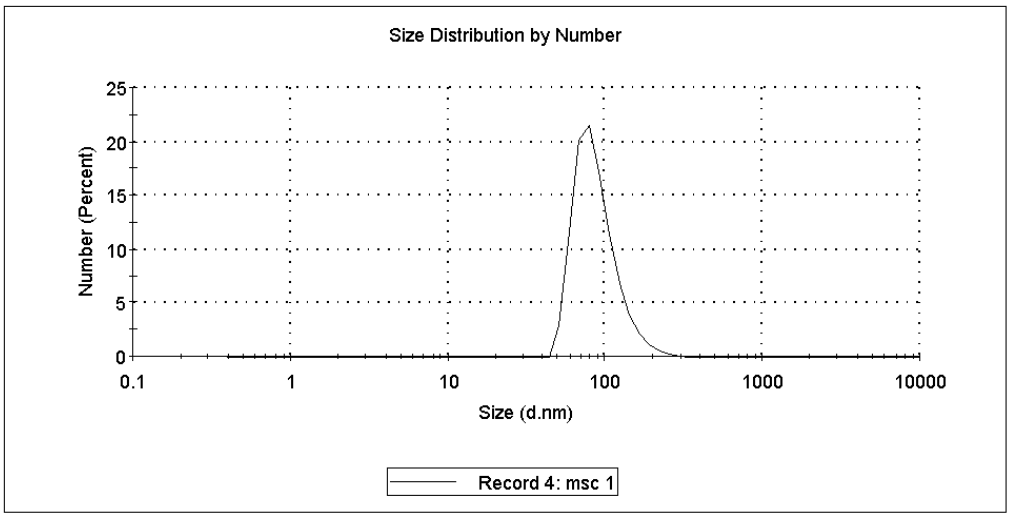

Figure 8.9: Effects of Matrix Alignment and Mechanical Properties on Heterotypic Cellular Interactions: Exosome Isolation. Particles were successfully isolated and following size distribution analysis using dynamic light scattering, the average diameter of particles was determined to be 92.62 ± 28.30 nm, suggesting exosomes can be successfully isolated. *n*=5.

CHAPTER 9: SUMMARY AND FUTURE DIRECTIONS

The objectives of this thesis were to 1) elucidate the cell-cell and cell-matrix interactions that take place following connective tissue injury and during repair and 2) determine the cellular and matrix-based cues that are critical for modulating the inflammatory response and controlling stem cell activity in order to promote stem cell-guided tissue regeneration following connective tissue injury. It was hypothesized that 1) mimicking the cell-cell communications between native tissue fibroblasts, macrophages, and stem cells following connective tissue injury would elucidate the effects of macrophage accumulation on scar tissue formation, as well as uncover the regenerative roles of stem cells during repair, and 2) matrix-based cues contribute to the inflammatory and fibrotic response following connective tissue injury, and could therefore be tuned in order to modulate the fibrotic response and promote stem cell-guided connective tissue regeneration.

To test these hypotheses, this thesis was divided into two specific aims. **Aim 1** focused on the development and optimization of a series of co- and tri-culture models for assessing the interactions between native ligament fibroblasts, infiltrating macrophage, and homed or exogenously delivered stem cells following connective tissue injury. The interactions between fibroblasts and macrophages during the early inflammatory response were first explored (*Chapter 2*), followed by determination of the role that MSC play during inflammation and the wound healing response (*Chapter 3*). In this aim, it was observed that fibroblast-macrophage interactions propagate the inflammatory response that occurs following connective tissue injury, as observed through increased macrophage activation toward pro- and anti-inflammatory phenotypes, as well as a pro-fibrotic response by fibroblasts.

Aim 2 centered on elucidating the effects of matrix alignment and mechanical properties on the response of each of these three cell types, as well as the heterotypic interactions among them, in order to design an optimal matrix for promoting stem cell-guided connective tissue regeneration. In *Chapter 4*, a series of electrospun nanofiber-based matrices were designed and optimized to assess the role of differences in matrix alignment and mechanical properties during connective tissue repair cell response. Using these matrices, the effects of matrix alignment and mechanical properties on stem cell response (*Chapter 5*), fibroblast activity (*Chapter 6*), and macrophage activation (*Chapter 7*), as well as the heterotypic interactions between all three cell types (*Chapter 8*) were analyzed. The major findings of each chapter are outlined below.

9.1 Aim 1: Role of Heterotypic Cellular Interactions in Connective Tissue Healing

Aim 1 focused on assessing the interactions between native tissue fibroblasts, infiltrating inflammatory macrophages, and homed or exogenously delivered stem cells following connective tissue injury. Specifically, a series of co- and tri-culture models were developed and utilized to assess fibroblast-macrophage interactions, fibroblast-MSC interactions, and MSC-macrophage interactions, as they related to connective tissue injury, early- and late-stage inflammation, and repair and remodeling. In *Chapter 2*, it was determined that interactions between fibroblasts and macrophages results in a heterogeneous inflammatory response by macrophages, as observed through both M1 and M2 polarization of M0 macrophages, as well as an early pro-fibrotic response by fibroblasts, resulting in enhanced proliferation and matrix synthesis. This is potentially due to a change in fibroblast phenotype following injury, as fibroblasts isolated from a healthy ACL did not have the same inflammatory effect on macrophages as fibroblasts isolated from an injured ACL.

The role of MSC in connective tissue healing was assessed in *Chapter 3*. In this chapter, it was found that MSC promote fibroblast proliferation, with the greatest increase in cell proliferation during early-stage repair. Mesenchymal stem cells were also observed to decrease collagen production by co-culture fibroblasts, while increasing their own matrix synthesis. This response may be valuable in reducing the production of scar tissue by native ligament/tendon cells, in exchange for MSC synthesis of a functional replacement matrix. Additionally, MSC modulate the immune response by decreasing macrophage polarization, resulting in release of lower total levels of both pro- and anti-inflammatory cytokines by macrophages, suggesting that M0 macrophages remain at M0. This may be through IL-10 signaling, as MSC were shown to release high levels of IL-10 in conditioned media from macrophage culture.

9.2 Aim 2: Effects of Matrix Alignment and Mechanical Properties on Cell Healing Response

Aim 2 explored the effects of matrix alignment and mechanical properties on the response of MSC, fibroblasts, and macrophages, as well as the interactions among these three cell types. In *Chapter 4*, a series of electrospun nanofiber-based matrices were fabricated and optimized to study the role of differences in matrix alignment and mechanical properties on cell response during connective tissue injury and repair. To this end, PDMS was incorporated into PCL-only nanofibers, resulting in fibers with lower mechanical properties at both the local and bulk level compared to PCL alone. PDMS-PCL and PCL-only

fibers were electrospun in aligned and unaligned fiber orientations, resulting in four distinct meshes. The local and bulk elastic moduli of PDMS-PCL blend fibers were lower than those of PCL-only meshes, with a ten- to twenty-fold lower local modulus than PCL-only fibers in both unaligned and aligned fiber orientations.

In *Chapter 5*, the effects of fiber alignment and mechanical properties on stem cell response were assessed. It was determined that, while alignment did not impact MSC proliferation, matrix synthesis, or differentiation, fibers with decreased mechanical properties (PDMS-PCL) resulted in enhanced cell proliferation while increased mechanical properties (PCL-only) caused an increase in collagen production. For fibroblasts, as analyzed in *Chapter 6*, proliferation was similarly enhanced on PDMS-PCL matrices regardless of fiber alignment, while the rate of collagen synthesis was greater on PCL-only matrices in both unaligned and aligned fiber orientations. Additionally, the rate of collagen synthesis at early time points was further enhanced on aligned fibers compared to unaligned fibers for both PCL-only and PDMS-PCL matrices.

Macrophages seeded on nanofibers showed lower attachment to all fibrous matrices compared to tissue culture plastic. Attachment was observed to decrease even further on aligned PDMS-PCL meshes compared to all other nanofiber groups. For cells which did attach, pro-inflammatory activation of M0 macrophages following attachment was mitigated on all fiber groups compared to monolayer culture, while anti-inflammatory response was upregulated for all meshes compared to macrophages on tissue culture plastic, suggesting a fibrous matrix may be a beneficial substrate for modulating the macrophage-driven inflammatory response observed following connective tissue injury, regardless of fiber organization or mechanical properties (*Chapter 7*).

The response on macrophages in co- and tri-culture in 3D on both unaligned and aligned fibers match those observed in Aim 1 in 2D. Interestingly, while it was observed for tri-culture on both unaligned and aligned fibers that the presence of MSC minimizes TNF and IL-10 release by macrophages, this effect is further enhanced on aligned fibers compared to unaligned fibers, indicating that an aligned matrix topography mimetic of healthy fibrous connective tissues(8;98) is optimal for minimizing the inflammatory response and promoting stem cell trophic signaling following connective tissue injury, while unaligned fibers mimetic of the matrix topography that is characteristic of early scar formation(8;103) results in a heightened inflammatory response by macrophages in tri-culture. Furthermore, overall secretion of both pro- and anti-

inflammatory cytokines is lowest on aligned nanofibers with a local elastic modulus ~1MPa (aligned PDMS-PCL). This is potentially because the topographical and mechanical cues provided by aligned PDMS-PCL fibers are mimetic of the fiber alignment(271;272) and local mechanical properties(272-274) observed in developing connective tissue in humans, leading to the promotion of a regenerative or healing response by cells, instead of fibrotic scar formation.

Based on these results, an aligned matrix with mechanical properties similar to those observed for connective tissue during embryonic development is optimal for promoting stem cell-guided tissue regeneration, as it promotes matrix synthesis and proliferation by both native ligament fibroblasts and homed or exogenously delivered MSC, while modulating the cellular interactions that are responsible for macrophage-driven inflammation. Additionally, macrophage attachment on these matrices is minimal compared to unaligned fibers, as well as aligned fibers with higher mechanical properties. These findings can be applied toward the development of an engineered matrix for implantation during surgical repair procedures following connective tissue injury. The optimized matrix could either be seeded with autologous stem cells prior to delivery to the injury site, or implanted as an acellular device, to modulate the response of cells during the native repair process. Specific to ACL repair, following implantation at the injury site during an ACL repair or reconstruction procedure, this matrix could minimize scar tissue formation to promote functional tissue healing, in order to minimize the potential for re-tear injuries.

9.3 Future Directions

9.3.1 Tri-Culture Models with Increasing Complexity

The 2D and 3D tri-culture models developed in this thesis are robust tools that can be used to better understand the individual response of each cell type. In this thesis, these models were utilized to determine the effects of communications with fibroblasts and/or MSC on macrophage polarization toward a pro- or anti-inflammatory phenotype, as determined by monitoring the release of pro- and anti-inflammatory cytokines. These models also allow for the assessment of other cell responses, including cell proliferation, matrix synthesis, and phenotypic changes, including stem cell differentiation. While cell response was assessed after 48 hours and 7 days in tri-culture, it is possible to use these models to monitor changes in cell-cell communications and their effects on the response of individual cell types at other time points, as well. Additionally, these models can be tuned to allow for cell-cell contact between two or more

cell types during tri-culture, offering indefinite tri-culture combinations to assess the effects of various modes of cell-cell interactions on cell response, over both short- and long-term time points. Finally, the complexity of these models can be further increased through study of the effects of timing the delivery of each cell type, to better mimic the time scale of the influx of cells during the inflammatory response following connective tissue injury. All of these adjustments may serve to further our understanding of the biology of connective tissue healing.

9.3.2 Other Immune Responses

This thesis has focused on determining the role that macrophages play in connective tissue inflammation and repair, as well as uncovering the means by which stem cells promote functional connective tissue healing following injury. Macrophages were chosen as a representative cell type of the body's native inflammatory response, as they are part of the body's first line of defense during injury, and are prevalent throughout inflammation and healing(275). It has been previously observed that macrophages are important players in tissue repair, as they are responsible not only for the clearance of debris, but also the release of signaling molecules that promote fibroblast proliferation, as well as extracellular matrix synthesis and degradation(1). Still, future work could assess the effects of stem cell delivery and the use of an artificial matrix microenvironment on the activation of other inflammatory cell types found at the injury site, including neutrophils and T cells. These cell types could be added to the current co- and tri-culture models to enhance their complexity and more accurately recapitulate the injured microenvironment observed *in vivo*, or substituted for current cell types to gain a better understanding of how stem cells interact with these immune cells. Findings from these studies may serve to uncover additional microenvironmental cues that are essential for modulating the inflammatory response and promoting MSC-driven immunomodulation following injury.

9.3.3 In Vivo *Models*

As the goal of this thesis is to design an optimal fiber-based matrix for modulating the inflammatory response and promoting stem cell-guided functional connective tissue regeneration, an animal model could be utilized to assess the impact of the nanofiber matrix, either seeded with autologous MSC to serve as a stem cell delivery vehicle or delivered as an acellular construct, on the inflammatory response *in vivo*.

Initially, matrices could be designed for subcutaneous implantation to assess host immune response over time. The model could be similar to the one used by Paul *et al*., in which matrices are implanted subcutaneously in immunocompetent rats and assessed for attachment of macrophages and other immune cells(276). Following a successful subcutaneous study, the matrix could then be evaluated in a physiologically relevant model of connective tissue injury, such as ACL injury and repair, in which the stem cell-seeded matrix could be implanted at the site following injury and surgical repair, to assess the ability of stem cells on the optimized matrix to promote healing and minimize scar tissue formation.

9.4 Innovation and Impact

In conclusion, a series of *in vitro* models have been developed and optimized for mimicking the cell-cell and cell-matrix interactions that occur following connective tissue injury, in order to uncover the role of macrophage accumulation in scar formation, as well as determine the mechanisms behind MSC trophic signaling and immunomodulation during tissue repair. Guided by the motivation to design an implantable matrix that is capable of promoting stem cell-guided tissue repair by 1) encouraging stem cell trophic signaling, 2) supporting proliferation and matrix synthesis by native tissue fibroblasts, and 3) modulating the macrophage-driven inflammatory response, this thesis emphasizes the importance of matrix topography and mechanical properties in guiding stem cell response, as well as the response of other cell types found at the injury site, and the interactions between these populations of cells. The broader implications of this work include the development of co- and tri-culture models for studying the mechanisms behind complex cellular interactions and processes, as well as demonstration of complex matrix design strategies for elucidating the interactions between biomaterial matrices and cells. These strategies provide critical insight into the events that are responsible for scar formation following connective tissue injury, as well as the environmental cues which are critical for guiding stem cell-based tissue regeneration. Findings from this thesis can be applied toward regenerative therapies for a variety of orthopaedic tissue types, as well as other fibrous tissues, including skin, cardiac tissue, and the liver.

REFERENCE LIST

(1) Kawamura S, Ying L, Kim HJ, Dynybil C, Rodeo SA. Macrophages accumulate in the early phase of tendon-bone healing. J Orthop Res 2005 Nov;23(6):1425-32.

(2) Hays PL, Kawamura S, Deng XH, Dagher E, Mithoefer K, Ying L, et al. The role of macrophages in early healing of a tendon graft in a bone tunnel. J Bone Joint Surg Am 2008 Mar;90(3):565-79.

(3) Fan H, Liu H, Toh SL, Goh JC. Enhanced differentiation of mesenchymal stem cells co-cultured with ligament fibroblasts on gelatin/silk fibroin hybrid scaffold. Biomaterials 2008 Mar;29(8):1017-27.

(4) Ryan GB, Majno G. Acute inflammation. A review. Am J Path 1977;86(1):183.

(5) Nauta AJ, Fibbe WE. Immunomodulatory properties of mesenchymal stromal cells. Blood 2007;110(10):3499-506.

(6) Kim J, Hematti P. Mesenchymal stem cell–educated macrophages: A novel type of alternatively activated macrophages. Experimental Hematology 2009;37(12):1445-53.

(7) Hukins DW, Aspden RM. Composition and properties of connective tissues. Trends Biochem Sci 1985;10(7):260-4.

(8) Frank CB. Ligament structure, physiology and function. J Musculoskelet Neuronal Interact 2004 Jun;4(2):199-201.

(9) Lo IK, Ou Y, Rattner J, Hart DA, Marchuk LL, Frank CB, et al. The cellular networks of normal ovine medial collateral and anterior cruciate ligaments are not accurately recapitulated in scar tissue. J Anat 2002;200(3):283-96.

(10) Corr DT, Hart DA. Biomechanics of scar tissue and uninjured skin. Adv Wound Care 2013;2(2):37-43.

(11) Lin VS, Lee MC, O'Neal S, McKean J, Sung KL. Ligament tissue engineering using synthetic biodegradable fiber scaffolds. Tissue Eng 1999 Oct;5(5):443-52.

(12) Riboldi SA, Sampaolesi M, Neuenschwander P, Cossu G, Mantero S. Electrospun degradable polyesterurethane membranes: potential scaffolds for skeletal muscle tissue engineering. Biomaterials 2005;26(22):4606-15.

(13) Matthews JA, Wnek GE, Simpson DG, Bowlin GL. Electrospinning of Collagen Nanofibers. Biomacromolecules 2002;3:232-8.

(14) O'Connor RS, Hao X, Shen K, Bashour K, Akimova T, Hancock WW, et al. Substrate rigidity regulates human T cell activation and proliferation. J Immunol 2012;189(3):1330-9.

(15) Palchesko RN, Zhang L, Sun Y, Feinberg AW. Development of polydimethylsiloxane substrates with tunable elastic modulus to study cell mechanobiology in muscle and nerve. PLoS ONE 2012;7(12):e51499.

(16) Wen JH, Vincent LG, Fuhrmann A, Choi YS, Hribar KC, Taylor-Weiner H, et al. Interplay of matrix stiffness and protein tethering in stem cell differentiation. Nat Mater 2014;13(10):979-87.

(17) Eroshenko N, Ramachandran R, Yadavalli VK, Rao RR. Effect of substrate stiffness on early human embryonic stem cell differentiation. J Biol Eng 2013;7(1):1.

(18) Brown XQ, Ookawa K, Wong JY. Evaluation of polydimethylsiloxane scaffolds with physiologically-relevant elastic moduli: interplay of substrate mechanics and surface chemistry effects on vascular smooth muscle cell response. Biomaterials 2005;26(16):3123-9.

(19) Zhang W, Choi DS, Nguyen YH, Chang J, Qin L. Studying cancer stem cell dynamics on PDMS surfaces for microfluidics device design. Scientific Reports 2013;3.

(20) Subramony SD, Dargis BR, Castillo M, Azeloglu EU, Tracey MS, Su A, et al. Effect of nanofiber alignment and mechanical loading on hMSC differentiation. International Symposium on Ligaments & Tendons XII. 2012. San Francisco, CA. 2-3-2012.

(21) Discher DE, Janmey P, Wang YL. Tissue cells feel and respond to the stiffness of their substrate. Science 2005 Nov 18;310(5751):1139-43.

(22) Engler AJ, Sen S, Sweeney HL, Discher DE. Matrix elasticity directs stem cell lineage specification. Cell 2006 Aug 25;126(4):677-89.

(23) Zemel A, Rehfeldt F, Brown AEX, Discher DE, Safran SA. Optimal matrix rigidity for stress-fibre polarization in stem cells. Nat Phys 2010 Jun;6(6):468-73.

(24) Moffat KL, Sun WS, Spalazzi JP, Doty SB, Levine WN, Lu HH. Nanofiber alignment in biodegradable polymer scaffold directs attachment and matrix elaboration of human rotator cuff fibroblasts. Transactions of the Orthopaedic Research Society 32, Paper #349. 2007.

(25) Saino E, Focarete ML, Gualandi C, Emanuele E, Cornaglia AI, Imbriani M, et al. Effect of electrospun fiber diameter and alignment on macrophage activation and secretion of proinflammatory cytokines and chemokines. Biomacromolecules 2011;12(5):1900-11.

(26) Caplan AI. Mesenchymal stem cells. J Orthop Res 1991 Sep;9(5):641-50.

(27) Haynesworth SE, Goshima J, Goldberg VM, Caplan AI. Characterization of cells with osteogenic potential from human marrow. Bone 1992;13(1):81-8.

(28) Prockop DJ. Marrow stromal cells as stem cells for nonhematopoietic tissues. Science 1997 Apr 4;276(5309):71-4.

(29) Pittenger MF, Mackay AM, Beck SC, Jaiswal RK, Douglas R, Mosca JD, et al. Multilineage potential of adult human mesenchymal stem cells. Science 1999 Apr 2;284(5411):143-7.

(30) Shokrgozar MA, Fattahi M, Bonakdar S, Ragerdi I, Majidi M, Haghighipour N, et al. Healing potential of mesenchymal stem cells cultured on a collagen-based scaffold for skin regeneration. Iran Biomed J 2012;16(2):68-76.

(31) Young RG, Butler DL, Weber W, Caplan AI, Gordon SL, Fink DJ. Use of mesenchymal stem cells in a collagen matrix for Achilles tendon repair. J Orthop Res 1998 Jul;16(4):406-13.

(32) S Subramony SD, Dargis BR, Castillo M, Azeloglu EU, Tracey MS, Su A, Lu HH. The guidance of stem cell differentiation by substrate alignment and mechanical stimulation. Biomaterials 2013 Mar 31;34(8):1942-53.

(33) Subramony SD, Su A, Yeager K, Lu HH. Combined effects of chemical priming and mechanical stimulation on mesenchymal stem cell differentiation on nanofiber scaffolds. J Biomech 2014 Jun 27;47(9):2189-96.

(34) Wakitani S, Saito T, Caplan AI. Myogenic cells derived from rat bone marrow mesenchymal stem cells exposed to 5-azacytidine. Muscle Nerve 1995;18(12):1417-26.

(35) Calvi LM, Adams GB, Weibrecht KW, Weber JM, Olson DP, Knight MC, et al. Osteoblastic cells regulate the haematopoietic stem cell niche. Nature 2003;425(6960):841-6.

(36) Doherty MJ, Ashton BA, Walsh S, Beresford JN, Grant ME, Canfield AE. Vascular pericytes express osteogenic potential in vitro and in vivo. J Bone Miner Res 1998;13(5):828-38.

(37) Zuk PA, Zhu M, Mizuno H, Huang J, Futrell JW, Katz AJ, et al. Multilineage cells from human adipose tissue: implications for cell-based therapies. Tissue Eng 2001 Apr;7(2):211-28.

(38) Toma JG, McKenzie IA, Bagli D, Miller FD. Isolation and characterization of multipotent skin–derived precursors from human skin. Stem Cells 2005;23(6):727-37.

(39) Bi Y, Ehirchiou D, Kilts TM, Inkson CA, Embree MC, Sonoyama W, et al. Identification of tendon stem/progenitor cells and the role of the extracellular matrix in their niche. Nat Med 2007 Oct;13(10):1219-27.

(40) Seo BM, Miura M, Gronthos S, Bartold PM, Batouli S, Brahim J, et al. Investigation of multipotent postnatal stem cells from human periodontal ligament. Lancet 2004 Jul 10;364(9429):149-55.

(41) Gronthos S, Mankani M, Brahim J, Robey PG, Shi S. Postnatal human dental pulp stem cells (DPSCs) in vitro and in vivo. Proc Natl Acad Sci U S A 2000 Dec 5;97(25):13625-30.

(42) Granero-Molto F, Weis JA, Longobardi L, Spagnoli A. Role of mesenchymal stem cells in regenerative medicine: application to bone and cartilage repair. Expert Opin Biol Ther 2008;8(3):255-68.

(43) Dominici MLBK, Le Blanc K, Mueller I, Slaper-Cortenbach I, Marini FC, Krause DS, et al. Minimal criteria for defining multipotent mesenchymal stromal cells. The International Society for Cellular Therapy position statement. Cytotherapy 2006;8(4):315-7.

(44) Simmons PJ, Torok-Storb B. Identification of stromal cell precursors in human bone marrow by a novel monoclonal antibody, STRO-1. Blood 1991 Jul 1;78(1):55-62.

(45) Kolf CM, Cho E, Tuan RS. Mesenchymal stromal cells: Biology of adult mesenchymal stem cells: regulation of niche, self-renewal and differentiation. Arthritis Res Ther 2007;9(1):1-10.

(46) Caplan AI, Dennis JE. Mesenchymal stem cells as trophic mediators. J Cell Biochem 2006 Aug 1;98(5):1076-84.

(47) Dimarino AM, Caplan AI, Bonfield TL. Mesenchymal stem cells in tissue repair. Front Immunol 2013;4:201.

(48) Le Blanc K, Ringden O. Immunobiology of human mesenchymal stem cells and future use in hematopoietic stem cell transplantation. Biol Blood Marrow Transplant 2005;11(5):321-34.

(49) Krampera M, Cosmi L, Angeli R, Pasini A, Liotta F, Andreini A, et al. Role for interferon-gamma in the immunomodulatory activity of human bone marrow mesenchymal stem cells. Stem Cells 2006;24(2):386-98.

(50) Ren G, Zhang L, Zhao X, Xu G, Zhang Y, Roberts AI, et al. Mesenchymal stem cell-mediated immunosuppression occurs via concerted action of chemokines and nitric oxide. Cell Stem Cell 2008;2(2):141-50.

(51) Ryan JM, Barry F, Murphy JM, Mahon BP. Interferon-gamma does not break, but promotes the immunosuppressive capacity of adult human mesenchymal stem cells. Clin Exp Immunol 2007;149(2):353-63.

(52) English K, Barry FP, Field-Corbett CP, Mahon BP. IFN-gamma and TNF-alpha differentially regulate immunomodulation by murine mesenchymal stem cells. Immunol Lett 2007;110(2):91-100.

(53) Lee RH, Pulin AA, Seo MJ, Kota DJ, Ylostalo J, Larson BL, et al. Intravenous hMSCs improve myocardial infarction in mice because cells embolized in lung are activated to secrete the anti-inflammatory protein TSG-6. Cell Stem Cell 2009;5(1):54-63.

(54) Di Nicola M, Carlo-Stella C, Magni M, Milanesi M, Longoni PD, Matteucci P, et al. Human bone marrow stromal cells suppress T-lymphocyte proliferation induced by cellular or nonspecific mitogenic stimuli. Blood 2002;99(10):3838-43.

(55) Le Blanc K, Tammik L, Sundberg B, Haynesworth SE, Ringden O. Mesenchymal stem cells inhibit and stimulate mixed lymphocyte cultures and mitogenic responses independently of the major histocompatibility complex. Scand J Immunol 2003;57(1):11-20.

(56) Potian JA, Aviv H, Ponzio NM, Harrison JS, Rameshwar P. Veto-like activity of mesenchymal stem cells: functional discrimination between cellular responses to alloantigens and recall antigens. J Immunol 2003;171(7):3426-34.

(57) William TT, Pendleton JD, Beyer WM, Egalka MC, Guinan EC. Suppression of allogeneic T-cell proliferation by human marrow stromal cells: implications in transplantation. Transplantation 2003;75(3):389-97.

(58) Bartholomew A, Sturgeon C, Siatskas M, Ferrer K, McIntosh K, Patil S, et al. Mesenchymal stem cells suppress lymphocyte proliferation in vitro and prolong skin graft survival in vivo. Exp Hematol 2002;30(1):42-8.

(59) Djouad F, Plence P, Bony C, Tropel P, Apparailly F, Sany J, et al. Immunosuppressive effect of mesenchymal stem cells favors tumor growth in allogeneic animals. Blood 2003;102(10):3837-44.

(60) Krampera M, Glennie S, Dyson J, Scott D, Laylor R, Simpson E, et al. Bone marrow mesenchymal stem cells inhibit the response of naive and memory antigen-specific T cells to their cognate peptide. Blood 2003;101(9):3722-9.

(61) Lui PPY, Kong SK, Lau PM, Wong YM, Lee YW, Tan C, et al. Allogeneic tendon-derived stem cells promote tendon healing and suppress immunoreactions in hosts: in vivo model. Tissue Eng Pt A 2014;20(21-22):2998-3009.

(62) Proffen BL, Haslauer CM, Harris CE, Murray MM. Mesenchymal stem cells from the retropatellar fat pad and peripheral blood stimulate ACL fibroblast migration, proliferation, and collagen gene expression. Connect Tissue Res 2013;54(1):14-21.

(63) Baraniak PR, McDevitt TC. Stem cell paracrine actions and tissue regeneration. Regenerative medicine 2010;5(1):121-43.

(64) Lange-Consiglio A, Rossi D, Tassan S, Perego R, Cremonesi F, Parolini O. Conditioned medium from horse amniotic membrane-derived multipotent progenitor cells: immunomodulatory activity in vitro and first clinical application in tendon and ligament injuries in vivo. Stem Cells Dev 2013;22(22):3015-24.

(65) Chen HS, Su YT, Chan TM, Su YJ, Syu WS, Harn HJ, et al. Human adipose-derived stem cells accelerate the restoration of tensile strength of tendon and alleviate the progression of rotator cuff injury in a rat model. Cell Transplantation 2015;24(3):509-20.

(66) Schofield R. The relationship between the spleen colony-forming cell and the haemopoietic stem cell. Blood Cells 1977;4(1-2):7-25.

(67) Li L, Xie T. Stem cell niche: structure and function. Annu Rev Cell Dev Biol 2005;21:605-31.

(68) Scadden DT. The stem-cell niche as an entity of action. Nature 2006 Jun 29;441(7097):1075-9.

(69) Tan Q, Lui PPY, Lee YW. In vivo identity of tendon stem cells and the roles of stem cells in tendon healing. Stem Cells Dev 2013;22(23):3128-40.

(70) Taichman RS, Emerson SG. Human osteoblasts support hematopoiesis through the production of granulocyte colony-stimulating factor. J Exp Med 1994;179(5):1677-82.

(71) Zhang J, Niu C, Ye L, Huang H, He X, Tong WG, et al. Identification of the haematopoietic stem cell niche and control of the niche size. Nature 2003;425(6960):836-41.

(72) Shen Q, Goderie SK, Jin L, Karanth N, Sun Y, Abramova N, et al. Endothelial cells stimulate self-renewal and expand neurogenesis of neural stem cells. Science 2004;304(5675):1338-40.

(73) Shi S, Gronthos S. Perivascular niche of postnatal mesenchymal stem cells in human bone marrow and dental pulp. J Bone Miner Res 2003;18(4):696-704.

(74) Devine SM, Bartholomew AM, Mahmud N, Nelson M, Patil S, Hardy W, et al. Mesenchymal stem cells are capable of homing to the bone marrow of non-human primates following systemic infusion. Exp Hematol 2001;29(2):244-55.

(75) Studeny M, Marini FC, Champlin RE, Zompetta C, Fidler IJ, Andreeff M. Bone marrow-derived mesenchymal stem cells as vehicles for interferon-β delivery into tumors. Cancer Res 2002;62(13):3603-8.

(76) Sole A, Spriet M, Padgett KA, Vaughan B, Galuppo LD, Borjesson DL, et al. Distribution and persistence of technetium-99 hexamethyl propylene amine oxime–labelled bone marrow–derived mesenchymal stem cells in experimentally induced tendon lesions after intratendinous injection and regional perfusion of the equine distal limb. Equine Vet J 2013;45(6):726-31.

(77) Becerra P, Valdes Vazquez MA, Dudhia J, Fiske–Jackson AR, Neves F, Hartman NG, et al. Distribution of injected technetium-labeled mesenchymal stem cells in horses with naturally occurring tendinopathy. J Orthop Res 2013;31(7):1096-102.

(78) Guest DJ, Smith MRW, Allen WR. Equine embryonic stem–like cells and mesenchymal stromal cells have different survival rates and migration patterns following their injection into damaged superficial digital flexor tendon. Equine Vet J 2010;42(7):636-42.

(79) Awad HA, Boivin GP, Dressler MR, Smith FN, Young RG, Butler DL. Repair of patellar tendon injuries using a cell-collagen composite. J Orthop Res 2003 May;21(3):420-31.

(80) Harris MT, Butler DL, Boivin GP, Florer JB, Schantz EJ, Wenstrup RJ. Mesenchymal stem cells used for rabbit tendon repair can form ectopic bone and express alkaline phosphatase activity in constructs. J Orthop Res 2004 Sep;22(5):998-1003.

(81) McNeilly CM, Banes AJ, Benjamin M, Ralphs JR. Tendon cells in vivo form a three dimensional network of cell processes linked by gap junctions. J Anat 1996 Dec;189 (Pt 3):593-600.

(82) Ralphs J, McNeilly C, Hayes A, Banes A, Benjamin M. 3D modeling of tendon cell shape in vivo by confocal microscopy cell-cell communication and the role of the gap junctions. Transactions of the Annual Meeting - Orthopaedic Research Society 1996 p. 5.

(83) Sharma P, Maffulli N. Tendon injury and tendinopathy: healing and repair. J Bone Joint Surg 2005;87(1):187-202.

(84) Lee IC, Wang JH, Lee YT, Young TH. The differentiation of mesenchymal stem cells by mechanical stress or/and co-culture system. Biochem Biophys Res Commun 2007 Jan 5;352(1):147-52.

(85) Mizuno N, Ozeki Y, Shiba H, Kajiya M, Nagahara T, Takeda K, et al. Humoral factors released from human periodontal ligament cells influence calcification and proliferation in human bone marrow mesenchymal stem cells. J Periodontol 2008;79(12):2361-70.

(86) Zhang L, Tran N, Chen HQ, Kahn CJ, Marchal S, Groubatch F, et al. Time-related changes in expression of collagen types I and III and of tenascin-C in rat bone mesenchymal stem cells under co-culture with ligament fibroblasts or uniaxial stretching. Cell Tissue Res 2008 Apr;332(1):101-9.

(87) Luo Q, Song G, Song Y, Xu B, Qin J, Shi Y. Indirect co-culture with tenocytes promotes proliferation and mRNA expression of tendon/ligament related genes in rat bone marrow mesenchymal stem cells. Cytotechnology 2009;61(1-2):1.

(88) Lovati AB, Corradetti B, Cremonesi F, Bizzaro D, Consiglio AL. Tenogenic differentiation of equine mesenchymal progenitor cells under indirect co-culture. Int J Artif Organs 2012;35(11):996-1005.

(89) Canseco JA, Kojima K, Penvose AR, Ross JD, Obokata H, Gomoll AH, et al. Effect on ligament marker expression by direct-contact co-culture of mesenchymal stem cells and anterior cruciate ligament cells. Tissue Eng Pt A 2012;18(23-24):2549-58.

(90) Kramer PR, Nares S, Kramer SF, Grogan D, Kaiser M. Mesenchymal stem cells acquire characteristics of cells in the periodontal ligament in vitro. J Dent Res 2004 Jan;83(1):27-34.

(91) Manning CN, Martel C, Sakiyama-Elbert SE, Silva MJ, Shah S, Gelberman RH, et al. Adipose-derived mesenchymal stromal cells modulate tendon fibroblast responses to macrophage-induced inflammation in vitro. Stem Cell Res Ther 2015;6(1):1.

(92) Wang IN, Bogdanowicz DR, Mitroo S, Shan J, Kala S, Lu HH. Cellular interactions regulate stem cell differentiation in tri-culture. Connect Tissue Res 2016;57(6):476-87.

(93) He P, Ng KS, Toh SL, Goh JC. In vitro ligament-bone interface regeneration using a trilineage coculture system on a hybrid silk scaffold. Biomacromolecules 2012 Sep 10;13(9):2692-703.

(94) Lee JH, Kosinski PA, Kemp DM. Contribution of human bone marrow stem cells to individual skeletal myotubes followed by myogenic gene activation. Exp Cell Res 2005;307(1):174-82.

(95) Lee JH, Kemp DM. Human adipose-derived stem cells display myogenic potential and perturbed function in hypoxic conditions. Biochem Biophys Res Commun 2006;341(3):882-8.

(96) Beier JP, Bitto FF, Lange C, Klumpp D, Arkudas A, Bleiziffer O, et al. Myogenic differentiation of mesenchymal stem cells co–cultured with primary myoblasts. Cell Biol Int 2011;35(4):397-406.

(97) Schneider PR, Buhrmann C, Mobasheri A, Matis U, Shakibaei M. Three–dimensional high–density co–culture with primary tenocytes induces tenogenic differentiation in mesenchymal stem cells. J Orthop Res 2011;29(9):1351-60.

(98) Kannus P. Structure of the tendon connective tissue. Scand J Med Sci Sports 2000 Dec;10(6):312-20.

(99) Frank C, Woo SL, Amiel D, Harwood F, Gomez M, Akeson W. Medial collateral ligament healing. A multidisciplinary assessment in rabbits. Am J Sports Med 1983 Nov;11(6):379-89.

(100) Amiel D, Frank CB, Harwood FL, Akeson WH, Kleiner JB. Collagen alteration in medial collateral ligament healing in a rabbit model. Connect Tissue Res 1987;16(4):357-66.

(101) Liu SH, Yang RS, al-Shaikh R, Lane JM. Collagen in tendon, ligament, and bone healing. A current review. Clin Orthop Relat Res 1995 Sep;(318):265-78.

(102) Woo SL, Hildebrand K, Watanabe N, Fenwick JA, Papageorgiou CD, Wang JH. Tissue engineering of ligament and tendon healing. Clin Orthop Relat Res 1999 Oct;(367 Suppl):S312-S323.

(103) Shrive N, Chimich D, Marchuk L, Wilson J, Brant R, Frank C. Soft-tissue "flaws" are associated with the material properties of the healing rabbit medial collateral ligament. J Orthop Res 1995 Nov;13(6):923-9.

(104) Corr DT, Hart DA. Biomechanics of scar tissue and uninjured skin. Adv Wound Care 2013;2(2):37-43.

(105) Vunjak-Novakovic G, Altman G, Horan R, Kaplan DL. Tissue engineering of ligaments. Annu Rev Biomed Eng 2004;6:131-56.

(106) Laurencin CT, Freeman JW. Ligament tissue engineering: an evolutionary materials science approach. Biomaterials 2005;26(36):7530-6.

(107) Yang PJ, Temenoff JS. Engineering orthopedic tissue interfaces. Tissue Eng Pt B Rev 2009 Jun;15(2):127-41.

(108) Altman GH, Diaz F, Jakuba C, Calabro T, Horan RL, Chen J, et al. Silk-based biomaterials. Biomaterials 2003 Feb;24(3):401-16.

(109) Altman GH, Horan RL, Lu HH, Moreau J, Martin I, Richmond JC, et al. Silk matrix for tissue engineered anterior cruciate ligaments. Biomaterials 2002 Oct;23(20):4131-41.

(110) Murugan R, Ramakrishna S. Design strategies of tissue engineering scaffolds with controlled fiber orientation. Tissue Eng 2007 Aug;13(8):1845-66.

(111) Pham QP, Sharma U, Mikos AG. Electrospun poly(epsilon-caprolactone) microfiber and multilayer nanofiber/microfiber scaffolds: characterization of scaffolds and measurement of cellular infiltration. Biomacromolecules 2006 Oct;7(10):2796-805.

(112) Czaplewski SK, Tsai TL, Duenwald-Kuehl SE, Vanderby R, Li WJ. Tenogenic differentiation of human induced pluripotent stem cell-derived mesenchymal stem cells dictated by properties of braided submicron fibrous scaffolds. Biomaterials 2014;35(25):6907-17.

(113) Yin Z, Chen X, Chen JL, Shen WL, Hieu Nguyen TM, Gao L, et al. The regulation of tendon stem cell differentiation by the alignment of nanofibers. Biomaterials 2010 Mar;31(8):2163-75.

(114) Engler AJ, Griffin MA, Sen S, Bonnemann CG, Sweeney HL, Discher DE. Myotubes differentiate optimally on substrates with tissue-like stiffness pathological implications for soft or stiff microenvironments. J Cell Biol 2004;166(6):877-87.

(115) Winer JP, Janmey PA, McCormick ME, Funaki M. Bone marrow-derived human mesenchymal stem cells become quiescent on soft substrates but remain responsive to chemical or mechanical stimuli. Tissue Eng Pt A 2008;15(1):147-54.

(116) Sharma RI, Snedeker JG. Biochemical and biomechanical gradients for directed bone marrow stromal cell differentiation toward tendon and bone. Biomaterials 2010;31(30):7695-704.

(117) Rehmann MS, Luna JI, Maverakis E, Kloxin AM. Tuning microenvironment modulus and biochemical composition promotes human mesenchymal stem cell tenogenic differentiation. J Biomed Mater Res A 2016.

(118) Xu B, Song G, Ju Y, Li X, Song Y, Watanabe S. RhoA/ROCK, cytoskeletal dynamics, and focal adhesion kinase are required for mechanical stretch-induced tenogenic differentiation of human mesenchymal stem cells. J Cell Physiol 2012;227(6):2722-9.

(119) Discher DE, Mooney DJ, Zandstra PW. Growth factors, matrices, and forces combine and control stem cells. Science 2009;324(5935):1673-7.

(120) Watt FM, Fujiwara H. Cell-extracellular matrix interactions in normal and diseased skin. CSH Perspect Biol 2011;3(4):a005124.

(121) Tang SW, Tong WY, Shen W, Yeung KW, Lam YW. Stringent requirement for spatial arrangement of extracellular matrix in supporting cell morphogenesis and differentiation. BMC Cell Biol 2014;15(1):10.

(122) Zhang C, Yuan H, Liu H, Chen X, Lu P, Zhu T, et al. Well-aligned chitosan-based ultrafine fibers committed teno-lineage differentiation of human induced pluripotent stem cells for Achilles tendon regeneration. Biomaterials 2015;53:716-30.

(123) Popielarczyk TL, Nain AS, Barrett JG. Aligned Nanofiber Topography Directs the Tenogenic Differentiation of Mesenchymal Stem Cells. Applied Sciences 2017;7(1):59.

(124) Cardwell RD, Dahlgren LA, Goldstein AS. Electrospun fibre diameter, not alignment, affects mesenchymal stem cell differentiation into the tendon/ligament lineage. J Tissue Eng and Regen Med 2014;8(12):937-45.

(125) Molloy T, Wang Y, Murrell G. The roles of growth factors in tendon and ligament healing. Sports Med 2003;33(5):381-94.

(126) Hankemeier S, Keus M, Zeichen J, Jagodzinski M, Barkhausen T, Bosch U, et al. Modulation of proliferation and differentiation of human bone marrow stromal cells by fibroblast growth factor 2: potential implications for tissue engineering of tendons and ligaments. Tissue Eng 2005 Jan;11(1-2):41-9.

(127) Sahoo S, Toh SL, Goh JC. A bFGF-releasing silk/PLGA-based biohybrid scaffold for ligament/tendon tissue engineering using mesenchymal progenitor cells. Biomaterials 2010 Apr;31(11):2990-8.

(128) Chang J, Thunder R, Most D, Longaker MT, Lineaweaver WC. Studies in flexor tendon wound healing: neutralizing antibody to TGF-B1 increases postoperative range of motion. Plast Reconstr Surg-Baltimore 2000;105(1):148-55.

(129) Holladay C, Abbah S, O'Dowd C, Pandit A, Zeugolis DI. Preferential tendon stem cell response to growth factor supplementation. J Tissue Eng and Regen Med 2016;10(9):783-98.

(130) Jenner JM, Van EF, Saris DB, Willems WJ, Dhert WJ, Creemers LB. Effect of transforming growth factor-beta and growth differentiation factor-5 on proliferation and matrix production by human bone marrow stromal cells cultured on braided poly lactic-co-glycolic acid scaffolds for ligament tissue engineering. Tissue Eng 2007 Jul;13(7):1573-82.

(131) Lou J, Tu Y, Burns M, Silva M, Manske P. BMP-12 gene transfer augmentation of lacerated tendon repair. J Orthop Res 2001;19(6):1199-202.

(132) Wang QW, Chen ZL, Piao YJ. Mesenchymal stem cells differentiate into tenocytes by bone morphogenetic protein (BMP) 12 gene transfer. J Biosci Bioeng 2005;100(4):418-22.

(133) Violini S, Ramelli P, Pisani LF, Gorni C, Mariani P. Horse bone marrow mesenchymal stem cells express embryo stem cell markers and show the ability for tenogenic differentiation by in vitro exposure to BMP-12. BMC Cell Biol 2009;10(1):29.

(134) Mohanty N, Gulati BR, Kumar R, Gera S, Kumar P, Somasundaram RK, et al. Immunophenotypic characterization and tenogenic differentiation of mesenchymal stromal cells isolated from equine umbilical cord blood. In Vitro Cell Dev Biol Anim 2014;50(6):538-48.

(135) Lee JY, Zhou Z, Taub PJ, Ramcharan M, Li Y, Akinbiyi T, et al. BMP-12 treatment of adult mesenchymal stem cells in vitro augments tendon-like tissue formation and defect repair in vivo. PLoS ONE 2011;6(3):e17531.

(136) Bottagisio M, Lopa S, Granata V, Talo G, Bazzocchi C, Moretti M, et al. Different combinations of growth factors for the tenogenic differentiation of bone marrow mesenchymal stem cells in monolayer culture and in fibrin-based three-dimensional constructs. Differentiation 2017;95:44-53.

(137) Wolfman NM, Hattersley G, Cox K, Celeste AJ, Nelson R, Yamaji N, et al. Ectopic induction of tendon and ligament in rats by growth and differentiation factors 5, 6, and 7, members of the TGF-beta gene family. J Clin Invest 1997 Jul 15;100(2):321-30.

(138) Park A, Hogan MV, Kesturu GS, James R, Balian G, Chhabra AB. Adipose-derived mesenchymal stem cells treated with growth differentiation factor-5 express tendon-specific markers. Tissue Eng Pt A 2010;16(9):2941-51.

(139) Rubini M, Werner H, Gandini E, Roberts CT, LeRoith D, Baserga R. Platelet-derived growth factor increases the activity of the promoter of the insulin-like growth factor-1 (IGF-1) receptor gene. Exp Cell Res 1994;211(2):374-9.

(140) Steenfos H. Insulin-like growth factor I has a major role in wound healing. InSurg Forum 1989 (pp. 68-71).

(141) Kurtz CA, Loebig TG, Anderson DD, DeMeo PJ, Campbell PG. Insulin-like growth factor I accelerates functional recovery from Achilles tendon injury in a rat model. Am J Sports Med 1999;27(3):363-9.

(142) Lynch SE, Colvin RB, Antoniades HN. Growth factors in wound healing. Single and synergistic effects on partial thickness porcine skin wounds. J Clin Invest 1989;84(2):640.

(143) Duffy FJ, Seiler JG, Gelberman RH, Hergrueter CA. Growth factors and canine flexor tendon healing: initial studies in uninjured and repair models. J Hand Surg Am 1995;20(4):645-9.

(144) Cheng X, Tsao C, Sylvia VL, Cornet D, Nicolella DP, Bredbenner TL, et al. Platelet-derived growth-factor-releasing aligned collagen-nanoparticle fibers promote the proliferation and tenogenic differentiation of adipose-derived stem cells. Acta Biomater 2014;10(3):1360-9.

(145) Zhang J, Keenan C, Wang JH. The effects of dexamethasone on human patellar tendon stem cells: implications for dexamethasone treatment of tendon injury. J Orthop Res 2013;31(1):105-10.

(146) Reed SA, Johnson SE. Expression of scleraxis and tenascin C in equine adipose and umbilical cord blood derived stem cells is dependent upon substrata and FGF supplementation. Cytotechnology 2014;66(1):27-35.

(147) Moreau JE, Chen J, Horan RL, Kaplan DL, Altman GH. Sequential growth factor application in bone marrow stromal cell ligament engineering. Tissue Eng 2005;11(11-12):1887-97.

(148) James R, Kumbar SG, Laurencin CT, Balian G, Chhabra AB. Tendon tissue engineering: adipose-derived stem cell and GDF-5 mediated regeneration using electrospun matrix systems. Biomed Mater 2011 Apr;6(2):025011.

(149) Butler DL, Goldstein SA, Guilak F. Functional tissue engineering: the role of biomechanics. J Biomech Eng 2000 Dec;122(6):570-5.

(150) Wang JH. Mechanobiology of tendon. J Biomech 2006;39(9):1563-82.

(151) Komi PV, Fukashiro S, Jarvinen M. Biomechanical loading of Achilles tendon during normal locomotion. Clin Sports Med 1992 Jul;11(3):521-31.

(152) Awad HA, Butler DL, Harris MT, Ibrahim RE, Wu Y, Young RG, et al. In vitro characterization of mesenchymal stem cell-seeded collagen scaffolds for tendon repair: Effects of initial seeding density on contraction kinetics. J Biomed Mater Res 2000 Aug;51(2):233-40.

(153) Van Eijk F, Saris DB, Creemers LB, Riesle J, Willems WJ, Van Blitterswijk CA, Verbout AJ, Dhert WJ. The effect of timing of mechanical stimulation on proliferation and differentiation of goat bone marrow stem cells cultured on braided PLGA scaffolds. Tissue Eng Pt A 2008 Aug 1;14(8):1425-33.

(154) Song G, Luo Q, Xu B, Ju Y. Mechanical stretch-induced changes in cell morphology and mRNA expression of tendon/ligament-associated genes in rat bone-marrow mesenchymal stem cells. MCB 2010;7(3):165-74.

(155) Morita Y, Watanabe S, Ju Y, Xu B. Determination of optimal cyclic uniaxial stretches for stem cell-to-tenocyte differentiation under a wide range of mechanical stretch conditions by evaluating gene expression and protein synthesis levels. Acta Bioeng Biomech 2013;15(3).

(156) Zhang J, Wang JH. Mechanobiological response of tendon stem cells: implications of tendon homeostasis and pathogenesis of tendinopathy. J Orthop Res 2010;28(5):639-43.

(157) Juncosa-Melvin N, Shearn JT, Boivin GP, Gooch C, Galloway MT, West JR, et al. Effects of mechanical stimulation on the biomechanics and histology of stem cell-collagen sponge constructs for rabbit patellar tendon repair. Tissue Eng 2006 Aug;12(8):2291-300.

(158) Juncosa-Melvin N, Matlin KS, Holdcraft RW, Nirmalanandhan VS, Butler DL. Mechanical stimulation increases collagen type I and collagen type III gene expression of stem cell-collagen sponge constructs for patellar tendon repair. Tissue Eng 2007 Jun;13(6):1219-26.

(159) Altman GH, Horan RL, Martin I, Farhadi J, Stark PR, Volloch V, et al. Cell differentiation by mechanical stress. FASEB J 2002 Feb;16(2):270-2.

(160) Kawasaki T, Sumita Y, Egashira K, Ohba S, Kagami H, Tran SD, et al. Transient Exposure to Hypoxic and Anoxic Oxygen Concentrations Promotes Either Osteogenic or Ligamentogenic Characteristics of PDL Cells. BioResearch open access 2015;4(1):175-87.

(161) Noth U, Schupp K, Heymer A, Kall S, Jakob F, Schutze N, et al. Anterior cruciate ligament constructs fabricated from human mesenchymal stem cells in a collagen type I hydrogel. Cytotherapy 2005;7(5):447-55.

(162) Butler DL, Juncosa-Melvin N, Boivin GP, Galloway MT, Shearn JT, Gooch C, et al. Functional tissue engineering for tendon repair: A multidisciplinary strategy using mesenchymal stem cells, bioscaffolds, and mechanical stimulation. J Orthop Res 2007 Aug 3.

(163) Shearn JT, Juncosa-Melvin N, Boivin GP, Galloway MT, Goodwin W, Gooch C, Dunn MG, Butler DL. Mechanical stimulation of tendon tissue engineered constructs: effects on construct stiffness, repair biomechanics, and their correlation. J Biomech Eng. 2007 Dec 1;129(6):848-54.

(164) Chen YJ, Huang CH, Lee IC, Lee YT, Chen MH, Young TH. Effects of cyclic mechanical stretching on the mRNA expression of tendon/ligament-related and osteoblast-specific genes in human mesenchymal stem cells. Connect Tissue Res 2008;49(1):7-14.

(165) Kuo CK, Tuan RS. Mechanoactive tenogenic differentiation of human mesenchymal stem cells. Tissue Eng Pt A 2008 Oct;14(10):1615-27.

(166) Zhang L, Kahn CJ, Chen HQ, Tran N, Wang X. Effect of uniaxial stretching on rat bone mesenchymal stem cell: Orientation and expressions of collagen types I and III and tenascin-C. Cell Biol Int 2008;32(3):344-52.

(167) Nirmalanandhan VS, Shearn JT, Juncosa-Melvin N, Rao M, Gooch C, Jain A, et al. Improving linear stiffness of the cell-seeded collagen sponge constructs by varying the components of the mechanical stimulus. Tissue Eng Pt A 2008;14(11).

(168) Nirmalanandhan VS, Juncosa-Melvin N, Shearn JT, Boivin GP, Galloway MT, Gooch C, et al. Combined effects of scaffold stiffening and mechanical preconditioning cycles on construct biomechanics, gene expression, and tendon repair biomechanics. Tissue Eng Pt A 2009 Aug;15(8):2103-11.

(169) Abousleiman RI, Reyes Y, McFetridge P, Sikavitsas V. Tendon tissue engineering using cell-seeded umbilical veins cultured in a mechanical stimulator. Tissue Eng Pt A 2009 Apr;15(4):787-95.

(170) Chokalingam K, Juncosa-Melvin N, Hunter SA, Gooch C, Frede C, Florert J, et al. Tensile stimulation of murine stem cell-collagen sponge constructs increases collagen type I gene expression and linear stiffness. Tissue Eng Pt A 2009 Sep;15(9):2561-70.

(171) Doroski DM, Levenston ME, Temenoff JS. Cyclic tensile culture promotes fibroblastic differentiation of marrow stromal cells encapsulated in poly (ethylene glycol)-based hydrogels. Tissue Eng Pt A 2010 Jul 23;16(11):3457-66.

(172) Thomopoulos S, Das R, Birman V, Smith L, Ku K, Elson EL, et al. Fibrocartilage tissue engineering: the role of the stress environment on cell morphology and matrix expression. Tissue Eng Pt A 2011 Apr;17(7-8):1039-53.

(173) Doroski DM, Levenston ME, Temenoff JS. Cyclic tensile culture promotes fibroblastic differentiation of marrow stromal cells encapsulated in poly (ethylene glycol)-based hydrogels. Tissue Eng A. 2010 Jul 23;16(11):3457-66.

(174) Kreja L, Liedert A, Schlenker H, Brenner RE, Fiedler J, Friemert B, et al. Effects of mechanical strain on human mesenchymal stem cells and ligament fibroblasts in a textured poly (L-lactide) scaffold for ligament tissue engineering. J Mater Sci Mater Med 2012;23(10):2575-82.

(175) Xu B, Song G, Ju Y. Effect of focal adhesion kinase on the regulation of realignment and tenogenic differentiation of human mesenchymal stem cells by mechanical stretch. Connect Tissue Res 2011;52(5):373-9.

(176) Zhang J, Wang JH. The effects of mechanical loading on tendons-an in vivo and in vitro model study. PLoS ONE 2013;8(8):e71740.

(177) Xu Y, Dong S, Zhou Q, Mo X, Song L, Hou T, et al. The effect of mechanical stimulation on the maturation of TDSCs-poly(L-lactide-co-e-caprolactone)/collagen scaffold constructs for tendon tissue engineering. Biomaterials 2014 Mar;35(9):2760-72.

(178) Chen J, Horan RL, Bramono D, Moreau JE, Wang Y, Geuss LR, et al. Monitoring mesenchymal stromal cell developmental stage to apply on-time mechanical stimulation for ligament tissue engineering. Tissue Eng 2006 Nov;12(11):3085-95.

(179) Nirmalanandhan VS, Dressler MR, Shearn JT, Juncosa-Melvin N, Rao M, Gooch C, Bradica G, Butler DL. Mechanical stimulation of tissue engineered tendon constructs: effect of scaffold materials. J Biomech Eng 2007 Dec 1;129(6):919-23.

(180) Petrigliano FA, English CS, Barba D, Esmende S, Wu BM, Mcallister DR. The effects of local bFGF release and uniaxial strain on cellular adaptation and gene expression in a 3D environment: implications for ligament tissue engineering. Tissue Eng 2007 Nov 1;13(11):2721-31.

(181) Moreau JE, Bramono DS, Horan RL, Kaplan DL, Altman GH. Sequential biochemical and mechanical stimulation in the development of tissue-engineered ligaments. Tissue Eng Pt A 2008 Jul;14(7):1161-72.

(182) Raabe O, Shell K, Fietz D, Freitag C, Ohrndorf A, Christ HJ, et al. Tenogenic differentiation of equine adipose-tissue-derived stem cells under the influence of tensile strain, growth differentiation factors and various oxygen tensions. Cell Tissue Res 2013;352(3):509-21.

(183) Nirmalanandhan VS, Rao M, Shearn JT, Juncosa-Melvin N, Gooch C, Butler DL. Effect of scaffold material, construct length and mechanical stimulation on the in vitro stiffness of the engineered tendon construct. J Biomech 2008 Dec 31;41(4):822-8.

(184) Rowlands AS, George PA, Cooper-White JJ. Directing osteogenic and myogenic differentiation of MSCs: interplay of stiffness and adhesive ligand presentation. Am J Physiol-Cell Ph 2008;295(4):C1037-C1044.

(185) Farng E, Urdaneta AR, Barba D, Esmende S, McAllister DR. The effects of GDF-5 and uniaxial strain on mesenchymal stem cells in 3-D culture. Clin Orthop Relat Res 2008 Aug 1;466(8):1930-7.

(186) Kishore V, Bullock W, Sun X, Van Dyke WS, Akkus O. Tenogenic differentiation of human MSCs induced by the topography of electrochemically aligned collagen threads. Biomaterials 2012 Mar;33(7):2137-44.

(187) Banks JM, Mozdzen LC, Harley BA, Bailey RC. The combined effects of matrix stiffness and growth factor immobilization on the bioactivity and differentiation capabilities of adipose-derived stem cells. Biomaterials 2014;35(32):8951-9.

(188) Durant TJS, Dyment N, McCarthy MB, Cote MP, Arciero RA, Mazzocca AD, et al. Mesenchymal stem cell response to growth factor treatment and low oxygen tension in 3-dimensional construct environment. Muscles Ligaments Tendons J 2014;4(1):46.

(189) Stroncek JD, Reichert WM. Overview of wound healing in different tissue types. Indwelling neural implants: strategies for contending with the in vivo environment. 2008:3-40.

(190) Tsuchiya S, Yamabe M, Yamaguchi Y, Kobayashi Y, Konno T, Tada K. Establishment and characterization of a human acute monocytic leukemia cell line (THP-1). Int J Cancer 1980 Aug;26(2):171-6.

(191) Daigneault M, Preston JA, Marriott HM, Whyte MK, Dockrell DH. The identification of markers of macrophage differentiation in PMA-stimulated THP-1 cells and monocyte-derived macrophages. PLoS One 2010;5(1):e8668.

(192) Gordon S, Taylor PR. Monocyte and macrophage heterogeneity. Nat Rev Immunol 2005 Dec;5(12):953-64.

(193) Alfaro-Moreno E, Nawrot TS, Vanaudenaerde BM, Hoylaerts MF, Vanoirbeek JA, Nemery B, et al. Co-cultures of multiple cell types mimic pulmonary cell communication in response to urban PM10. Eur Respir J 2008 Nov;32(5):1184-94.

(194) Klegeris A, Walker DG, McGeer PL. Regulation of glutamate in cultures of human monocytic THP-1 and astrocytoma U-373 MG cells. J Neuroimmunol 1997 Sep;78(1-2):152-61.

(195) Saad B, Matter S, Ciardelli G, Uhlschmid GK, Welti M, Neuenschwander P, et al. Interactions of osteoblasts and macrophages with biodegradable and highly porous polyesterurethane foam and its degradation products. J Biomed Mater Res 1996 Nov;32(3):355-66.

(196) Freytes DO, Kang JW, Marcos-Campos I, Vunjak-Novakovic G. Macrophages modulate the viability and growth of human mesenchymal stem cells. J Cell Biochem 2013 Jan;114(1):220-9.

(197) Fronza M, Heinzmann B, Hamburger M, Laufer S, Merfort I. Determination of the wound healing effect of Calendula extracts using the scratch assay with 3T3 fibroblasts. J Ethnopharmacol 2009;126(3):463-7.

(198) Walter MNM, Wright KT, Fuller HR, MacNeil S, Johnson WE. Mesenchymal stem cell-conditioned medium accelerates skin wound healing: an in vitro study of fibroblast and keratinocyte scratch assays. Exper Cell Res 10;316(7):1271-81.

(199) Reddy GK, Enwemeka CS. A simplified method for the analysis of hydroxyproline in biological tissues. Clin Biochem 1996 Jun;29(3):225-9.

(200) Hildebrand KA, Frank CB. Scar formation and ligament healing. Can J Surg 1998;41(6):425.

(201) Fine A, Goldstein RH. The effect of transforming growth factor-beta on cell proliferation and collagen formation by lung fibroblasts. J Biol Chem 1987;262(8):3897-902.

(202) Tardif F, Ross G, Rouabhia M. Gingival and dermal fibroblasts produce interleukin-1beta converting enzyme and interleukin-1beta but not interleukin-18 even after stimulation with lipopolysaccharide. J Cell Physiol 2004;198(1):125-32.

(203) Sugarman BJ, Aggarwal BB, Hass PE, Figari IS, Palladino MA, Shepard HM. Recombinant human tumor necrosis factor-alpha: effects on proliferation of normal and transformed cells in vitro. Science 1985;230(4728):943-5.

(204) Battegay EJ, Raines EW, Colbert T, Ross R. TNF-alpha stimulation of fibroblast proliferation. Dependence on platelet-derived growth factor (PDGF) secretion and alteration of PDGF receptor expression. J Immunol 1995;154(11):6040-7.

(205) Postlethwaite AE, Raghow R, Stricklin GP, Poppleton H, Seyer JM, Kang AH. Modulation of fibroblast functions by interleukin 1: increased steady-state accumulation of type I procollagen messenger RNAs and stimulation of other functions but not chemotaxis by human recombinant interleukin 1 alpha and beta. J Cell Biol 1988;106(2):311-8.

(206) Glowacka E, Lewkowicz P, Rotsztejn H, Zalewska A. IL-8, IL-12 and IL-10 cytokines generation by neutrophils, fibroblasts and neutrophils-fibroblasts interaction in psoriasis. Adv Med Sci 2010;55(2):254-60.

(207) Clegg PD, Strassburg S, Smith RK. Cell phenotypic variation in normal and damaged tendons. Int J Exp Pathol 2007;88(4):227-35.

(208) Gotoh M, Hamada K, Yamakawa H, Tomonaga A, Inoue A, Fukuda H. Significance of granulation tissue in torn supraspinatus insertions: An immunohistochemical study with antibodies against interleukin-1beta, cathepsin D, and matrix metalloprotease-1. J Orthop Res 1997;15(1):33-9.

(209) Menke NB, Ward KR, Witten TM, Bonchev DG, Diegelmann RF. Impaired wound healing. Clin Dermatol 2007;25(1):19-25.

(210) Manning CN, Martel C, Sakiyama-Elbert SE, Silva MJ, Shah S, Gelberman RH, et al. Adipose-derived mesenchymal stromal cells modulate tendon fibroblast responses to macrophage-induced inflammation in vitro. Stem Cell Res Ther 2015;6(1):1.

(211) Schnoor M, Cullen P, Lorkowski J, Stolle K, Robenek H, Troyer D, et al. Production of type VI collagen by human macrophages: a new dimension in macrophage functional heterogeneity. J Immunol 2008;180(8):5707-19.

(212) Choi J-J, Yoo S–A, Park S–J, Kang Y–J, Kim W–U, Oh I–H, et al. Mesenchymal stem cells overexpressing interleukin–10 attenuate collagen–induced arthritis in mice. Clin Exp Immunol 2008;153(2):269-76.

(213) Qu X, Liu X, Cheng K, Yang R, Zhao RC. Mesenchymal stem cells inhibit Th17 cell differentiation by IL-10 secretion. Exper Hematol 2012;40(9):761-70.

(214) Schofer MD, Roessler PP, Schaefer J, Theisen C, Schlimme S, Heverhagen JT, et al. Electrospun PLLA nanofiber scaffolds and their use in combination with BMP-2 for reconstruction of bone defects. PLoS ONE 2011;6(9):e25462.

(215) Seyedjafari E, Soleimani M, Ghaemi N, Shabani I. Nanohydroxyapatite-coated electrospun poly (l-lactide) nanofibers enhance osteogenic differentiation of stem cells and induce ectopic bone formation. Biomacromolecules 2010;11(11):3118-25.

(216) Aviss KJ, Gough JE, Downes S. Aligned electrospun polymer fibres for skeletal muscle regeneration. Eur Cell Mater 2010;19:193-204.

(217) Bashur CA, Dahlgren LA, Goldstein AS. Effect of fiber diameter and orientation on fibroblast morphology and proliferation on electrospun poly(D,L-lactic-co-glycolic acid) meshes. Biomaterials 2006 Nov;27(33):5681-8.

(218) Moffat KL, Levine WN, Lu HH. *In vitro* evaluation of rotator cuff tendon fibroblasts on aligned composite scaffold of polymer nanofibers and hydroxyapatite nanoparticles. Transactions of the 54th Orthopaedic Research Society. 2008.

(219) Lee CH, Shin HJ, Cho IH, Kang YM, Kim IA, Park KD, et al. Nanofiber alignment and direction of mechanical strain affect the ECM production of human ACL fibroblast. Biomaterials 2005 Apr;26(11):1261-70.

(220) Sahoo S, Ouyang H, Goh JC, Tay TE, Toh SL. Characterization of a novel polymeric scaffold for potential application in tendon/ligament tissue engineering. Tissue Eng 2006 Jan;12(1):91-9.

(221) Subramony SD, Qu D, Ma R, Schaer M, Guo XE, Doty S.B., et al. *In vitro* optimization and *in vivo* evaluation of a multi-phased nanofiber-based synthetic ACL scaffold. Transactions of the 60th Orthopaedic Research Society. 2014.

(222) Li WJ, Tuli R, Okafor C, Derfoul A, Danielson KG, Hall DJ, et al. A three-dimensional nanofibrous scaffold for cartilage tissue engineering using human mesenchymal stem cells. Biomaterials 2005 Feb;26(6):599-609.

(223) Casper ME, Fitzsimmons JS, Stone JJ, Meza AO, Huang Y, Ruesink TJ, et al. Tissue engineering of cartilage using poly-ε-caprolactone nanofiber scaffolds seeded in vivo with periosteal cells. Osteoarthr Cartilage 2010;18(7):981-91.

(224) Lee NM, Erisken C, Iskratsch T, Sheetz M, Levine WN, Lu HH. Polymer fiber-based models of connective tissue repair and healing. Biomaterials 2017;112:303-12.

(225) Yang DY, Liu X, Jin Y, Zhu Y, Zeng DD, Jiang XY, et al. Electrospinning of Poly(dimethylsiloxane)/Poly(methyl methacrylate) Nanofibrous Membrane: Fabrication and Application in Protein Microarrays. Biomacromolecules 2009 Dec;10(12):3335-40.

(226) Kim YB, Cho D, Park WH. Electrospinning of Poly(Dimethyl Siloxane) by Sol-Gel Method. J Appl Polym Sci 2009 Dec 15;114(6):3870-4.

(227) Yoshimoto H, Shin YM, Terai H, Vacanti JP. A biodegradable nanofiber scaffold by electrospinning and its potential for bone tissue engineering. Biomaterials 2003 May;24(12):2077-82.

(228) Li WJ, Danielson KG, Alexander PG, Tuan RS. Biological response of chondrocytes cultured in three-dimensional nanofibrous poly(epsilon-caprolactone) scaffolds. J Biomed Mater Res A 2003 Dec 15;67(4):1105-14.

(229) Baker BM, Mauck RL. The effect of nanofiber alignment on the maturation of engineered meniscus constructs. Biomaterials 2007 Apr;28(11):1967-77.

(230) Nerurkar NL, Elliott DM, Mauck RL. Mechanics of oriented electrospun nanofibrous scaffolds for annulus fibrosus tissue engineering. J Orthop Res 2007 Aug;25(8):1018-28.

(231) Costa KD, Lee EJ, Holmes JW. Creating alignment and anisotropy in engineered heart tissue: role of boundary conditions in a model three-dimensional culture system. Tissue Eng 2003 Aug;9(4):567-77.

(232) Sahin O, Erina N. High-resolution and large dynamic range nanomechanical mapping in tapping-mode atomic force microscopy. Nanotechnology 2008 Nov 5;19(44):445717.

(233) Sahin O, Magonov S, Su C, Quate CF, Solgaard O. An atomic force microscope tip designed to measure time-varying nanomechanical forces. Nat Nanotechnol 2007 Aug;2(8):507-14.

(234) Yang D, Liu X, Jin Y, Zhu Y, Zeng D, Jiang X, et al. Electrospinning of poly (dimethylsiloxane)/poly (methyl methacrylate) nanofibrous membrane: Fabrication and application in protein microarrays. Biomacromolecules 2009;10(12):3335-40.

(235) Wang Z, Volinsky AA, Gallant ND. Crosslinking effect on polydimethylsiloxane elastic modulus measured by custom–built compression instrument. J Appl Polym Sci 2014;131(22).

(236) Selby JC. Composite diaphragm inflation: A method for probing the rheological functions of cell-cell anchoring junctions and cytoskeletal networks within a living normal human epidermal keratinocyte sheet. (Doctoral dissertation, University of Illinois at Urbana-Champaign) ProQuest; 2007.

(237) Song J, Tranchida D, Vancso GJ. Contact mechanics of UV/ozone-treated PDMS by AFM and JKR testing: mechanical performance from nano-to micrometer length scales. Macromolecules 2008;41(18):6757-62.

(238) Xie J, Li X, Xia Y. Putting electrospun nanofibers to work for biomedical research. Macromol Rapid Commun 2008;29(22):1775-92.

(239) Ma M, Hill RM, Lowery JL, Fridrikh SV, Rutledge GC. Electrospun poly (styrene-block-dimethylsiloxane) block copolymer fibers exhibiting superhydrophobicity. Langmuir 2005;21(12):5549-54.

(240) Bhattacharya S, Datta A, Berg JM, Gangopadhyay S. Studies on surface wettability of poly (dimethyl) siloxane (PDMS) and glass under oxygen-plasma treatment and correlation with bond strength. J Microelectromech Syst 2005;14(3):590-7.

(241) Bodas D, Khan-Malek C. Hydrophilization and hydrophobic recovery of PDMS by oxygen plasma and chemical treatment - An SEM investigation. Sens Actuators B Chem 2007;123(1):368-73.

(242) Gruber HE, Somayaji S, Riley F, Hoelscher GL, Norton HJ, Ingram J, et al. Human adipose-derived mesenchymal stem cells: serial passaging, doubling time and cell senescence. Biotech Histochem 2012 May;87(4):303-11.

(243) Jiang X, Cao HQ, Shi LY, Ng SY, Stanton LW, Chew SY. Nanofiber topography and sustained biochemical signaling enhance human mesenchymal stem cell neural commitment. Acta Biomater 2012 Mar;8(3):1290-302.

(244) Lu HH, Cooper JA, Jr., Manuel S, Freeman JW, Attawia MA, Ko FK, et al. Anterior cruciate ligament regeneration using braided biodegradable scaffolds: in vitro optimization studies. Biomaterials 2005 Aug;26(23):4805-16.

(245) Gruber HE, Somayaji S, Riley F, Hoelscher GL, Norton HJ, Ingram J, et al. Human adipose-derived mesenchymal stem cells: serial passaging, doubling time and cell senescence. Biotech Histochem 2012 May;87(4):303-11.

(246) Greenwood SK, Hill RB, Sun JT, Armstrong MJ, Johnson TE, Gara JP, et al. Population doubling: a simple and more accurate estimation of cell growth suppression in the in vitro assay for chromosomal aberrations that reduces irrelevant positive results. Environ Mol Mutagen 2004;43(1):36-44.

(247) Mathur A, Moore SW, Sheetz MP, Hone J. The role of feature curvature in contact guidance. Acta Biomater 2012 Jul;8(7):2595-601.

(248) Vogel V, Sheetz M. Local force and geometry sensing regulate cell functions. Nat Rev Mol Cell Biol 2006 Apr;7(4):265-75.

(249) Jahani H, Kaviani S, Hassanpour-Ezatti M, Soleimani M, Kaviani Z, Zonoubi Z. The effect of aligned and random electrospun fibrous scaffolds on rat mesenchymal stem cell proliferation. Cell Journal (Yakhteh) 2012;14(1):31.

(250) Chen CS, Mrksich M, Huang S, Whitesides GM, Ingber DE. Geometric control of cell life and death. Science 1997 May 30;276(5317):1425-8.

(251) McBeath R, Pirone DM, Nelson CM, Bhadriraju K, Chen CS. Cell shape, cytoskeletal tension, and RhoA regulate stem cell lineage commitment. Dev Cell 2004;6(4):483-95.

(252) Wheatley DN, Wang AM, Strugnell GE. Expression of primary cilia in mammalian cells. Cell Biol Int 1996;20(1):73-81.

(253) Tummala P, Arnsdorf EJ, Jacobs CR. The role of primary cilia in mesenchymal stem cell differentiation: a pivotal switch in guiding lineage commitment. Cell Molec Bioeng 2010;3(3):207-12.

(254) Hoey DA, Tormey S, Ramcharan S, O'Brien FJ, Jacobs CR. Primary cilia–mediated mechanotransduction in human mesenchymal stem cells. Stem Cells 2012;30(11):2561-70.

(255) Pelham RJ, Wang Yl. Cell locomotion and focal adhesions are regulated by substrate flexibility. Proc Natl Acad Sci 1997;94(25):13661-5.

(256) Solon J, Levental I, Sengupta K, Georges PC, Janmey PA. Fibroblast adaptation and stiffness matching to soft elastic substrates. Biophys J 2007 Dec 15;93(12):4453-61.

(257) Xie J, Li X, Lipner J, Manning CN, Schwartz AG, Thomopoulos S, et al. "Aligned-to-random" nanofiber scaffolds for mimicking the structure of the tendon-to-bone insertion site. Nanoscale 2010 Jun 9;2(6):923-6.

(258) Park SH, Hong JW, Shin JH, Yang DY. Quantitatively controlled fabrication of uniaxially aligned nanofibrous scaffold for cell adhesion. J Nanomater 2011;2011:8.

(259) Fee T, Surianarayanan S, Downs C, Zhou Y, Berry J. Nanofiber alignment regulates NIH3T3 cell orientation and cytoskeletal gene expression on electrospun PCL+ Gelatin nanofibers. PLoS ONE 2016;11(5):e0154806.

(260) Garg K, Sell SA, Madurantakam P, Bowlin GL. Angiogenic potential of human macrophages on electrospun bioresorbable vascular grafts. Biomed Mater 2009;4(3):031001.

(261) Smith MJ, White KL, Smith DC, Bowlin GL. In vitro evaluations of innate and acquired immune responses to electrospun polydioxanone-elastin blends. Biomaterials 2009;30(2):149-59.

(262) Smith MJ, Smith DC, Bowlin GL, White KL. Modulation of murine innate and acquired immune responses following in vitro exposure to electrospun blends of collagen and polydioxanone. J Biomed Mater Res A 2010;93(2):793-806.

(263) Shaw LM, Messier JM, Mercurio AM. The activation dependent adhesion of macrophages to laminin involves cytoskeletal anchoring and phosphorylation of the alpha 6 beta 1 integrin. J Cell Biol 1990;110(6):2167-74.

(264) Ma J, Chen T, Mandelin J, Ceponis A, Miller NE, Hukkanen M, et al. Regulation of macrophage activation. Cell Mol Life Sci 2003;60(11):2334-46.

(265) Cao H, Liu T, Chew SY. The application of nanofibrous scaffolds in neural tissue engineering. Adv Drug Deliv Rev 2009;61(12):1055-64.

(266) Cao H, Mchugh K, Chew SY, Anderson JM. The topographical effect of electrospun nanofibrous scaffolds on the in vivo and in vitro foreign body reaction. J Biomed Mater Res A 2010;93(3):1151-9.

(267) Blakney AK, Swartzlander MD, Bryant SJ. The effects of substrate stiffness on the in vitro activation of macrophages and in vivo host response to poly (ethylene glycol)-based hydrogels. J Biomed Mater Res A 2012;100(6):1375.

(268) Fereol S, Fodil R, Labat B, Galiacy Sp, Laurent VrM, Louis B, et al. Sensitivity of alveolar macrophages to substrate mechanical and adhesive properties. Cell Motil Cytoskeleton 2006;63(6):321-40.

(269) Adlerz KM, randa-Espinoza H, Hayenga HN. Substrate elasticity regulates the behavior of human monocyte-derived macrophages. Eur Biophys J 2016;45(4):301-9.

(270) Thery C, Amigorena S, Raposo G, Clayton A. Isolation and characterization of exosomes from cell culture supernatants and biological fluids. Curr Protoc Cell Biol 2006;3-22.

(271) Provenzano PP, Vanderby R. Collagen fibril morphology and organization: implications for force transmission in ligament and tendon. Matrix Biology 2006;25(2):71-84.

(272) Marturano JE, Arena JD, Schiller ZA, Georgakoudi I, Kuo CK. Characterization of mechanical and biochemical properties of developing embryonic tendon. Proc Natl Acad Sci 2013;110(16):6370-5.

(273) Provenzano PP, Martinez DA, Grindeland RE, Dwyer KW, Turner J, Vailas AC, et al. Hindlimb unloading alters ligament healing. J Appl Physiol 2003;94(1):314-24.

(274) Galloway MT, Lalley AL, Shearn JT. The role of mechanical loading in tendon development, maintenance, injury, and repair. J Bone Joint Surg 2013;95(17):1620.

(275) Kawamura S, Ying L, Kim HJ, Dynybil C, Rodeo SA. Macrophages accumulate in the early phase of tendon-bone healing. J Orthop Res 2005 Nov;23(6):1425-32.

(276) Paul A, Manoharan V, Krafft D, Assmann A, Uquillas JA, Shin SR, et al. Nanoengineered biomimetic hydrogels for guiding human stem cell osteogenesis in three dimensional microenvironments. J Mater Chem B 2016;4(20):3544-54.

(277) Oh M, Nör JE. The perivascular niche and self-renewal of stem cells. Frontiers Physiol 2015;6.